THERMODYNAMIC MODELLING OF WAX

AND

INTEGRATED WAX - HYDRATE

By

Hongyan Ji

Submitted for the Degree of Doctor of Philosophy in

Petroleum Engineering

Institute of Petroleum Engineering

Heriot-Watt University

Edinburgh, UK

May 2004

ABSTRACT

Deposition of wax in wellbore and pipelines is of major concern for the flow assurance in oil industry. Wax can be considered as a solid phase of hydrocarbon compounds, which forms if operating temperature and pressure conditions are inside the wax phase boundary for a given fluid system. The work described in this thesis is sought to develop a comprehensive thermodynamic wax model that can be used to determine the wax phase boundary for complex reservoir fluids. Reservoir fluid systems are prone to both wax and hydrate formation at low temperature and high pressure conditions. It is speculated that the formation of one solid phase may affect the thermodynamic behaviour of the other. This was also considered in this study through integrated modelling of wax-hydrate.

The new wax model was developed based on wax disappearance temperatures (WDTs), rather than wax appearance temperature (WAT) as used in most previous models. Reliable WDTs were measured at precise solid-liquid equilibrium conditions in the laboratory. A systematic approach was adopted in the model construction. First, basic thermodynamic equations were derived and modified in order to properly represent the wax phase equilibrium. Then, the model was tuned using binary mixtures of synthetic n-paraffins with accurate compositional data. Finally, the model was extended to real reservoir fluids using a well-proven fluid characterisation procedure based on conventional oil compositional data.

New correlations were developed for calculating thermo-physical properties of pure compounds, in order to improve the calculated fugacity for pure solids. The α functions of SRK and PR EoS were then modified for improving the calculated fugacity for wax-forming compounds in liquid phase. A new approach based on the UNIQUAC equation was developed to describe solid mixtures of wax. The effect of pressure on wax solid phase was also modelled using reliable fusion temperatures for pure compounds.

The wax model based on synthetic n-paraffin mixtures was extended to real reservoir fluids by considering the roles of different hydrocarbon classes in wax formation, which was in line

with experimental and field observations. To facilitate the practical application of the model, the extension was based on the fluid compositional data measured from conventional reservoir fluid analysis. A programme was developed for splitting the plus fraction (e.g. C_{20+}) into single carbon number (SCN) groups, and an empirical correlation was established to further separate each SCN group heavier than C_{20} into an n-paraffin and a non-n-paraffin pseudo-component.

The new wax model can be used for predicting the wax phase boundary, as well as the amount and composition of wax precipitated in different fluids. The reliability of model has been examined and validated using independent experimental data.

The wax model developed in this work was integrated with the hydrate model developed from the previous studies in the research group, in order to quantify the effect of wax formation on hydrate phase boundary, and vice versa, in complex reservoir fluid systems.

ACKNOWLEDGEMENTS

This work was carried out between October 2000 and December 2003 in Centre for Gas Hydrate Research, Institute of Petroleum Engineering, Heriot-Watt University. I am particularly grateful to Professor Bahman Tohidi and Professor Ali Danesh for their extremely precious guidance, invaluable suggestions, continuous encouragements, and strong supports. I also owe my thanks to Professor Adrian C. Todd for his very helpful and inspiring discussions.

I would truly appreciate all the help given by my colleague Mr. Rod W. Burgass, for his close cooperation and considerable contributions to experimental work. I also would like to thank other members in Centre for Gas Hydrate Research, particularly Dr. Kasper Korsholm Østergaard, Dr. Shaoran Ren, Mr. Ross Anderson, who helped me at different stages of this work. Thanks are also extended to Mr. Amir Masoudi, Dr. Jinhai Yang, and Mr. Jahan Arjmandi, for their encouragements.

The contribution of Reservoir Fluid Studies Group for their valuable experimental data is highly appreciated. I would also appreciate the support from academic and research staff, the assistance from support staff, of the Institute of Petroleum Engineering at Heriot-Watt University.

This work was part of a Joint Industrial project funded by ABB Offshore Systems Ltd, the UK Department of Trade and Industry, Petrobras, Shell UK Exploration and Production, and TOTAL, whose support is gratefully acknowledged. I also wish to thank James-Watt Scholarship and the ORS Award Scheme for financial support.

Finally, I will express my deep thanks to all members of my family, for their unlimited encouragement and excessive support, without which it would be impossible for me to achieve the goal of pursuing this degree.

TABLE OF CONTENT

ABSTRACT			i
ACKNOWLEDGEMENTS			iii
TABLE OF CONTENTS			iv
LIST OF TABLES			xi
LIST OF FIGURES			xiii
LIST OF SYMBOLS			xxi
CHAPTER-1		INTRODUCTION	1
	1.1	WAX	2
		1.1.1 Mechanism of Wax Deposition	3
		1.1.2 Control of Wax Deposition	4
	1.2	GAS HYDRATE	6
	1.3	WAX AND HYDRATE	7
	1.4	OUTLINE OF THE THESIS	8
CHAPETR-2		MEASUREMENTS AND EXPERIMENTAL DATA	11
	2.1	INTRODUCTION	11
	2.2	WAT AND WDT	12
	2.3	TECHNQIUES USED FOR WDT MEASUREMENTS	13
		2.3.1 Experimental Equipments	13
		2.3.2 Experimental Procedures	15
	2.4	TESTED FLUIDS AND EXPERIMENTAL DATA	15
		2.4.1 Fluid Samples	15
		2.4.2 Experimental Results for Synthetic Binaries	16

		2.4.3 Experimental Data for Multi-component Mixtures and Real Reservoir Fluids	18
	2.5	SUMMARY	20
	2.6	TABLES	21
	2.7	FIGURES	23
CHAPETR-3		THERMODYNAMIC DESCIPTION OF PHASES AND PHASE EQUILIBRIUM	27
	3.1	INTRODUCTION	27
	3.2	WAX AND HYDRATE STRUCTURES	28
		3.2.1 Wax	28
		3.2.2 Hydrate	30
	3.3	MULTI-PHASE EQUILIBRIUM	31
	3.4	VAPOUR AND LIQUID PHASES	33
	3.5	SOLID PHASE – WAX	34
	3.6	SOLID PHASE – HYDRATE	35
		3.6.1 Calculation of f_w^{β}	36
		3.6.2 Calculation of $\Delta\mu_w^{\beta-H}$	37
		3.6.3 Kihara Potential Parameters	38
	3.7	SOLID PHASE – ICE	39
	3.8	SUMMARY	40
	3.9	TABLES	41
	3.10	FIGURES	42
CHAPTER-4		DEVELOPMENT OF WAX THERMODYNAMIC MODEL	44
	4.1	INTRODUCTION	44
	4.2	REVIEW OF EXISTING WAX MODELS AND PROPOSAL OF A NEW WAX MODEL	44
		4.2.1 Review of Existing Wax Thermodynamic Models	44

		4.2.2 New Wax Model Proposal	49
	4.3	FUSION PROPERTIES AND HEAT CAPACITY	49
	4.4	MODIFICATION OF SRK AND PR EOS FOR HEAVY HYDROCARBONS	50
		4.4.1 Approach	51
		4.4.2 Proposed New m vs ω Correlations	53
		4.4.3 Optimised Binary Interaction Parameters (BIPs)	54
		4.4.4 Comparison of Several α Functions	55
	4.5	DESCRIPTION OF WAX SOLIDS	55
	4.6	MODELLING HIGH PRESSURE CONDITIONS	57
	4.7	CONCLUSIONS	57
	4.8	TABLES	59
	4.9	FIGURES	61
CHAPTER-5		MODELLING OF WAX IN REAL RESERVOIR FLUIDS	65
	5.1	INTRODUCTION	65
	5.2	CLASSIFICATION OF HYDROCARBONS AND THEIR ROLES IN WAX FORMATION	66
		5.2.1 Classification of Hydrocarbons for Reservoir Fluids	66
		5.2.2 Composition of Wax Formed in Real Reservoir Fluids	66
		5.2.3 Roles of Different Hydrocarbons in Wax Formation	67
	5.3	MODELLING OF WAX IN REAL RESERVOIR FLUIDS	68
		5.3.1 Review of Existing Wax Models for Real Reservoir Fluids	69
		5.3.2 Considerations of the New Wax Model Developed in This Work	71
	5.4	EXTENSION OF THE NEW WAX MODEL TO REAL RESERVOIR FLUIDS	71
		5.4.1 Splitting of the Plus Fraction into SCN Groups	72
		5.4.2 Estimation of n-Paraffin Concentration	74
		5.4.3 Estimation of non-n-Paraffin Melting Point	

		Temperature	74
	5.4.4	Flow-chart for Modelling Wax in Real Reservoir Fluids	75
5.5	DISCUSSIONS		75
	5.5.1	The Approach for Splitting the Plus Fraction	76
	5.5.2	Estimation of n-Paraffin Concentrations	76
5.6	CONCLUSIONS		78
5.7	TABLES		80
5.8	FIGURES		82
CHAPTER-6	VALIDATION OF THE WAX MODEL		90
6.1	INTRODUCTION		90
6.2	WAX PHASE BOUNDARY		92
	6.2.1	Validation of the Correlations for Fusion Properties and Heat Capacity	92
	6.2.2	Validation of the New Wax Solid Model	92
	6.2.3	Effects of Pressure and Light End on Wax Phase Boundary	94
	6.2.4	Real Reservoir Fluids	97
6.3	AMOUNT AND COMPOSITION OF WAX PRECIPITATED		98
	6.3.1	Synthetic Mixture	98
	6.3.2	Real Reservoir Fluids	99
6.4	CONCLUSIONS		100
6.5	TABLES		102
6.6	FIGURES		106
CHAPTER-7	INTEGRATED MODELLING OF WAX AND HYDRATE		124
7.1	INTRODUCTION		124
7.2	COMBINING THE WAX AND HYDRATE MODELS		125

		7.2.1 Programme Outline	125
		7.2.2 Fluid Characterisation	126
		7.2.3 EoS and BIP	127
	7.3	APPLICATION OF THE INTEGRATED MODEL	127
		7.3.1 Hydrate Phase Boundary: Effect of Wax Formation	128
		7.3.2 Wax phase Boundary: Effect of Hydrate Formation	129
	7.4	CONCLUSIONS	130
	7.5	TABLES	132
	7.6	FIGURES	135
CHAPTER-8		CONCLUSIONS	139
	8.1	EXPERIMENTAL WORK	140
	8.2	DEVELOPMENT AND VALIDATION OF THE NEW WAX MODEL	140
		8.2.1 Development of the Wax Model	141
		8.2.2 Modelling of Real Reservoir Fluids	142
		8.2.3 Validation of the Wax Model	143
	8.3	INTEGRATED MODELLING OF WAX AND HYDRATE	144
	8.4	RECOMMENDATIONS FOR FUTURE WORK	145
		8.4.1 Further Improving the Wax Model Using New Experimental Data	145
		8.4.2 Effects of Wax and Hydrate Co-Formation	146
APPENDIX-A		EXPERIMENTAL DATA	147
APPENDIX-B		EQUATION OF STATE AND BINARY INTERACTION PARAMETER	155
	B.1	EQUATION OF STATE	155
		B.1.1 General Form of EoS	155

B.1.2 EoS Parameters 157
B.2 MIXING RULES AND BINARY INTERACTION PARAMETERS 159
B.2.1 Mixing Rules 159
B.2.2 Binary Interaction Parameters 160
B.3 TABLES 162

APPENDIX-C THERMO0PHYSICAL PROPERTIES 165
C.1 FUSION AND SOLID-SOLID TRANSITION TEMPERATURES 165
C.1.1 Fusion Temperature 165
C.1.2 Solid-solid Transition Temperature 166
C.2 HEAT OF FUSION AND SOLID-SOLID TRANSITION 167
C.2.1 Sum of Enthalpy of Fusion and Enthalpy of Solid-solid Transition 167
C.2.2 Enthalpy of Fusion and Solid-solid Transition 167
C.3 HEAT CAPACITY 168
C.3.1 Heat Capacity for n-Paraffin Liquids 168
C.3.2 Heat Capacity for n-Paraffin Solids 169
C.4 FIGURES 170

REFERENCES 174

LIST OF TABLES

TABLES

Table 2.1	Experimental WDT data (this work) for nC_6-nC_{16} and nC_6-nC_{17} binaries	21
Table 2.2	Experimental WDT data (this work) for nC_{16}-nC_{18}, nC_{16}-nC_{20} and nC_{15}-nC_{19} binaries.	22
Table 3.1	Geometric and physical properties for cavities of structure I, II and H hydrates.	41
Table 4.1	The VLE and SLE binary systems containing heavy n-paraffins.	59
Table 4.2	Heavy compound T/T_c ranges used for developing the EoS parameter in this work.	60
Table 5.1	Melting point temperatures for several hydrocarbons.	80
Table 5.2	The constants determined in this work for estimating the n-paraffin concentrations.	80
Table 5.3	Experimental data (Ronningsen et al. 1991) and the calculated WDTs for several North Sea crude oils.	81
Table 6.1	Experimental WDT data (Metivaud et al., 1999) and different model predictions for C_{14}-C_{15}-C_{16} ternary, at 0.1MPa.	102
Table 6.2	Experimental WDT data (Metivaud et al., 1999) and different model predictions for C_{18}-C_{19}-C_{20} ternary, at 0.1MPa.	103
Table 6.3	Experimental WDT data (this laboratory) and different model predictions for C_6-C_{16}-C_{17} ternary, at 0.1MPa.	104

Table 6.4 Compositions of four mixtures containing methane (Daridon et al. 1996). 104

Table 6.5 Experimental (this laboratory) and predicted (using the HWWAX model) WDTs for real reservoir fluids, at 0.1 MPa. 105

Table 6.6 Compositions for the multi-component mixture representing a highly simplified crude oil system (Pauly et al., 2001). 105

Table 7.1 Compositions (mole%) for several mixtures based on different mixing ratios of C_1-C_5 with the dead fluid. 132

Table 7.2 Calculated wax disappearance temperature (WDT) at 5.07 MPa and the hydrate dissociation points without and with taking into account wax formation. 132

Table 7.3 Distributions (mole %) of equilibrium phases and compositions of the fluid with removal of wax at several temperature and pressure conditions. 133

Table 7.4 The calculated hydrate dissociation temperatures (HDT) and the wax disappearance temperatures (WDT) with and without hydrate. 133

Table 7.5 Distributions (mole %) of equilibrium phases and compositions of the fluid with removal of hydrate at several temperature and pressure conditions. 134

Table A.1 Compositions (mole%) for synthetic Mixtures A, B, C and D without light ends (Centre for Gas Hydrate Research, HWU). 147

Table A.2 Experimental WDT data for synthetic Mixtures A, B, C and D without light ends (Centre for Gas Hydrate Research, HWU). 148

Table A.3 Compositions (mole%) for synthetic Mixtures B, C and D with light ends (Centre for Gas Hydrate Research, HWU). 149

Table A.4 Experimental WDT data for synthetic Mixtures B, C and D with light ends (Centre for Gas Hydrate Research, HWU). 150

Table A.5	Compositions (mole%) for synthetic Mixture E with different amounts of light-ends (Centre for Gas Hydrate Research. HWU).	150
Table A.6	Experimental WAT and WDT data for synthetic Mixture E with different amounts of light-ends (Centre for Gas Hydrate Research, HWU).	151
Table A.7.	Compositions and physical properties (Reservoir Fluid Studies Group, HWU) of North Sea crude oil LTA97-1 (WDT is measured as 328 K, Centre for Gas Hydrate Research, HWU).	152
Table A.8.	Compositions and physical properties (Reservoir Fluid Studies Group, HWU) of Base condensate LTB98-1 (WDT is measured as 309 K, Centre for Gas Hydrate Research, HWU).	153
Table A.9.	Single phase compositions and physical properties (Reservoir Fluid Studies Group, HWU) of Black oil RFS-1 (WDT for the dead fluid is measured as 323 K, Centre for Gas Hydrate Research, HWU).	154
Table B.1.	Binary interaction parameters between light and intermediate compounds in SRK EoS.	162
Table B.2.	Binary interaction parameters between light and intermediate compounds in PR EoS.	163
Table B.3.	Binary interaction parameters between light and intermediate compounds in VPT EoS.	164
Table B.4.	Binary interaction parameters between water and several compounds in VPT EoS.	164

LIST OF FIGURES

FIGURES

Figure 2.1. Schematic illustration of the simple visual set-up. 23

Figure 2.2. Schematic illustration of the QCM. 23

Figure 2.3. Schematic illustration of the QCM apparatus (atmosphere pressure). 24

Figure 2.4. Schematic of the combined visual and QCM apparatus. 24

Figure 2.5. The nC_6-nC_{16} wax phase boundaries based on the WDT data determined in this work and the literature data 25

Figure 2.6. The nC_6-nC_{17} wax phase boundaries based on the WDT data from this work and the literature data. 25

Figure 2.7. The nC_{16}-nC_{18} wax phase boundaries based on the WDT data from this work and the literature data. 26

Figure 2.8. WAT and WDT measured using QCM on a North Sea crude oil (measured by Burgass R.W.). 26

Figure 3.1. Schematic representation of crystal packing modes in terms of carbon chain (the line in figure) arrangement (Craig et al., 1998): (a) ideal packing without disorder, (b) inter-chain mixing, (c) end-chain twisting/folding, and (d) combined carbon chain mixing and twisting/folding. 42

Figure 3.2. Five types of cavities in structure I, II and H hydrates. 42

Figure 3.3. Flowchart for calculating wax phase boundary in a multi-phase system. 43

Figure 4.1. Experimental and estimated critical temperatures for heavy n-paraffins (C_n>C_{20}). 61

Figure 4.2. Experimental and estimated critical pressures for heavy n-paraffins (C_n>C_{20}). 61

Figure 4.3. Comparison of heavy compound (C_n>C_{20}) *m* values optimised using critical properties estimated by several empirical correlations to *m* values of $C_1 - C_{20}$, SRK EoS. 62

Figure 4.4. Comparison of heavy compound (C_n>C_{20}) *m* values optimised using critical properties estimated by several empirical correlations to *m* values of $C_1 - C_{20}$, PR EoS. 62

Figure 4.5. Binary interaction parameters optimised using binary SLE data and the SRK EoS modified in this work (Cn: carbon number). 63

Figure 4.6. Binary interaction parameters optimised using binary SLE data and the PR EoS modified in this work (Cn: carbon number). 63

Figure 4.7. Comparison of α values calculated by several methods as functions of acentric factor for the SRK EoS. 64

Figure 4.8. Comparison of α values calculated by several methods as functions of acentric factor for the PR EoS. 64

Figure 5.1. Relative errors (%) of specific gravities estimated using the logarithm function in conjunction with the directly obtained parameters (experimental data: Pedersen et al., 1991b). 82

Figure 5.2. Relative errors (%) of specific gravities estimated using the logarithm function in conjunction with the corrected parameters (experimental data: Pedersen et al., 1991b). 82

Figure 5.3. Flowchart of generating fluid composition data to model wax in reservoir fluids. 83

Figure 5.4. Experimental data (Pedersen et al., 1991b) and calculated SCN molar distributions for the North Sea crude oil 1. 84

Figure 5.5. Experimental data (Pedersen et al., 1991b) and calculated SCN molar distributions for the North Sea crude oil 2. 84

Figure 5.6. Experimental data (Pedersen et al., 1991b) and calculated SCN molar distributions for the North Sea crude oil 3. 85

Figure 5.7. Experimental data (Pedersen et al., 1991b) and calculated SCN specific gravities against molecular weight for the North Sea crude oil 1. 85

Figure 5.8. Experimental data (Pedersen et al., 1991b) and calculated SCN specific gravities against molecular weight for the North Sea crude oil 2. 86

Figure 5.9. Experimental data (Pedersen et al., 1991b) and calculated SCN specific gravities against molecular weight for the North Sea crude oil 3. 86

Figure 5.10. Independent experimental data (Oil 1, Pan et al., 1997) and predicted specific gravities using several correlations. 87

Figure 5.11. Independent experimental data (Roehner et al., 2002) and predicted specific gravities using several correlations. 87

Figure 5.12. The SCN (heavier than C_{35}) molar distributions predicted for the North Sea Crude Oils 1 and 6. 88

Figure 5.13. The SCN (heavier than C_{35}) specific gravities predicted for the North Sea Crude Oils 1 and 6. 88

Figure 5.14. The SCN (heavier than C_{35}) molar distributions estimated for the North Sea Crude Oils 7, 8 and 17. 89

Figure 5.15. The SCN (heavier than C_{35}) specific gravities estimated for the North Sea Crude oils 7, 8 and 17. 89

Figure 6.1. Experimental (this work) and predicted WDTs for C_6-C_{16} and C_6-C_{17} binaries. 106

Figure 6.2. Comparison of experimental WDT data (this laboratory) for C_{16} -C_{18} binaries with model predictions using several approaches. 106

Figure 6.3. Comparison of experimental WDT data (this laboratory) for C_{16}-C_{20} binaries with model predictions using several approaches. 107

Figure 6.4 Comparison of experimental WDT data (this laboratory) for C_{15}-C_{19} binaries with model predictions using several approaches. 107

Figure 6.5. Comparison of experimental WDT data (Robles et al., 1996) for C_{17}-C_{19} binaries with model predictions using several approaches. 108

Figure 6.6. Experimental data (Vanderkooi et al., 1995) compared with the HWWAX predictions of P_b and WDT for C_1-C_{20} binaries. 108

Figure 6.7. Experimental data (Peters et al., 1987a) compared with the HWWAX predictions of P_b and WDT for C_2-C_{24} binaries. 109

Figure 6.8. Measured (Daridon et al., 1996) and predicted (using the HWWAX model) phase boundaries for Mixture A. 109

Figure 6.9. Measured (Daridon et al., 1996) and predicted (using the HWWAX model) phase boundaries for Mixture B. 110

Figure 6.10. Measured (Daridon et al., 1996) and predicted (using the HWWAX model) phase boundaries for Mixture C. 110

Figure 6.11. Measured (Daridon et al., 1996) and predicted (using the HWWAX model) phase boundaries for Mixture D. 111

Figure 6.12. Experimental data (this laboratory) and predicted WDTs (using the HWWAX model) for Mixtures A, B and C and their live fluids with C_1-C_4. 111

Figure 6.13. Measured (this laboratory) and predicted (using the HWWAX model) WDTs for Mixture D, with and without natural gas. 112

Figure 6.14. Experimental data (Reservoir Fluid Studies Group) and the calculated SCN mole concentrations against molecular weight for the North Sea crude oil LTA97-1. 112

Figure 6.15. Experimental data (Reservoir Fluid Studies Group) and the calculated SCN specific gravities against molecular weight for the North Sea crude oil LTA97-1. 113

Figure 6.16. Experimental data (Reservoir Fluid Studies Group) and the calculated SCN mole concentrations against molecular weight for Base Condensate LTB98-1. 113

Figure 6.17. Experimental data (Reservoir Fluid Studies Group) and the calculated SCN specific gravities against molecular weight for Base Condensate LTB98-1. 114

Figure 6.18. Experimental data (Reservoir Fluid Studies Group) and the calculated SCN mole concentrations against molecular weight for Black Oil RFS-1 (dead fluid). 114

Figure 6.19 Experimental data (Reservoir Fluid Studies Group) and the calculated SCN specific gravities against molecular weight for Black Oil RFS-1 (dead fluid). 115

Figure 6.20. Measured wax amounts (mass %) (Pauly et al., 2001) and predicted values using different wax models. 115

Figure 6.21 Measured (Pauly et al., 2001) and predicted wax compositions using different wax models at 290.2 K and 0.1 MPa. 116

Figure 6.22. Measured (Pauly et al., 2001) and predicted (using HWWAX) wax compositions at different temperature conditions, at 0.1MPa. 116

Figure 6.23. Experimental (Pauly et al., 2001) and predicted (using HWWAX) wax compositions at different pressure conditions (290.2K). 117

Figure 6.24. Experimental (Pedersen et al., 1991a) and predicted (using HWWAX) wax amounts for crude Oil 1. 117

Figure 6.25. Experimental (Pedersen et al., 1991a) and predicted (using HWWAX) wax amounts for crude Oil 2. 118

Figure 6.26. Experimental (Pedersen et al., 1991a) and predicted (using HWWAX) wax amounts for crude Oil 3. 118

Figure 6.27. Experimental (Pedersen et al., 1991a) and predicted (using HWWAX) wax amounts for crude Oil 5. 119

Figure 6.28. Experimental (Pedersen et al., 1991a) and predicted (using HWWAX) wax amounts for crude Oil 6. 119

Figure 6.29. Experimental (Pedersen et al., 1991a) and predicted (using HWWAX) solid amounts for crude Oil 7. 120

Figure 6.30. Experimental (Pedersen et al., 1991a) and predicted (using HWWAX) wax amounts for crude Oil 8. 120

Figure 6.31. Experimental (Pedersen et al., 1991a) and predicted (using HWWAX) wax amounts for crude Oil 9. 121

Figure 6.32. Experimental (Pedersen et al., 1991a) and predicted (using HWWAX) wax amounts for crude Oil 10. 121

Figure 6.33. Experimental (Pedersen et al., 1991a) and predicted (using HWWAX) wax amounts for crude Oil 11. 122

Figure 6.34. Experimental (Pedersen et al., 1991a) and predicted (using HWWAX) wax amounts for crude Oil 12. 122

Figure 6.35. Experimental (Pedersen et al., 1991a) and predicted (using HWWAX) wax amounts for crude Oil 15. 123

Figure 6.36. Experimental (Pedersen et al., 1991a) and predicted (using HWWAX) wax amounts for crude Oil 17. 123

Figure 7.1. Schematic flow-chart for integrated modelling of wax and hydrate (*WDT* and WDT_{pres} are the wax disappearance

temperatures in the absence and presence of hydrate, respectively. HDT and HDT_{pres} are the hydrate dissociation temperatures in the absence and presence of wax, respectively). 135

Figure 7.2. Schematic flow-chart for calculating the hydrate dissociation temperature (HDT/HDT_{pres}) in absence/presence of wax. 136

Figure 7.3. Hydrate phase boundaries predicted for several mixtures with different mixing ratios of light ends (C_1-C_5). 137

Figure 7.4. Wax phase boundaries for fluids with different concentrations of light end, as compositions listed in Table A.5. 137

Figure 7.5. The wax and hydrate phase boundaries for the fluid containing 69 mole% light ends (experimental data are generated in this laboratory. Wax and hydrate predictions are based on the HWWAX and HWHYD models). 138

Figure C.1. Experimental data (Schaerer et al., 1955; Broadhurst, 1962) and regressed fusion temperatures for n-paraffins. 170

Figure C.2. Experimental data (Schaerer et al., 1955; Broadhurst, 1962) and regressed solid-solid transition temperatures for n-paraffins. 170

Figure C.3. Experimental data (Schaerer et al., 1955; Broadhurst, 1962) and regressed enthalpies of fusion and solid-solid transition for n-paraffins. 171

Figure C.4. Experimental data (Schaerer et al., 1955; Broadhurst, 1962) and regressed enthalpies of fusion for n-paraffins. 171

Figure C.5. Experimental data (Huffman et al., 1931; Jin et al., 1991; van Miltenburg et al., 1999) and regressed heat capacities for liquid n-paraffins with odd carbon numbers. 172

Figure C.6. Experimental data (Huffman et al., 1931; Jin et al., 1991; van Miltenburg et al., 1999) and regressed heat capacities for liquid n-paraffins with even carbon numbers. 172

Figures C.7. Experimental data (Huffman et al., 1931; Jin et al., 1991; van Miltenburg et al., 1999) and regressed heat capacities for solid n-paraffins with odd carbon numbers. 173

Figures C.8. Experimental data (Huffman et al., 1931; Jin et al., 1991; van Miltenburg et al., 1999) and regressed heat capacities for solid n-paraffins with even carbon numbers. 173

LIST OF SYMBOLS

SYMBOLS

a^A	The asymmetric contribution in the non-random mixing rules (Equation B.22)
a^C	The conventional random mixing term (Equation B.22)
a, b, c	Parameters of EoS
A, B	Constants related with the general EoS parameters (Equations B.5 and B.6)
B', C', D'	The second, third and fourth virial coefficients of the virial equation (B.1)
a_{SG}, b_{SG}, c_{SG}	Constants related to specific gravity calculations
A_{np}, B_{np}, C_{np}	Constants of the correlation (Equation 5.7) to estimate n-paraffin concentration
$C_{j\,m}$	Langmuir constant between guest component '*j*' and hydrate cavity '*m*'
C_n	Carbon number
C_p	Heat capacity
e	Energy (used in the UNIQUAC equation)
f	Fugacity
F^k	The mole fraction of phase '*k*'
g	Molar Gibbs energy
h	Molar enthalpy
i	Component '*i*'

k_{ij}	Binary interaction parameter between component 'i' and component 'j'
$K(r)$	Kihara potential energy of interaction between two molecules
m	The parameter for calculating the temperature dependency term of EoS
n	Number of components
$p(MW)$	The probability density function of molecular weight
P	Pressure
q	Molecular external surface
r	Molecular size parameter (Equations 4.10 and 4.12) or the distance measured from the centre of cavity (Equation 3.19)
R	Universal gas constant
R_c	The cavity radius
s	Solid mole fraction
T	Temperature
u, w	Parameters of the general form of EoS
u_i^k	The chemical potential of component 'i' in phase 'k'
U, W	Parameters of the general EoS expressed in terms of compressibility factor (Equations B.7 and B.8)
$U(r)$	The spherically symmetric cell potential in the hydrate cavity
v	Molar volume
x	Liquid mole fraction
z	Coordination number
z_i	The feed composition (in mole fraction) of component 'i'

Z	Compressibility factor

GREEK LETTERS

α	Temperature dependency of the attraction term in equation of state
δ	Constant of EoS
Ω	EoS parameter coefficient
φ	Fugacity coefficient
γ	Activity coefficient
θ_m	The number of type m cavity for each water molecule in the unit cell
κ	Boltzmann's constant (Equation 3.19)
ε	The depth of Kihara potential energy well
σ	The collision diameter
β	The hard-core redius
δ^M	Parameters of Equation 3.21
ϑ	Parameter related with molecular size (Equations 4.9 and 4.10)
$\breve{\xi}$	Parameter related with molecular external surface (Equations 4.9 and 4.11)
τ	Parameter related with characteristic energy of UNIQUAC equation
λ	Parameter used to calculate the characteristic energy μ
$\Gamma(\chi)$	Gamma function
η	The minimum molecular weight included in the gamma distribution
χ, β	Parameter determining the shape of the gamma distribution function

Δ	variation
ω	acentric factor
π	Phase number

SUPERSCRIPTS

E	Excess
H	Hydrate Phase
I	Ice phase
k	Phase
L	Liquid phase
O	Pure component
S	Solid phase of wax
sat	Saturation
β	The empty hydrate lattice

SUBSCRIPTS

b	Bubble point
c	Critical condition
cal	Calculated data
exp	Experimental data
f	Fusion

ice	Ice
o	Reference condition
r	Reduced
subl	Sublimation
sum	Sum of heats of fusion and heat of solid-solid transition
tr	Solid-solid transition
w	Water

ABBREVIATIONS

BIP	Binary interaction parameter
Cal.	Calculated
Comp.	Compound or component
Dev.	Deviation
DSC	Differential Scanning Calorimetry
EoS	Equation of State
Exp.	Experimental
GC	Gas chromatography
HDT	Hydrate dissociation temperature
HWHYD	The Heriot-Watt HYDrate model
HWWAX	The Heriot-Watt WAX model
MW	Molecular weight

non-np	None normal paraffin
np	Normal paraffin
PNA	Paraffins, Naphthenes and Aromatics
PR EoS	The Peng-Robinson Equation of State
Pres	Presence of wax or hydrate
QCM	Quartz Crystal Microbalance
SLE	Solid-liquid equilibrium
SRK EoS	The Soave-Redlich-Kwong Equation of State
SCN	Single carbon number
SDS	Solid Detection System
SG	Specific gravity
sH	Hydrate structure H
sI	Hydrate structure I
sII	Hydrate structure II
VLE	Vapour-liquid equilibrium
VPT EoS	Valderrama modification of the Patel and Teja Equation of State
WAT	Wax appearance temperature
WDT	Wax disappearance temperature
wt%	Weight percent

CHAPTER-1

INTRODUCTON

Solid deposition is the main issue for flow assurance in oil production and transportatic systems. Different forms of solids can be formed when reservoir fluids flow into wellbo and pass through pipelines due to pressure, temperature and fluid composition change These include the precipitation of scales due to aqueous phase composition changes, th deposition of asphaltene in wellbore as a result of temperature and pressure changes, and th formation of wax and gas hydrates in multiphase pipelines at low temperature Understanding and properly modelling these processes is essential in implementation of co effective flow assurance remedies in oilfield operations. This thesis is mainly concerne with the thermodynamic modelling of wax in various hydrocarbon systems, as well as th thermodynamic effect between wax and gas hydrate formation at conditions when both wa and hydrate can be formed.

The wax deposited from an oil system is a mixture containing heavy molecules of severa hydrocarbon homologues, such as normal paraffins (n-paraffins), branched paraffins (isc paraffins) and naphthenes. Paraffins, also called alkanes, are non-aromatic saturate hydrocarbons with straight (normal) or branched (iso) carbon chains. Molecules for r paraffins and iso-paraffins are symbolised with general chemical formula C_nH_{2n+} Naphthenes, also termed cyclo-paraffins, are homologues of hydrocarbons containing at lea one ring structure and saturated with respect to hydrogen. Their molecules are symbolise with the chemical formula C_nH_{2n}. Other hydrocarbons, such as aromatics, a group c chemicals containing one or more six-carbon rings characteristic of the benzene series i molecular structure, do not precipitate in wax formation.

Gas hydrates are crystalline molecular complexes formed from mixtures of water an suitably sized gas molecules. The water (host) molecules, upon hydrogen bonding, forı unstable lattice structures with several interstitial cavities. The gas (guest) molecules ca occupy the lattice cavities. When a minimum number of cavities are occupied, the crystallir structure will become stable and solid gas hydrates will form, even at temperatures we above the ice point. The formation of hydrate in hydrocarbon systems can be promoted ; high pressure and low temperature conditions.

In general, reservoir fluid systems, containing oil, gas and water, are prone to both wax an hydrate formation when they are subjected to low temperature conditions. It is speculate that the formation of one phase could affect the thermodynamic and kinetic behaviour of th other. The formation of wax or hydrate will change the composition of the fluid, an consequently it will affect the thermodynamics of the system. More importantly, it is likel that any wax (or hydrate) formation will provide nucleation sites for the other to precipitat Traditionally, wax and hydrate have been studied separately. One of the main objectives c this work is to develop a reliable wax model for complex hydrocarbon systems, then t formulate an integrated wax-hydrate thermodynamics model, capable of predicting th impact of wax formation on hydrate phase boundary, and vice versa.

1.1. WAX

Produced petroleum fluids from an oil reservoir consist of mainly hydrocarbons, water a well as small amounts of non-hydrocarbons, such as N_2, CO_2, and H_2S. The phase behaviou of a hydrocarbon system is determined by its fluid composition and the prevailin temperature and pressure conditions. Generally, at reservoir conditions, hydrocarbons exi: mainly in vapour and liquid phases. However, when the fluids are subjected to lo temperature environments, heavy hydrocarbons may precipitate to form a solid phase - wax.

The occurrence of wax deposition in wellbore and transfer lines was documented as far a back to 1865 (Bone, 1865), in the early beginning of the oil industry. Wax deposited from petroleum fluid is a mixture containing predominantly paraffins, so the wax deposition commonly referred as 'paraffin deposition'. Wax deposit contains predominantl hydrocarbon molecules heavier than C_{20} (Newberry et al., 1986; Labes-Carrier et al., 2002

It appears as a mushy gel to a firmly hard solid, with colour from lightly white to brown dar (Bucaram, 1966; Newberry et al., 1986). When wax forms, a variety of organic an inorganic materials, in their liquid or solid states, may be entrapped or combined, leading t an increased bulk of wax deposit.

Wax deposition may occur in almost every oil-producing area (Shock et al., 1955). It can b found in reservoir formation, down-hole equipment, surface-line, separator, and storage tan (Bucaram, 1966; Bilderback et al., 1969). Wax deposition has been causing many problem in the production and transportation of hydrocarbon fluids (EnDean, 1981; Sifferman, 197 Newberry, 1983). In order to solve and alleviate these problems, the oil industry has directe considerable efforts towards understanding wax deposition mechanisms and finding efficier wax control techniques.

1.1.1. Mechanism of Wax Deposition

Wax formation is a crystallisation process. It includes two successive stages: cryst nucleation and crystal growth (Singhal et al., 1991). Nucleation of wax crystals is the fir step in the formation of a new phase - the solid wax phase, from liquid phase. Formation of new phase requires the creation of an interface between the two phases. The interface i created when the intermolecular attraction force between the heavy hydrocarbons is greate than that with the light components, then the molecules of the heavy components wi combine to form wax crystal nuclei.

When wax nuclei form, crystals will grow on the sites where the surface energy of cohesio between the crystal and the liquid heavy components is significantly large (Singhal, et al 1991). Wax particles with considerable size will be formed by crystal agglomeration.

Wax particles will then deposit on cold surfaces. The growth of wax deposition could b facilitated, due to molecular diffusion and Brownian motion (Burger et al., 1981). Normall there is a temperature gradient between bulk fluid and cold surface, which can lead to concentration gradient and force the wax-forming compounds moving toward the wall b molecular diffusion. In addition, small wax particles suspended in the fluid will continuous collide to form large particles due to Brownian motion, the movement of a particle in a flu owing to thermal agitation. On the other hand, the growth of wax deposition could b

mitigated due to shear dispersion. The shear force imposed by fluid flow along the streamline tends to suspend wax particles in the fluid.

Wax formation is a phase transition: transformation of heavy hydrocarbons from liquid phase to solid phase. Between the two phases, there is a phase boundary, the so-called wax phase boundary, which can be used to determine the appearance and disappearance of wax. Wax phase boundary is strongly dependent on fluid composition. For any given fluid, wax forms only if the temperature and pressure conditions are inside its wax phase boundary. Hence wax phase boundary needs to be accurately determined for the fluid, in order to evaluate the tendency and severity of wax deposition.

1.1.2. Control of Wax Deposition

In oil industry, methods for handling paraffin deposition are divided into four categories (McClaflin et al., 1984):

- Mechanical approach
- Thermal method
- Chemical treatment
- Combinations among the above three methods

Mechanical approach. Mechanical methods involve running a scraper or a cutter to remove wax deposits in pipelines. Commonly used scraper or cutters include devices such as pigs, rod scrappers, plastic line, and plastic-coated rods.

Mechanical removal of wax deposit has been widely used in oil fields. However, mechanical removal of wax generally needs frequent application and interrupts the normal production (Bilderback et al., 1969). The time interval between operations may be several days or number of months, depending on the deposition rate. Use of mechanical approaches for removing wax in pipelines may add problems of wax deposition at oil storage tank (Bilderback et al., 1969). Mechanical approach may also lead to severe tube wear, broke wireline, stuck plunger, and loss of production due to shutdown (Newberry et al, 1986).

When using mechanical approaches, the technique specifications are dependent on the hardness of wax deposit. The wax hardness may reply on wax composition. For instance, higher 'critical carbon number', above which wax molecules diffuse into wax gel matrix

may yield a mechanically harder wax (Paso et al., 2003). Hence, knowledge of wax composition for a given system should be beneficial for designing mechanical wax-removal methods. Furthermore, mechanical technique specifications such as operation pressure may also depend on the amount of wax deposited. Wax amount needs to be estimated in order to design the optimum operation pressure.

Thermal method. Thermal methods are based on minimisation of heat loss and/or addition of external heat to the system (McClaflin et al., 1984). Examples of thermal methods include injection of hot oil, circulation of hot water, insulation of pipelines, and installation of bottom-hole heaters.

When using thermal methods to introduce heat or reduce heat loss, the quantity of heat necessary for maintaining the fluid temperature needs to be estimated. Accurate prediction of wax phase boundary is required for calculating the required heat. For instance, when using hot oil injection to maintain pipeline temperature, the oil used is mostly from bottom of the sales tank (Addison, 1984), which may be the most paraffin-laden. When the oil is pumped down pipes, it may reach its wax phase boundary before it gets to the objective location. The approach of hot oil injection can be improved through accurate estimation of the wax phase boundary for the injected oil.

Chemical treatment. Chemical control methods are based on

- Using solvents (generally having high aromatic contents) to dissolve wax deposits;
- Using inhibitors to avoid wax crystallisation, slow down wax crystal growth, and/or prevent wax adherence to pipe walls.

Wax inhibitors for avoiding wax crystallisation work by reducing the crystallisation temperature (Brownawell et al., 1962). Wax inhibitors for slowing down crystal growth and/or reducing wax adherence usually possess chemical structures that have segments to combine with wax crystals (Becker, 2000). The incorporation of inhibitors into wax molecules can prevent wax crystals from forming network with each other, and diminishing their tendency to grow and adhere.

Wax inhibitors are unfortunately system selective. One inhibitor that is effective in a given system can fail in other systems. The mechanisms of some wax inhibitors are not full

understood, and the selection of inhibitors is commonly undertaken by experiments in each case. Understanding of wax composition is important for the selection of wax inhibitor.

Combined method. It is common that a combination of mechanical, thermal and chemical methods is used in practice for wax control. For instance, injection of hot diesel can combine thermal with chemical treatments. A 'pigging' method is usually combined with chemical treatment, in order to extend the time interval required for pigging (McClaflin et al., 1984).

Control of wax deposition is very costly. An insulated offshore pipeline is approximately 50% more expensive compared to the standard pipeline (Carniani et al., 1996). The chemical treatment can cost $0.05 per barrel of oil produced at a moderate chemical dosage of 10(ppm (Carniani et al., 1996). According to the U.S. DOE (2001), remediation of subsea pipeline blockage caused by wax can cost $1 million per mile (Psao et al., 2003). Field data show that wax control costs over $15 to 20 million in India (Rai et al., 1995).

It is believed that the accuracy of existing wax models for predicting wax appearance temperature (WAT) is very poor, which can have a significant impact on implementing a cost effective wax remediation in field applications. The cost of wax control should be reduced if the wax phase equilibrium, in terms of wax phase boundary and wax composition, can be accurately predicted.

1.2. GAS HYDRATE

Water is present with hydrocarbons in oil reservoirs. In addition, water may be introduced through hydrocarbon recovery processes such as water flooding. The influence of water on hydrocarbon phase behaviour in convention reservoirs is generally small. Hence, water is usually not taken into account when studying the phase behaviour of hydrocarbon systems. Ignoring the effect of water will not introduce significant error to the hydrocarbon phase equilibrium, unless gas hydrates are formed.

Gas hydrates can form with compounds, such as methane (C_1), ethane (C_2), propane (C_3), iso-butane (iC_4), n-butane (nC_4), iso-pentane (iC_5), carbon dioxide (CO_2), nitrogen (N_2) and H_2S, which are generally present in vapour and liquid states in reservoir fluids. The

formation of hydrates from vapour phase is more common. However. in the absence of vapour phase, hydrates can also form from liquid phase.

Hydrate formation, like wax, can lead to blockage and damage of facilities, causing substantial problems for production and transportation of hydrocarbons. The negative impacts of gas hydrate formation on hydrocarbon transportation are well documented in the literature (Hammerschmidt, E. G., 1934, 1940; Mansoori, 1996; Reyna et al., 2001).

Prevention of hydrate formation can be carried out through operating the system outside the hydrate phase boundary. This can be achieved by thermal methods, such as insulating the pipeline, introducing heat to the system. On the other hand, thermodynamic hydrate inhibitors, such as methanol and glycols, can be used for shifting hydrate phase boundary toward lower-temperature and higher-pressure regions. Therefore, a cost effective hydrate control is also largely dependent on accurate determination of hydrate phase boundary.

1.3. WAX AND HYDRATE

In a reservoir fluid system containing water, light and heavy hydrocarbons, formation of both wax and hydrate is possible at certain pressure and temperature conditions. The formation of one solid may affect the thermodynamic behaviour of the other solid. The formation of gas hydrate removes light constituents (e.g. C_1, C_2, C_3, iC_4, nC_4, CO_2, N_2, H_2S) from the fluid phases, which could lead to the increased concentration of waxy compounds, affecting the wax phase behaviour. On the other hand, the formation of wax removes heavy hydrocarbons, increasing the concentration of light compounds in the remaining fluid. Small difference in the composition of hydrate-formers may dramatically affect hydrate formation temperature and pressure (Sloan, 1998, page 266). Furthermore, although beyond the scope of this work, the formation of wax will provide necessary nucleation sites and may promote the formation of hydrate by reducing the required sub-cooling, and vice versa.

While wax and hydrate phase equilibrium have been widely studied, they were traditionally investigated as unrelated problems. Hydrate phase boundaries estimated while ignoring the effect of wax formation may be over-optimistic (i.e., showing lower hydrate formation

temperatures). Similarly, when ignoring the hydrate formation, wax problems may be underestimated. Hence, it is necessary to conduct an integrated wax and hydrate study.

1.4. OUTLINE OF THE THESIS

The main objective of this work is to develop an accurate wax model and integrate it with the current hydrate model, available from the previous studies in the research group (Avlonitis, 1992; Tohidi, 1995; Østergaard, 2000). The integrated wax-hydrate model will be capable of predicting wax and hydrate phase equilibrium and the impact of one solid formation on the other. The model will also be capable of predicting the amount and composition of different phases (including wax and gas hydrate) at any given temperature and pressure condition. The reliability of the hydrate model, HWHYD, has been demonstrated by comparative studies against extensive independent experimental data.

However, the current wax thermodynamic models reported in the literature are far less accurate than the hydrate model. When comparing wax formation temperatures predicted using some existing models with field and experimental data, errors in order of 20 K have been observed (Monger-McClure et al., 1999).

It is, therefore, necessary to modify and improve the wax model, prior to coupling it with the well-validated hydrate model. In this study, a new wax model will be developed and validated by proper experimental data (Ji et al., 2003, 2004; Tohidi et al., 2002, 2004). The wax model will then be integrated with the existing hydrate model.

When developing the wax model, several parameters, such as the adjustable parameter of UNIQUAC equation for describing the wax phase, need to be tuned using experimental data. Reliability of experimental data can strongly affect the model accuracy. In most previous studies, wax appearance temperature (WAT) was measured in laboratory and used for tuning the model. WAT is, however, dependent on experimental procedure, and not necessarily the solid-liquid equilibrium point. The model based on experimental WAT data is consequently subjected to questions of reliability. In this laboratory, wax disappearance temperatures (WDTs) are measured at precise solid-liquid equilibrium conditions (Ji et al., submitted; Ji et al., in preparation). The experimental equipments and the test procedure are described in

Chapter-2. With the reliable experimental technique, WDTs are measured for synthetic and real reservoir fluids. Experimental data generated in this work for tuning a new wax model are presented in Chapter-2, while data used for validation of the model are given in Appendix-A.

Chapter 3 describes the fundamental formulations of the wax and hydrate models. These include descriptions of phases, such as vapour (V), liquid hydrocarbon (L_2), aqueous phase (L_1), Ice (I), solid phase of hydrate (H), and solid phase of wax (S). Basic thermodynamic formulas for calculating fugacity in each phase are also presented.

N-paraffins are present in reservoir fluids, and they are essential for determining the wax phase equilibrium. However, concentrations of n-paraffins in reservoir fluids are generally not known, which may result in the uncertainty when tuning the model parameter directly using conventional reservoir fluid composition data. Hence, in this work the wax model is first tuned with synthetic n-paraffin mixtures with accurate compositional data (Ji et al., 2004). In Chapter-4, development of the wax model based on pure n-paraffins and their mixtures is detailed.

Chapter-5 extends the wax model to real reservoir fluids. The compositional data obtained from laboratory analysis for reservoir fluids are generally up to limited carbon numbers. However, modelling of wax phase equilibrium requires compositions for heavy hydrocarbons, which are not available experimentally. Hence, numerical methods will be needed for obtaining the required compositional data, which will be presented in this chapter. Furthermore, reservoir fluids are mixtures containing different hydrocarbon homologues that have considerably different properties. Discussion and modelling of effects of different hydrocarbons on wax formation are also presented.

In Chapter-6, validation of the new wax model will be presented by comparing its predictions against independent experimental data and with some existing wax models. A wide range of experimental data for both synthetic mixtures and real reservoir fluids are used.

The wax model is then coupled with the existing hydrate model, which is detailed in Chapter-7. The integrated model is capable of predicting the separate wax and hydrate phase equilibrium, and combined wax-hydrate phase equilibria. Hydrate/wax phase boundaries with different light end concentrations are modelled, in order to demonstrate the effects

caused by removal of heavy/light hydrocarbons due to wax/hydrate formation. Furthermore, the predictions of the integrated wax and hydrate model are compared with independent experimental data, demonstrating the effect of one solid formation on the other. in terms of shifting phase boundary.

The conclusion of this work and some recommendations for future work are presented in Chapter-8.

CHAPTER-2

MEASUREMENTS AND EXPERIMENTAL DATA

2.1. INTRODUCTION

In field operations, the precipitation of wax solids is generally due to temperature decrease when reservoir streams passing through cold equipment and pipelines. Wax appearance temperature (WAT) can be determined or observed in laboratory and in field operations. A wax phase boundary is usually plotted using WAT as a function of either the system pressure, or the concentration of wax forming compounds. However, it is well known that the wax phase boundary determined by wax appearance temperature is strongly dependent on experimental and observation procedures; very different results have been reported in the literature even for the same hydrocarbon system. In fact, most wax appearance observations were not or cannot be made at thermodynamic equilibrium conditions, since it is practically impossible for giving sufficiently long time for wax to appear at a solid-liquid equilibrium temperature. Instead, a wax disappearance temperature (WDT) can be measured at equilibrium or near equilibrium conditions.

This chapter describes the importance of measuring wax disappearance temperature as basis for modelling wax phase boundary. Several reliable techniques were used for determining the WDT in this study. The experimental set-ups and procedures will be described. Experimental WDT data are measured for different synthetic and real reservoir fluids, which can be used for tuning and validation of the new wax model developed in this study.

2.2. WAT AND WDT

Wax phase boundary is traditionally determined by measuring wax appearance temperature or cloud point temperature, in which the first appearance of wax is detected during cooling. As described in Chapter-1, formation of wax may include two successive stages: wax nucleation and crystal growth. Wax nucleation is the most important wax formation stage, which needs substantial external energies for the creation of wax crystal seeds. The required energy is obtained through reducing temperature below the solid-liquid equilibrium (SLE) point. The difference between the system temperature (or WAT) and SLE temperature is referred as subcooling. During WAT measurement, cooling rate will have a great effect on the energy transfer process, subsequently on the seeding of wax. Generally, faster cooling rate may cause less time for energy transfer during the cooling process, therefore a lower temperature for wax appearance. Hence, the measured wax appearance temperature may not necessarily be the equilibrium point.

The measured wax appearance temperature is also dependent on experimental techniques used on quantifying the wax formation. Techniques such as visual observation (without or with microscopy), latent-heat-based Differential Scanning Calorimetry (DSC), viscosity measurement, and laser-based Solid Detection System (SDS) are commonly used in laboratories for measuring the WAT (Ronningsen et al., 1991; Hammami et al., 1997). The visual technique is sensitive for transparent sample and requires a minimum amount of wax for detection. It may give a higher WAT value, compared to the other techniques. For example, WATs measured using visual microscopy could be over 10 K higher than those determined using DSC and SDS (Ronningsen et al., 1991; Hammami et al., 1997).

In order to improve wax phase boundary determination using WAT data, some researchers modified the measured WAT by adding an estimated subcooling value (Monger-McClure et al., 1999). This method could make the measured wax phase boundary nearer to the SLE points, if a correct subcooling value was given. Monger-McClure et al. (1999) suggested an empirical correlation for estimating the subcooling to be added to the WAT, which in K was 1.1 times of the cooling rate in K/min (i.e. the subcooling in ^{o}F was 2 times of the cooling rate in ^{o}F/min). They claimed that this estimation was valid up to the cooling rate of around 2.8 K/min (i.e. 5 ^{o}F/min). However, experimental results in this laboratory show that the subcooling to be added is not only dependent on cooling rate, but also on fluid composition.

When using a similar cooling rate, very different values of subcooling required for wax appearance have been found for different mixtures. For example, with the cooling rate of 1 K per 30 minutes, the subcooling of approximately 18 K was required for a North Sea crude oil, while the subcooling needed for a North Sea gas condensate was approximately 6 K.

In order to establish a wax model based on thermodynamic equilibrium, the wax phase boundary should be determined by directly measuring real SLE points. Instead of WAT, the wax disappearance temperature (WDT) measured with equilibrium step-heating is a proper approach to the SLE point. The difference between measured WDT and WAT for a given system can be very significant, as shown later in Figure 2.8.

In this study, the WDT data will be used to tune and validate a new wax model. The required experimental data were generated in this laboratory or obtained from the literature. In order to generate accurate experimental data, a number of experimental techniques have been developed in this laboratory (Ji et al., submitted; Ji et al., in preparation).

2.3. TECHNIQUES USED FOR WDT MEASUREMENTS

Techniques used in this laboratory for detecting wax disappearance temperature are based on the visual observation and a unique method based on Quartz Crystal Microbalance (QCM). The visual observation of wax formation and dissolution can be used for transparent fluids. The QCM technique shows a high sensitivity for detecting wax formed and dissolved in real reservoir fluids, in which visual observation is impossible. The experimental set-ups and procedure are described below.

2.3.1. Experimental Equipments

Experimental equipments used in this laboratory for WDT measurements include a simple visual set-up for the tests at atmosphere pressure, a QCM apparatus operated at atmosphere pressure, and a combined visual and QCM apparatus with a maximum operating pressure of 50 MPa.

The visual set-up

The visual set-up consists of a test vial and a temperature-controlled bath, as schematically shown in Figure 2.1. The test vial is a 7 cc thin-walled glass tube with diameter of approximately 12 mm. The bath temperature can be maintained with kerosene in the range of 243 K and 333 K (i.e. –30 °C and 60 °C). A thermometer is submerged in the bath fluid to measure the fluid temperature, with an accuracy of 0.1 K.

The QCM apparatus (atmosphere pressure)

QCM (Quartz Crystal Microbalance) set-up is comprised of a thin disc of AT cut (i.e., a cut in particular orientation where the resonance frequency to first order does not depend on temperature) quartz sandwiched between two electrodes (see Figure 2.2). The principle is that, when solids adhere to or remove from the QCM surface, the resonant frequency of the QCM declines or increases. The QCM is very sensitive, requiring masses in the order of micrograms only to cause a significant change in resonant frequency.

The low-pressure QCM apparatus comprises of a QCM suspended in a small vessel (15 cc), as shown in Figure 2.3. A magnetic stirrer mixes the vessel contents, while a water jacket around the cell connected to a circulating heater/cooler allows temperature to be controlled. The resonant frequency of the QCM was measured using a Hewlett Packard 4194A Impedance/Gain Phase Analyser.

The combined visual and QCM apparatus (up to 50 MPa)

The combined visual and QCM apparatus is mainly consisted of a high pressure equilibrium cell, injection pump and a rocking device for stirring, as well as temperature and pressure control/recording equipment, as shown schematically in Figure 2.4.

The equilibrium cell (maximum effective volume of 100 cc) is comprised of a metal body housing a cylindrical sample chamber. The system pressure (up to 50 MPa) is controlled by injecting or withdrawing the test fluid using a pump. The cell is mounted on a pivot frame that allows a rocking motion around a horizontal axis, in order to ensure adequate mixing of the sample fluid. The cell is rocked through 90 degrees at a rate of up to 8 times per minute.

A QCM device is suspended in the test fluid inside the cell. The measurement with QCM can be combined with the visual observation through the sapphire windows of the equilibrium cell.

2.3.2. Experimental Procedures

During each test, the test fluid was first heated to a temperature high enough (313-323 K for synthetic fluids and 333-338K for reservoir fluids) to dissolve all the wax present. The bath temperature was then reduced to form wax, being detected by visual observation, or the QCM technique through a significant and sudden drop in resonant frequency. After significant amount of wax formed, the temperature was raised stepwise allowing at least 30 minutes at each temperature for equilibrium to be achieved. The WDT could be detected with visual observation, or QCM by the change of resonant frequency vs. temperature (as indicated later in Figure 2.8).

2.4. TESTED FLUIDS AND EXPERIMENTAL DATA

With the experimental equipments described above, WDTs can be measured for clear or dark fluids with and without light ends (such as compounds C_1 – C_4) at different pressure conditions. Two types of fluids have been tested in the laboratory, and they are synthetic fluids and real reservoir fluids. Experimental WDT data for synthetic binary systems will be presented in this chapter, while those for multi-component synthetic fluids and real reservoir fluids will be given in Appendix-A.

2.4.1. Fluid Samples

Synthetic mixtures

The test fluids comprised of synthetic fluids containing normal paraffins with known compositions. WDTs for transparent synthetic fluids were measured with the visual technique. Both synthetic binaries and multi-component synthetic systems were tested in this laboratory.

Binary systems were deliberately designed for parameter tuning in the development of a new wax model, as will be detailed in Chapters 3 and 4. The binaries designed for the model

tuning in this work include nC_6-nC_{16}, nC_6-nC_{17}, nC_{16}-nC_{18}, nC_{16}-nC_{20} and nC_{15}-nC_{19}. For the binary systems, WDTs were measured with different composition distributions, and the wax phase boundary was established by plotting the WDT as a function of the concentration of the heavier component in a binary.

Multi-component synthetic systems are needed for validation of the new wax model. Compositions for synthetic fluids were designed in such a way that the component concentration decreases with an increase in the carbon chain length, in order to represent a simplified crude oil system. For the multi-component systems, WDTs were measured at different pressures, and consequently the wax phase boundary was plotted (i.e., WDT versus pressure).

Real reservoir fluids

Experimental WDT data for real reservoir fluids were measured with the QCM technique, which will be used to validate the new wax model for predicting wax problems in field operations.

2.4.2. Experimental Results for Synthetic Binaries

Experimental WDT data for nC_6-nC_{16}, nC_6-nC_{17}, nC_{16}-nC_{18}, nC_{16}-nC_{20} and nC_{15}-nC_{19} binaries were generated in this work. The test sample was prepared with a procedure as described below, in order to minimise the evaporation of light end. Measurements of WDT were made with the simple visual set-up. The sample was weighed after the test, in order to evaluate the weight loss due to evaporation upon heating, which was found to be minimal. The WDT data measured in this work will be given and compared with the wax phase boundary data reported in the literature.

Sample preparation

The binaries were prepared with normal paraffins (i.e. n-alkanes, purity $\geq 99\%$), purchased from Aldrich Chemical Company, Inc., without further purification. In preparation of a test sample, first, a portion of the heavier compound for the binaries was weighed and put into a 7 cc vial, then the lighter compound was added. The test vial was then quickly sealed with a lid. The system composition was determined using weights measured with the accuracy of

approximately 1 mg for each component, equivalent to an error band (in absolute value) of 0.01 to 0.1 mole% in composition.

Measurements of WDT were conducted in the closed system in order to prevent the evaporation of any light end. The test mixture was weighed after the measurement of WDT, which showed an ignorable weight loss during the test, which might cause deviations less than 0.2 mole% in composition. Several repeated tests showed the WDT measured was reproducible within ±1 K.

Experimental WDT data

Experimental WDT data generated for nC_6-nC_{16} and nC_6-nC_{17} binaries in this work are given in Table 2.1.

Table 2.2 lists experimental WDT data measured for nC_{16}-nC_{18}, nC_{16}-nC_{20} and nC_{15}-nC_{19} binaries in this work.

Comparison with literature data

The wax phase boundaries for nC_6-nC_{16} and nC_6-nC_{17} systems were measured and reported in the literature (Hoerr et al., 1951). However, the experimental procedure was not clearly specified by the authors. So it was not possible to indicate whether the data were based on WAT or WDT.

The nC_6-nC_{16} and nC_6-nC_{17} wax phase boundaries were plotted, comparing the WDT data generated in this work with the data reported in the literature. As shown in Figures 2.5 and 2.6, the WDT values determined in this work are approximately 2 – 5 K higher than those reported in the literature. One explanation for the difference might be that the literature data were generated via measuring WATs.

A set of wax phase boundary data for nC_{16}-nC_{18} can also be found in the literature, which was based on melting temperatures (WDT) measured with a dilatometer (Parczewska, 2000). The author observed two forms of solid in the binary, which were referred as the high-temperature solid and the low temperature solid. The nC_{16}-nC_{18} wax phase boundary based on the literature data is shown in Figure 2.7, where the circle (o) and cross (+) denote the high-temperature solid and the low temperature solid, respectively. The nC_{16}-nC_{18} wax

phase boundary based on the WDT from this work was also plotted in the figure. As shown in Figure 2.8, a good agreement is observed for the wax phase boundaries between this work and the literature. The WDT data from this work are of approximately 1 - 2 K higher than the wax melting temperatures marked for the low temperature solids (the cross points) from the literature. The visual technique used in this work does not differentiate different solid forms.

2.4.3. Experimental Data for Multi-component Mixtures and Real Reservoir Fluids

WDTs for multi-component mixtures and real reservoir fluids were measured by R.W. Burgass in Centre for Gas Hydrate Research (JIP Reports 1999-2004), and composition data for real reservoir fluids were provided by Reservoir Fluid Studies Group, Institute of Petroleum Engineering, Heriot-Watt University. The experimental data are given in details in Appendix-A. These data are used in Chapters 6 and 7 for validating the wax model developed in this work. In the following sections, a brief description is given to the fluid systems tested and the experimental techniques used in the measurements.

Multi-component mixtures

In order to investigate the effect of light end (such as C_1 –C_4) on wax phase boundary, experimental WDT data were generated for several mixtures with and without light ends. The systems studied include 10 synthetic multi-component systems with C_n up to 40, as given in Appendix-A.

Table A.1 lists the composition for four multi-component mixtures (A, B, C and D) measured in this laboratory, and these mixtures contain the heaviest component as C_{30} – C_{40}. WDTs for these mixtures were measured by the visual observation using the combined visual and QCM apparatus. Experimental WDT data at different pressures are given in Table A.2.

Mixtures B, C were added light compounds of C_1 – C_4, and the mixture D was added a natural gas. Table A.3 shows the composition for the mixtures with light ends, and Table A.4 lists the experimental WDT data measured at different pressures.

The mixture E without light end was prepared using normal paraffins of C_{10} and C_{21}-C_{26} in this laboratory. The concentration for components C_{21}-C_{26} decreases following an exponential decay function of mole fraction against molecular weight (or carbon number). The mole fractions for consecutive components can be equivalently correlated as $x_i = q \times x_{i-1}$

with q of 0.70. Then a natural gas was added with different proportions, two live fluids were obtained, which contain 45 mole% light end and 69 mole% light end. The compositions for the three mixtures of E without and with light ends are shown in Table A.5. Bubble point pressures were measured for the two fluids with natural gas. which are also given in Table A.5.

For the fluid E without light end, the WAT at 0.1 MPa was measured as 275.9 K (2.7 °C) using the QCM technique, while the WDT at 0.1 MPa was measured as 276.2 K (3 °C). Due to the small subcooling of this mixture, experimental WAT data were measured, as given in Table A.6. For the similar reason, WATs were measured for the fluid with 45 mole% light end, as also given in Table A.6. When using the measured WAT data for validating the wax model, a subcooling of approximately 1 K will be taken into account. Experimental WAT and WDT data (Table A.6) were generated for the fluid E with 69 mole% light end, which show a subcooling of approximately 2 K.

Real reservoir fluids

Burgass measured WDTs for three reservoir fluids including a North Sea crude oil, a condensate and a black oil. The WDT for a real reservoir fluid from North Sea was measured using the QCM technique. Table A.7 lists the fluid composition obtained from laboratory analysis of Reservoir Fluid Studies Group in Institute of Petroleum Engineering at Heriot-Watt University. The detection of the WAT and WDT using the QCM method is reproduced in Figure 2.8, a significant change in resonant frequency at points near WAT can be observed. WDT was identified as the point at which the resonant frequency during heating went back to the curve during cooling. With the method of QCM, the WDT was measured as 327 K, which was 18 K higher than the WAT (309 K).

Table A.8 gives the composition and physical properties of a condensate (Base Condensate LTB98-1). For the stabilised fluid, the WDT measured using the QCM was 309 K at 0.1 MPa, while a similar value of WDT (309 K) was observed by visual. Table A.9 shows the composition and physical properties of a black oil (Black Oil RFS-1). and the WDT measured using the QCM technique was 323 K at 0.1 MPa.

2.5. SUMMARY

Reliable experimental SLE data are important for developing an accurate wax model. The wax disappearance temperatures measured with proper techniques. instead of the traditionally used WAT data, represent the solid-liquid equilibrium.

Reliable experimental techniques have been developed and used in this laboratory, which combine sensitive wax detecting methods with deliberately designed step-cooling and step-heating procedure to achieve equilibrium. A visual observation was used for measuring WDTs in transparent fluids, and a QCM technique was used for real reservoir fluids, both showing good accuracy and repeatability.

Wax phase boundaries have been measured for several binaries, which can be used for developing the new wax model. WDTs were also measured at different pressures for several multi-component mixtures with and without light ends and for three real reservoir fluids. These data will be used for validating the new wax model.

2.6. TABLES

Table 2.1. Experimental WDT data (this work) for nC_6-nC_{16} and nC_6-nC_{17} binaries.

Composition/mole% (±0.3 mole%)		WDT/K (±1 K)
	nC_6-nC_{16}	
nC_6	nC_{16}	
100.0	0.0	178
98.6	1.4	247
95.9	4.1	256
93.1	6.9	262
90.4	9.6	265
75.3	24.7	275
0.0	100.0	291
	nC_6-nC_{17}	
nC_6	nC_{17}	
100.0	0.0	178
98.9	1.1	248
96.9	3.1	257
94.4	5.6	262
91.7	8.3	265
79.3	20.7	274
0.0	100.0	295

Table 2.2. Experimental WDT data (this work) for nC_{16}-nC_{18}, nC_{16}-nC_{20} and nC_{15}-nC_{19} binaries.

Composition/mole% (±0.3 mole%)		WDT/K (±1 K)
	nC_{16}-nC_{18}	
nC_{16}	nC_{18}	
100.0	0.0	291
92.7	7.3	291
83.3	16.7	291
73.0	27.0	292
59.9	40.1	293
56.3	43.7	294
46.3	53.7	295
28.6	71.4	298
24.2	75.8	299
22.2	77.8	299
22.2	77.8	299
17.6	82.4	299
0.0	100.0	301
	nC_{16}-nC_{20}	
nC_{16}	nC_{20}	
100.0	0.0	291
95.9	4.1	291
84.6	15.4	290
70.3	29.7	297
60.8	39.2	301
57.3	42.7	302
41.2	58.8	305
37.0	63.0	306
0.0	100.0	310
	nC_{15}-nC_{19}	
nC_{15}	nC_{19}	
100.0	0.0	283
94.2	5.8	283
88.1	11.9	283
79.9	20.1	286
69.3	30.7	290
51.7	48.3	296
0.0	100.0	305

2.7. FIGURES

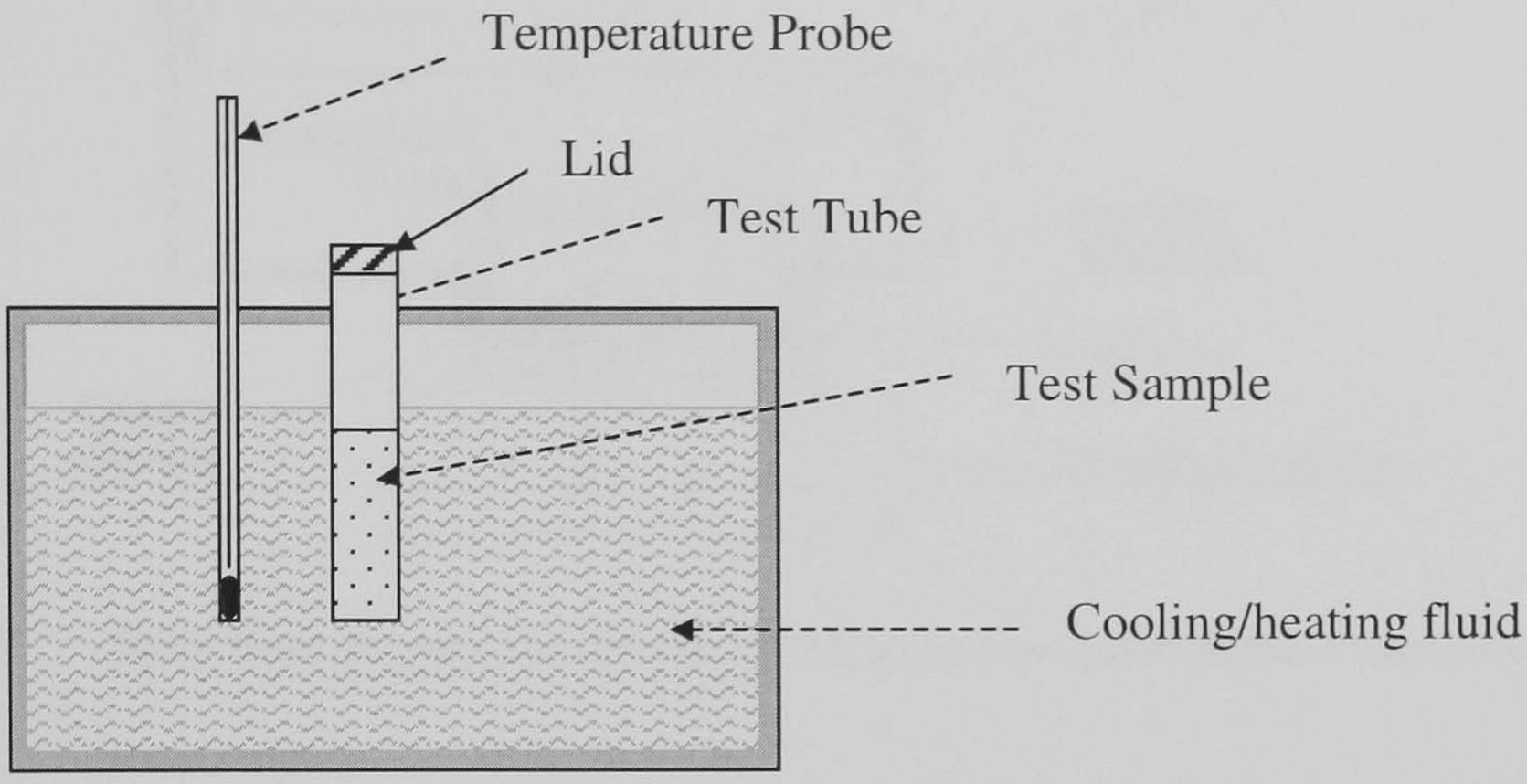

Figure 2.1. Schematic illustration of the simple visual set-up.

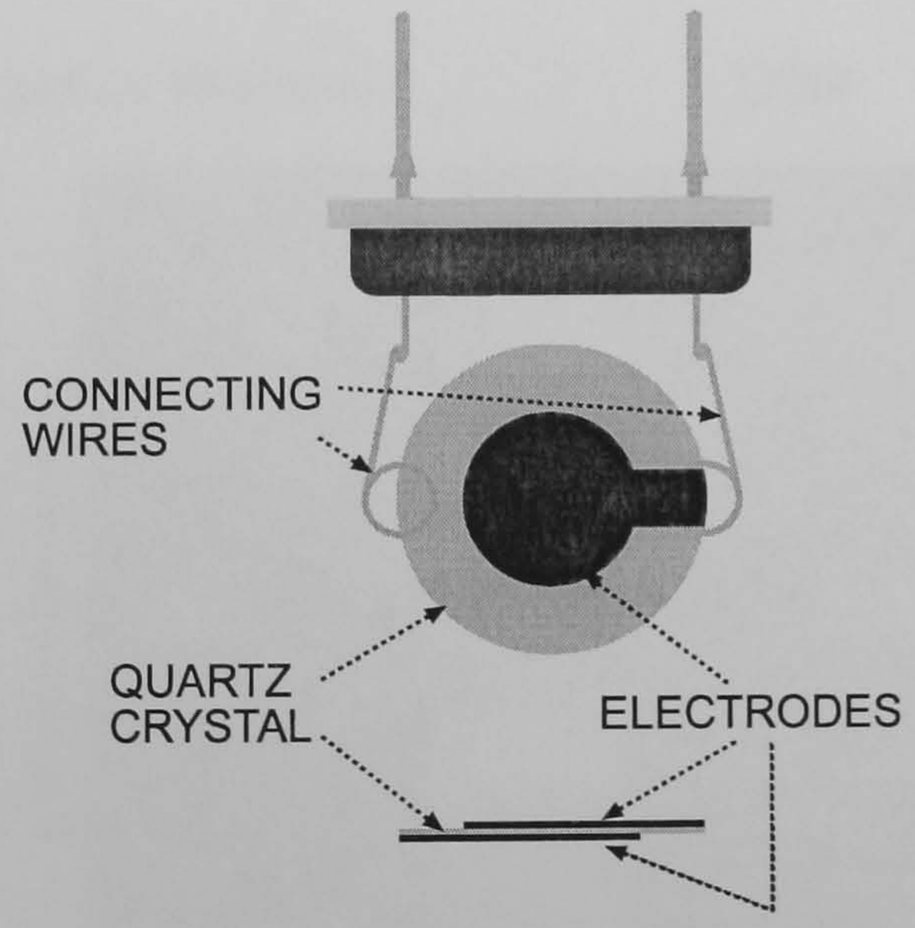

Figure 2.2. Schematic illustration of the QCM.

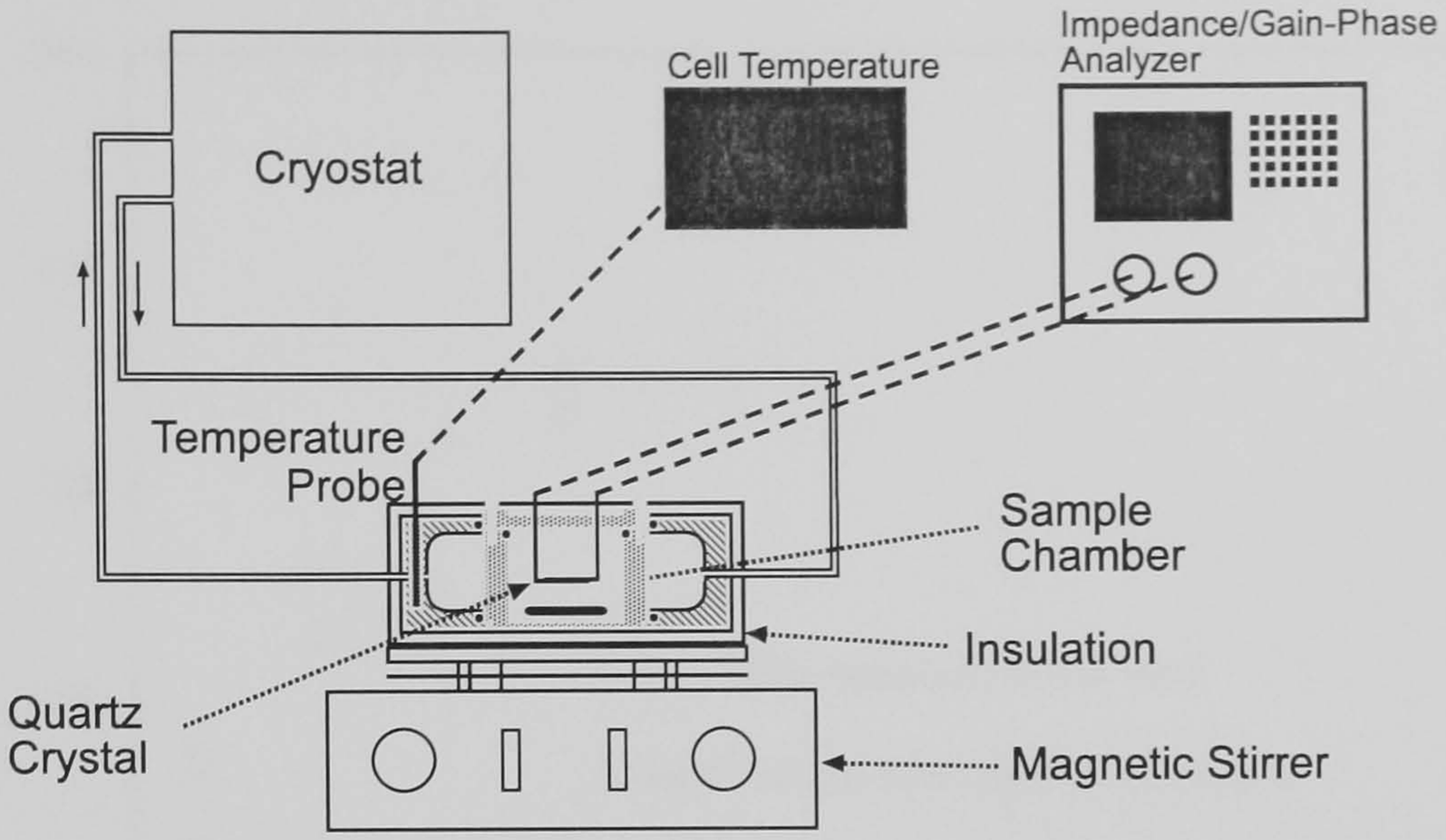

Figure 2.3. Schematic illustration of the QCM apparatus (atmosphere pressure).

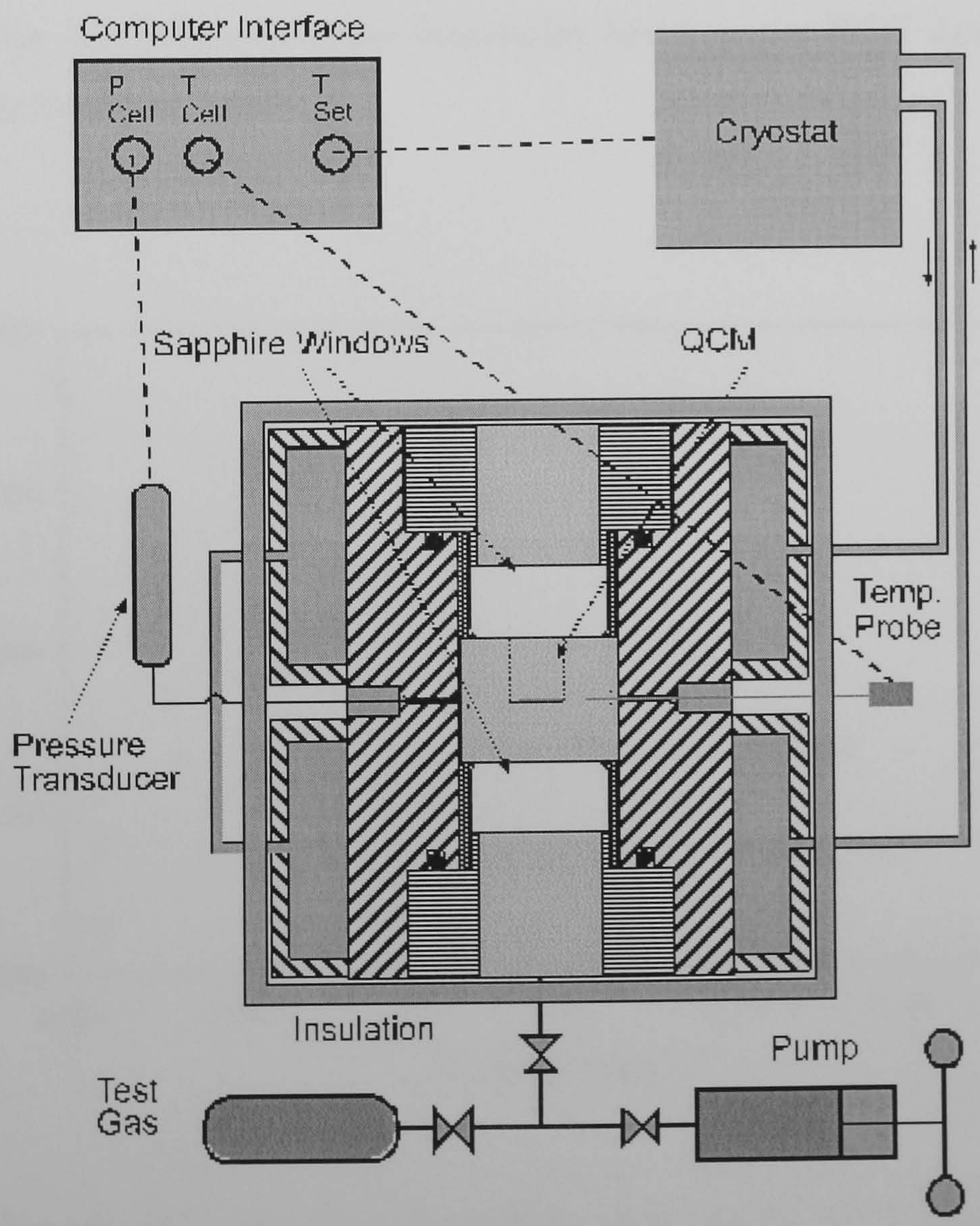

Figure 2.4. Schematic of the combined visual and QCM apparatus.

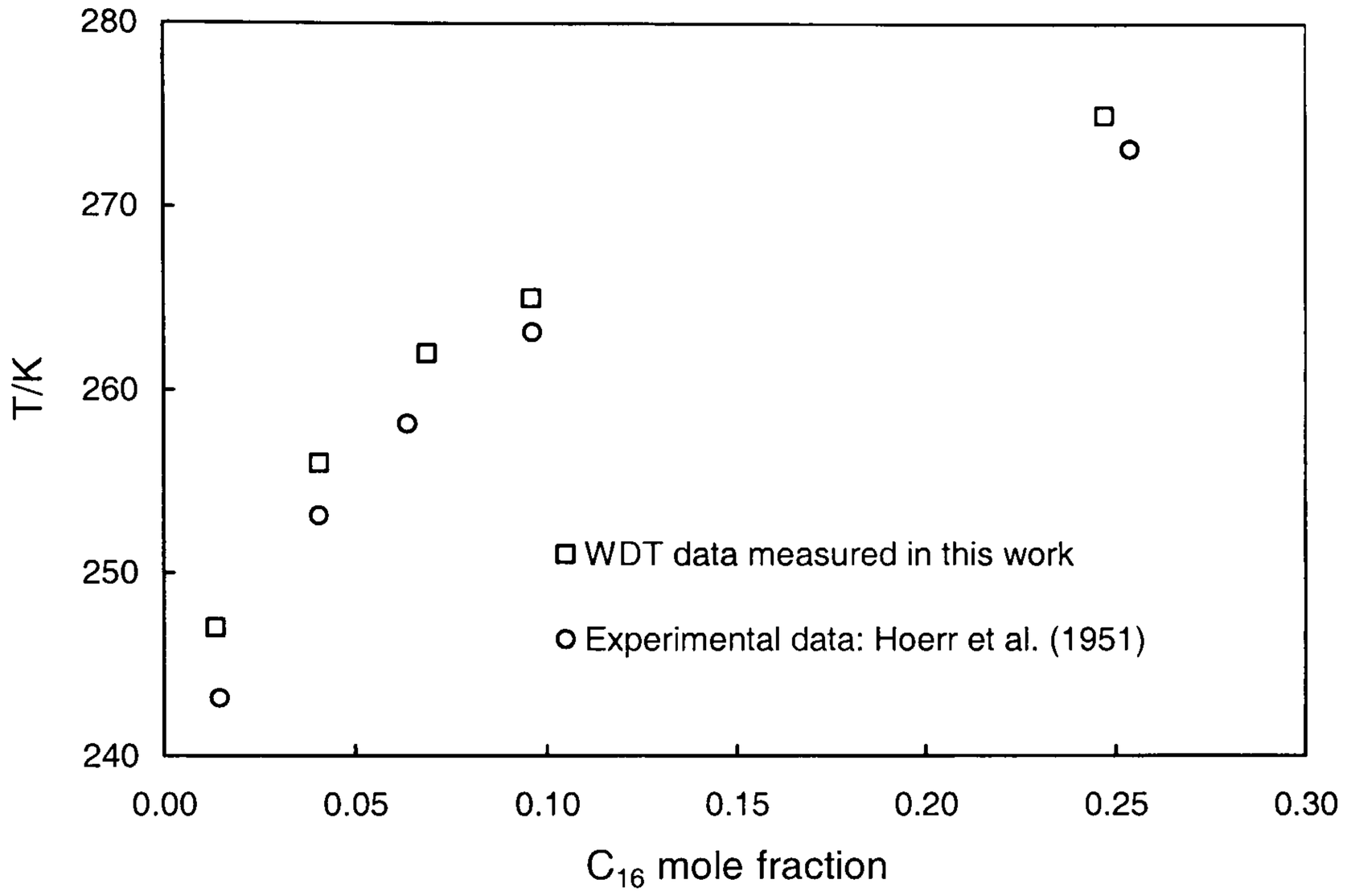

Figure 2.5. The nC_6-nC_{16} wax phase boundaries based on the WDT data determined in this work and the literature data.

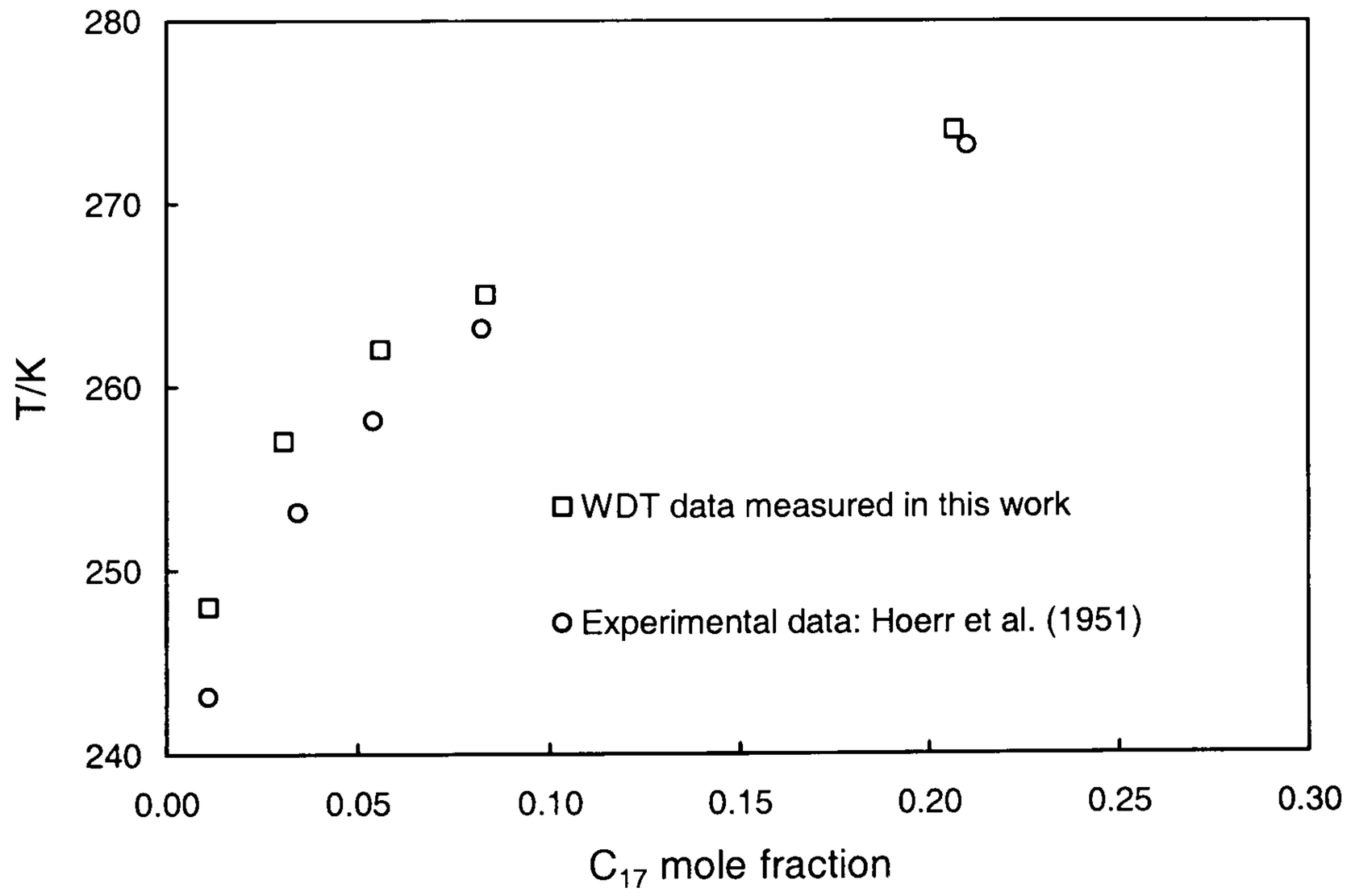

Figure 2.6. The nC_6-nC_{17} wax phase boundaries based on the WDT data from this work and the literature data.

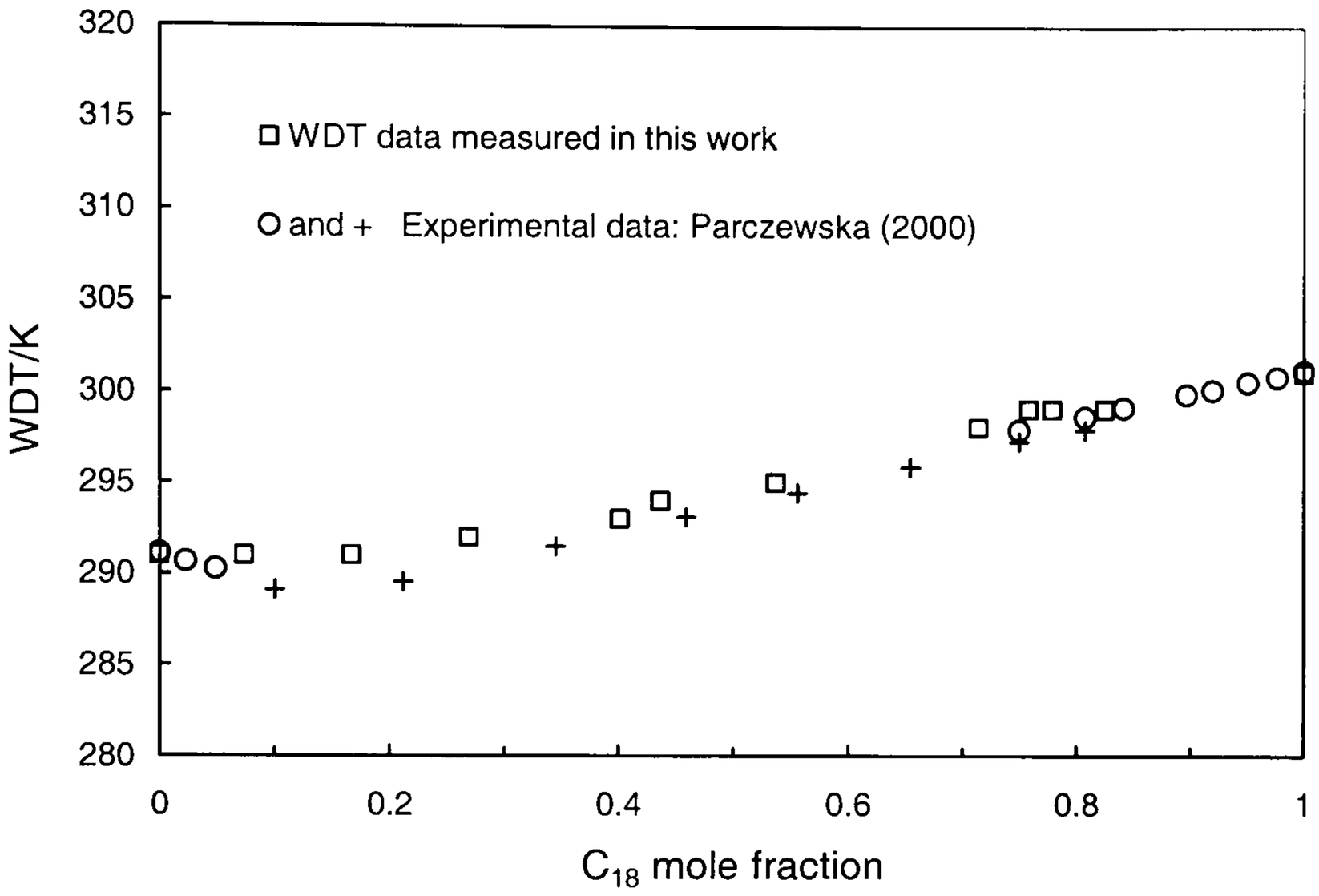

Figure 2.7. The nC_{16}-nC_{18} wax phase boundaries based on the WDT data from this work and the literature data.

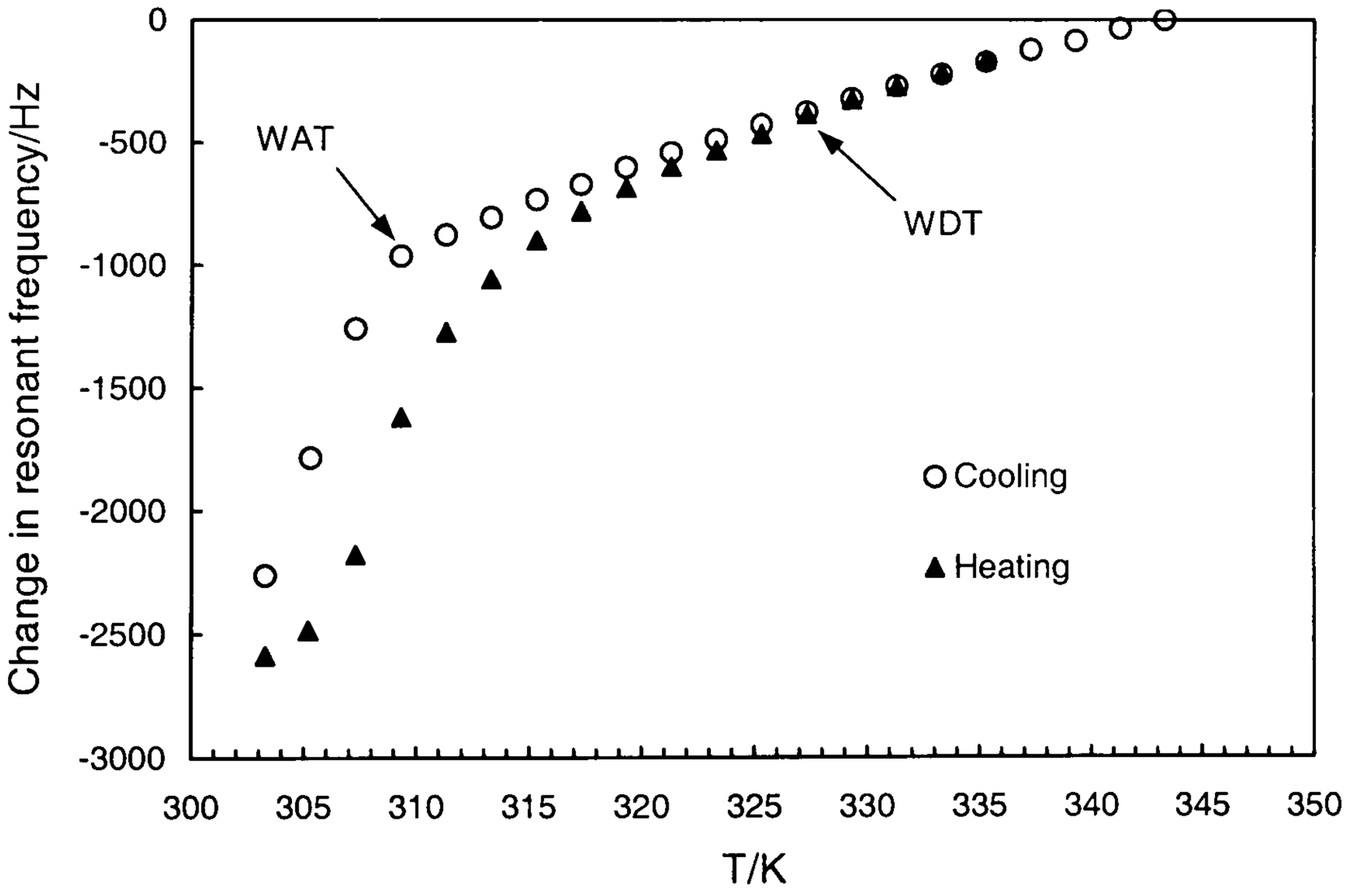

Figure 2.8. WAT and WDT measured using QCM on a North Sea crude oil (measured by Burgass R.W.).

CHAPTER-3

THERMODYNAMIC DESCIPTION OF PHASES AND PHASE EQUILIBRIUM

3.1. INTRODUCTION

A petroleum reservoir fluid contains a variety of components, which may form different phases. Light constituents such as methane, ethane and propane are predominantly in the vapour and liquid hydrocarbon phases, while they can also dissolve in water. Intermediate hydrocarbons with carbon number between 6 and 20 are liquid at normal operating conditions. Heavy hydrocarbons are usually in the liquid phase, but they can precipitate to form a solid phase of wax at low temperatures. Water generally coexists with hydrocarbons, and it can be in both vapour and liquid phases, and also solid phases when forming ice or gas hydrates at low temperature and high pressure conditions. This work does not consider asphaltene phase, which is predominantly composed of poly-nuclear aromatics.

For thermodynamic modelling of wax and hydrate in complex real reservoir fluids, the following phases need to be considered:

- Vapour phase (V), containing hydrocarbon gases and water in the vapour form.
- Aqueous phase (L_1), i.e. the liquid phase consisting mainly of water and water-dissolved components.
- Liquid hydrocarbon phase (L_2).
- Wax phase (S), a mixture of solids formed by heavy paraffinic hydrocarbons.
- Hydrate phase (H), a solid mixture formed by water and light hydrocarbons and other hydrate formers such as H_2S and N_2.
- Ice (I), the solid phase of water.

In this chapter, the fundamental thermodynamics for modelling multi-phase equilibrium will be presented. Thermodynamic equations used for calculating chemical potential and fugacity in different phases will be given. Modelling of wax and hydrate is based on their crystalline structures, which will also be summarised.

3.2. WAX AND HYDRATE STRUCTURES

3.2.1 Wax

Wax precipitation is the crystallisation of heavy hydrocarbon molecules from the liquid phase. The crystal structures of wax have been studied and well documented in the literature. The wax crystallography study is commonly carried out using n-paraffins, due to their vital role in wax formation (will be described in details in Chapter-5).

Pure n-paraffin solids generally can show four types of crystal structures, namely hexagonal, triclinic, orthorhombic and monoclinic (Broadhurst, 1962). Molecules with a hexagonal structure can rotate around their long chain axes, whilst the rotation is restricted for molecules having other structures. The crystal structure of a compound depends not only on its carbon number (C_n) but also on the odd or even nature of C_n.

Temperature is also important for determining the crystal structure for a given compound. For example, nC_{29} solid shows orthorhombic structure at temperatures lower than 331.4 K, but hexagonal structure at temperatures between 331.4 K and the melting temperature 336.6 K. When increasing temperature, there is a conversion of crystal structures, which is referred as solid-solid transition.

The solid-solid transition can affect the thermodynamic description of a melting process, since an extra energy is required for converting the solid from a low-temperature crystal structure to a high-temperature one. The latent heat of solid-solid transition is comparable to that of melting. For instance, 7.54 kcal heat is needed for converting 1 mole nC_{29} solid from the orthorhombic structure to the hexagonal structure, and further 15.80 kcal heat is required for melting the hexagonal solid.

In the liquid phase, hydrocarbons with different carbon numbers can mix with each other to form a homogeneous solution, but in the solid phase the tendency of mixing for different hydrocarbons is strongly dependent on their carbon number differences. In a solid system comprising of only one component (i.e. pure compound system). the component molecules have the same carbon chain length, so they can mix with each other in an orderly arrangement of carbon chains without bending. This case is referred as the ideal packing mode of molecules, as schematically illustrated in Figure 3.1a, using the line to stand for the carbon chain of a molecule (Craig et al., 1998).

However, for a solid system containing several components, the differences of carbon chain lengths between components will affect their molecule packing. Disorders of arranging carbon chains will be introduced; consequently the molecules will be packed in non-ideal modes. The manner of non-ideal packing depends mainly on the carbon number (C_n) difference. The molecules of components with small C_n differences may pack mainly by the carbon chain mixing (i.e. the long chain connects with the short chain), as schematically shown in Figure 3.1b. The molecules of compounds with high C_n differences may pack predominantly by twisting/folding long carbon chains, as schematically shown in Figure 3.1c. Apparently, for a system containing compounds with both small and high C_n differences, the molecules may pack by combination of the carbon chain mixing and bending, as schematically shown in Figure 3.1d.

The molecule packing disorder can have a significant effect on the nature of solid mixtures (Craig et al., 1998). Compounds with small C_n differences form a "solid solution", a thermodynamic term used to describe a homogeneous and stable mixture of one solid substance in another. The co-solubility of compounds in the solid state decreases as the C_n difference increases. When the C_n difference is significantly high, different compounds are completely "insoluble" in each other, consequently form multi-pure-solids, i.e. each compound forms a solid phase.

For instance, solid solutions were observed in the binary systems such as nC_{23}-nC_{24}, nC_{23}-nC_{25} and nC_{26}-nC_{28} (AchourBoudjema et al., 1996; Dirand et al., 1996; Jouti et al., 1996; Provost et al. 1999). On the other side, multi-pure-solids were observed in the binaries or ternaries such as nC_{30}-nC_{40}, nC_{16}-nC_{28}, nC_{16}-nC_{41}, nC_{28}-nC_{41} and nC_{16}-nC_{28}- nC_{41} (Dorset, 1997; Paunovic et al., 2000).

Real reservoir fluids consist of hydrocarbons with continuously distributed carbon numbers. The crystallography of wax has been studied using synthetic multi-component mixtures containing continuous C_n and reservoir fluids (Dirand et al., 1998; Chevallier et al., 2000). It was found that solid solutions formed in these systems. Furthermore, solid-solid transitions were observed during the wax melting process upon increasing temperature (Chevallier et al., 1999).

Therefore, in this study, the non-ideal solid solution theory will be used to describe the solid phase of wax. The solid-solid transition will be taken into account when using a thermodynamic equation to represent the wax melting process.

3.2.2. Hydrate

Gas hydrate has different structures, depending on the chemical nature and geometry of guest molecules. The two most common hydrate structures are known as structure I (sI) and structure II (sII). The unit cell of structure I hydrate is a 12 Å cube consisting of 46 water molecules that form two types of cavity: 2 small cavities and 6 large cavities. The small cavity is 12-sided (dodecahedron) with 12 pentagonal faces (5^{12}), whereas the large cavity is 14-sided (tetrakaidecahedron) with 12 pentagonal and 2 hexagonal faces ($5^{12}6^2$). The 5^{12} cavity is almost spherical with a radius of 3.95 Å., while the $5^{12}6^2$ cavity resembles an oblate ellipsoid with a radius of 4.33 Å. Of the natural gas components which form simple hydrates, methane, ethane, carbon dioxide and hydrogen sulphide are known to form structure I. Methane and hydrogen sulphide can stabilise the 5^{12} cavities and can occupy the large $5^{12}6^2$ cavities. Ethane and carbon dioxide occupy the $5^{12}6^2$ cavities.

The unit cell of structure II hydrate is a 17.3 Å cube consisting of 136 water molecules. The sII unit cell also contains two types of cavity: 16 small cavities and 8 large cavities (von Stackelberg and Muller, 1954). The small cavity is pentagonal dodecahedra (5^{12}), while the large cavity is 16-sided (hexakaidecahedron) including 12 pentagonal and 4 hexagonal faces ($5^{12}6^4$). The small cavity is a distorted shape having a radius of 3.91 Å. while the large cavity is very spherical with a radius of 4.73 Å. Propane and iso-butane form structure II hydrates. and they only fit into the large cavity ($5^{12}6^4$). Normal butane does not form a simple hydrate, but sII hydrate can be formed from n-butane with methane or hydrogen sulphide as a help gas in the small cages. Natural gas mixtures containing propane, iso-butane, and n-butane usually form structure II hydrate.

Ripmeester et al. reported a new hexagonal hydrate structure (sH) in 1987. The unit cell of sH hydrate contains 34 water molecules that form a hexagonal lattice in which each side of the hexagonal face 'a' is 12.26 Å and the height 'c' is 10.17 Å. The sH unit cell contains three types of cavity: 3 small cavities (5^{12}), 2 medium cavities, and 1 large cavity. The medium cavity is irregular 12-sided (dodecahedron) having 3 square faces, 6 pentagonal faces and 3 hexagonal faces ($4^3 5^6 6^3$). The large cavity has 12 pentagonal faces as well as 6 hexagonal faces encircled with 2 hexagonal faces at the top and bottom of cavity ($5^{12} 6^8$). Due to the absence of single-crystal diffraction data, the radius of the small cavity was assumed to be 3.91 Å, and the radius of the medium and large cavities were estimated to be 4.06 and 5.71 Å, respectively (Mehta and Sloan, 1994). Simple sH hydrates do not form. The sH hydrate can be formed from alkanes and cycloalkanes such as 2-methybutane, 2,2-dimethylbutane, methylcyclopentane and cycloheptane with a help gas (e.g. methane, hydrogen sulphide, nitrogen and carbon dioxide).

Figure 3.2 shows different cavities presented in structure I, II and H hydrates.

Table 3.1 summarises the geometric and physical properties for structure I. II and H hydrates and their cavities.

In the statistical thermodynamic model, the hydrate phase is modelled using the ideal solid solution theory of van der Waals and Platteeuw (1959), as developed by Parrish and Prausnitz (1972). The hydrate equilibrium point can be determined by the fact that at equilibrium the chemical potentials of water between the hydrate phase and other coexisting phases are equal.

3.3. MULTI-PHASE EQUILIBRIUM

For a closed system consisting of n components and π phases at an equilibrium condition, the chemical potential of each component in all phases must be uniform:

$$\mu_i^1 = \cdots = \mu_i^k = \cdots = \mu_i^\pi \qquad (i = 1, \ldots, n) \qquad (3.1)$$

where μ_i^k is the chemical potential of component i in the phase k.

For an isothermal system, the chemical potential of component *i* in any phase, of vapour, liquid or solid, can be related to the fugacity as follows:

$$\mu_i - \mu_{i,O} = RT \ln \frac{f_i}{f_{i,O}} \tag{3.2}$$

where μ_i and f_i are the chemical potential and fugacity, respectively, of species *i* at a given temperature (T) and pressure (P). $\mu_{i,O}$ and $f_{i,O}$ are the chemical potential and fugacity, respectively, of species *i* at an arbitrary reference state of pressure and composition. R is the universal gas constant.

$\mu_{i,O}$ and $f_{i,O}$ are dependent, and when one is chosen the other will be fixed. The equilibrium criteria in terms of chemical potential can, hence, be replaced by the following equivalent equation in terms of fugacity,

$$f_i^1 = \cdots = f_i^k = \cdots = f_i^\pi \qquad (i = 1, \ldots, n) \tag{3.3}$$

where the subscripts and superscripts designate components and their phases, respectively.

When applying Equation 3.3 to n components, $n(\pi\text{-}1)$ equations of fugacity equality are obtained for a general case where all of the system species are presented in each phase.

Mass balance for the closed system requires the following $n+\pi$ equations to be fulfilled,

$$z_i = \sum_{k=1}^{\pi} F^k x_i^k \qquad (i = 1, \ldots, n) \tag{3.4}$$

and

$$\sum_{i=1}^{n} x_i^k = 1 \qquad (k = 1, \ldots, \pi) \tag{3.5}$$

where z_i is the feed composition (in mole fraction) of component *i*, x_i^k is the mole fraction of component *i* in the phase *k*, and F^k is the mole fraction of phase *k* in the system.

The $(n+1)\pi$ equations in total, as given in Equations 3.3 - 3.5, are used to solve the phase equilibrium problem that has an equal number of unknown variables. The unknown

variables can be [x_i^k , F^k] ($i = 1, \ldots, n$ and $k = 1, \ldots, \pi$) at specified (known) temperature T and pressure P, and this is a typical isothermal flash problem. If the unknown variables are [x_i^k , F^k] ($k \neq r$) and either P or T at the condition $F^r = 0$, this will be a general phase boundary problem. In order to solve these problems, proper thermodynamic equations are required for calculating the fugacity in different phases.

Figure 3.3 shows the flowchart to calculate wax phase boundary in a multi-phase system.

3.4. VAPOUR AND LIQUID PHASES

The fugacities of component i in the vapour (V), liquid hydrocarbon (L_2) and aqueous (L_1) phases can be calculated using a cubic equation of state (EoS):

$$f_i = x_i \varphi_i P \tag{3.6}$$

where f_i, x_i and φ_i are the fugacity, mole fraction and fugacity coefficient of component i. P is the system pressure.

In the modelling of hydrate phase equilibrium in previous studies (Avlonitis, 1992; Tohidi, 1995; Østergaard, 2000), the Valderrama modification of Patel and Teja (VPT) EoS (Valderrama, 1990) was adopted to determine the fluid fugacity. However, in the petroleum industry, the Soave-Redlich-Kwong (Soave, 1972) and the Peng-Robinson (Peng and Robinson, 1976) EoS have been widely used for calculating vapour-liquid equilibrium of hydrocarbons. Therefore, in this study, the SRK and PR EoS will be used to calculate the fluid fugacity in the modelling of wax phase equilibrium.

The SRK and PR EoS can be described using the following general form:

$$P = \frac{RT}{v-b} - \frac{a}{(v+\delta_1 b)(v+\delta_2 b)} \tag{3.7}$$

where P, v, T and R are the pressure, molar volume, temperature and universal gas constant. δ_1 and δ_2 are constants equal to 1 and 0 in the SRK EoS, and $1+\sqrt{2}$ and $1-\sqrt{2}$ in the PR EoS, respectively.

a and b in Equation 3.7 are terms related to the molecular attraction and repulsion. They are given by:

$$a = \Omega_{ac} \frac{R^2 T_c^2}{P_c} \alpha \tag{3.8}$$

$$b = \Omega_b \frac{RT_c}{P_c} \tag{3.9}$$

where T_c and P_c are the critical temperature and the critical pressure. Ω_{ac} and Ω_b are constants, which are 0.42747 and 0.08664 in the SRK EoS, and 0.45724 and 0.07780 in the PR EoS.

α (in Equation 3.8) expresses the temperature dependency of the attraction term; being a function of the reduced temperature and acentric factor. The α function was suggested by Soave (1972), and later selected by Peng and Robinson (1976), is of the form:

$$\alpha = \left[1 + m\left(1 - T_r^{0.5}\right)\right]^2 \tag{3.10}$$

where T_r is the reduced temperature, which equals T/T_c and m is a constant for each compound.

The detailed description of SRK and PR EoS will be given in Appendix-B. When using the EoS to mixtures, binary interaction parameters are usually needed. Binary interaction parameters for light constituents (such as C_1, C_2, C_3, C_4, C_5, CO_2, N_2) and intermediate compounds (i.e. $C_6 - C_{20}$) can be found from literature (e.g. Danesh, 1998), and they are also given in Appendix-B.

3.5. SOLID PHASE - WAX

The fugacity (f_i^S) of component i in the solid phase of wax, at P and T, is related to pure solid fugacity (f_i^{OS}) at a reference pressure (P_O), based on the solid solution theory, as expressed in Equation 3.11.

$$f_i^S = s_i \gamma_i^S f^{OS} \exp\left(\int_{P_o}^{P} \frac{\bar{v}_i^S}{RT} dP \right) \tag{3.11}$$

where s_i and γ_i^S are the mole fraction and activity coefficient of component i in the solid phase.

f_i^{OS} is calculated from pure liquid fugacity at the same temperature. As some n-paraffins exhibit solid-solid transitions before melting, the fugacity ratio of subcooled liquid versus solid can be calculated using Equation 3.12:

$$ln\frac{f_i^{OL}}{f_i^{OS}} = \frac{\Delta h_{tr,i}}{RT}\left(1-\frac{T}{T_{tr,i}}\right)+\frac{\Delta h_{f,i}}{RT}\left(1-\frac{T}{T_{f,i}}\right)+\frac{1}{RT}\int_{T_{f,i}}^{T}\Delta C_{p,i}^{LS}dT-\frac{1}{R}\int_{T_{f,i}}^{T}\frac{\Delta C_{p,i}^{LS}}{T}dT \tag{3.12}$$

where $T_{tr,i}$ and $T_{f,i}$ are the solid-solid transition and fusion temperatures of component i, respectively. $\Delta h_{tr,i}$ and $\Delta h_{f,i}$ are the latent heats of the solid-solid and solid-liquid transitions. $\Delta C_{p,i}^{LS}$ is the heat capacity difference between liquid and solid (the heat capacity differences between the two solid forms are ignored).

$$\Delta C_{p,i}^{LS} = C_{p,i}^{L} - C_{p,i}^{S} \tag{3.13}$$

The pure liquid fugacity of compound i (f_i^{OL} in Equation 3.12) can be calculated using a cubic equation of state.

3.6. SOLID PHASE - HYDRATE

Hydrate phase equilibrium was modelled using a statistical thermodynamic theory proposed by van der Waals and Platteeuw (1959). In this theory, the hydrate phase was described using an ideal solution. Hydrate forming molecules were viewed as adsorbed in the cavity sites, which was described with the Langmuir adsorption theory. The fundamental assumptions are:

1. The contribution from host molecules to the free energy is independent of the occupation of the cavity. This assumption also implies that encaged molecules do not distort the cavity.

2. Each cavity can contain at most one guest molecule, which cannot diffuse from the cavity.

3. There are no interactions of the solute molecules, i.e., the energy of each encaged guest molecule is independent of the number and types of other solute molecules.

4. No quantum effects are needed; classical statistics are valid.

The fugacity of water in the hydrate phase, f_w^H, is calculated by (Anderson and Prausnitz, 1986):

$$f_w^H = f_w^\beta \, exp\left(-\frac{\Delta\mu_w^{\beta-H}}{RT}\right) \tag{3.14}$$

where f_w^β is the fugacity of water in the empty hydrate lattice. $\Delta\mu_w^{\beta-H}$ is the difference of chemical potential for water between the empty hydrate lattice ($\Delta\mu_w^\beta$) and the hydrate phase ($\Delta\mu_w^H$).

3.6.1. Calculation of f_w^β

The fugacity of water in the empty hydrate lattice, f_w^β in Equation 3.14, is given by:

$$f_w^\beta = f_w^{L_1/I} \, exp\left(\frac{\Delta\mu_w^{\beta-L_1/I}}{RT}\right) \tag{3.15}$$

where $f_w^{L_1/I}$ is the fugacity of pure water or ice. $\Delta\mu_w^{\beta-L_1/I}$ represents the difference of chemical potential for water between the empty hydrate lattice and pure water/ice.

The term inside the brackets of Equation 3.15, i.e. $\frac{\Delta\mu_w^{\beta-L_1/I}}{RT}$, is calculated with:

$$\frac{\Delta\mu_w^{\beta-H/L_1}}{RT} = \frac{\Delta\mu_w^{O}}{RT_0} - \int_{T_0}^{T} \frac{\Delta h_w^{\beta-L_1/I}}{RT^2} dT + \int_0^P \frac{\Delta v_w^{\beta-L_1/I}}{RT} dP \tag{3.16}$$

where $\Delta\mu_w^O$ is the reference chemical potential difference between water in the empty hydrate lattice and pure water in the ice phase at 273.15 K. $\Delta h_w^{\beta-L_1/I}$ and $\Delta v_w^{\beta-L_1/I}$ are the molar enthalpy difference and the molar volume difference, respectively, between an empty hydrate lattice and water/ice. The $\Delta\mu_w^O$ and $\Delta v_w^{\beta-L_1/I}$ values for hydrates of different structure were given by Parrish and Prausnitz (1972). Dharmawardhana et al. (1980) and Mehta and Sloan (1994).

$\Delta h_w^{\beta-L_1/I}$ in Equation 3.16 is given by:

$$\Delta h_w^{\beta-L_1/I} = \Delta h_w^O + \int_{T_o}^{T} \Delta C_{p,w} dT \tag{3.17}$$

where Δh_w^O is the enthalpy difference between the empty hydrate lattice and ice at the ice point and zero pressure. $\Delta C_{p,w}$ is the heat capacity difference between the empty hydrate lattice and the pure liquid water. Values of Δh_w^O can be found from the literature, while $\Delta C_{p,w}$ can be calculated using an empirical correlation (Dharmawardhana et al., 1980; Holder et al. 1980; Mehta and Sloan, 1994)

3.6.2. Calculation of $\Delta\mu_w^{\beta-H}$

The chemical potential difference between water in the empty hydrate lattice and the hydrate phase, i.e. $\Delta\mu_w^{\beta-H}$ in Equation 3.14, is given by (Parrish and Prausnitz, 1972):

$$\Delta\mu_w^{\beta-H} = RT\sum_m \theta_m \ln\left(1+\sum_j C_{jm} f_j\right) \tag{3.18}$$

where θ_m is the number of type m cavity for each water molecule in the unit cell. f_j is the fugacity of guest component j. C_{jm} is the Langmuir constant, which is calculated as:

$$C_{jm} = \frac{4\pi}{\kappa T}\int_0^R \exp\left(-\frac{U(r)}{\kappa T}\right) r^2 dr \tag{3.19}$$

where κ is the Boltzmann's constant. r is the distance measured from the centre of cavity. $U(r)$ is the spherically symmetric cell potential in the cavity.

$U(r)$ is dependent on the intermolecular potential function chosen for describing the encaged guest-water interaction. McKoy and Sinanoglu (1963) suggested to use the Kihara potential model to represent the potential energy of interaction between spherically symmetric molecules that have impenetrable hard cores surrounded by penetrable soft electron clouds.

The Kihara potential functions are given as follows:

$$\mathrm{K}(r) = \infty \qquad (r = 2\beta) \qquad (3.20a)$$

$$\mathrm{K}(r) = 4\varepsilon\left[\left(\frac{\sigma - 2\beta}{r - 2\beta}\right)^{12} - \left(\frac{\sigma - 2\beta}{r - 2\beta}\right)^{6}\right] \qquad (r > 2\beta) \qquad (3.20b)$$

where $\mathrm{K}(r)$ is the potential energy of interaction between two molecules. ε is the depth of the energy well, i.e., the minimum potential energy. β is the hard-core radius. σ is the collision diameter, the distance when $K = 0$.

McKoy and Sinanoglu (1963) suggested calculating the overall cell potential ($U(r)$) with:

$$U(r) = 2z^{H}\varepsilon\left[\frac{(\sigma^{*})^{12}}{R_c^{11} r}\left(\delta^{10} + \frac{\beta}{R_c}\delta^{11}\right) - \frac{(\sigma^{*})^{6}}{R_c^{5} r}\left(\delta^{4} + \frac{\beta}{R_c}\delta^{5}\right)\right] \qquad (3.21)$$

where z^H is the coordination number of hydrate cavity. R_c is the cavity radius. σ^* is given by $\sigma^* = \sigma\text{-}2\beta$. The general form for calculating δ^M ($M = 4, 5, 10, or\ 11$) is as:

$$\delta^{M} = \frac{1}{M}\left[\left(1 - \frac{r}{R_c} - \frac{\beta}{R_c}\right)^{-M} - \left(1 + \frac{r}{R_c} - \frac{\beta}{R_c}\right)^{-M}\right] \qquad (3.22)$$

3.6.3. Kihara Potential Parameters

The Kihara potential model is used to calculate the interaction energy between spherically symmetric molecules. In this model, each molecule has an impenetrable (hard) core

surrounded by penetrable (soft) electron clouds; the intermolecular distance is taken as the minimum distance between the surfaces of the molecules cores.

The Kihara potential model has three adjustable parameters, i.e. the hard-core radius (β), the collision diameter (σ) and the depth of energy well (ε), which are required for modelling hydrate. The value of β was found to be not a strong factor affecting the calculation of hydrate dissociation pressures, so in the hydrate model β was estimated using a correlation (Avlonitis, 1992; Tohidi, 1995). The values of σ and ε for different hydrate formers were determined using an optimisation method to match the experimental data in terms of hydrate dissociation pressure (Tohidi, 1995).

The Kihara potential parameters were determined for hydrate formers such as methane, ethane, propane, i-butane, n-butane, carbon dioxide, hydrogen sulphide and nitrogen, which are commonly present in real reservoir fluids. The Kihara potential parameters were also determined for heavy hydrate formers such as benzene, cyclohexane and methylcyclohexane (Tohidi, 1995).

In this work, hydrate modelling will only take into account the light compounds such as C_1, C_2, C_3, iC_4, nC_4, CO_2 and N_2, as they are the major compounds forming hydrate in real reservoir fluids.

3.7. SOLID PHASE - ICE

Ice is considered as a sub-cooled liquid. The following formula is used for calculating the fugacity of water in ice phase:

$$f_w^I = P_{ice}^{sat} \times \left(\varphi_w^V\right)_{P_{ice}^{sat}} \times exp\left[\left(v_{ice} / RT\right) \times \left(P - P_{ice}^{sat}\right)\right] \tag{3.23}$$

where f_w^I is the fugacity of water in the ice phase. P_{ice}^{sat} and P are the ice vapour pressure and the system pressure, respectively. v_{ice} is the ice molar volume. $\left(\varphi_w^V\right)_{P_{ice}^{sat}}$ is the water fugacity coefficient in the vapour phase at the ice vapour pressure P_{ice}^{sat}. Both v_{ice} and P_{ice}^{sat} can be calculated using empirical correlations (Tohidi, 1995).

3.8. SUMMARY

This chapter has detailed the thermodynamic basis for multi-phase equilibrium. For a closed isothermal system, modelling of multi-phase equilibrium is based on the uniformity of fugacity for each component throughout all phases.

The fugacity in each fluid phase was calculated using an equation of state. The VPT EoS was used for modelling the hydrate phase equilibrium, and the SRK/PR EoS was independently used for calculating the wax phase equilibrium.

The fugacity of each compound in the wax solid phase was related to the pure solid fugacity, based on the non-ideal solid solution theory. The pure solid fugacity was calculated from the fugacity of pure sub-cooled liquid, where fusion properties and heat capacities were required. The solid-solid transition was also formulated into the thermodynamic equation in order to properly represent the actual melting process of wax. In the non-ideal solid solution theory, the activity coefficient was required, which will be discussed and estimated in Chapter-4.

The hydrate phase was described using the ideal solid solution theory, in which the activity coefficient equals unity. The Kihara potential was used for expressing the guest-water molecular interaction. The required Kihara potential parameters were determined in previous studies (Avlonitis, 1992; Tohidi, 1995).

Ice was regarded as a sub-cooled liquid, and the fugacity of water in ice phase was calculated by correcting the saturation fugacity of water at the same temperature with an exponential factor (the Poynting correction).

3.9. TABLES

Table 3.1. Geometric and physical properties for cavities of structure I. II and H hydrates

Structure	I		II		H		
Crystal type	Cubic		Cubic		Hexagonal		
Lattice parameter, Å	a=12		a=17.3		a=12.26. c=10.17		
Water molecules/unit cell	46		136		34		
Cavity	5^{12}	$5^{12}6^2$	5^{12}	$5^{12}6^4$	5^{12}	$4^35^66^3$	$5^{12}6^8$
Number of cavities/unit cell	2	6	16	8	3	2	1
Average cavity radius, Å	3.95	4.33	3.91	4.73	3.91	4.06	5.71
Coordination number	20	24	20	28	20	20	36

3.10. FIGURES

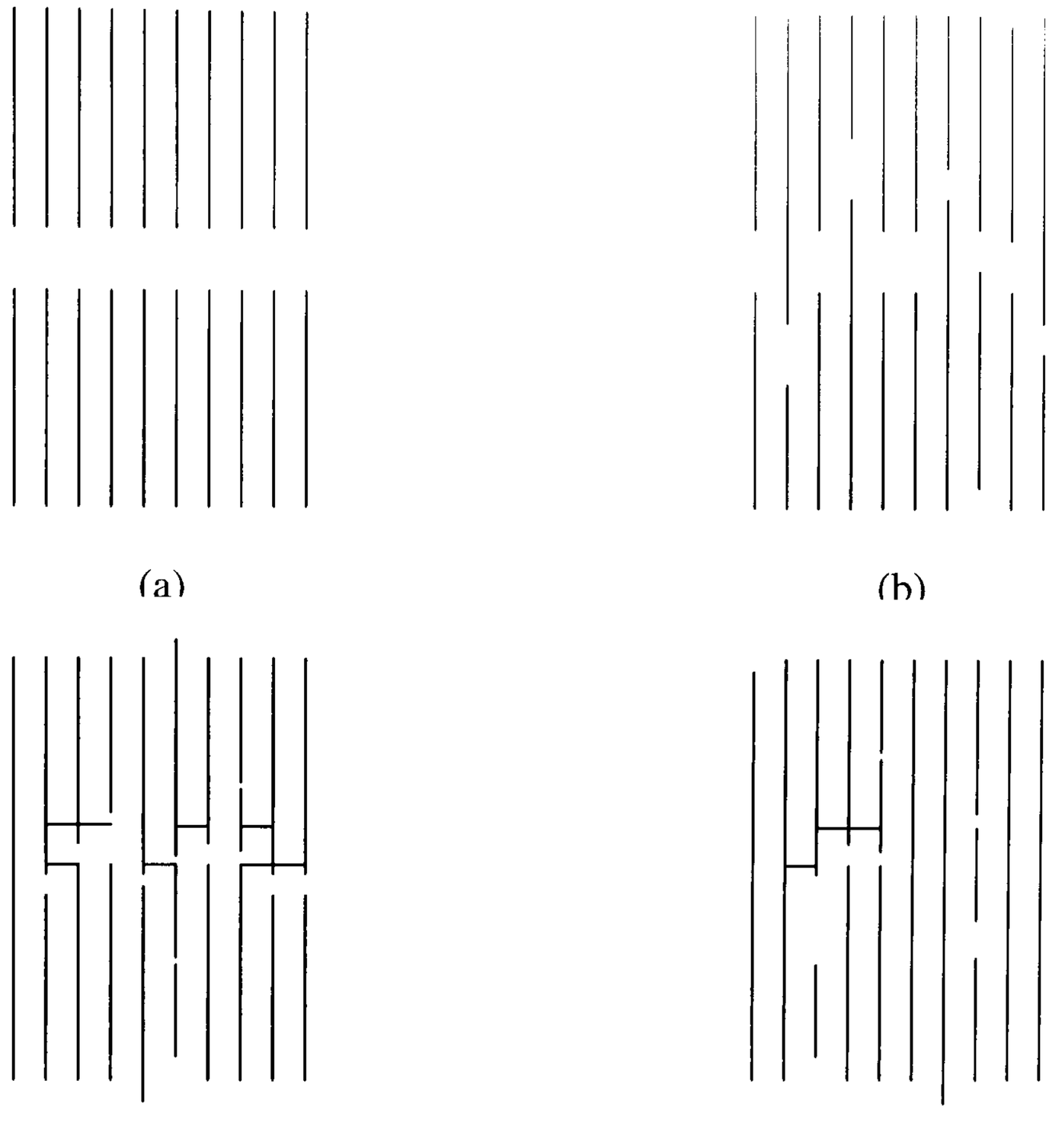

Figure 3.1. Schematic representation of crystal packing modes in terms of carbon chain (the line in figure) arrangement (Craig et al., 1998): (a) ideal packing without disorder, (b) inter-chain mixing, (c) end-chain twisting/folding, and (d) combined carbon chain mixing and twisting/folding.

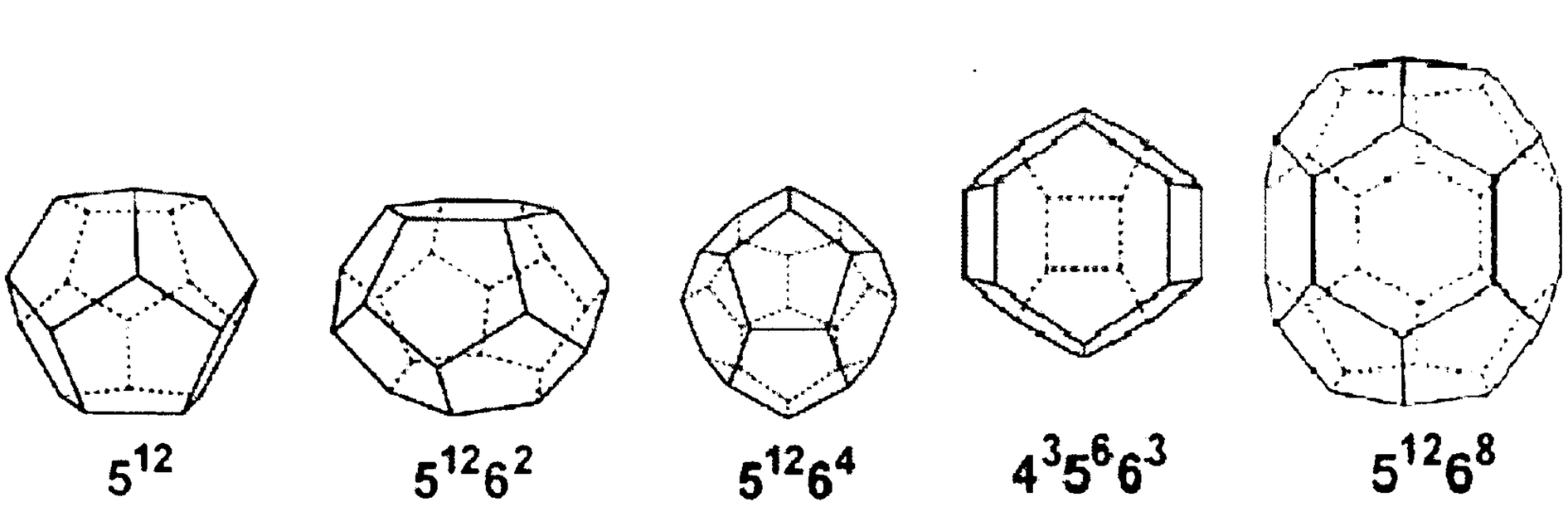

Figure 3.2. Five types of cavities in structure I, II and H hydrates

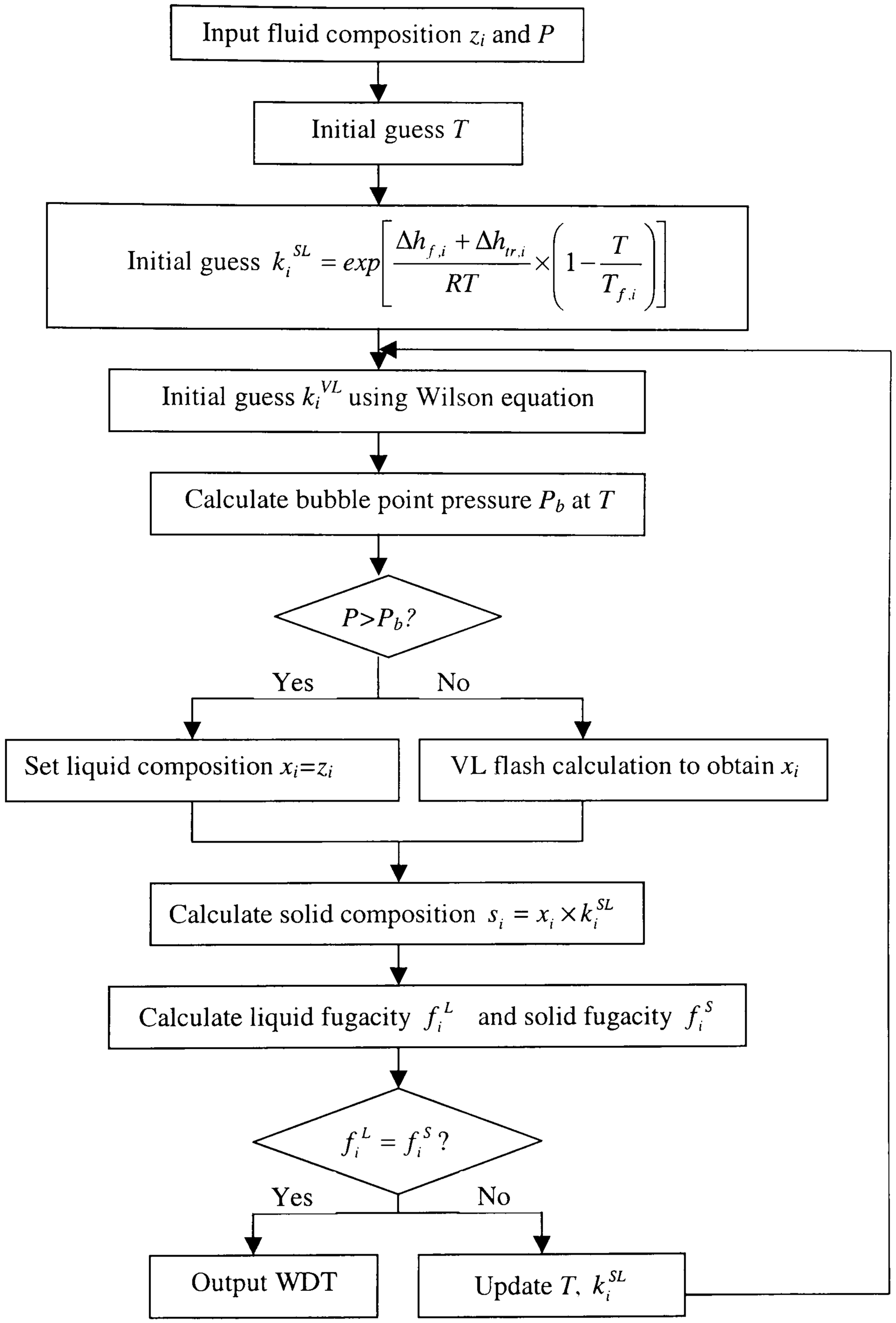

Figure 3.3. Flowchart for calculating wax phase boundary in a multi-phase system.

CHAPTER-4

DEVELOPMENT OF WAX THERMODYNAMIC MODEL

4.1. INTRODUCTION

In this chapter, the existing wax thermodynamic models will be reviewed, focusing on their main features in terms of description of fluid and solid phases, the tuning and validation method. Limitations of the existing wax models will be discussed. Then, the development of a new wax model will be given by several modifications.

Correlations for calculating thermo-physical properties will be based on the experimental data of pure compounds. Comparing with the existing models, the new wax model will consider using a modified EoS to calculate the fugacity in fluid phases, and a non-ideal solid solution to model the solid phase. In order to improve the calculation of fugacity in the liquid and solid phases, the new wax model will be tuned using experimental WDT data of different synthetic binaries with known compositions. The model capability will be extended to high-pressure conditions in this chapter. The extension of the new wax model for real reservoir fluids will be detailed in Chapter-5, and the model validation will be given in Chapter-6.

4.2. REVIEW OF EXISTING WAX MODELS AND PROPOSAL OF A NEW WAX MODEL

4.2.1 Review of Existing Wax Thermodynamic Models

Several predictive thermodynamic models for wax have been presented in the literature. Some of the more popular models are detailed below:

Won (1986, 1989).

In 1986, Won presented early efforts to use a thermodynamic model for predicting wax phase boundaries (Won, 1986). The Soave–Redlich–Kwong (SRK) equation of state (EoS) was used for vapour–liquid equilibrium (VLE) calculations. A modified regular solution approach was employed for solid–liquid equilibrium (SLE) calculations, where activity coefficients were calculated using solubility parameters of individual components. Critical temperature, critical pressure and acentric factor were estimated using correlations suggested by Spencer and Daubert (1973), Lydersen (1955), and Lee–Kesler (1975). The fusion temperature and heat of fusion were correlated to molecular weight using experimental data predominantly for pure *n*-paraffins with odd carbon numbers.

In 1989, Won modified the model by combining the modified regular solution with the equation of Flory–Huggins (Flory, 1941, 1942; Huggins, 1941, 1942) for calculating activity coefficients in the liquid phase (Won, 1989).

The wax model proposed by Won was validated against cloud point temperatures measured for synthetic fuels, diesel fuels, and North Sea gas condensates. Many other researchers adopted the model suggested by Won (1986, 1989), sometimes without any modification, when developing their own model.

However, there are several major shortcomings in Won's model, which can limit its capability and reliability for predicting wax phase boundaries. Firstly, two different methods are applied to the liquid phase for VLE and SLE; an EoS is used for VLE, while an activity coefficient model is applied to SLE. This leads to inconsistency in the description of liquid phase, and very often results in convergence issues. A further problem is that the modified regular solution approach used for describing wax solids does not differ greatly from the ideal solid solution approach, due to the similarity of the solubility parameters for *n*-paraffins. Both these approaches lead to overestimation of wax phase boundary temperatures. In addition, the model cannot provide reliable predictions of wax phase boundaries at high-pressure conditions, as the effect of pressure on wax equilibria is ignored. Finally the model is based on WAT data, which, as discussed, are not reliable for tuning and/or validating a model.

Hansen et al (1988).

In 1988, Hansen et al. presented a wax model that used the SRK EoS for VLE calculations, with the ideal solid solution approach applied to the solid phase, and a polymer solution approach applied to the liquid phase for SLE. As parameters required in the polymer solution approach were determined by fitting to the measured cloud point temperatures (WAT) for 13 North Sea crude oils, it was not surprising that predicted WATs were in good agreement with measured WAT data for the same North Sea crude oils.

The model proposed by Hansen et al. (1988) has similar limitations to that of Won (1986, 1989). Furthermore, the polymer solution approach used by authors leads to activity coefficients in the liquid phase of the order of 10^{-10}, which does not correspond with reality (Pedersen et al., 1991b; Pedersen, 1995).

Pedersen et al (1991, 1995).

In 1991, Pedersen et al. (1991b) presented a wax model based on modifications to the approach of Won (1986). A modified regular solution approach was applied to both the liquid and solid phases. Fusion properties and heat capacities for pure compounds were tuned to fit measured wax precipitation data for the North Sea oils. The model was validated using experimental WAT data for the North Sea oils.

In 1995, Pedersen further modified this model, employing a cubic equation of state for consistency in description of the liquid phase for VLE and SLE calculations. The ideal solid solution approach was applied to the solid phase. Fusion properties were calculated using correlations suggested by Won (1986).

The main problem with the model of Pedersen et al. (1991b) is that it uses unreliable values for fusion properties and heat capacity. The approaches used to describe wax solids in the models proposed in 1991 and 1995 (i.e. the approaches of regular solid solution and ideal solid solution), may lead to an overestimation of wax phase boundary temperatures. Again, the models are flawed in that they are based upon non-equilibrium WAT data.

Erickson et al (1993).

The model proposed by Erickson et al. in 1993 was also a modification of that of Won (1986). The ideal solution approach was applied to SLE calculations. Heat of fusion for pure compounds was tuned against experimental SLE data for binary mixtures. The proposed model was validated against experimental WAT data for crude oil and condensate samples. The model proposed by Erickson et al. (1993) has similar limitations to that of Won (1986).

LiraGaleana et al (1996).

LiraGaleana et al. (1996) presented a wax thermodynamic model in which a multi-pure-solid approach was used for description of wax solids. This approach assumed wax solids consisting of multiple solid phases, and each solid phase was a pure compound. The PR EoS was used for calculating fugacity in the liquid and vapour phases. Critical properties and the acentric factors were estimated using correlations suggested by Cavett (1964). The model was validated using experimental SLE data for binaries, and measured cloud point temperatures (WAT) for the North Sea crude oils.

Studies on crystal structure in recent years reveal that the miscibility of *n*-paraffins in a solid state depends strongly on differences in molecular sizes (i.e. carbon number). An *n*-paraffin mixture with a significant carbon number difference (e.g. nC_{30}–nC_{40}) appears to form pure solids (Dorset et al., 1997), whereas an *n*-paraffin mixture with a consecutive carbon number distribution forms a single solid solution (Dirand et al., 1998). Thus assumptions of the multi-pure-solid approach are not consistent with real wax crystal behaviour. Therefore, the reliability of the model proposed by LiraGaleana et al. (1996) is of question for systems consisting of compounds with similar molecular sizes.

Coutinho et al. (1995, 1996, 1998)

In 1995 and 1996, Coutinho et al. evaluated several approaches for calculating activity coefficients in SLE, including the Flory–Huggins, Universal Functional Group Activity Coefficient (UNIFAC), Flory free-volume, and entropic free-volume (Coutinho et al., 1995, 1996). In 1998, Coutinho presented a wax thermodynamic model which used a combined UNIFAC and Flory free-volume approach to describe the liquid phase, with the universal quasi-chemical (UNIQUAC) equation being used to describe wax solids. In this UNIQUAC

approach, the characteristic energy, Δe_{ij}, for calculating the adjustable binary parameter, τ_{ij}, with Equation 4.14, is expressed using λ_{ij} and λ_{ii} as below:

$$\Delta e_{ij} = \frac{z}{2q_i}\left(\lambda_{ij}-\lambda_{ii}\right) \tag{4.1}$$

where q_i is the external surface area parameter of pure compounds. λ_{ii} is calculated using enthalpy of sublimation for component i as follows:

$$\lambda_{ii} = -\frac{2}{z}\left(\Delta h_{subl,i} - RT\right) \tag{4.2}$$

where z is the coordination number (set to 6 by the authors). λ_{ij} is given by λ_{kk} as below. where k designates the smaller n-paraffin of the pair ij :

$$\lambda_{ij} = \lambda_{kk} \tag{4.3}$$

Using the above correlations, when k is i, Δe_{ij} is zero, and Δe_{ji} has a nonzero value. The model proposed by Coutinho (1998) was validated using experimental data for the amount and composition of wax precipitated for mixtures.

In 2000, Pauly et al. further modified the model of Coutinho (1998) by using SRK EoS–G^E for the description of liquid and vapour phases. G^E was obtained using a modified UNIFAC equation. Critical properties were estimated using correlations proposed by Twu (1984). The Poynting correction term was used to extend the model to high-pressure conditions. Partial molar volumes required for calculating the Poynting correction were estimated in accordance with crystallographic studies of *n*-paraffin solids. The model was validated using experimental WDT data for *n*-paraffin mixtures.

Hydrocarbon solids present a positive deviation from the ideal solid solution, as shown later in Chapter-6. This positive deviation can be described using the UNIQUAC equation. The accuracy of this equation depends on parameters defined for the equation. Coutinho used thermodynamic properties to calculate binary parameters. Examining the model proposed by Coutinho (1998) (as will be presented in Chapter-6) shows that Coutinho's UNIQUAC approach lacks reliability for mixtures containing molecules of similar sizes.

4.2.2. New Wax Model Proposal

Considering the limitations and lack of reliability of the existing wax models reviewed above, a new wax model will be developed in this study. The new wax model will consider ensuring consistency in description of the liquid phase for VLE and SLE calculations, by using a cubic equation of state for calculating fugacity in all hydrocarbon fluid phases. SRK and PR EoS are widely used for calculating fugacities in vapour–liquid hydrocarbon systems, therefore, they will be used for the description of fluid phases in the new wax model.

The new wax model will be developed using a systematic approach (Ji et al., 2004). First, we will develop correlations for calculating thermo-physical properties, such as the temperatures and latent heats of fusion, for pure substances. Then, the SRK and PR EoS will be modified in order to improve the calculation of fugacity for heavy hydrocarbons. New correlations will be suggested to calculate coefficients of temperature dependency functions for the attraction term of the EoS. Following this, a new approach based on the UNIQUAC equation will be developed for describing wax solids. The tuning of EoS and UNIQUAC equation will be conducted by matching the calculated SLE points to experimental WDT data, using specially designed binary mixtures. Finally, a method will be proposed for extension of the developed wax model to high-pressure conditions based on pure compound fusion properties.

4.3. FUSION PROPERTIES AND HEAT CAPACITY

As shown in Equations 3.12 and 3.13, fusion properties and heat capacity are required for calculating the fugacity of solids. Their accuracy is vital for developing a reliable wax model. Experimental data show that fusion properties and heat capacities of n-paraffins are dependent not only on the carbon chain length, but also on whether carbon numbers are odd or even. This has been considered in the new model when developing correlations for fusion properties and heat capacity.

In the new model, properties for both solid-solid (T_{tr} and ΔH_{tr}) and solid-liquid (T_f and ΔH_f) transitions (at 0.1 MPa) have been regressed into correlations using available experimental data for pure n-paraffins up to C_{70} (Broadhurst, 1962; Schaerer et al., 1955). A

third order polynomial function has been developed to represent transition temperature as a function of carbon number, acknowledging the difference between odd and even carbon numbers. Latent heats for transitions have been correlated with the product of molecular weight and fusion temperature using a linear function.

Several correlations have been developed to calculate heat capacity for solid n-paraffins of odd or even carbon numbers (as a function of temperature and carbon number) using available experimental data (Huffman et al., 1931; Jin et al.. 1991; van Miltenburg et al., 1999). A single correlation as a function of temperature and carbon number has been developed in this study for calculating the heat capacity of liquid n-paraffins. Correlations for both fusion properties and heat capacity are detailed in the Appendix-C.

4.4. MODIFICATION OF SRK AND PR EOS FOR HEAVY HYDROCARBONS

The SRK and PR EoS, as described using the general form of Equation 3.7, have two parameters, a and b, which are related to the molecular attraction and repulsion. The attraction term a is calculated by Equation 3.8, using critical temperature (T_c) critical pressure (P_c) and α. Clearly, the accuracy of T_c, P_c, and α values affects the calculated attraction term a, which further impacts the precision of calculated fugacity with EoS.

α is a function of reduced temperature ($T_r = T/T_c$) and acentric factor (ω). The accuracy of α function is dependent on the ranges of T_r and ω with which the correlation is developed. When using EoS far beyond correlation ω and T/T_c ranges, the EoS reliability can be radically reduced.

Traditionally, the α function was developed by matching vapour pressures of pure substances. In the original SRK and PR EoS, α was related to T_r and ω using Equation 3.10 (as given in Chapter-3 and reproduced below) in conjunction with Equations 4.4 and 4.5. based on vapour pressure data for hydrocarbons up to C_{10} (with an acentric factor of 0.492). The temperatures from normal boiling points to critical points (i.e. T/T_c range of approximately 0.6-1.0) were considered in the PR EoS (Peng and Robinson, 1976). whereas data at $T_r = 0.7$ were used in the original SRK (Soave, 1972).

$$\alpha = \left[1 + m\left(1 - T_r^{0.5}\right)\right]^2 \qquad \text{(for SRK and PR)} \qquad (3.10)$$

$$m = 0.480 + 1.574\omega - 0.176\omega^2 \qquad \text{(for SRK)} \qquad (4.4)$$

$$m = 0.37464 + 1.54226\omega - 0.26992\omega^2 \qquad \text{(for PR)} \qquad (4.5)$$

In order to improve the SRK and PR EoS for representation of heavy substances, many researchers attempted to modify the EoS by introducing new generalised correlations for α and/or *m* when heavier compounds and lower temperatures were taken into account. For instance, Soave (1993) and Twu et al. (1995a) suggested the modified α functions for SRK EoS, while Robinson and Peng (1978), Twu et al. (1995b) and Gasem et al. (2001) proposed the modified α functions for PR EoS. These modifications were also based on vapour pressures of pure compounds. C_{20} (acentric factor of approximately 0.91) and C_{28} (acentric factor of approximately 1.16) were probably the heaviest compounds taken into account for the modified SRK and PR EoS (Twu et al, 1995a; Gasem et al., 2001), respectively, while the lowest T/T_c for compounds heavier than C_{20} was approximately 0.57 in the modified PR EoS (Gasem et al., 2001).

The wax phase equilibrium is determined mainly by hydrocarbons between C_{20} to C_{60} (as will be detailed in Chapter-5). The temperature at which wax precipitates is generally low. Assuming a maximum and minimum reservoir and pipeline temperatures of 473 K to 273 K, the T/T_c of interest is between 0.28 to 0.6. This demonstrates the importance of reliable α function for heavy hydrocarbons at low temperatures. However, due to difficulties in vapour pressure measurements, it appears difficult to consider the interested acentric factor and T/T_c ranges when using experimental data for pure compounds to develop the α function.

Therefore, in this work, we will use VLE and SLE experimental data of binary systems to optimise the α values for heavy hydrocarbons in order to improve the wax model. The binary systems used contain hydrocarbons up to C_{36}, with low T/T_c values for heavy components.

4.4.1. Approach

The following approach was employed to develop the *m* correlation for modifying the α function of the SRK and PR EoS:

(1). The α form of Equation 3.10 was adopted in this work, due to its significant success and flexibility. The temperature dependency coefficients (i.e., *m* in the α function) for compounds heavier than C_{20} were optimised to match experimental VLE and SLE data for binaries. At this stage of optimisation, binary interaction parameters were set to zero.

The objective function used for the optimisation was as follows:

$$F = \frac{1}{n_1 + n_2}\left(\sum_{i=1}^{n_1} \left| \frac{P_{b,exp} - P_{b,cal}}{P_{b,exp}} \right| + \sum_{i=1}^{n_2} \left| \frac{WDT_{exp} - WDT_{cal}}{WDT_{exp}} \right| \right) \tag{4.6}$$

where P_b is the bubble point pressure, and *WDT* is the wax disappearance temperature for the binaries. The subscript "*exp*" designates experimental data, and "*cal*" designates calculated data. n_1 and n_2 are number of P_b and *WDT* data points, respectively.

(2). The optimised *m* values for heavy paraffins (C_n>C_{20}) were plotted against acentric factors estimated using the correlations suggested by Lee-Kesler (1975). As the original SRK and PR EoS have been successfully applied to light hydrocarbons, the original α and *m* functions (Equations 3.10 and 4.4 or 4.5) were considered to be valid for paraffins lighter than C_{20}. The *m* values for light paraffins (C_n≤C_{20}) were calculated using the original EoS parameters, and plotted against acentric factor. Finally, *m* values for heavy and light compounds were correlated with acentric factor (as presented later). Hydrocarbons up to C_{36} have been taken into account when developing the proposed *m* versus ω correlations for the modified EoS.

(3). Binary interaction parameters are generally required to match experimental equilibrium data for binary systems consisting of light and heavy compounds due to significant molecular size differences. Binary interaction parameters determined for binary systems are generally applied directly to multi-component systems. In this work, binary interaction parameters for pairs of compounds were determined through minimisation of the differences between calculated and experimental SLE data for binary systems. When optimising binary interaction parameters, the *m* correlations developed in this work were used for calculating the EoS parameters.

Table 4.1 gives the binary systems used in this work for developing the new m vs ω correlations.

4.4.2. Proposed New m vs ω Correlations

When optimising the m value, critical temperature (T_c) and pressure (P_c) data are required. Reliable experimental data for these properties are available for n-paraffins up to C_{20}. It is difficult and can be inaccurate to measure directly the critical properties for heavy hydrocarbons (C_n>C_{20}) due to thermal decomposition at high temperatures. It is customary to estimate the T_c and P_c for long chain paraffins using empirical correlations. Figures 4.1 and 4.2 compare T_c and P_c estimated using the correlations suggested by Ambrose (1978, 1979 and 1980), Twu (1984), Teja et al. (1990), Constantinou et al. (1994) and Riazi et al. (1995). Considerable differences in the estimated values for different correlations are observed. The experimental T_c and P_c data for several heavy hydrocarbons (Nikitin et al., 1997) are also shown in Figures 4.1 and 4.2, respectively.

Initially, the m values for C_{22}, C_{24}, C_{32} and C_{36} were optimised using the T_c and P_c values estimated by each set of empirical correlations. Optimised m values were then plotted against the acentric factor (ω), as shown in Figures 4.3 and 4.4, using the SRK and PR EoS, respectively. It is clear that the critical property estimation can have a significant effect on optimised m values.

The m values of C_1-C_{20} calculated by the original EoS function (Equations 4.4 and 4.5) are also plotted against their acentric factors (ω) in Figures 4.3 and 4.4. Clearly m values of all compounds investigated must be consistent with respect to their acentric factors. The optimised m values for heavy compounds using the empirical correlations suggested by Ambrose (1978, 1979 and 1980) and Teja et al. (1990) did not follow the expected trend of C_1-C_{20}, thus these correlations were deemed not suitable for a reliable application.

As shown in Figure 4.3, the correlations suggested by Riazi et al. (1995) lead to consistent m vs ω, and were therefore selected to calculate the T_c and P_c values when using the SRK EoS. The m values, optimised for compounds heavier than C_{20} and calculated for C_1-C_{20}, were correlated with the acentric factor (ω), as given by:

$$m = 0.4806 + 1.7137\omega - 0.9207\omega^2 + 0.9620\omega^3 - 0.2595\omega^4 \qquad \text{(for SRK EoS)} \quad (4.7)$$

As shown in Figure 4.4, the correlations suggested by Twu (1984), which similarly gave consistent values, were selected to estimate T_c and P_c when using the PR EoS. The m values of paraffins from C_1 up to C_{36} have been correlated to the acentric factor (ω), and the proposed form is presented as:

$$m = 0.3748 + 1.5932\omega - 0.5706\omega^2 + 0.3968\omega^3 - 0.092\omega^4 \qquad \text{(for PR EoS)} \quad (4.8)$$

The m correlations (i.e. Equations 4.7 and 4.8) developed in this work are expressed as fourth order polynomial functions and span a wider range of ω than the original second order polynomial functions (i.e. Equations 4.4 and 4.5) based on compounds up to C_{10} (Soave, 1972; Peng and Robinson, 1976).

The data used in the development of the above two correlations covered a range of acentric factor up to 1.37 (i.e., C_{36}). However, the correlations show a consistent trend up to an acentric value of 1.83 (i.e., C_{60}).

The T/T_c of C_{22}, C_{24}, C_{32} and C_{36} were calculated using the binary equilibrium (VLE and SLE) temperature and the component critical temperature, as listed in Table 4.2. For hydrocarbons heavier than C_{20}, the lowest T/T_c used for developing the EoS parameters in this work was approximately 0.32-0.37, compared to the value of approximately 0.57 reported in the previous modifications (Gasem et al., 2001).

4.4.3. Optimised Binary Interaction Parameters (BIPs)

In the optimisation of m values, the binary interaction parameters were initially set to zero. They were then optimised for matching to the experimental SLE data for light-heavy hydrocarbon binaries. Since binary interaction parameters are generally considered as fitting parameters for hydrocarbon systems, but not rigorous physical terms, their values may depend on the EoS being used.

Figure 4.5 shows the binary interaction parameters optimised using the SLE binaries (as listed in Table 4.1) and the modified SRK EoS presented in this work. T_c and P_c were calculated with the correlations suggested by Riazi et al. (1995), as discussed above. The binary interaction parameters for different binaries are almost constant and independent of the combination (pairing) of compounds, and their value is approximately –0.02 for all the

binaries investigated. A similar result was observed for the PR EoS with an average binary interaction parameter value of –0.024, as shown in Figure 4.6.

4.4.4. Comparison of Several α Functions

The temperature dependency multiplier, α, of the SRK EoS was calculated according to the suggestions of Soave (1972), Soave (1993), Twu et al. (1995a) and this work. The α values at $T_r=T/T_c$ of 0.3, 0.5, 0.7 and 0.9 were plotted against acentric factor (ω). As shown in Figure 4.7, for hydrocarbons heavier than C_{20} (i.e., $\omega > 0.91$), the α values obtained by the different approaches are in good agreement at $T_r = 0.9$. Indeed the deviation should vanish totally at the critical point where $T_r = 1$ and α=1. The deviation between this work and those reported in the literature increases with a decrease in T/T_c. At the interested T/T_c of approximatley 0.28 to 0.6, the α values based on this work show siginificant differences comparing with those reported in the literature for the SRK EoS.

Similarly, the temperature dependency parameters (i.e. α values) of the PR EoS have been calculated using the functions proposed by Peng and Robinson (1976), Robinson and Peng (1978), Twu et al. (1995b), Gasem et al. (2001) and this work. The calculated α values were plotted against the acentric factor, as presented in Figure 4.8. The observation is similar to that of SRK, albeit, the difference between the proposed correlation and those of previously modified correlation is relatively small.

4.5 DESCRIPTION OF WAX SOLIDS

The UNIQUAC equation with parameters determined in this work is used for describing wax solids, i.e., for calculating activity coefficients in the solid phase. The general UNIQUAC equation in terms of molar excess Gibbs energy is given as:

$$\frac{g^E}{RT} = \sum_{i=1}^{n} s_i \ln\left(\frac{\vartheta_i}{s_i}\right) + \frac{z}{2}\sum_{i=1}^{n} q_i s_i \ln\left(\frac{\xi_i}{\vartheta_i}\right) - \sum_{i=1}^{n} q_i s_i \ln\left(\sum_{j=1}^{n} \xi_j \tau_{ji}\right) \tag{4.9}$$

with

$$\vartheta_i = \frac{r_i s_i}{\sum_{j=1}^{n} r_j s_j} \tag{4.10}$$

$$\xi_i = \frac{q_i s_i}{\sum_{j=1}^{n} q_i s_i} \tag{4.11}$$

where g^E is the molar excess Gibbs energy. r_i and q_i are molecular structure parameters of pure compounds, which depend on molecular sizes and external surface areas. z is the coordination number ($6 \le z \le 12$).

The coordination number, z, is set to 10 here, according to the value suggested by Abrams and Prausnitz (1975). Based on the n-paraffin structure parameters provided in the literature (Abrams and Prausnitz, 1975; Prausnitz, 1986), the following correlations have been developed for calculating r_i and q_i.

$$r_i = 0.675 C_{n,i} + 0.4483 \tag{4.12}$$

$$q_i = 0.540 C_{n,i} + 0.6200 \tag{4.13}$$

where $C_{n,i}$ is the carbon number for compound i.

As shown in Equation 4.9, for each pair of compounds, there are two adjustable parameters, τ_{ij} and τ_{ji}. These are given in terms of characteristic energies Δe_{ij} and Δe_{ji}. The general formulation for calculating τ_{ij} is:

$$\tau_{ij} = exp\left(-\frac{\Delta e_{ij}}{RT}\right) \tag{4.14}$$

The characteristic energy, Δe_{ij}, is correlated with $\Delta C_{n,ij}$, the difference in carbon numbers for a pair of compound i and j:

$$\Delta e_{ij} = a_{UNIQUAC} \times \Delta C_{n,ij} \tag{4.15}$$

where $a_{UNIQUAC}$ is a constant determined as 11 cal·mol^{-1} in this work using the experimental WDT data generated in this laboratory for C_{16}-C_{18}, C_{16}-C_{20} and C_{15}-C_{19} binaries.

It is also assumed that:

$$\Delta e_{ji} = \Delta e_{ij} \tag{4.16}$$

4.6 MODELLING HIGH PRESSURE CONDITIONS

The exponential term in Equation 3.11, referred as the Poynting correction term, takes into account the effect of the difference between the operating pressure (P) and the reference pressure (P_O). In this work, the reference pressure is set to be the operating pressure, where the Poynting correcting term becomes unity. To calculate the pure solid fugacity at the reference pressure (f_i^{OS}), fusion properties of pure compounds have to be those at the operating pressure conditions (i.e., the reference pressure in this work).

Based on experimental measurements for pure n-paraffins (Floter et al., 1997; Wurflinger et al., 2000), the following generalized correlation is proposed for calculating fusion temperatures at increased pressure conditions.

$$T_{f\,(P)} = T_{f\,(P=0.1MPa)} + 0.2 \times (P - 0.1) \tag{4.17}$$

where $T_{f\,(P=0.1MPa)}$ and $T_{f\,(P)}$ are the fusion temperatures (in K) of pure compounds at 0.1 MPa and the operating pressure (P) in MPa, respectively.

4.7 CONCLUSIONS

In this chapter, a new wax model has been developed using data on pure and binaries of n-paraffins. The model can be used for calculating the wax phase equilibrium for systems with known compositions. The accuracy of calculated WDTs at different pressures, amounts and compositions of wax precipitated at different temperatures and pressures will be validated using independent experimental data in Chapter-6.

Comparing with the existing models, the new wax model has the following improvements:

(1). The EoS was invariably used for calculating the liquid fugacity in both VLE and SLE, showing the thermodynamic consistency.

(2). The experimental WDT data for systems with known compositions were used for the model tuning, which improved its reliability.

(3). The parameters of the model were determined using a systematic approach. as follows:

- The acknowledgement of the differences in behaviour of odd and even carbon number improved the accuracy of calculated thermo-physical properties of pure compounds, consequently improving the calculated fugacity of pure solids.

- The α functions of SRK and PR EoS were modified by taking into account data on heavy hydrocarbons at low temperatures, which improved the calculated fugacity for wax-forming compounds in the liquid phase.

- A constant binary interaction parameter was established for intermediate (C_5-C_{20}) and heavy (C_n>C_{20}) compounds when using the modified SRK and PR EoS.

- A new approach based on the UNIQUAC equation was developed for calculating the activity coefficient in the solid phase. The activity coefficient representing the non-ideality of a solution was correlated with the carbon number difference, which was in agreement with the nature of wax mixtures, hence improved the calculated solid fugacity.

- The pressure effect on the solid fugacity was considered, which improved the model capability for calculating wax phase equilibrium at high pressures.

4.8 TABLES

Table 4.1. The VLE and SLE binary systems containing heavy n-paraffins. (Data source: Seyer, 1938; Dernini et al., 1976; Madsen et al.. 1976; Madsen, 1979; Peters et al.. 1987. 1988, 1989; Kniaz, 1991; Roberts et al., 1994; Aalto et al., 1996).

Light comp.	VLE /SLE	x (heavy comp.)	T/K	P/MPa	Data points
		Binaries consisting of C_{22}			
C_2	VLE	0.21 - 0.95	350	0.3 - 8.2	7
C_6	SLE	0.0889 - 0.9861	291.3 - 316.9	0.1	14
		Binaries consisting of C_{24}			
C_2	VLE	0.0328 - 0.8803	300.9 - 368.7	0.4 - 13.6	104
C_6	SLE	0.0140 - 0.1240	279.7 - 299.8	0.1	6
C_7	SLE	0.0147 - 0.5414	283.3 - 317.1	0.1	21
		Binaries consisting of C^*_{28}			
C_5	SLE	0.0031 - 0.0346	284.6 - 301.9	0.1	9
C_7	SLE	0.0048 - 0.1138	287.3 - 312	0.1	14
C_8	SLE	0.0036 - 0.0815	285.9 - 309.8	0.1	19
C_{10}	SLE	0.0039 - 0.0493	287.4 - 306.3	0.1	19
		Binaries consisting of C_{32}			
C_3	VLE	0.019	373.7 - 374.7	4.5 - 4.6	12
C_5	SLE	0.0013 - 0.0073	288.8 - 300.2	0.1	12
C_6	SLE	0.0037 - 0.8954	299.4 - 341.5	0.1	14
C_7	SLE	0.0014 - 0.1999	289.3 - 326.8	0.1	15
C_8	SLE	0.0026 - 0.6800	292.0 - 338.4	0.1	21
C_{10}	SLE	0.0061 - 0.8566	299.6 - 340.6	0.1	13
C_{12}	SLE	0.0039 - 0.8280	296.5 - 340.8	0.1	20
		Binaries consisting of C_{36}			
C_3	VLE	0.0009 - 0.0192	353.1 - 372.6	3.2 - 4.4	20
C_5	SLE	0.0001 - 0.0024	284.7 - 304	0.1	17
C_6	SLE	0.0001 - 0.0032	284.5 - 305.4	0.1	16
C_7	SLE	0.0001 - 0.5997	284.5 - 344.4	0.1	52
C_8	SLE	0.0001 - 0.0024	283.8 - 303.2	0.1	19
C_{10}	SLE	0.0001 - 0.0027	285.7 - 304.2	0.1	20
C_{12}	SLE	0.0001 - 0.0033	285.9 - 306.3	0.1	21

Note: comp.: component; x: mole fraction; *: data used for optimisation of binary interaction parameters, but not used in the development of the m correlation.

Table 4.2. Heavy compound T/T_c ranges used for developing the EoS parameter in this work.

Compound	*T/Tc*
C_{22}	0.37 - 0.44
C_{24}	0.35 - 0.46
C_{32}	0.34 - 0.44
C_{36}	0.32 - 0.42

4.9 FIGURES

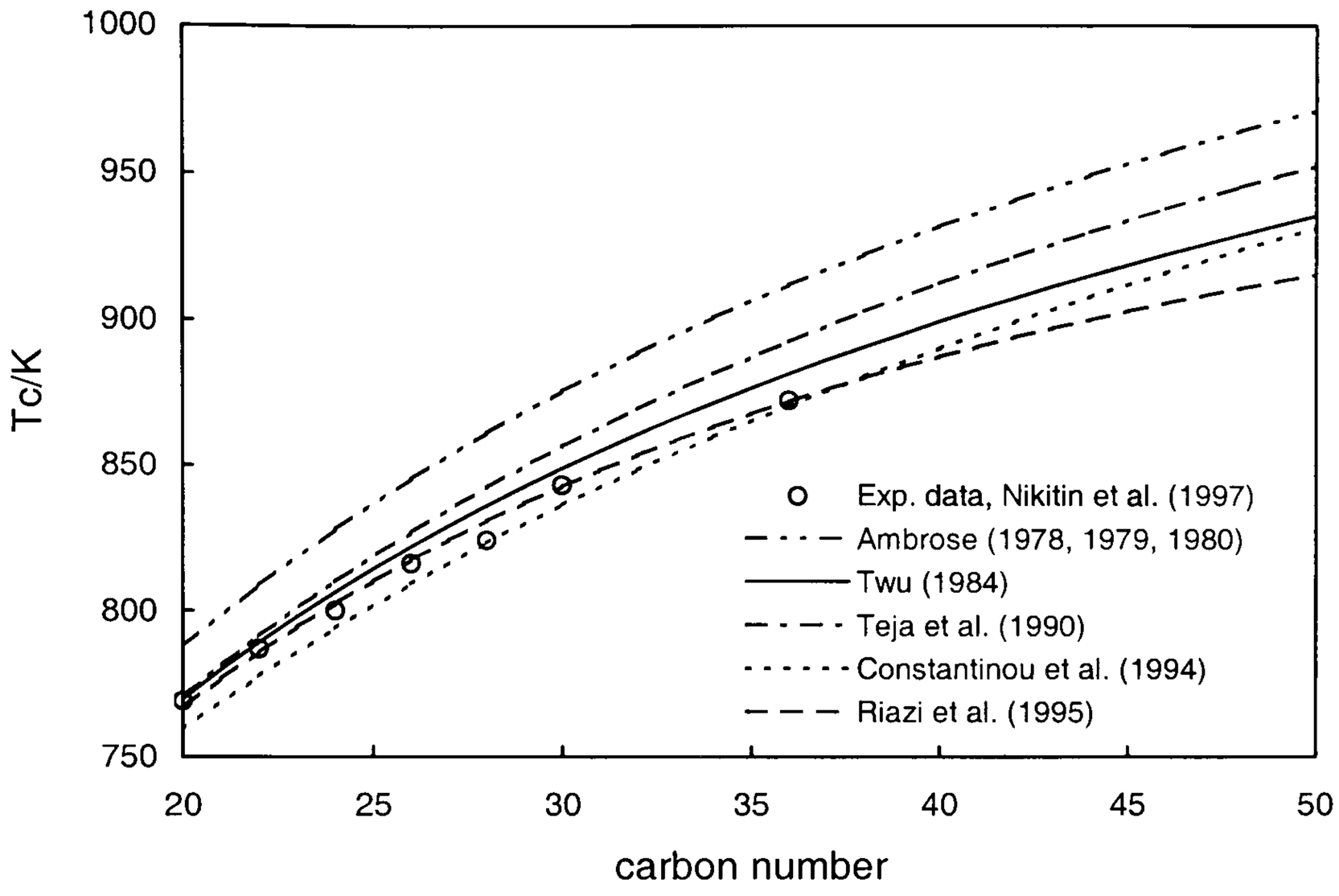

Figure 4.1. Experimental and estimated critical temperatures for heavy n-paraffins (C_n>C_{20}).

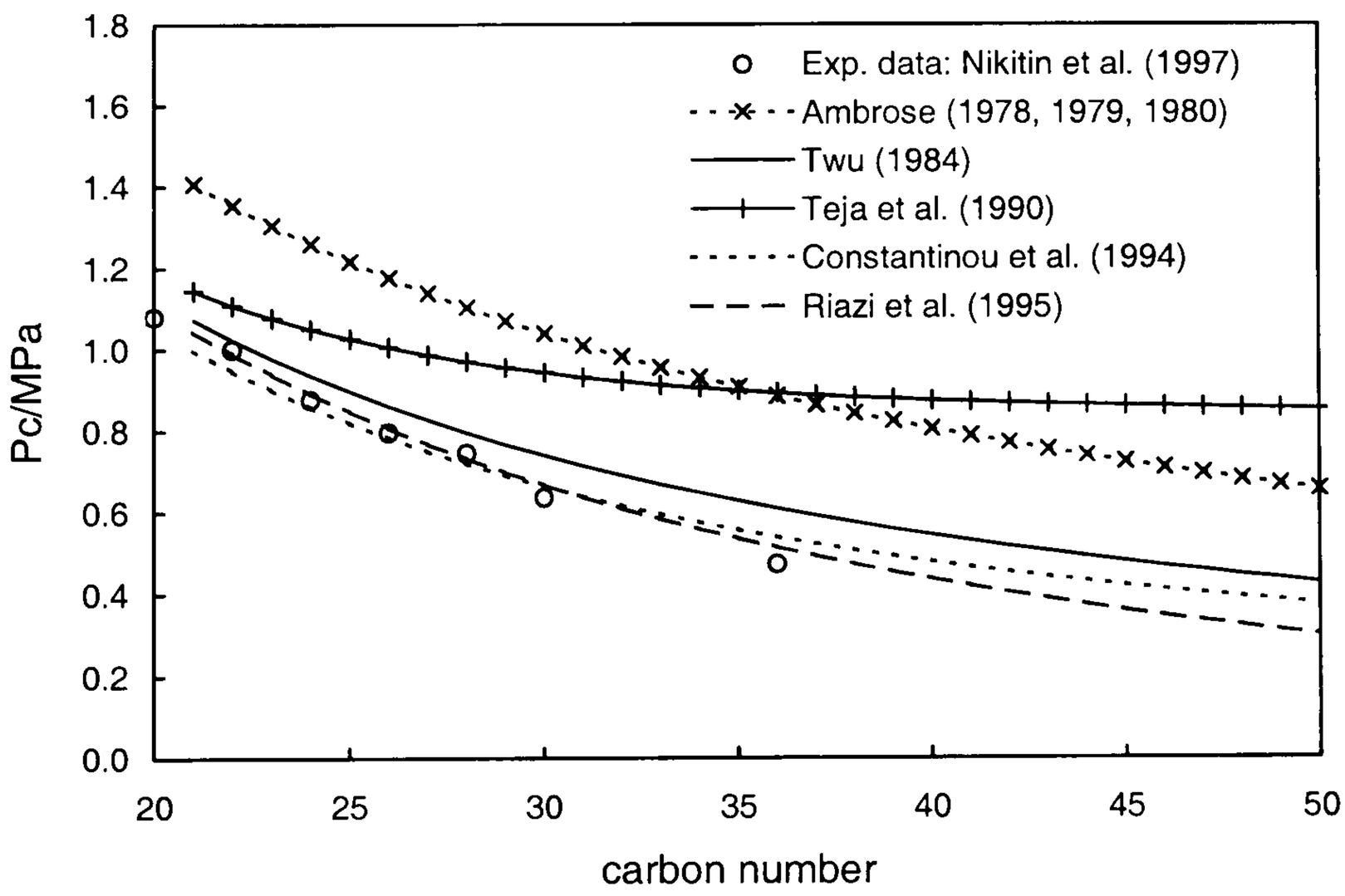

Figure 4.2. Experimental and estimated critical pressures for heavy n-paraffins (C_n>C_{20}).

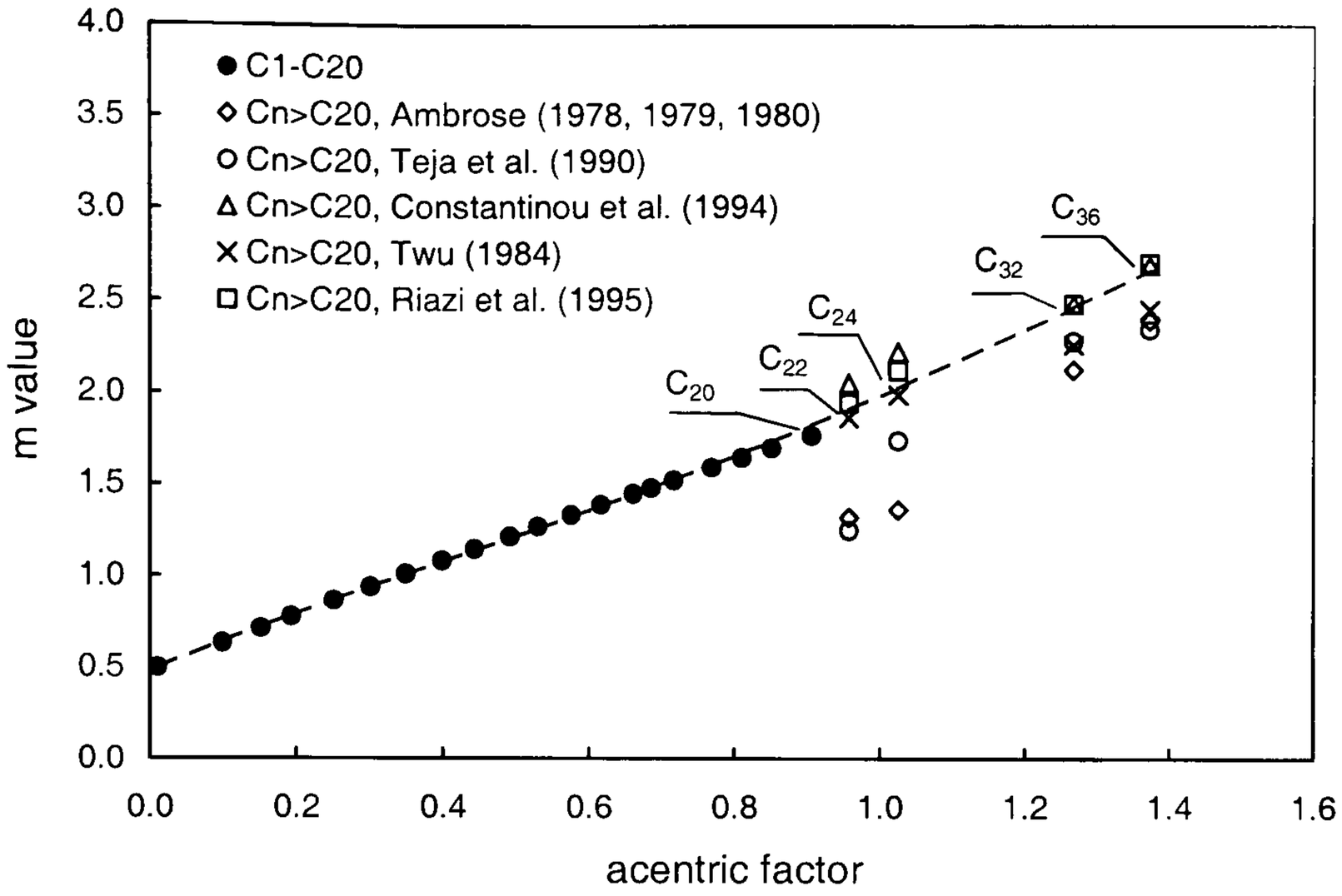

Figure 4.3. Comparison of heavy compound (C_n>C_{20}) *m* values optimised using critical properties estimated by several empirical correlations to *m* values of C_1 – C_{20}, SRK EoS.

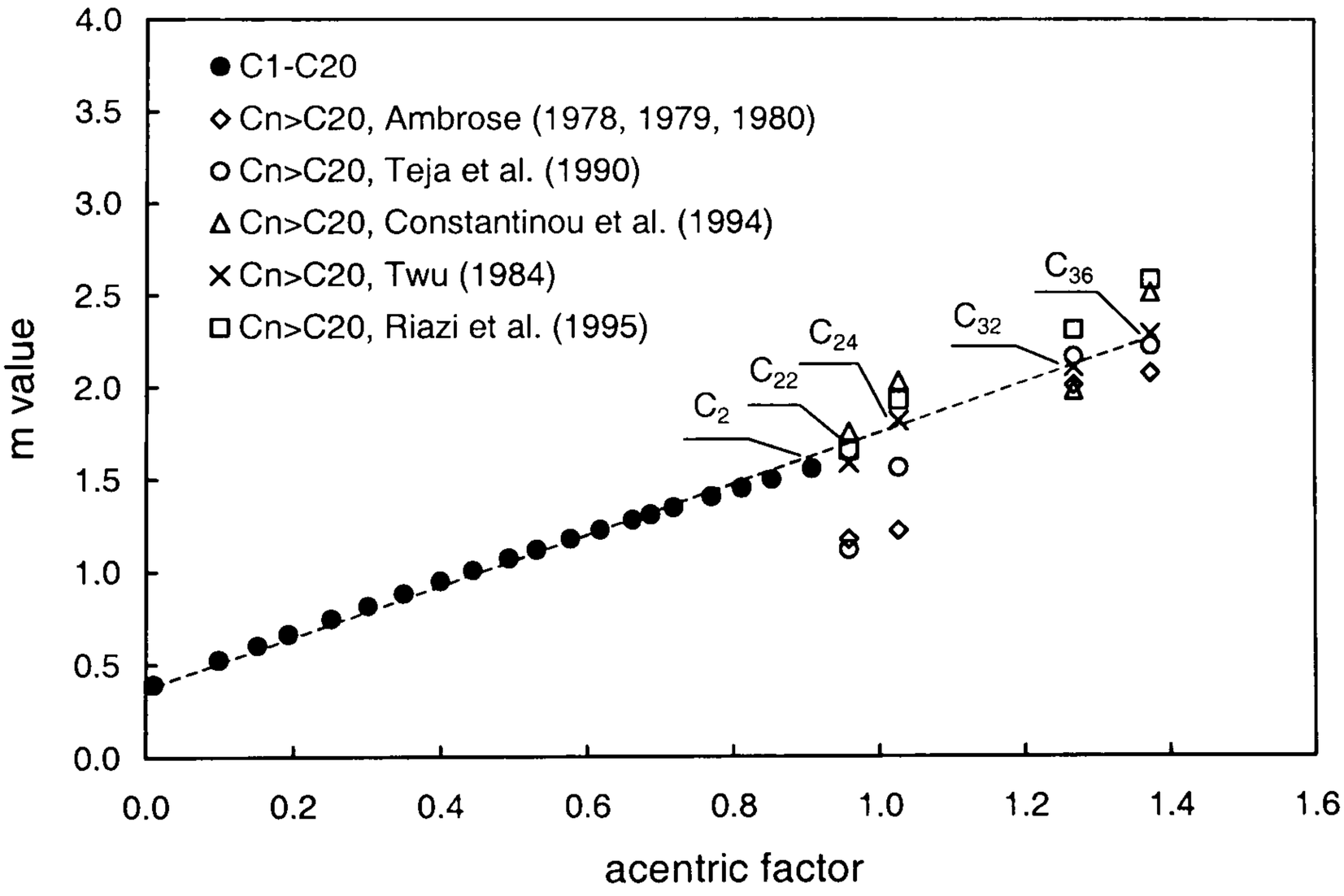

Figure 4.4. Comparison of heavy compound (C_n>C_{20}) *m* values optimised using critical properties estimated by several empirical correlations to *m* values of C_1 – C_{20}, PR EoS.

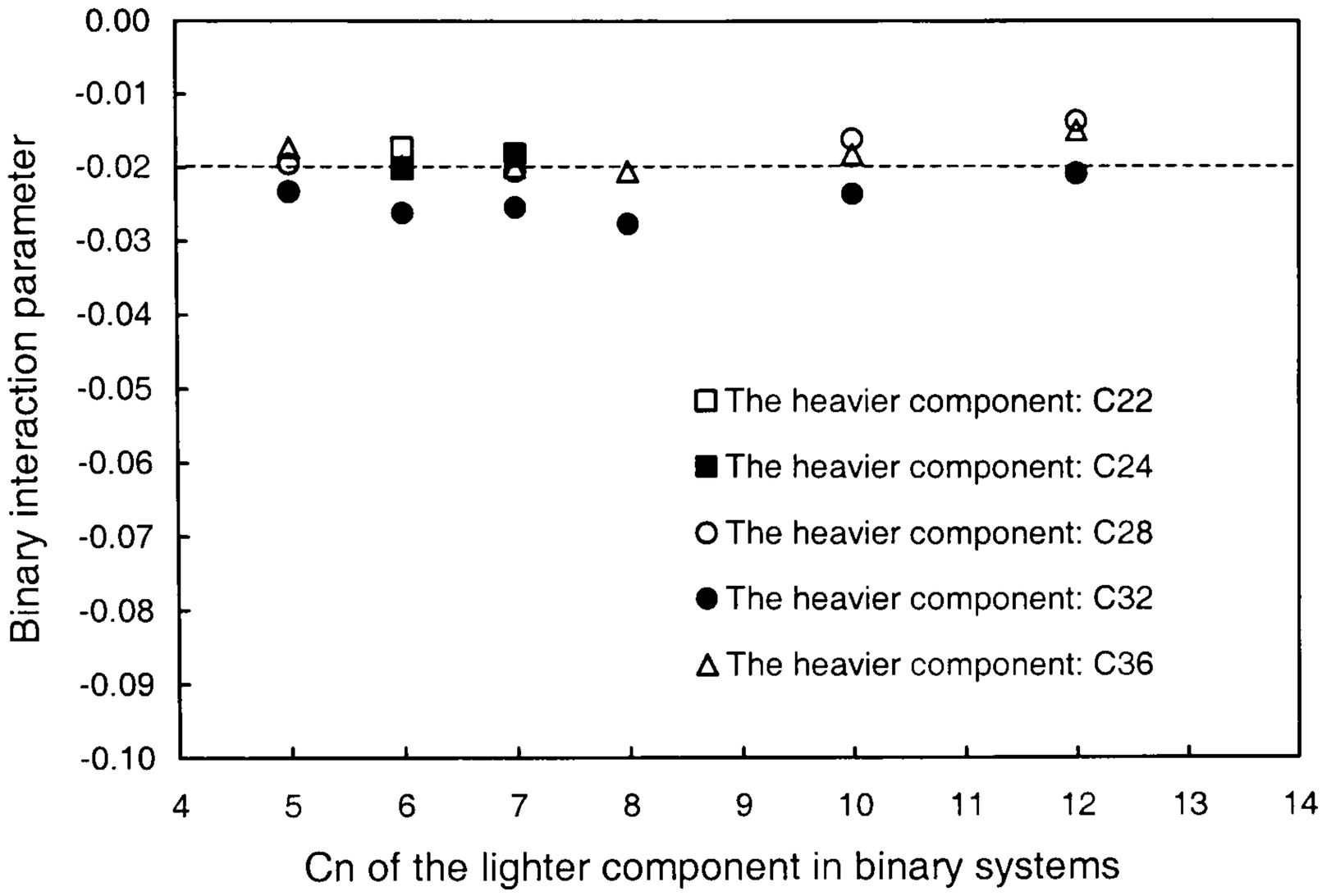

Figure 4.5. Binary interaction parameters optimised using binary SLE data and the SRK EoS modified in this work (Cn: carbon number).

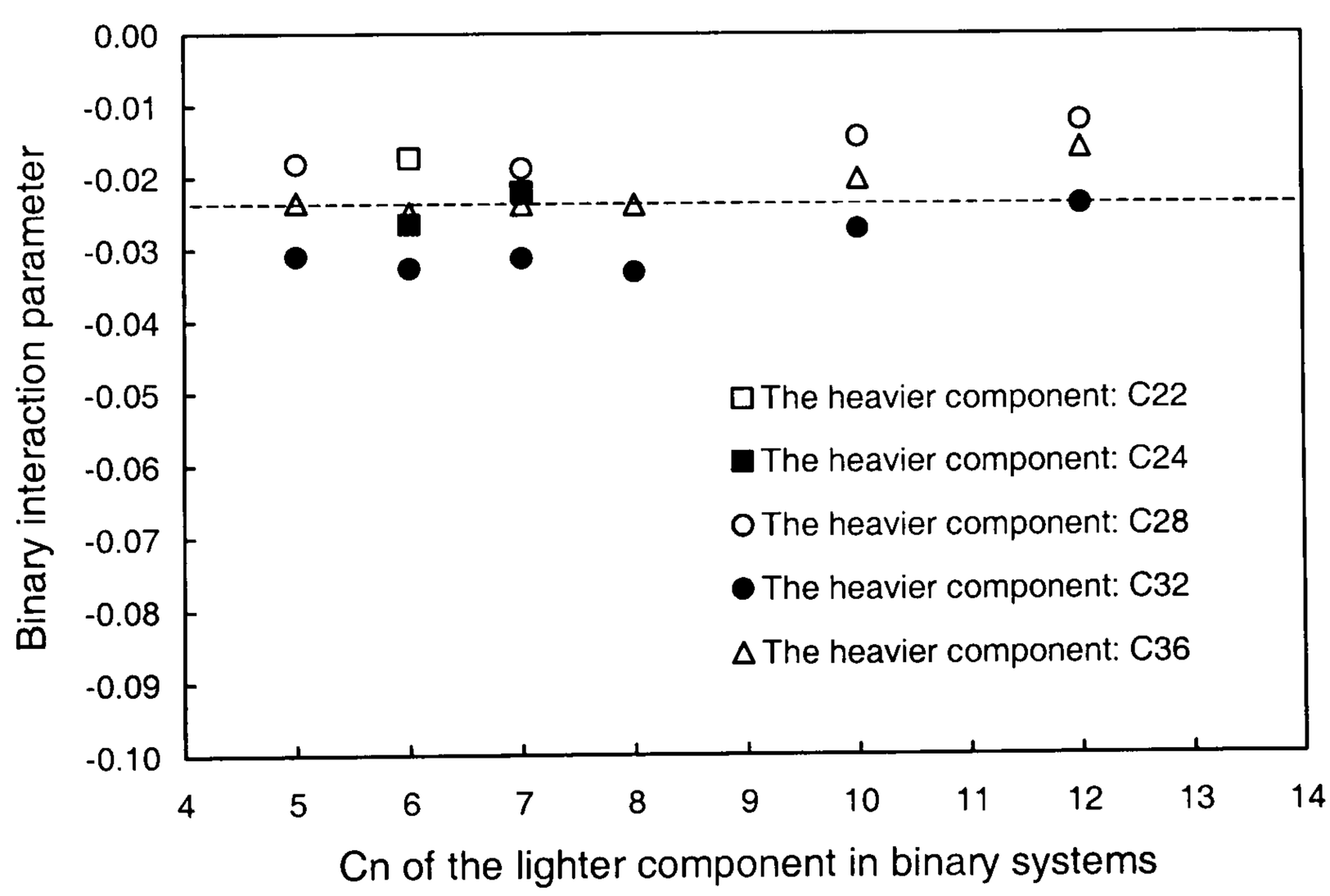

Figure 4.6. Binary interaction parameters optimised using binary SLE data and the PR EoS modified in this work (Cn: carbon number).

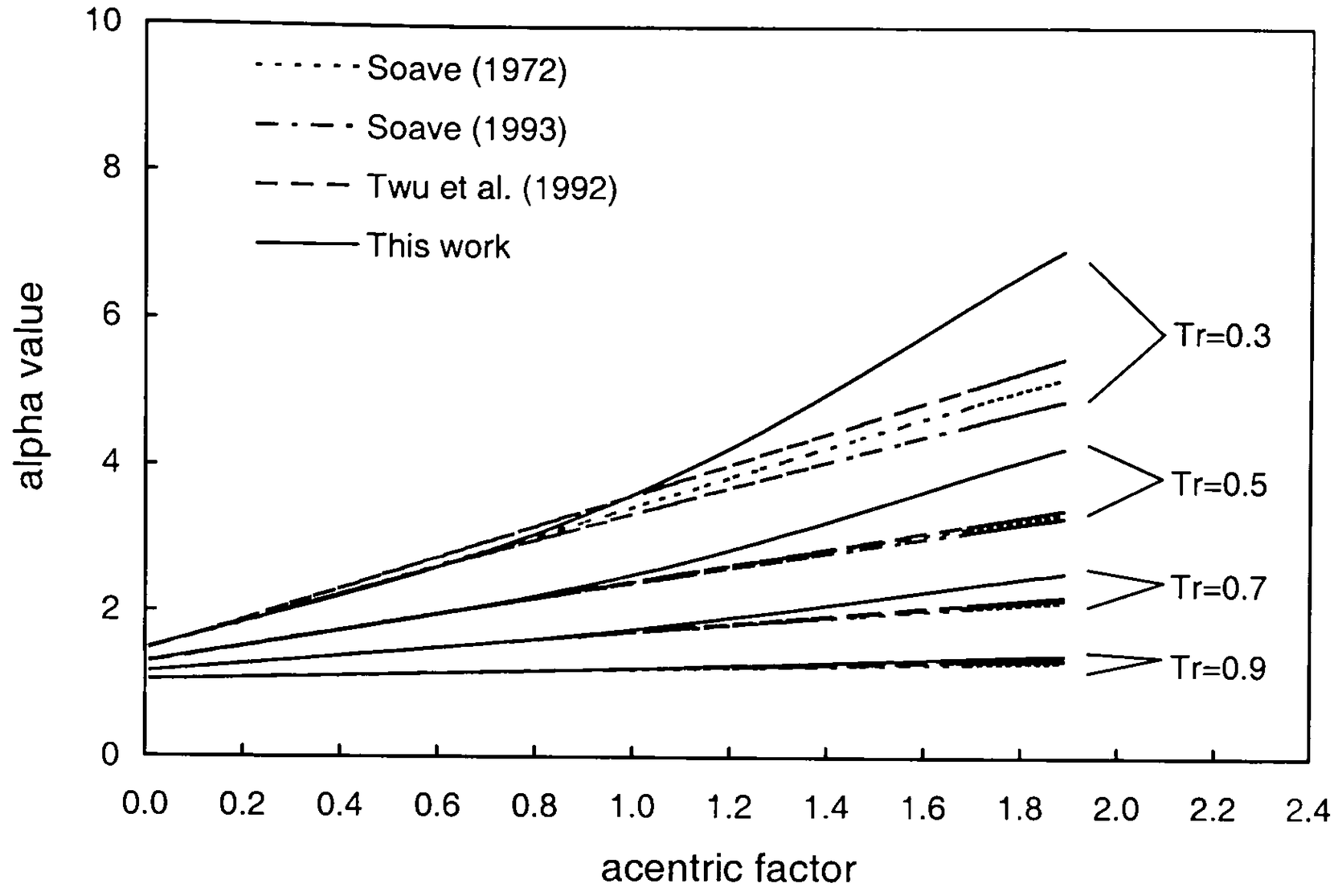

Figure 4.7. Comparison of α values calculated by several methods as functions of acentric factor for the SRK EoS.

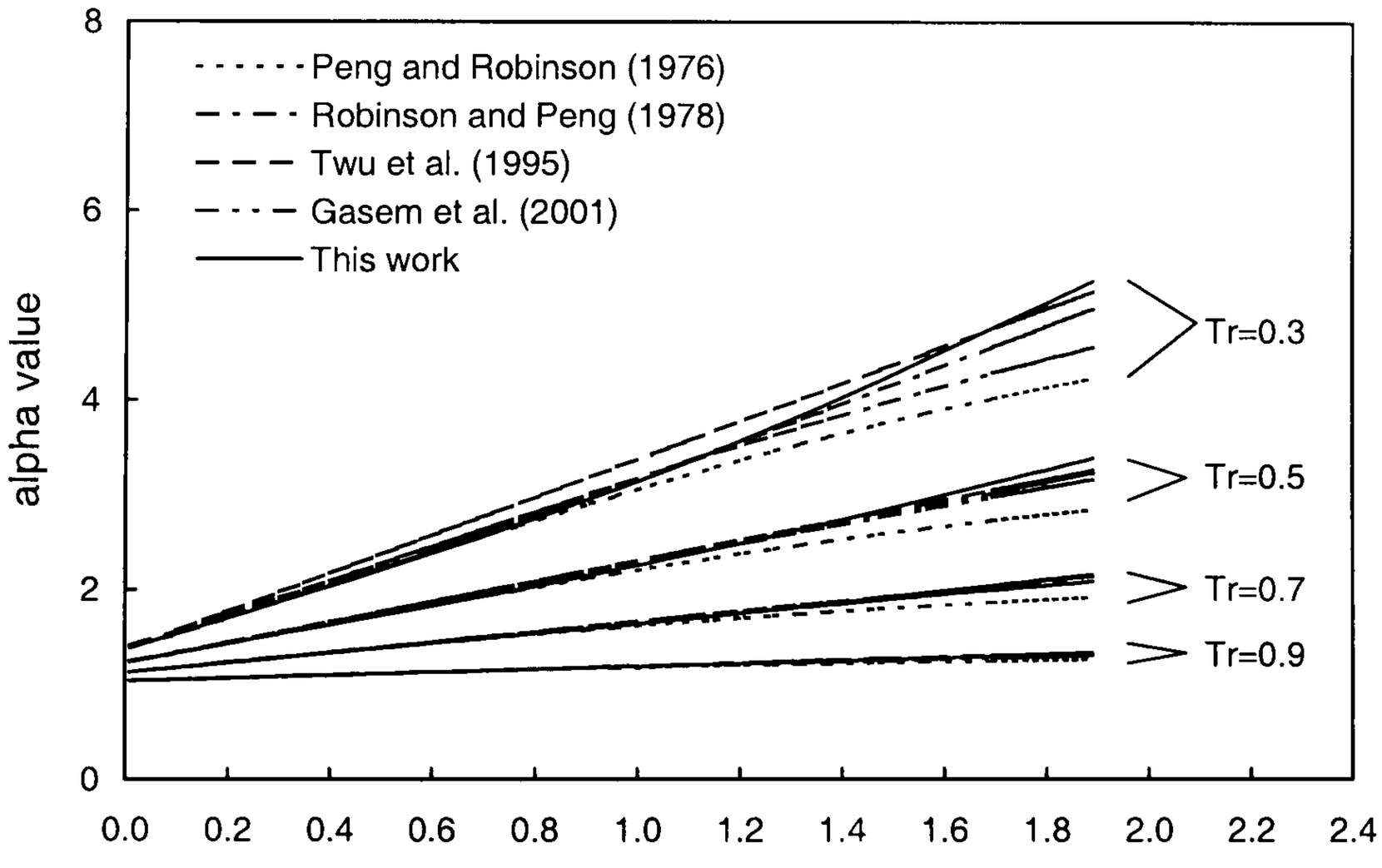

Figure 4.8. Comparison of α values calculated by several methods as functions of acentric factor for the PR EoS.

CHAPTER-5

MODELLING OF WAX IN REAL RESERVOIR FLUIDS

5.1. INTRODUCTION

The model formulated in Chapters 3 and 4 can be used to predict wax phase equilibrium for n-paraffin systems with known compositions. A real reservoir fluid contains n-paraffins as well as large amounts of non-normal paraffins, which may affect the wax phase equilibrium. Furthermore, for a real reservoir fluid, compositional data based on laboratory analysis are usually limited. Hence, for modelling the wax phase equilibrium in real reservoir fluids, the model needs to be extended by adding the non-n-paraffin hydrocarbons and a proper approach for estimating the required compositional data.

It is very difficult to experimentally detect which hydrocarbon initiates wax formation in a real reservoir fluid. The question can only be speculated by examining the content of wax deposits, and the wax phase boundaries formed with various proportions of different hydrocarbons.

In this chapter, I will briefly introduce different hydrocarbon types present in real reservoir fluids, and then evaluate their possible roles in wax formation. Accordingly, a method will be proposed to extend the wax model developed in the previous chapters to real reservoir fluids using commonly available experimental composition data.

5.2. CLASSIFICATION OF HYDROCABONS AND THEIR ROLES IN WAX FORMATION

5.2.1. Classification of Hydrocarbons for Reservoir Fluids

Hydrocarbons in reservoir fluids can be classified as **P**araffins (including n-paraffins and iso-paraffins), **N**aphthenes and **A**romatics, which are abbreviated as PNA. The physical and thermo-physical properties of a hydrocarbon are strongly dependent on its PNA class and its carbon number. Variation of properties against carbon number within a hydrocarbon class is often predictable. For instance, boiling point temperature increases with the increase in carbon number for hydrocarbons in the same class. The properties of hydrocarbons having the same carbon number but in different classes can differ significantly. For a given carbon number, iso-paraffins have the lowest boiling point temperatures, followed by n-paraffins, naphthenes and aromatics. The density of hydrocarbons follows the same trend, which can be used for differentiating the different hydrocarbon types with numerical correlations.

Melting point temperature, an important parameter for determining wax phase boundary, is strongly affected by hydrocarbon classes. In general, n-paraffins have much higher melting point temperatures compared to the other hydrocarbon classes with the same or even higher carbon number (as shown in Table 5.1), since the molecular geometry of n-paraffins allows them to pack together easily forming crystalline structures. The different melting point temperatures can affect the potentials of different hydrocarbon types to form wax.

5.2.2. Composition of Wax Formed in Real Reservoir Fluids

Wax deposits contain largely paraffins with small amounts of naphthenes and aromatics, as revealed by the early studies (Buchler et al., 1927; Bennett et al., 1944; Schanen, 1945; Fontana, 1946; Horne et al., 1946; Nelson et al., 1949; Clarke, 1951, Shock et al. 1955). More detailed wax compositions were given in recent years by analysing wax sample with advanced experimental techniques such as gas chromatography (GC).

It is clear that wax contains predominantly hydrocarbons heavier than C_{20}. For example, based on the GC analysis, the wax deposited in a production tubing was found containing hydrocarbons with carbon number between C_{18} to C_{66}, and C_{38} was at the peak concentration, while the wax deposited in a pipeline was of carbon number between C_{18} to C_{60}, and C_{30} was

at the peak concentration (Newberry et al., 1986). The wax collected from a pig receiver showed that hydrocarbons in the range of C_{30} – C_{60} were the major compounds (Labes-Carrier et al., 2002).

It is shown that n-paraffins, iso-paraffins and naphthenes all can take part in wax formation. The predominant hydrocarbon types of wax may be n-paraffins or non-n-paraffins such as iso-paraffins, depending on the real reservoir fluid. For instance, n-paraffins were reported as the principal constituents of wax for the oil studied by Srivastava et al. (1993), while iso-paraffins were found as the most abundant fraction of wax for the North Sea crude oil studied by Pedersen et al. (1991a). Moreover, as shown by the latter researchers, n-paraffins and naphthenes also contributed considerably to the wax deposit, but little amount of aromatics was found in the wax.

The composition of wax is also dependent on the temperature at which the wax sample is collected. For a given crude oil, the wax deposited and collected at different temperatures can show significantly different n-paraffin fractions. In general, lower temperatures can lead to smaller n-paraffin fractions and higher proportions of non-n-paraffins, based on the experimental data of wax composition at different temperatures (Pedersen et al., 1991a; Roehner et al., 2002).

It is also shown that the deposition location can significantly affect the wax composition, because of the change in temperature, pressure and fluid composition at different locations (Roehner et al., 2002).

5.2.3. Roles of Different Hydrocarbons in Wax Formation

Heavy n-paraffins, iso-paraffins and napthenes are all wax forming compounds, but n-paraffins generally have the highest melting point temperatures comparing to the others, so the composition of n-paraffins could be the determining factor for the wax phase boundary. This speculation was supported by the experimental WDT data measured for mixtures with different proportions of n-paraffins.

For instance, distillates were obtained from a real reservoir fluid, and each distillate was then further separated into three fractions: n-paraffin fraction, iso-paraffin & naphthene fraction, and aromatic fraction (Srivastava et al., 2002). The wax disappearance temperature (WDT)

was measured with a DSC technique for the different hydrocarbon fractions. The n-paraffin fraction gave the WDT value of approximately 40 - 60 °C higher than the iso-paraffin & naphthene fraction and the aromatic fraction. In further experiments, the separated n-paraffin fraction was mixed with the iso-paraffin & naphthene or the aromatic with different ratios, and the WDTs were measured for these mixtures. It was found that the mixtures with higher n-paraffin concentrations showed higher WDT values.

5.3. MODELLING OF WAX IN REAL RESERVOIR FLUIDS

It is plausible to make the following assumptions for modelling wax phase equilibrium in real reservoir fluids:

- The concentration of n-paraffins is the dominant factor deterderming the wax phase boundary.
- Iso-paraffins and naphthenes may be important in affecting the rate and amount of wax accumulation, due to their high concentrations in real reservoir fluids.
- Aromatics, commonly known as solvents for paraffinic wax, do not precipitate to form wax.

According to these assumptions, the composition will be required for n-paraffins, iso-paraffins, napthenes and aromatics. However, the compositional analysis for real reservoir fluids is generally based on single carbon number (SCN), where all hydrocarbons within a given boiling temperature range are grouped into a pseudo-component designated by a carbon number. Experimental data of compositions with the differentiation of different hydrocarbon types are very limited.

In the following sections, I will review a number of existing wax models regarding their treatments of different hydrocarbon types in the modelling of wax phase equilibrium. The methods for obtaining the required composition data in those wax models will also be given. Finally, I will describe the approach adopted in this work for modelling wax phase equilibrium in real reservoir fluids.

5.3.1. Review of Existing Wax Models for Real Reservoir Fluids

Models based on SCN groups

Several wax models developed in 1980's and 1990's assumed that compounds with the same carbon number for different hydrocarbon types have the same potential to form wax (Won, 1986, 1989; Hansen et al., 1988; Pedersen et al, 1991b, LiraGaleana et al., 1996). They used average values of physical and thermo-physical properties for single carbon number (SCN) groups without differentiation of n-paraffin, iso-paraffin, naphthene, and aromatics.

As mentioned earlier, n-paraffins have significantly higher melting point temperatures than the other hydrocarbons. In order to obtain the average value, the melting point temperature for the n-paraffin were reduced, which may impair the model's ability in estimating wax problem.

The assumption that all hydrocarbon classes have the same potential to form wax needs the SCN composition as input data. For real reservoir fluids, it will be difficult to determine the heaviest SCN group taking part in wax formation. Won (1986) used a 'cut-off' molecular weight to determine the heaviest SCN group forming wax. The value of the 'cut-off' must be obtained for each fluid studied by fitting to its experimental wax equilibrium data, limiting the model's capability for wide applications.

Models based on only n-paraffins

Erickson et al. (1993) assumed that n-paraffins determine the cloud point of crude oils, while iso-paraffins and naphthenes do not take part in wax formation. Accurate and detailed compositional data with differentiation of n-paraffin from the other hydrocarbon classes are required for using the model suggested by the authors. They suggested using an exponential decay function for estimating the required n-paraffin composition. The function was based on the last known n-paraffin concentrations measured in laboratory. Therefore, experimental data of n-paraffin concentration must be generated at least for parts of SCN groups. This is the minimum requirement when using the exponential decay function.

The exponential decay function correlates n-paraffin concentration against molecular weight, and it does not include fluid properties that relate with amounts of different hydrocarbons. The function parameters must be determined for each individual case. The function

established for a given crude oil has little reliability when applying to other independent fluids for which no experimental data of n-paraffin concentration is available. This restricts the exponential decay function for general application.

The wax models suggested by Daridon et al. (2001) and Coutinho et al. (2001) also assumed that only n-paraffins take part in wax formation. This assumption is not in agreement with the experimental and practical observations that non-n-paraffin hydrocarbons can also be the predominant constituent of wax. Ignoring the non-n-paraffins' potential for forming wax may lead to underestimating wax accumulation problems.

Model based on n-paraffins and non-n-paraffins

In the model presented by Pedersen (1995), it claimed that 'the wax forming components seem to consist mainly of n-paraffins. ... Also C_{7+} *iso-paraffins and naphthenes, especially the light ones*, will contribute to the wax phase'. The author argued that 'the presence of very heavy branched paraffins and cyclo-paraffins in the wax phase may be questioned'. Clearly, this argument is not in agreement with the experimental data about wax composition.

Pedersen used an empirical correlation for dividing the C_{7+} SCN group into a wax-forming part and a non-wax-forming part. The concentrations for wax-forming parts were estimated from the SCN concentrations by comparing the SCN density against the density of the n-paraffin with the same molecular weight. The empirical correlation has three constants, which were determined by matching experimental WAT data for the North Sea crude oils in that model.

The methodology suggested by Pedersen (1995) for estimating the n-paraffin concentration is reasonable. The correlation also considered that the relative amounts of different hydrocarbons affect the SCN properties, such as specific gravity. A correlation with parameters determined using accurate experimental data might present reasonable capability for estimating n-paraffin compositions for independent reservoir fluids. However, in the model of Pedersen (1995), the parameters of the correlation were determined using WAT data, which may limit the reliability of the correlation.

5.3.2. Considerations of the New Wax Model Developed in This Work

The new model will take into account different roles for various hydrocarbon classes in wax formation (Ji et al., 2003), generally in line with the experimental and field observations. First, the wax phase boundary of a real reservoir fluid is determined by n-paraffins. Then iso-paraffins, naphthenes and aromatics in each SCN group are considered as a pseudo-compound (referred as non-n-paraffin), since at present it is difficult to differentiate these hydrocarbon classes for modelling purposes. The non-n-paraffin will contribute to wax formation by increasing the amount of precipitated wax. The heaviest parts in a real reservoir fluid, i.e. compounds with molecular weight higher than 842 (equivalent to nC_{60}), are considered as the material that will 'precipitate' as asphaltenes (Pan et al., 1997), and will not form wax.

The new wax model will use the method suggested by Pedersen (1995) for estimating n-paraffin concentrations. The correlation constants will be determined by matching experimental WDT data in this work, instead of WAT data in the model of Pedersen (1995).

Since non-n-paraffins will take part in wax accumulation in the new wax model, their thermo-physical properties are required. The melting point temperatures of non-n-paraffins are dependent on both their carbon numbers and their molecular structures. For compounds with the same carbon number but different molecular structures such as different branched carbon chains, melting point temperatures may be different. However, due to lack of experimental data about detailed molecular structures of compounds in real reservoir fluids, the effect of molecular structure on melting point temperature will be ignored in this work.

5.4. EXTENSION OF THE NEW WAX MODEL TO REAL RESERVOIR FLUIDS

For modelling wax phase equilibrium in real reservoir fluids with the new wax model, n-paraffin concentrations are required, which can be estimated using the mole fraction, molecular weight and specific gravity of single carbon number (SCN) groups.

For real reservoir fluids, the compositions based on conventional laboratory analysis are described using discrete compounds up to C_5 and SCN groups for compounds heavier than C_5. SCN groups are determined according to their boiling point temperatures using

experimental techniques such as distillation and/or gas chromatography. The heavy end of hydrocarbon fluid is commonly described using the plus fraction, such as C_{7+}, C_{10+} and so on. In order to model wax phase equilibrium, the plus fraction needs to be split into SCN groups, in which the mole fraction, molecular weight and specific gravity for each SCN group are estimated.

5.4.1. Splitting of the Plus Fraction into SCN Groups

Estimation of mole fraction and molecular weight

A Gamma distribution function is used in this work for estimating the mole fraction and molecular weight when breaking the plus fraction into SCN groups. It is given as follows (Whitson, 1983):

$$p(MW) = \frac{(MW-\eta)^{\chi-1}\, exp[-(MW-\eta)/\beta']}{\beta'^{\chi}\, \Gamma(\chi)} \tag{5.1}$$

where $\Gamma(\chi)$ is the gamma function. η is the minimum molecular weight (MW) included in the distribution. χ and β' determine the shape of the distribution function.

β' is correlated to χ using η and the average molecular weight of the plus fraction (MW_{C_n+}) as follows:

$$\beta' = (MW_{C_n+} - \eta)/\chi \tag{5.2}$$

The compounds with molecular weight in the range of MW_{i-1} to MW_i are grouped as the SCN i with mole fraction given by:

$$z_i = z_{C_n+} \int_{M_{i-1}}^{M_i} p(MW)d(MW) \tag{5.3}$$

The average molecular weight for the SCN group i is

$$MW_i = \frac{z_{C_n+}}{z_i} \int_{M_{i-1}}^{M_i} p(MW)MWd(MW) \tag{5.4}$$

Estimation of specific gravity

The specific gravities of SCN groups can be estimated using their molecular weights. Riazi et al. (1996) suggested a general empirical correlation, which can be used to calculate the specific gravity when there is no experimental data available on the fluid system.

On the other hand, when there are experimental data, a logarithm function can be used to express the dependence of specific gravity against molecular weight, as given by:

$$SG_i = a_{SG}\, ln(MW_i) + b_{SG} \tag{5.5}$$

where SG_i and MW_i are the specific gravity and molecular weight for SCN group i.

a_{SG} and b_{SG} in Equation 5.5 are constants for a given real reservoir fluid. Their values can be calculated from experimental data of specific gravity and molecular weight for the C_7 group and the dead fluid. However, in this work, it was found that the determined constants needed to be adjusted in order to improve their accuracy when using the correlation for heavy SCN groups with $C_n > C_{20}$.

For instance, constants of a_{SG} and b_{SG} for a number of North Sea crude oils (Pedersen et al., 1991b) were calcuated using experimental data on C_7 group and the dead fluid. The specific gravities for SCN groups up to C_{20}/C_{30} were then estimated with Equation 5.5, and the estimated specific gravities were compared against experimental data. Figure 5.1 shows relative errors (i.e. relative error $\% = \frac{SG_{cal} - SG_{exp}}{SG_{exp}} \times 100$) for estimated specific gravities.

As shown in Figure 5.1, specific gravities estimated for SCN groups heavier than C_{20} show considerable deviations compared to the experimental data. But the compounds above C_{20} are the major wax forming constituents. Therefore, their specific gravities need to be accurately estimated for modelling the wax phase equilibrium.

Based on the data shown in Figure 5.1, it is suggested in this work that the values of a_{SG} and b_{SG} determined with the C_7 and the dead fluid data are further modified by a molecular-weight-depedent correction term, given by:

$$c_{SG,i} = 1 + (0.0126 MW_i - 2.2667) \times 0.01 \tag{5.6}$$

where $c_{SG,i}$ is the correction dividing factor for a_{SG} and b_{SG} when estimating the specific gravity of SCN group i. MW_i is the molecular weight of SCN group i.

The corrected constants, $a_{SG}/c_{SG,i}$ and $b_{SG}/c_{SG,i}$, were used for estimating the specific gravities for SCN groups and then compared with the experimental data. As shown in Figure 5.2, the estimated specipifc gravities for SCN groups heavier than C_{20} are closer to the experimental data when compared to Figure 5.1.

5.4.2. Estimation of n-Paraffin Concentration

As mentioned earlier, the correlation suggested by Pedersen (1995) is used for estimating n-paraffin concentrations in the extended new wax model. In this correlation, the n-paraffin concentration is related to the concentration, molecular weight and specific gravity for SCN groups, as expressed by:

$$z_{np,i} = z_{SCN,i}\left[1.0 - \left(A_{np} + B_{np} \times MW_i\right) \times \left(\frac{SG_{SCN,i} - SG_{np,i}}{SG_{np,i}}\right)^{C_{np}}\right] \tag{5.7}$$

where $z_{SCN,i}$ and $z_{np,i}$ are the mole fractions of SCN and n-paraffin. $SG_{SCN,i}$ and $SG_{np,i}$ are the specific gravities for SCN i and n-paraffin i with the same molecular weight (MW_i).

A_{np}, B_{np} and C_{np} in Equation 5.7 are constants, which express the effect of n-paraffin concentration on SCN specific gravity. Values of A_{np}, B_{np} and C_{np} are determined in this work by matching the experimental WDT data for the North Sea crude oils (Ronningsen et al., 1991, Pedersen et al., 1991b). The A_{np}, B_{np} and C_{np} values are listed in Table 5.2. The calculated WDTs are compared with the experimental data, as shown in Table 5.3, and will be discussed later.

5.4.3. Estimation of non-n-Paraffin Melting Point Temperature

In the new wax model, melting point temperatures (T_f) for non-n-paraffins are estimated by subtracting a constant value (D) from the n-paraffin melting point temperature (T_f), as given by:

$$T_{f,non-np,i} = T_{f,np,i} - D \tag{5.8}$$

where $T_{f,non-np,i}$ and $T_{f,np,i}$ are the melting point temperatures for non-n-paraffin and n-paraffin with the same carbon number. D is a constant, indicating that the melting point temperature of an n-paraffin is generally higher than that of a non-n-paraffin with the same molecular weight.

Constant D in Equation 5.8 was determined in this work by matching the amount of wax measured at 233 K for a waxy crude oil (Oil 3, Pedersen et al., 1991a). The wax amount measured with a pulsed nuclear magnetic resonance (NMR) technique was 10.5 mass%. An optimised D value was calculated as 70 K.

5.4.4. Flow-chart for Modelling Wax in Real Reservoir Fluids

Figure 5.3 summaries the procedure used in this work to generate the required concentration data using conventional fluid properties.

5.5. DISCUSSIONS

The wax model developed in Chapters 3 and 4 for synthetic mixtures, has been extended to real reservoir fluids, by developing the fluid characterisation approach to split the plus fraction into SCN groups, and further separate them into n-paraffins and non-n-paraffins, as described above. The new wax model is named as the HWWAX (Heriot-Watt WAX) model, in parallel with our hydrate model, HWHYD (Heriot-Watt HYDrate). They will be integrated into a general wax and hydrate model as described in Chapter 7.

In this section, I will evaluate the reliability of the HWWAX model by examining the approach used for splitting the plus fraction, and by discussing the effect of the method used for estimating the n-paraffin concentrations.

5.5.1. The Approach for Splitting the Plus Fraction

Discription of mole fraction and molecular weight

The experimental data on the mole fraction and molecular weight for SCN groups up to C_{20}/C_{30} are available for a number of North Sea crude oils in the literature (Pedersen et al., 1991b). Figures 5.4 – 5.6 show the match of developed distribution function to experimental data for crude oils 1, 2 and 3, respectively. The distribution function proved to be reliable for the other crude oils studied in this work.

Estimation of specific gravity

The specific gravities for SCN groups of the North Sea crude oils (Pedersen et al., 1991b) were calculated using several methods, such as the correlation suggested by Riazi et al. (1996), the logarithm function with and without correction of parameters. Figures 5.7 – 5.9 compare the estimated specific gravities against the experimental data for crude oils 1, 2 and 3, respectively. When using the logarithm function, the parameters modified with Equation 5.6 improved the calculation accuracy. It should be noted that the experimental specific gravity data on these oils were used for determining the correction coefficient in Equation 5.6.

Some independent experimental data on specific gravities for crude oils are available in the literature (Pan et al., 1997; Roehner et al., 2002). As shown in Figures 5.10 and 5.11, the specific gravities calculated using the logarithm function with the corrected parameters are in better agreement with the experimental data. The general correlation of Riazi et al. (1996) gives overestimated specific gravities for the oil reported by Pan et al. (1997) (as show in Figure 5.10), but underestimated values for the oil reported by Roehner et al. (2002) (as show in Figure 5.11).

5.5.2 Estimation of n-Paraffin Concentrations

The method based on specific gravity, as shown in Equation 5.7, was used in this work for the estimation of n-paraffin concentrations. The constants in the equation were optimised using the North Sea crude oils, for which WDTs were measured using the microscopy technique at a cooling and heating rate of 0.5 K/min (Ronningsen et al., 1991; Pedersen et al., 1991b). The calculated WDT data and the experimental data were compared in Table 5.3.

As shown in Table 5.3, the calculated WDTs are in good agreements with the experimental data for the majority of crude oils studied, indicating the reliability of the new wax model for real reservoir fluids. For instance, comparing Oil 6 with Oil 1, the heavy SCN molar distributions for the two oils are close, as shown in Figure 5.12. But the specific gravities for the heavy SCN groups of Oil 6 are lower than Oil 1, as shown in Figure 5.13. suggesting that Oil 6 may contain more n-paraffin and should have a higher WDT than Oil 1. This was indeed properly calculated with the new wax model. As shown in Table 5.3, the WDTs calculated for Oils 6 and 1 are 326 K and 323 K, respectively, in excellent agreement with the experimental data.

It should also be noted that there are some significant deviations between the model calculated WDTs and the experimental data for Oils 9, 12, 15, and 17, as shown in Table 5.3. Though the accuracy of experimental data can be questioned when using a visual technique and continuous heating to measure WDTs, this could also be attributed to the methods used in the model for estimating n-paraffin concentrations, which is based on specific gravities and may have limitations in some cases.

For instance, comparing Oil 17 with Oils 7 and 8 in Table 5.3, the measured WDT for Oil 17 is 315 K, and the experimental WDTs for Oils 7 and 8 are 326 K and 324 K, respectively. The calculated WDTs for Oils 17, 7 and 8 are 323 K, 323 K and 321 K, respectively. The higher WDT value calculated for Oil 17 is the result of a close molar distribution (Figure 5.14) and a low specific gravity (Figure 5.15) for the heavy SCN groups, when comparing with Oils 7 and 8. The molar distribution and specific gravity were calculated using the plus fraction splitting method described earlier.

This disagreement can be caused by the implicit assumption used in the n-paraffin concentration estimation method, i.e. that all non-n-paraffins have higher specific gravities than the n-paraffin with the same molecular weight. However, the specific gravities of iso-paraffin are generally lower than n-paraffins. So if a real reservoir fluid contains a significantly large amount of iso-paraffins, its n-paraffin concentrations can be overestimated, resulting in an overestimated WDT. Oil 17 might contain a relatively high quantity of iso-paraffins than Oils 7 and 8, which cannot be modelled by the current method.

The model can be improved by classifying real reservoir fluids according to their n-paraffinic, iso-paraffinic, naphthenic or aromatic natures, in order to suit different real fluids.

However, this is beyond the scope of this study due to lack of experimental data for the time being.

5.6. CONCLUSIONS

The wax model developed in Chapters 3 and 4 for synthetic mixtures has been extended to real reservoir fluids using an approach to split the plus fractions given by the conventional reservoir fluid analysis. The new wax model was named as the HWWAX model. The reliability of the new model will be examined by comparing its predictions with independent experimental data in Chapter 6.

The method and its features used to develop the HWWAX model for real fluid applications can be summarised below:

(1). Experimental data and field observations have indicated that hydrocarbons heavier than C_{20} are the major compounds of wax deposits; n-paraffins, iso-paraffins and naphthenes can all take part in wax formation, while the composition of n-paraffins is the determing factor for the wax phase boundary of real reservoir fluids, and the higher the n-paraffin concentration, the higher the WDT values. This is the basis of the HWWAX model for calculating wax phase equilibrium in real reservoir fluids.

(2). Hydrocarbons in reservoir fluids are classified as n-paraffins, iso-paraffins, naphthenes and aromatics, and their relative impacts on wax formation have been evaluated and modelled. The HWWAX model took into account different roles of these hydrocarbon classes in wax formation, considering that the wax phase boundary was determined by n-paraffins, while iso-paraffins, naphthenes and aromatics only contributed to the amount of precipitated wax.

(3). A plus fraction splitting method has been established. The programmes based on a Gamma distribution function was used for estimating the mole fraction and molecular weight, and a logarithmic function with corrected coefficients was adopted for calculating the specific gravity. A good agreement was observed between the estimated and experimental data of molar distribution and specific gravity distribution for heavy SCN groups.

(4). The correlation has been determined for estimating n-paraffin concentrations, using the data estimated from (3).

The HWWAX model can be used to predict the wax phase boundary, the amount and composition of the precipitated wax for different fluids. To model real reservoir fluids, the input data required are the standard oil compositions given by conventional analytical method used in the oil industry, such as concentrations, molecular weights and specific gravities of C_1, C_2, C_3, C_4, C_5, SCN groups up to C_{19}, and the C_{20+} fraction.

5.7. TABLES

Table 5.1. Melting point temperatures for several hydrocarbons.

Hydrocarbon	Melting point temperature/K
Normal tritetracontane, $C_{43}H_{88}$ CH_3-$(CH_2)_{41}$-CH_3	358
Methyl-di-heneicosyl-methane, $C_{44}H_{90}$ CH_3-$(CH_2)_{20}$-CH-$(CH_2)_{20}$-CH_3 CH_3	335
Nonyl-di-heicosyl-methane, $C_{52}H_{104}$ CH_3-$(CH_2)_{20}$-CH-$(CH_2)_{20}$-CH_3 C_9H_{19}	306

Table 5.2. The constants determined in this work for estimating the n-paraffin concentrations.

Constant	Value
A_{np}	0.8133
B_{np}	5.737×10^{-4}
C_{np}	0.1281

Table 5.3. Experimental data (Ronningsen et al. 1991) and the calculated WDTs for several North Sea crude oils.

	Exp. data	Calculated WDT and deviation (Dev.)	
Oil num.	WDT/K	WDT/K	Dev./K
1	323	323	0
2	324	321	-3
3	326	325	-1
5	323	327	4
6	326	326	0
7	326	323	-3
8	324	321	-3
9	319	325	6
10	315	317	2
11	323	323	0
12	311	321	10
15	323	317	-6
17	315	323	8

Oil num: oil numbers, the same as those in the literature.

5.8. FIGURES

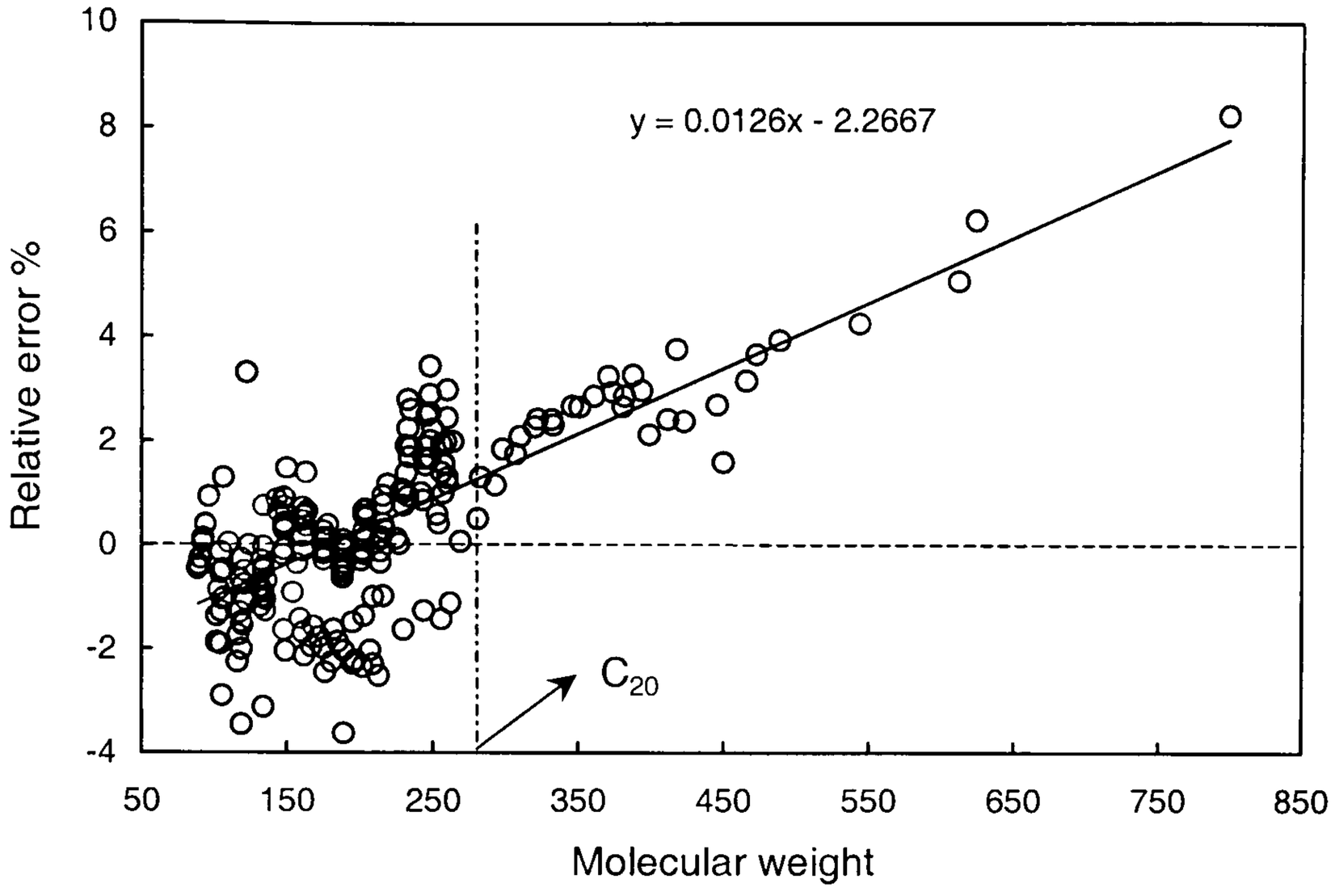

Figure 5.1. Relative errors (%) of specific gravities estimated using the logarithm function in conjunction with the directly obtained parameters (experimental data: Pedersen et al., 1991b).

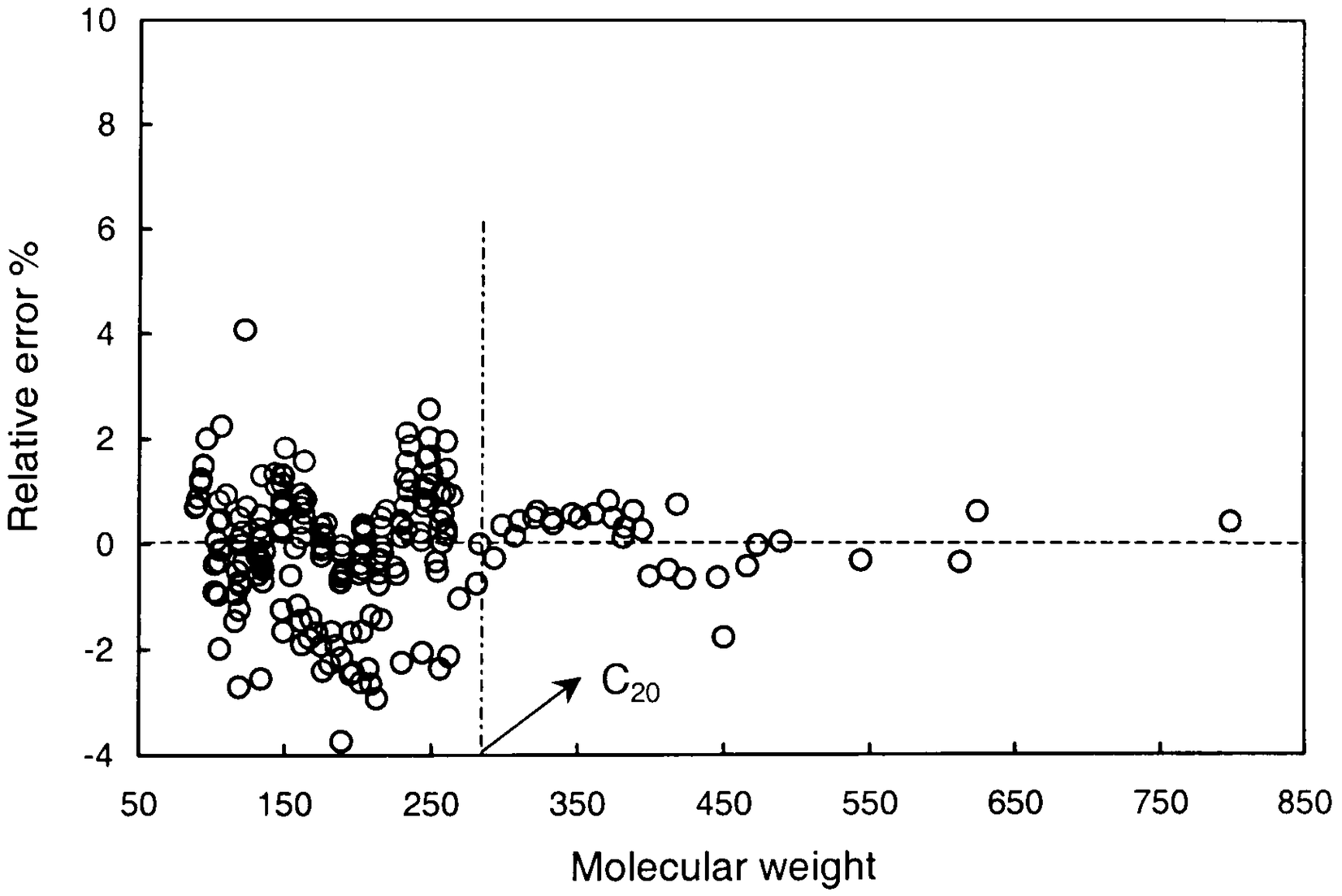

Figure 5.2. Relative errors (%) of specific gravities estimated using the logarithm function in conjunction with the corrected parameters (experimental data: Pedersen et al., 1991b).

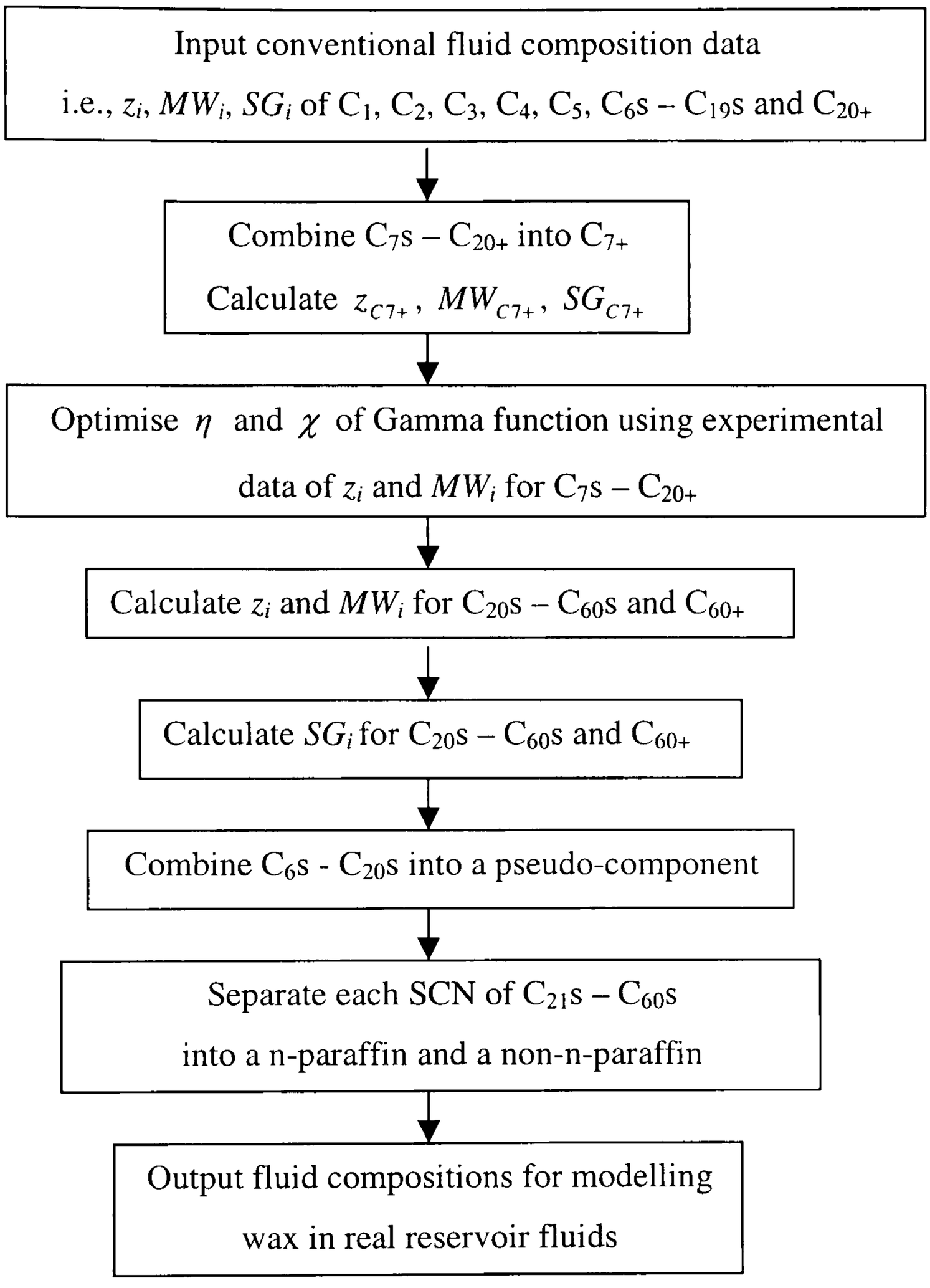

Figure 5.3. Flow-chart of generating fluid composition data to model wax in reservoir fluids.

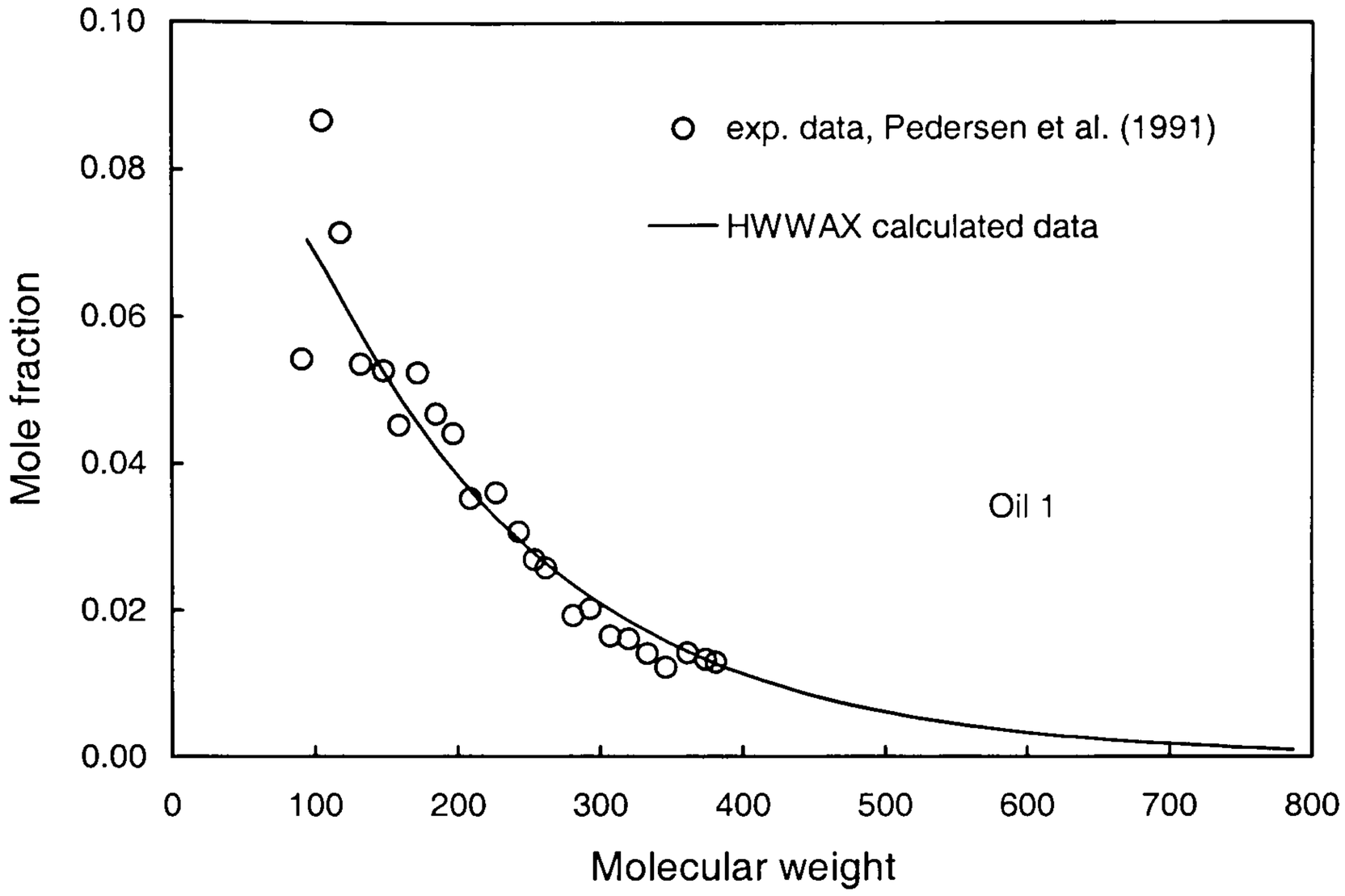

Figure 5.4. Experimental data (Pedersen et al., 1991b) and calculated SCN molar distributions for the North Sea crude oil 1.

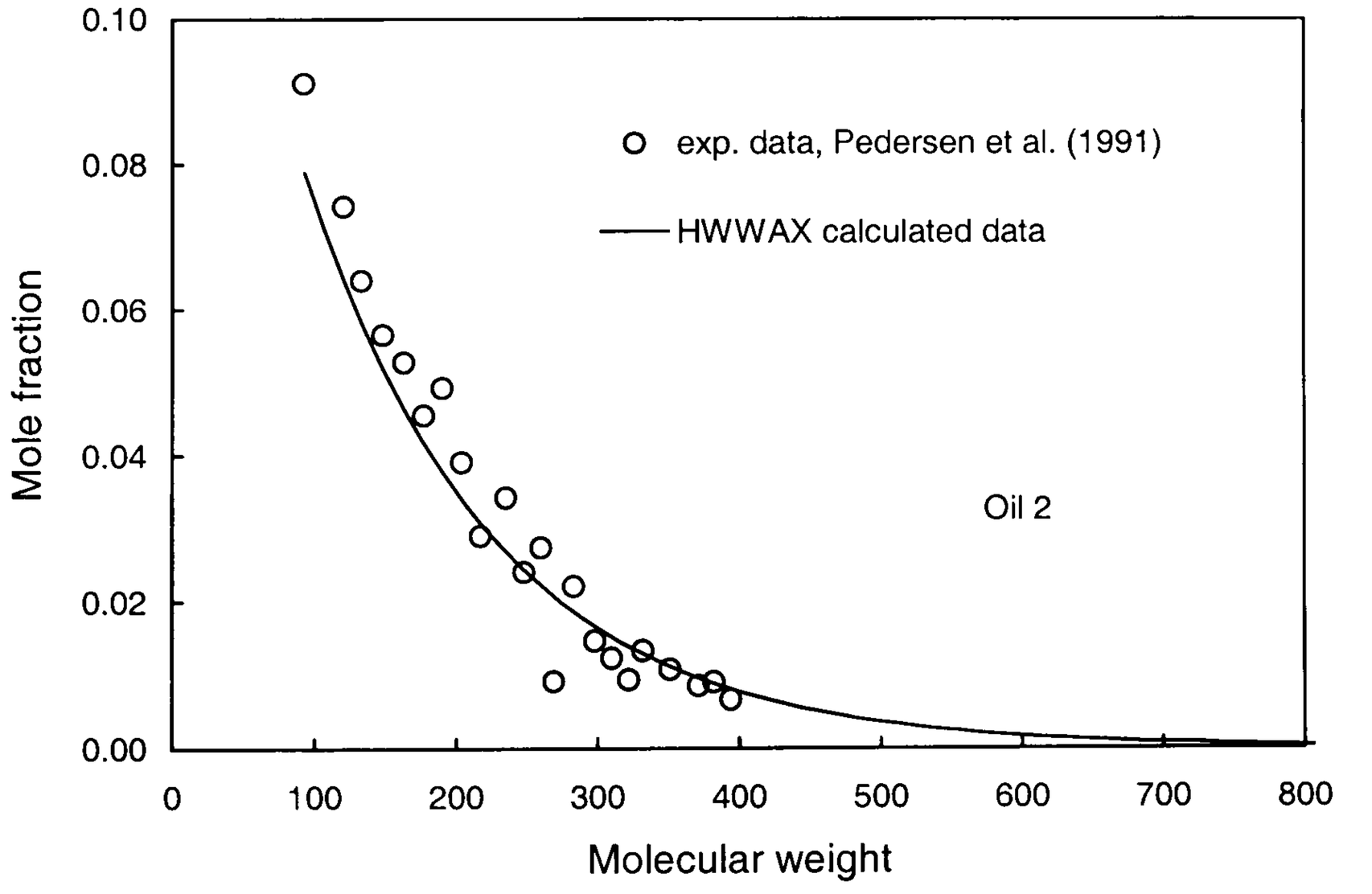

Figure 5.5. Experimental data (Pedersen et al., 1991b) and calculated SCN molar distributions for the North Sea crude oil 2.

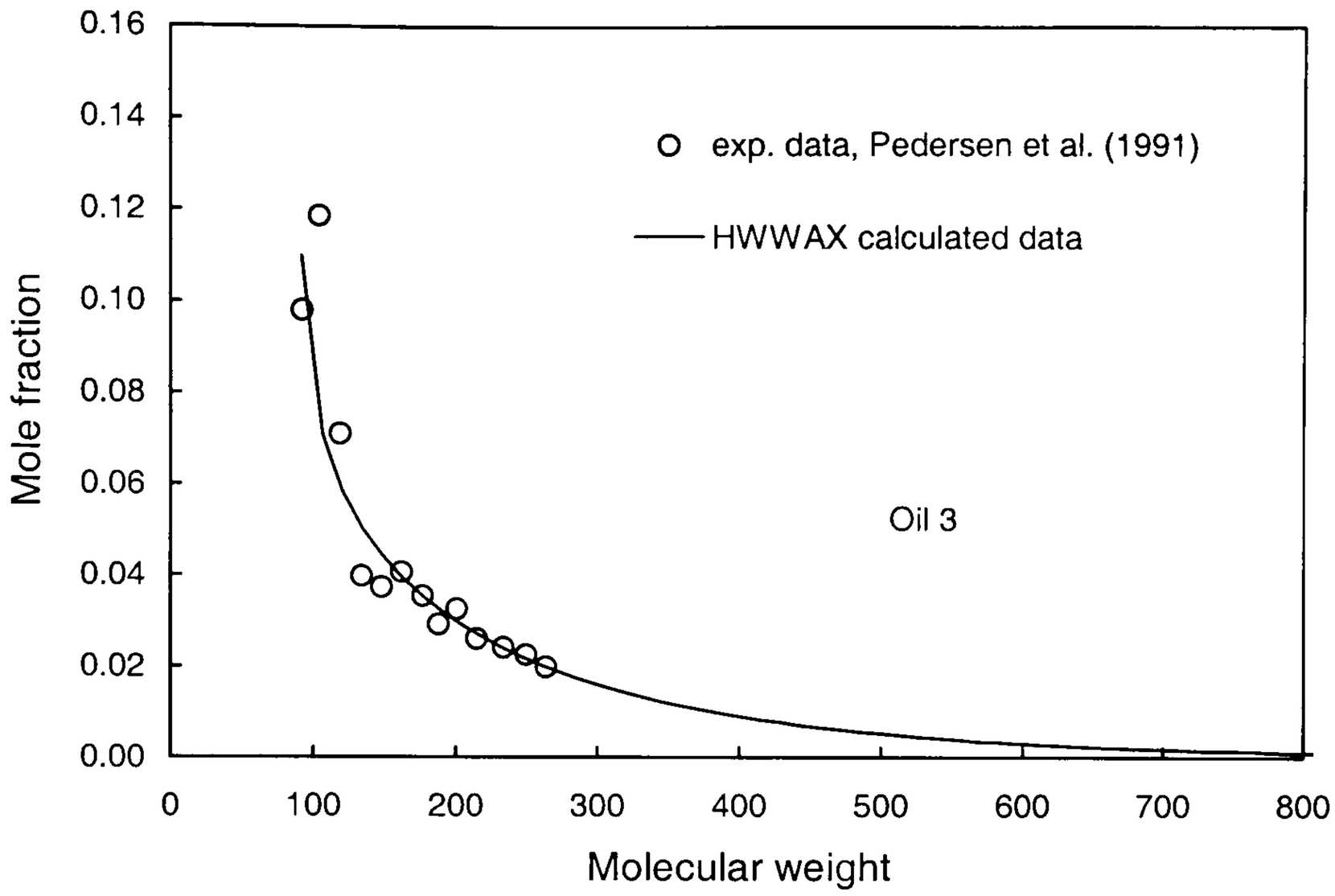

Figure 5.6. Experimental data (Pedersen et al., 1991b) and calculated SCN molar distributions for the North Sea crude oil 3.

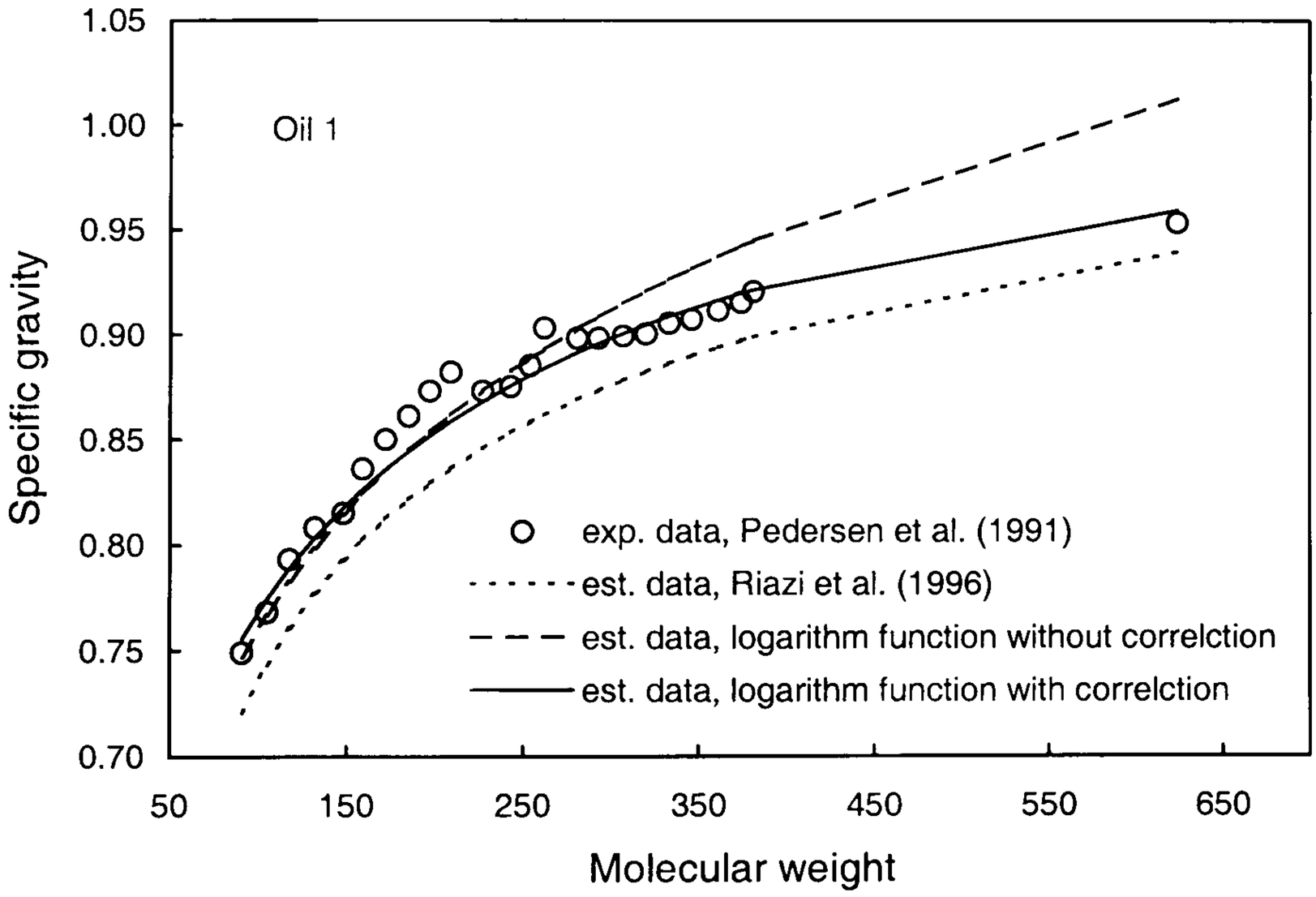

Figure 5.7. Experimental data (Pedersen et al., 1991b) and calculated SCN specific gravities against molecular weight for the North Sea crude oil 1.

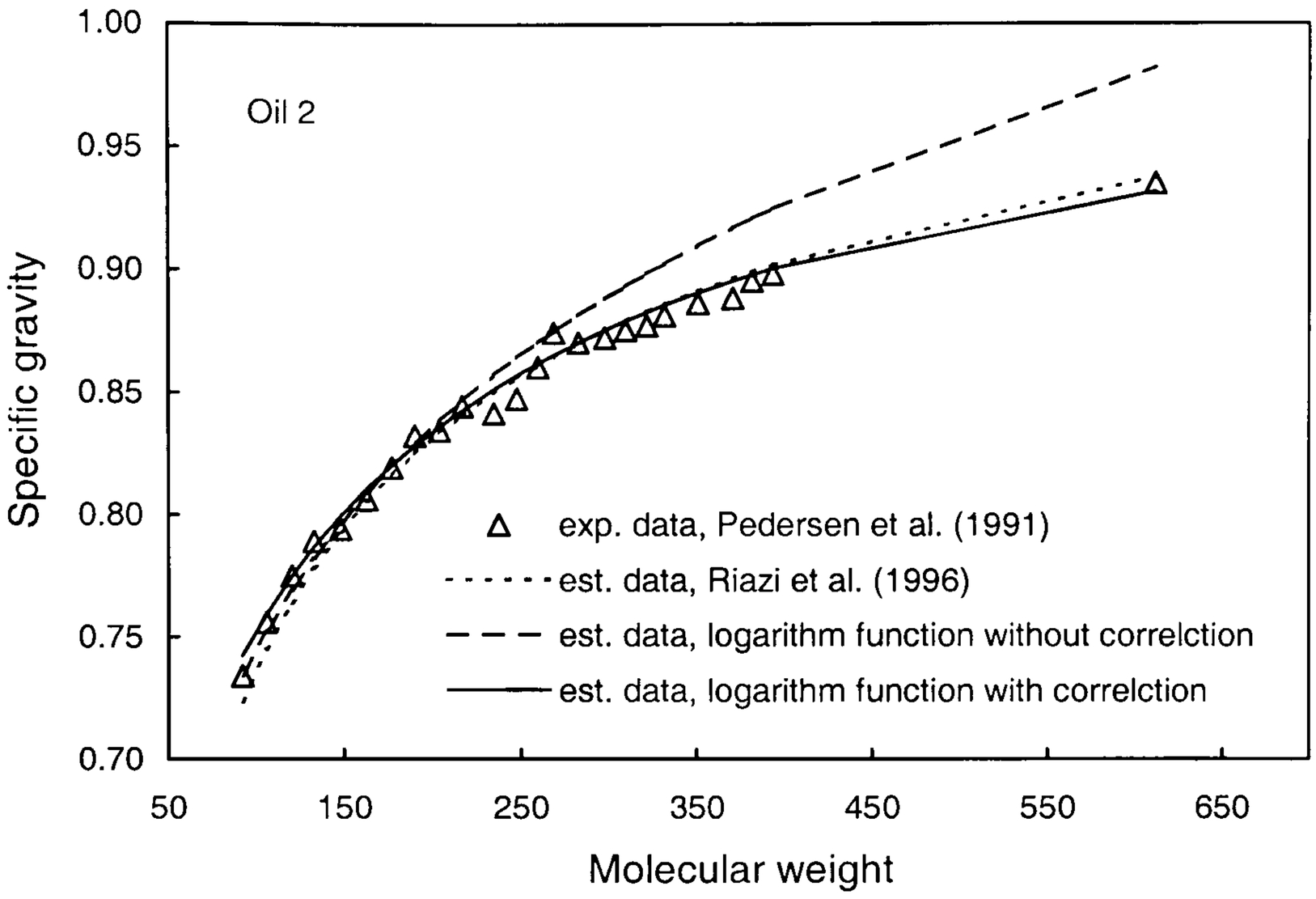

Figure 5.8. Experimental data (Pedersen et al., 1991b) and calculated SCN specific gravities against molecular weight for the North Sea crude oil 2.

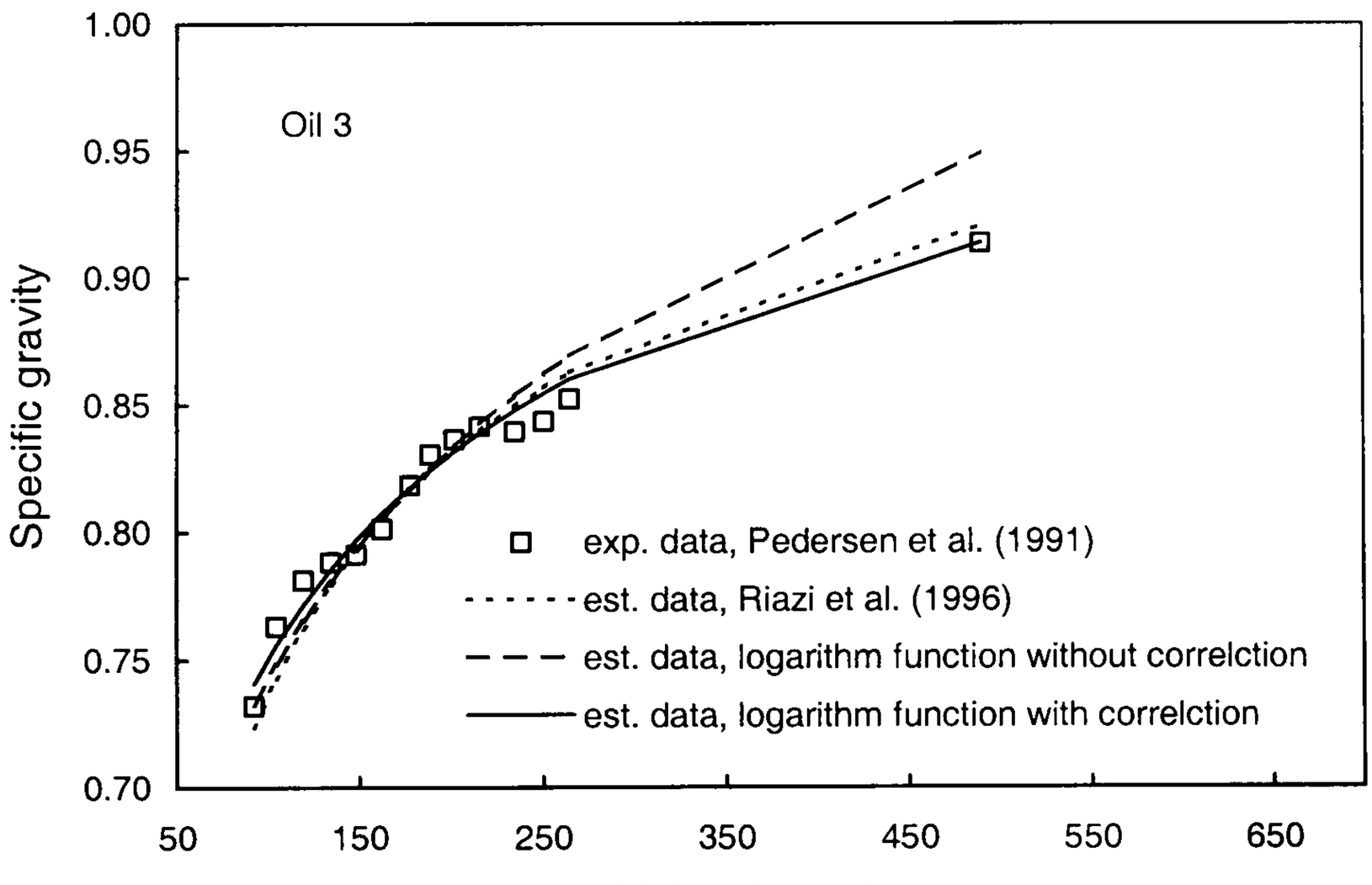

Figure 5.9. Experimental data (Pedersen et al., 1991b) and calculated SCN specific gravities against molecular weight for the North Sea crude oil 3.

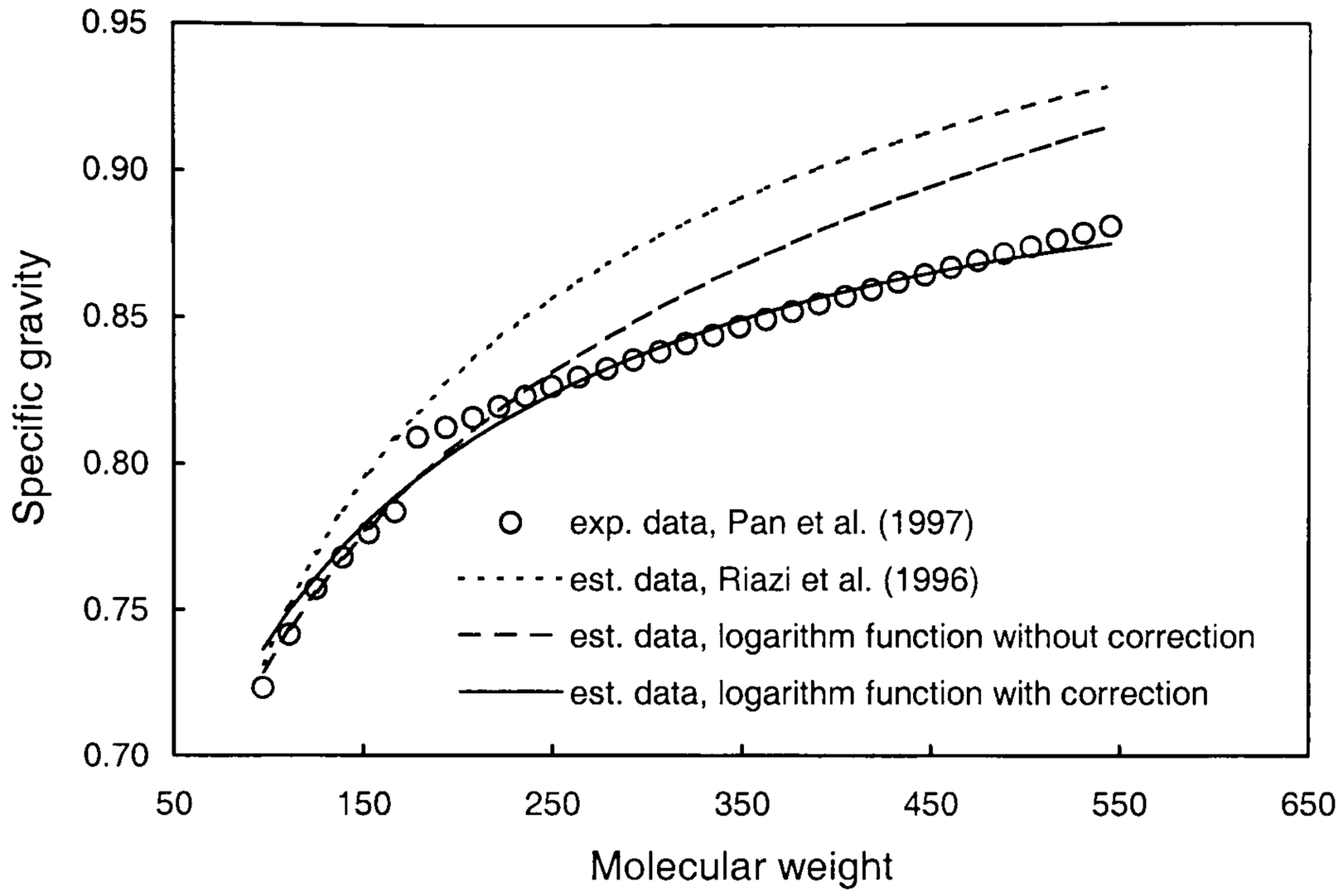

Figure 5.10. Independent experimental data (Oil 1, Pan et al., 1997) and predicted specific gravities using several correlations.

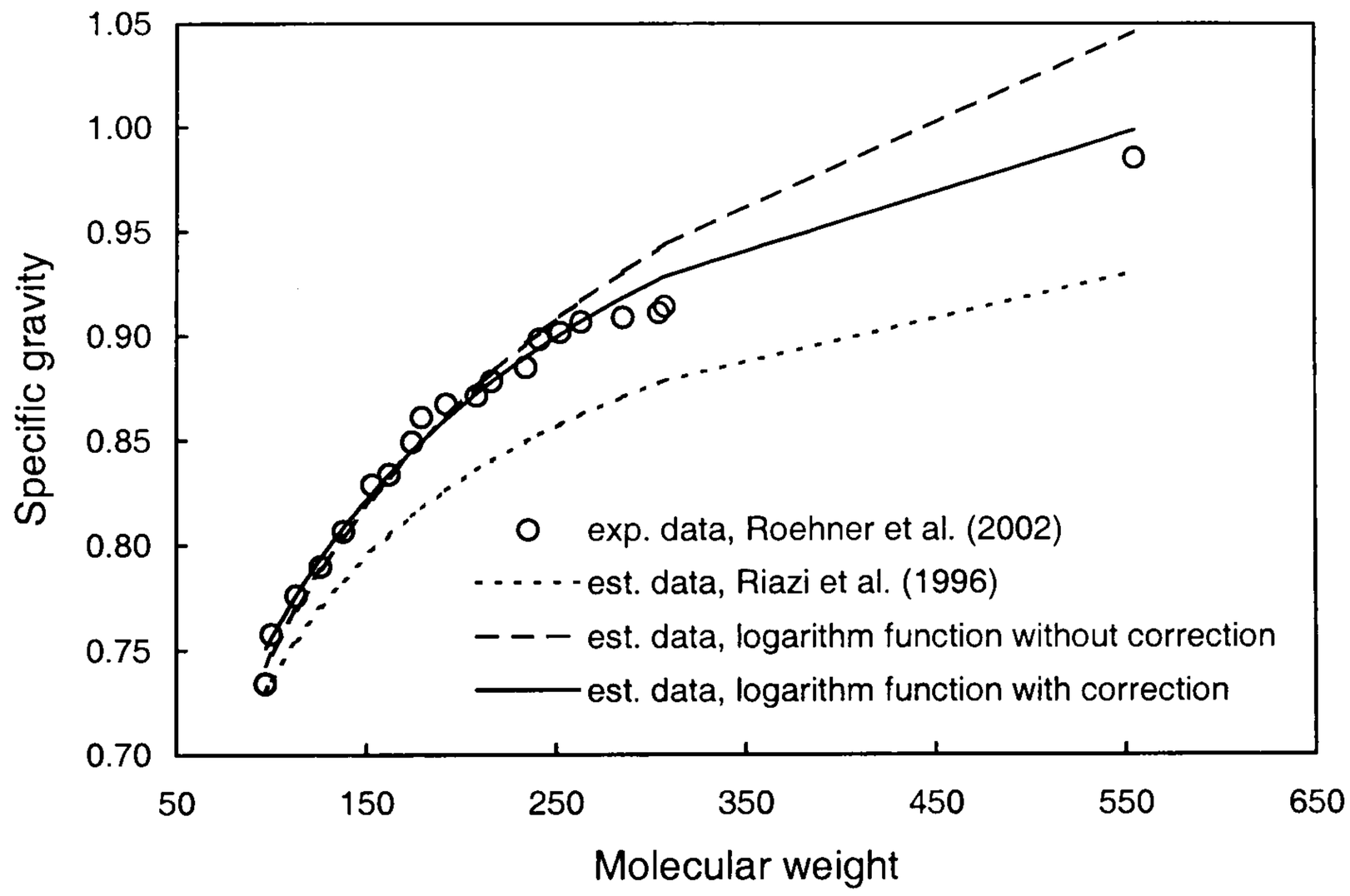

Figure 5.11. Independent experimental data (Roehner et al., 2002) and predicted specific gravities using several correlations.

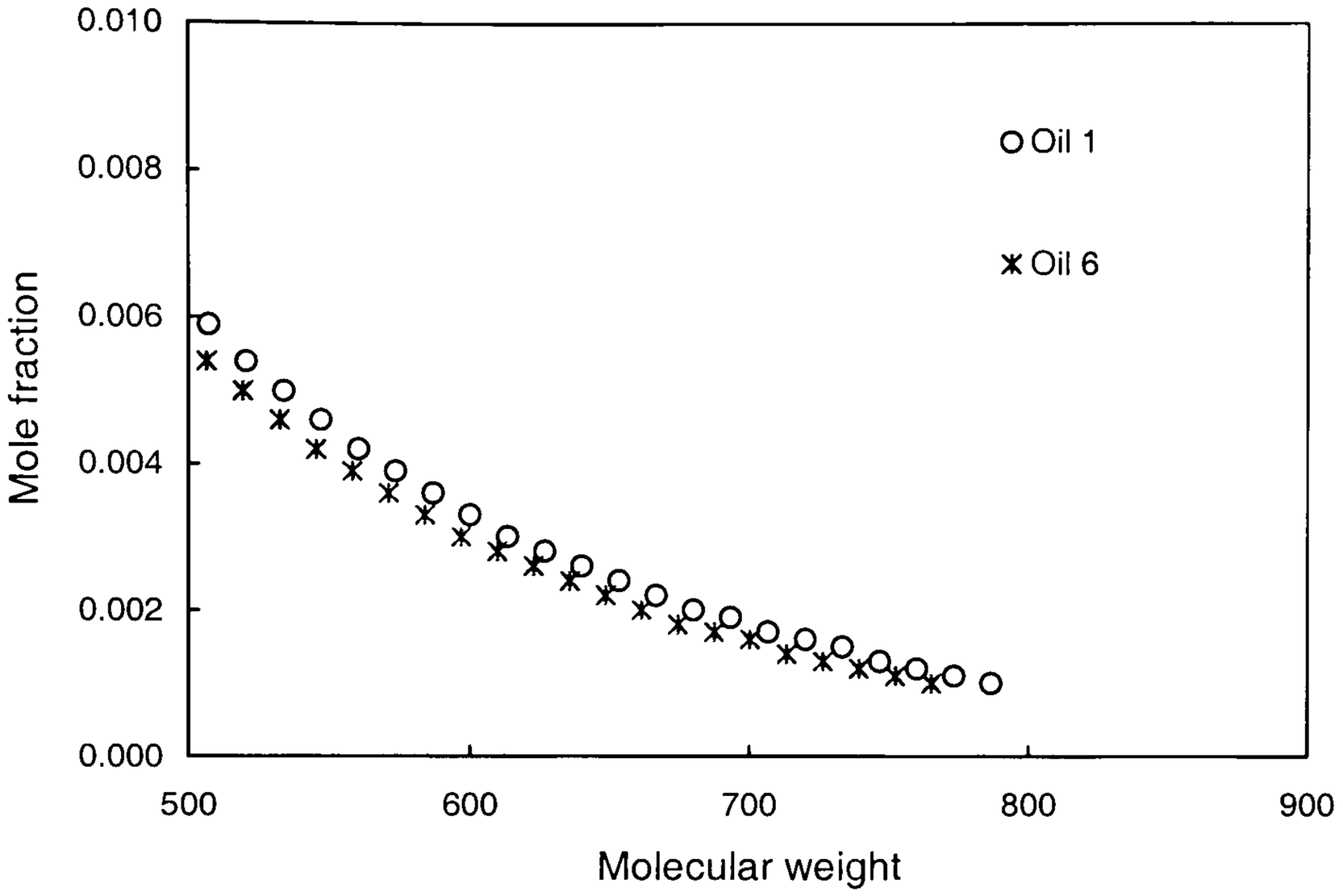

Figure 5.12. The SCN (heavier than C_{35}) molar distributions predicted for the North Sea Crude Oils 1 and 6.

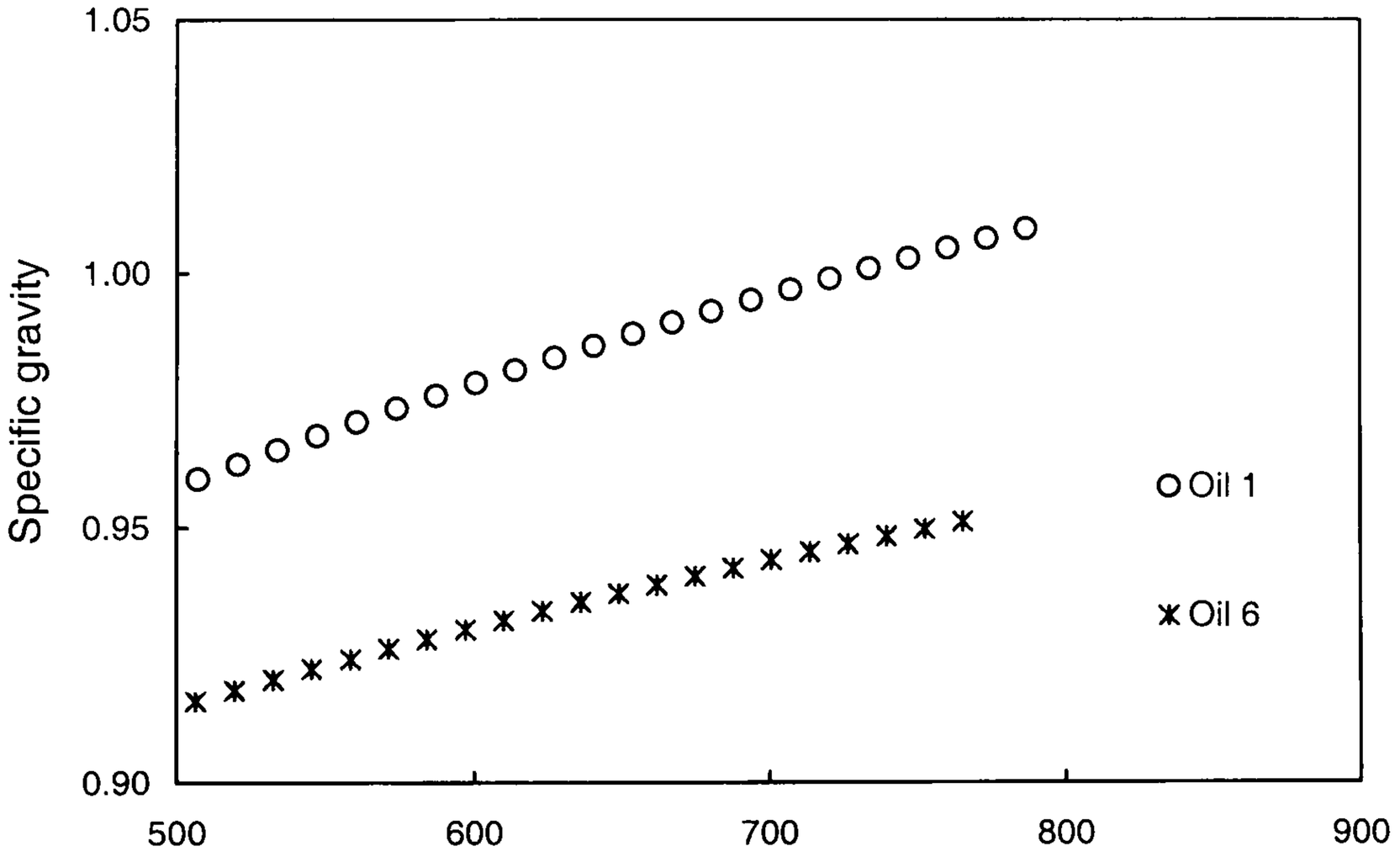

Figure 5.13. The SCN (heavier than C_{35}) specific gravities predicted for the North Sea Crude Oils 1 and 6.

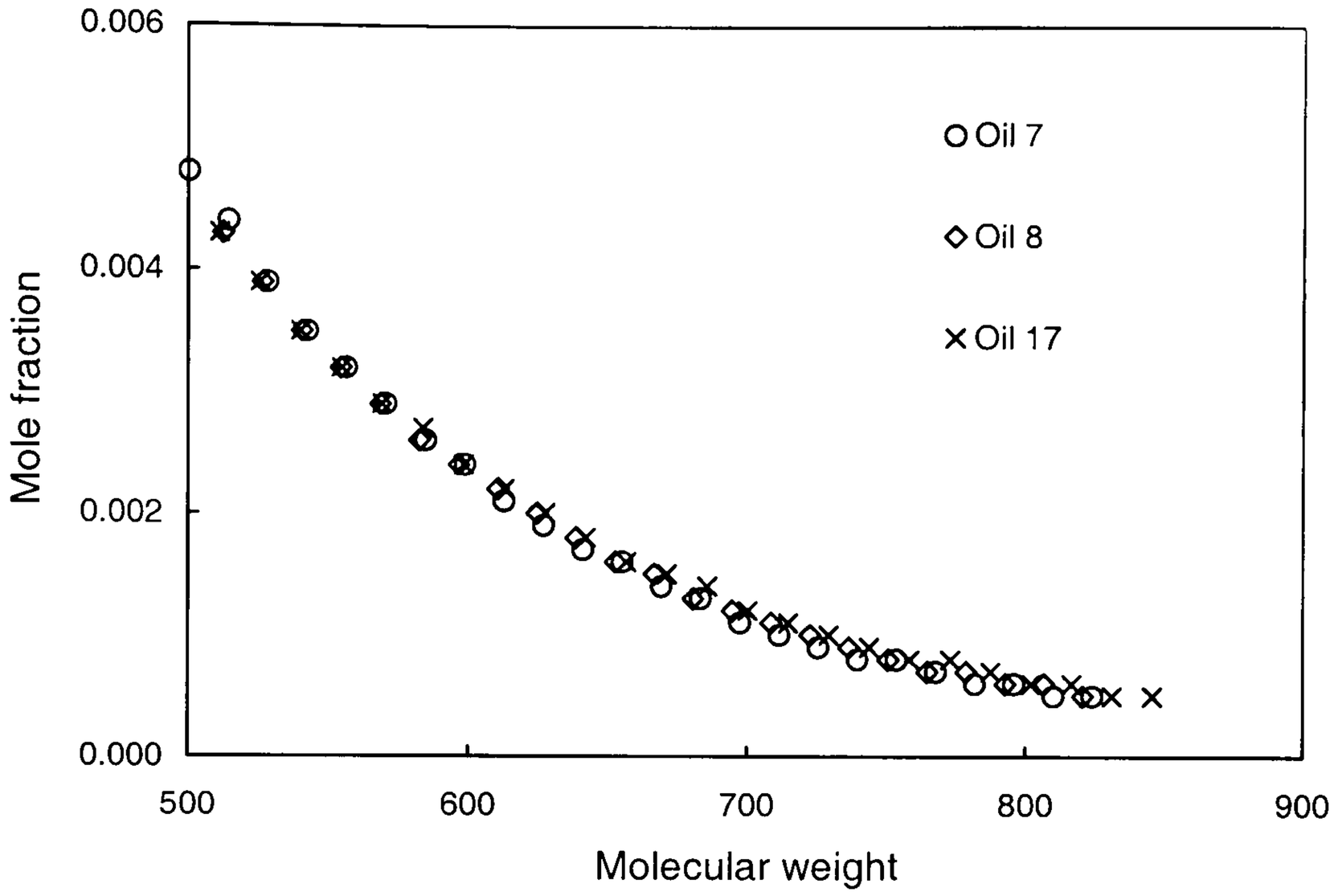

Figure 5.14. The SCN (heavier than C_{35}) molar distributions estimated for the North Sea Crude Oils 7, 8 and 17.

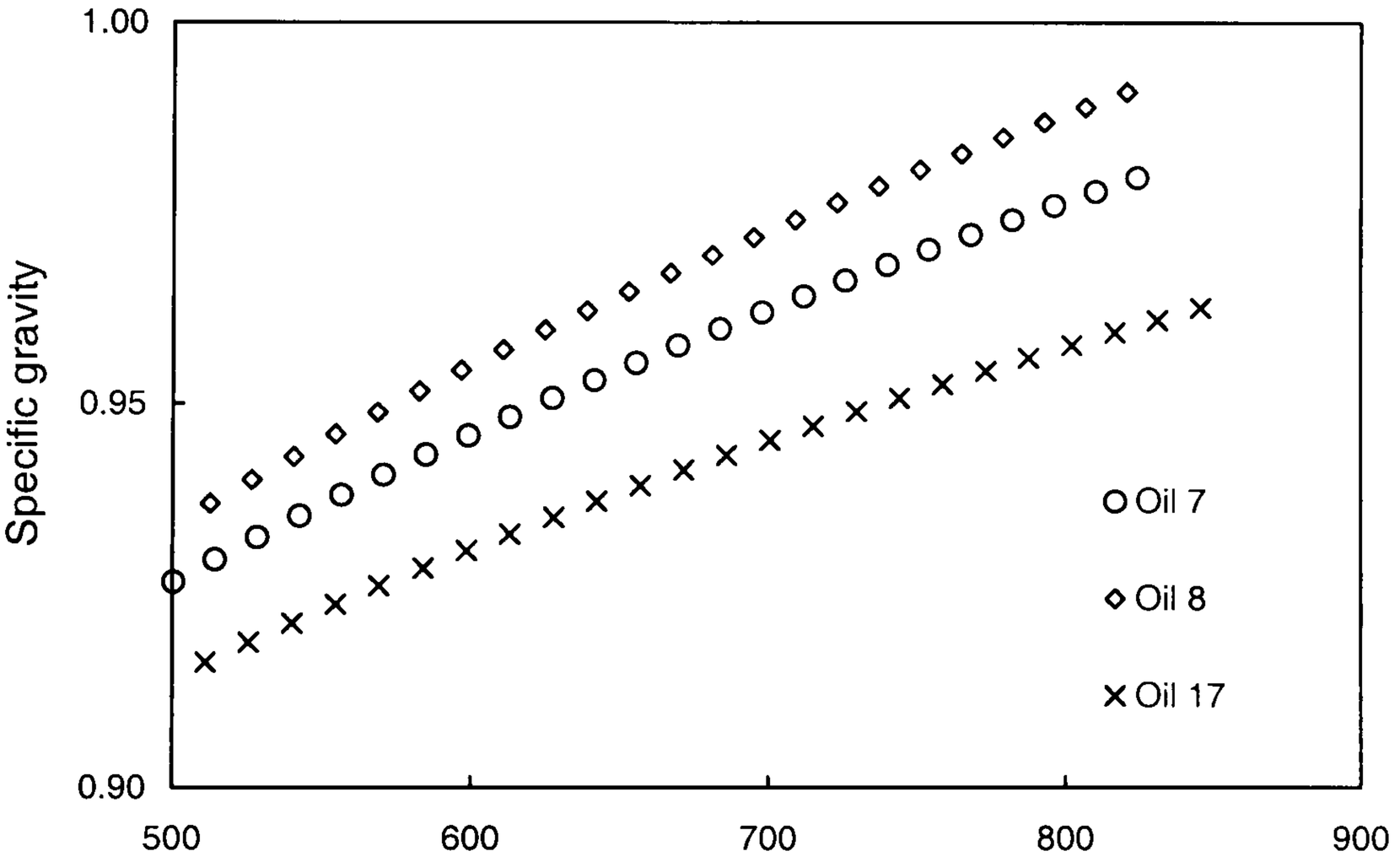

Figure 5.15. The SCN (heavier than C_{35}) specific gravities estimated for the North Sea Crude oils 7, 8 and 17.

CHAPTER-6

VALIDATION OF THE WAX MODEL

6.1. INTRODUCTION

In the development of the HWWAX model, first it was tuned using synthetic mixtures as described in Chapter 4, and then it was extended to real reservoir fluids in Chapter-5. The new model has the following improvements, modifications and new features over the existing wax models:

- New correlations with differentiation of odd or even carbon number were formulated for calculating the thermo-physical properties (e.g. fusion temperature, heat of fusion, heat capacity) of pure compounds with improved accuracy.

- The solid-solid transition was included into the thermodynamic equation for SLE calculations.

- The α functions of SRK and PR EoS were modified to consider heavy hydrocarbons at low temperatures. A single binary interaction parameter (BIP) was established for heavy hydrocarbons.

- A new approach based on the UNIQUAC equation was developed for describing wax solids.

- The effect of pressure on wax phase was included in the model using more reliable data of pure compound properties.

- For modelling real reservoir fluids, the roles of different hydrocarbons on wax formation were considered. N-paraffins were considered as the determining factor on

wax phase boundary, while the effect of iso-paraffins, naphthenes and aromatics on wax accumulation was also taken into account.

- A programme was developed for splitting the plus fraction into SCN groups and then separating each SCN heavier than C_{20} into an n-paraffin and a non-n-paraffin.

After these developments and modifications, the new wax model can be used for predicting the wax phase boundary, as well as the amount and composition of wax precipitated in different fluids. In this chapter, the reliability of predictions will be examined using independent experimental data generated in this laboratory and those available in the literature. These include:

- Wax phase boundaries.

The wax phase boundary can be plotted as WDT versus composition for binary and ternary systems. Experimental data with wide ranges of composition distributions will be used to validate the model, with special considerations on the accuracy of the thermo-physical properties, the inclusion of solid-solid transition, and the new formulation for describing wax solids.

For complex hydrocarbon systems, the wax phase boundary is based on WDT as a function of pressure. The effects of pressure and light end fractions on wax phase boundary will be examined by comparing the model predictions against experimental data.

- Amounts and compositions of wax formed.

The amounts and compositions of wax at different temperatures and pressures in a multi-component synthetic fluid will be predicted. The HWWAX predictions will be compared with the experimental data and the predictions using other existing wax models. The HWWAX model will also be examined and validated using literature experimental data on the amount of wax in various real reservoir fluids.

It is worth mentioning that, the experimental data (except those specially pointed out) used in this chapter for model validation have not been used in the model tuning as described in the previous chapters, so they are independent data. In the validation of the HWWAX model,

the SRK EoS modified in this work will be used. However, similar results can also be observed for the modified PR EoS.

6.2. WAX PHASE BOUNDARY

6.2.1. Validation of the Correlations for Fusion Properties and Heat Capacity

The new correlations for fusion properties and heat capacity developed in this work can be indirectly validated via comparing the model predictions with experimental WDT data for binary systems. For these binaries, the critical properties and acentric factors of the compounds involved are reported in ''Perry's Chemical Engineers' Handbook''. In addition, pure solids form in these binaries, due to the significant difference in molecular sizes of their components. Therefore, the accuracy of predicted WDTs for these binaries depends largely on the reliability of the fusion and heat capacity data.

As shown in Figure 6.1, the WDT predictions using the new model are in good agreement with the experimental data generated on C_6-C_{16} and C_6-C_{17} binaries in this work (Chapter-2). The curves in the figure also indicate that the reliability of the HWWAX model has been improved by the inclusion of a solid-solid transition in SLE calculations and the differentiation of odd and even carbon number.

6.2.2. Validation of the New Wax Solid Model

Experimental data for binaries and ternaries, generated in this laboratory or reported in the literature, are used for comparing several approaches for the description of wax solids. These include the ideal solid solution, the multi-pure-solid, Coutinho's UNIQUAC approach, and finally the HWWAX UNIQUAC approach (as described in Chapter-4). Compounds in the binaries and ternaries are lighter than C_{20}. Their critical properties and acentric factors have been measured experimentally and reported in reference handbooks (e.g. Perry's Chemical Engineer's Handbook). Hence the reliability of WDT predictions for these mixtures depends on the thermodynamic equation used for describing wax solids.

Binaries

Experimental WDT data have been generated for C_{16}-C_{18}, C_{16}-C_{20} and C_{15}-C_{19} binaries in this work (as given in Chapter-2), as shown in Figures 6.2-6.4. The wax phase boundaries of C_{16}-C_{18}, C_{16}-C_{20} and C_{15}-C_{19} are independently predicted using the ideal solid solution approach, the multi-pure-solid approach and Coutinho's UNIQUAC approach, as also shown in Figures 6.2-6.4.

The predictions using the ideal solid solution approach generally overestimate WDTs for all the binaries investigated (as shown in Figures 6.2 to 6.4). This suggests that the solid solution for these binaries is non-ideal, and the deviation from ideal is positive. As also shown in Figures 6.3 and 6.4, the multi-pure-solid approach is suitable for mixtures with components having significant differences in chain-length (e.g., C_{16}-C_{20} and C_{15}-C_{19} binaries), whereas, it is not satisfactory for binary systems with small molecular size difference (e.g., C_{16}-C_{18} system). Coutinho's UNIQUAC approach also shows limitations in the description of the non-ideality of solid solutions formed by n-paraffins with similar carbon numbers (e.g., C_{16}-C_{18} binary).

Experimental SLE data for C_{16}-C_{18}, C_{16}-C_{20} and C_{15}-C_{19} binaries have been used in the optimisation process for determining the constant in Equation 4.15 when developing the HWWAX UNIQAUC approach for describing wax solids. Calculated wax phase boundaries using HWWAX are compared with the experimental measurements, as shown in Figures 6.2 to 6.4.

Experimental WDT data for binary C_{17}-C_{19} system were reported (Robles et al., 1996). As shown in Figure 6.5, independent WDT predictions using the HWWAX model are in excellent agreement with the measurements, demonstrating the reliability of the approach used for describing wax solids.

Ternaries

Experimental WDT data for C_{14}-C_{15}-C_{16} and C_{18}-C_{19}-C_{20} ternaries were reported in the literature (Metivaud et al., 1999), and experimental WDT data for C_6-C_{16}-C_{17} ternaries were generated in this laboratory. As shown in Tables 6.1 to 6.3, the HWWAX predictions show very good agreement with the above experimental data over a wide range of compositional

distributions; generally the deviations are within 2 K. The ideal solid solution approach generally overestimates WDTs, while the multi-pure-solid approach and Coutinho's UNIQUAC approach shows significant deviations for some ternary systems.

6.2.3. Effects of Pressure and Light End on Wax Phase Boundary

Wax precipitation is normally induced by temperature reduction, but the effect of pressure on wax formation is also significant in some cases. Although wax may not form within operating temperatures at atmospheric pressure (the condition under which WATs and WDTs are often measured), wax precipitation may occur at higher pressures. The new wax model has the ability to predict wax phase boundaries at high-pressures.

Pressure can affect wax precipitation in two opposing ways. First, the gas solubility in liquid phase increases with an increase in the system pressure at conditions below the original mixture bubble point. This extra dissolved gas will reduce the relative mole fractions of heavy compounds in the liquid phase, which may reduce the tendency for wax formation. On the other hand, as pressure increases, the fusion temperatures of pure compounds will increase, and the wax phase boundary may shift to higher temperatures. The impact of pressure on fugacity of condensed phases away from the critical point is not very significant in comparison with the above two effects.

In a gas-liquid system, both factors mentioned above may affect the wax phase boundary. Depending on the dominant factor, the WDTs at high-pressures may be shifted with respect to the atmospheric pressure condition. Apparently, for a system above the saturation pressure, only the second factor will influence the wax phase boundary; the WDT will increase due to high pressure.

Binaries

Experimental WDT data for various binaries were reported in the literature (Vanderkooi et al., 1995; Peters et al, 1987). As shown in Figures 6.6 and 6.7, the bubble point pressures and WDTs independently predicted using the HWWAX model are in good agreement with experimental data for the C_1-C_{20} and C_2-C_{24} systems. Deviations between predicted WDTs and experimental data are less than 3 K over a wide range of compositional distribution. As also shown in Figures 6.6 and 6.7, compared to the fusion temperature (i.e., T_f) of the pure

heavier n-paraffin in the binaries, the presence of C_1 or C_2 reduces WDTs at pressures above bubble point pressures.

Multi-component mixtures with methane

Experimental data of bubble point pressure and WDT were reported for four mixtures containing C_1 with compositions given in Table 6.4 (Daridon et al., 1996).

Figure 6.8 shows the measured and predicted (using the HWWAX model) phase boundaries of SL/L, SLV/LV and L/LV for Mixture A. The predicted phase boundaries are in good agreement with the experimental data, indicating a good reliability in using HWWAX for predicting the influence of pressure and composition on WDT. It is noted that the experimental bubble pressure data were not used to tune the model, therefore the phase boundary predictions for this mixture are completely independent.

As also shown in Figure 6.8, when the operating pressure is below the bubble point pressure, wax can form in the system containing L+V phases. As shown on the wax phase boundary of SLV/LV, WDT decreases slightly as pressure increases, as a result of extra dissolved gas. As the pressure increases from atmospheric pressure to bubble point pressure (approximately 12 MPa), the WDT reduces by 3 K.

The influence of wax formation on bubble point pressure is also predicted using the HWWAX model. As shown in Figure 6.8, at temperatures within 20 K below WDTs, the predicted bubble point pressure increases slightly at lower temperatures due to solidification of heavy compounds leading to relatively higher mole concentration of light fractions in the liquid phase. However, due to small amounts of heavy fractions in the mixture, the increase in bubble point pressure is not siginificant. The bubble point pressure increases approximately by 0.2 MPa at most at temperatures below the WDT.

The measured (Daridon et al., 1996) and predicted (using the HWWAX model) phase boundaries for mixture B, C and D are shown in Figures 6.9 to 6.11. Similar to Mixture A, good agreement is observed beween the predictions and experimental data. The deviations of WDT predictions are –1 K, -3 K and –2 K for Mixture B, C and D, while the relative errors of predicted P_b are 6%, 7% and 3% for Mixture B, C and D, respectively. The predictions of P_b and WDT are independent of experimental measurements for these mixtures.

Multi-component mixtures without and with light ends (C_1-C_4)

The WDTs for several multi-component mixtures with and without light ends were measured in this laboratory, and they are also used for the model validation. The compositions of the mixtures without light ends are listed in Table A.1 (Appendix-A), and their experimental WDT data are given in Table A.2. The composition and WDT data for the mixtures with light ends are given in Tables A.3 and A.4.

As shown in Table A.1, mixtures A, B and C contain heavy components up to C_{30} or C_{36}. The measured and predicted wax phase boundaries for these mixtures are shown in Figure 6.12, which are reasonably in good agreement. The pressure effect on WDT is quite significant. As the pressure increases from 0.1 MPa to 40 MPa, the WDT increases by approximately 8 K.

Live fluids of B and C were prepared by mixing the dead mixtures with C_1 – C_4, and their bubble point pressures (P_b) were measured as given in Table A.3. In order to match the experimental P_b data, it is plausible to tune the binary interaction parameter (BIP) between the light compound with the highest mole concentration and the compounds predominantly in the liquid phase. A single BIP was tuned for C_1 against the pseudo-component (C_6-C_{20}) and the heavy components (C_n>C_{20}). The tuned BIP value of 0.12 was obtained for both live Fluids B and C. Then the wax phase boundaries were predicted for the live fluids, as also shown in Figure 6.12. A general agreement is observed between the predictions and experimental data with deviations between 1 and 2 K. Addition of light end to the system shifts the wax phase boundary toward lower temperatures.

Multi-component mixtures without and with natural gas

Multi-component Mixture D (Table A.1), containing components up to C_{40}, was prepared in this laboratory. The WDTs were measured at several pressures, as given in Table A.2.

A live fluid (Table A.3) was formed in the laboratory by adding natural gas into Mixture D. The fluid contains 42.85 mole% light ends. Its bubble point pressure (P_b) was measured as 12.6 MPa at 299 K. To match the experimental P_b data, a single binary interaction parameter was tuned as 0.06 for C_1 and hydrocarbons above C_6. The wax phase boundary for the live fluid was predicted using the HWWAX model, as shown in Figure 6.13. The measured and predicted wax phase boundaries for the dead Fluid D also are shown in the figure.

Reasonable agreements are observed between the predicted and measured WDTs in both cases. The prediction deviations are within 1 K for the mixture without light ends, and between 0 and 3 K for the fluid with light ends. It should be noted that there could be some errors in the measurement of WDT at pressures below the bubble point for the live fluid.

6.2.4. Real Reservoir Fluids

Three real reservoir fluids, North Sea crude oil LTA97-1, Base Condensate LTB98-1 and Black Oil RFS-1 (dead fluid), with compositions measured in Reservoir Fluid Studies Group and WDTs measured in Centre for Gas Hydrate Research, are used for the model validation. The fluid compositions based on the laboratory analysis are given in Tables A.7 – A.9.

In order to facilitate the modelling, the SCN groups from C_7 to C_{19} and C_{20+} were lumped into a C_{7+} fraction. Then the C_{7+} fraction was split into SCN groups up to C_{60}. For the splitting, Equations 5.3 and 5.4 were used to calculate the SCN mole fractions and molecular weights. The SCN specific gravities were calculated using Equations 5.5 and 5.6. Finally, the SCN groups from C_6 to C_{20} were grouped into one pseudo-component, and each SCN heavier than C_{20} was separated into an n-paraffin and a non-n-paraffin component using Equation 5.7.

The experimental and calculated SCN molar distributions for North Sea crude oil LTA97-1 are compared in Figures 6.14, while the measured and calculated SCN specific gravities are compared in Figure 6.15. Similarly, for Base Condensate LTB98-1, the calculated SCN molar distribution is compared with the experimental data in Figure 6.16, while the experimental and calculated SCN specific gravities are given in Figure 6.17. Figures 6.18 and 6.19 show the SCN molar distributions and the SCN specific gravity distributions for Black Oil RFS-1. Good agreement is observed between the calculated and experimental data for the three reservoir fluids investigated, indicating the reliability of the fluid characterisation programme developed in this work.

The WDTs were predicted using the HWWAX model, and compared with the experimental data measured using the QCM technique in this laboratory. As shown in Table 6.5, the predicted WDTs are very close to the measured values for Base Condensate LTB98-1 and Black Oil RFS-1 (dead fluid).

6.3. AMOUNT AND COMPOSITION OF WAX PRECIPITATED

6.3.1. Synthetic Mixture

Experimental data for the composition and amount of wax precipitated for a multi-component mixture under several temperature and pressure conditions have been reported in the literature (Pauly et al., 2001). Table 6.6 gives the composition data for the mixture. The mixture consists of consecutive normal alkanes from C_6 to C_{36}, with decreasing concentration as a function of increasing chain-length, representing a highly simplified crude oil system.

Amount of wax

The amounts of wax (mass % of the feed) predicted using different models (i.e., HWWAX, Coutinho's UNIQUAC approach, and the ideal solid solution approach) are compared against independent experimental data in Figure 6.20. It is obvious that the ideal solid solution approach overestimates the solid amounts over the whole temperature range (i.e., 256 K – 290 K). Predictions of the HWWAX model are in good agreement with the experimental data. As expected, the amount of wax deposit increases with a decrease in the system temperature.

The reliability of the HWWAX model for prediction of the pressure effect on wax deposition is also demonstrated in Figure 6.20. In this case, as the pressure increases from atmospheric pressure to 50 MPa, the amount of wax precipitated increases from 4.6 mass% to 9.3 mass% at 273.2 K.

Wax composition

Figure 6.21 shows the measured and predicted data for the wax composition (mass%) as a function of carbon number. Clearly, the ideal solid solution approach overestimates the amount of light components, especially for n-paraffins below C_{28}, in the precipitated wax. The predictions based on Coutinho's UNIQUAC approach are in reasonable agreement with the experimental data, but show significant deviation for heavy hydrocarbons over C_{30}. The predictions using the HWWAX model are in close agreement with the experimental data over a wide range of carbon number. The HWWAX model has greatly improved the predictions of wax composition. The predicted wax deposit at 290 K and 0.1 MPa consists

predominantly of paraffins heavier than C_{25}, which are in good agreement with the measured data.

Figure 6.22 shows the effect of temperature on the composition of wax precipitates (at 0.1 MPa). As temperature reduces, more light hydrocarbons take part in wax formation. The predictions of HWWAX are in good agreement with experimental data at different temperatures.

Figure 6.23 shows the impact of pressure on the wax composition. An increase in pressure has a similar effect as a reduction in temperature; both cause more light hydrocarbons to take part in the wax phase. The predictions using the HWWAX model are in good agreement with experimental data at different pressures.

6.3.2. Real Reservoir Fluids

The amounts of wax precipitated at different temperatures in several North Sea crude oils of different origins were measured using the Nuclear Magnetic Resonance (NMR) technique (Pedersen et al., 1991a). The wax amount measured at 233K for crude oil 3 was used for tuning the constant in Equation 5.8, in order to estimate the non-n-paraffin melting point temperatures (as described earlier in Chapter–5). The other experimental wax amount data were not used for tuning the HWWAX model, so they can be regarded as independent data to validate the HWWAX model. Figures 6.24 – 6.36 show the experimental and predicted (using the HWWAX model) wax amounts as a function of temperature for these crude oils.

The wax amounts in Oil 3 are also predicted using Won's model (1986). As mentioned in Chapters 4 and 5, modelling of wax for reservoir fluids in Won's model is based on SCN groups, and the ideal solid solution approach is used for describing the solid phase of wax. The heaviest SCN group that takes part wax formation is determined through matching the measured WDT (i.e. 326 K). As shown in Figure 6.26, the wax amounts predicted using Won's model (1986) are significantly higher than the experimental data. It is noted that, based on the predictions of Won's model, the majority of hydrocarbons heavier than C_{20} form wax at 273 K, which is not in agreement with the measurement.

As shown in figures 6.24 – 6.36, in general, a good agreement is observed between the experimental and wax amounts predicted using the HWWAX model for the oils studied,

except that the wax amounts for crude oil 1 were overestimated and the wax amounts for Oils 5 and 11 were underestimated by the model.

It was reported that Oil 1 was a 'biodegraded aromatic oil', and Oil 11 was 'heavy, biodegraded, naphthenic oil' (Pedersen et al., 1991a). It is speculated that Oil 1 may contain more aromatic fractions, and Oil 11 may contain more naphthenic fractions, comparing with the other oils. These could be the reason for the overestimation of wax amount for Oil 1 and the underestimation of wax amount for Oil 11, since the HWWAX model has not been tuned to differentiate the effects of aromatic and naphthenic relative amounts on wax accumulation. In fact, in the model, iso-paraffin, naphthene and aromatic fractions in each SCN group are all lumped into one pseudo-component designated as non-n-paraffin, which is assumed contributing to wax accumulation. However, aromatics actually do not form wax. In this work, no attempt was made to differentiate aromatic components from the others, due to lack of experimental data. Therefore, for crude oils with significant amounts of aromatics, e.g. Oil 1 (Figure 6.24), the model overestimates the amount of wax deposited. On the other hand, for crude oils with relatively high amounts of iso-paraffins or naphthenes, e.g. Oil 11 (Figure 6.33), the wax amounts are generally underestimated.

Oil 5 was reported as a 'waxy oil' (Pedersen et al., 1991a). Oil 5 could be rich with iso-paraffins and/or naphthenes, consequently the amount of wax could be underestimated using the HWWAX model, as shown in Figure 6.27.

6.4. CONCLUSIONS

In this chapter, the HWWAX model has been applied to various synthetic mixtures and real reservoir fluids, in order to examine and validate the model against experimental data generated in this laboratory or available in the literature. Most of the experimental data used here were not used for tuning the model, so they are considered as independent and viable for the validation purpose.

The model was examined in terms of wax phase boundary (i.e. WDT) and the amount of wax deposited at various temperature and pressure conditions. In general, for synthetic mixtures when the details of their compositions were known, excellent agreement between the model

predictions and the experimental data was observed. For real reservoir fluids with limited compositional data, the model also showed good reliability.

The new correlations for calculating the thermo-physical properties of pure compounds and the inclusion of solid-solid transition were examined using reliable experimental data of binary systems generated in this laboratory. The HWWAX model has demonstrated significant improvement in predicting WDTs.

The new wax solid model was validated using WDT data for various binary and ternary systems, and was compared against the existing models, such as the ideal solid solution, multi-pure-solid and Countiho's UNIQUAC approach. Comparing to the experimental data, the new model has reduced the prediction deviations to within 2 K from approximately 7-10 K of the existing models.

One important improvement of the HWWAX model is the inclusion of pressure effect on wax phase by using more reliable data of pure compound properties. This has been validated using binary and multi component mixtures with and without light ends (C_1 to C_4 or natural gas mixture). The comparison between predicted and experimental data indicated that the HWWAX model has excellent capability for modelling the pressure effect by considering both gas solubility and the fusion temperature of pure compounds under pressures.

Various real reservoir fluids have been used to validate the HWWAX model for predicting WDT and the amount of wax deposited at different temperatures. Generally, the model can provide acceptable WDT and wax amount predictions for different real reservoir fluids using the compositional data generally provided in the petroleum industry. It is also realised that the HWWAX model can be further improved by differentiating the effects of aromatics against iso-paraffins and naphthenes on wax accumulation when new experimental data are available.

6.5. TABLES

Table 6.1. Experimental WDT data (Metivaud et al., 1999) and different model predictions for C_{14}-C_{15}-C_{16} ternary, at 0.1MPa.

Experimental data			Predictions and deviations (Dev)								
				Ideal solid solution		Mutli-pure-solid		Countinho UNIQUAC		HWWAX	
Mole fraction			Exp. WDT /K	WDT /K	Dev /K	WDT /K	Dev /K	WDT /K	Dev /K	WDT /K	Dev /K
C_{14}	C_{15}	C_{16}									
0.06	0.57	0.37	283	287	4	277	-6	280	-3	285	2
0.14	0.23	0.63	285	288	3	284	-1	285	0	287	2
0.17	0.06	0.77	286	289	3	287	1	287	1	288	2
0.24	0.33	0.43	282	286	4	279	-3	281	-1	284	2
0.21	0.56	0.23	281	285	4	272	-10	276	-5	283	2
0.27	0.66	0.07	280	283	3	275	-5	278	-2	281	1
0.37	0.05	0.58	283	287	4	283	0	284	1	285	2
0.32	0.24	0.44	282	286	4	280	-2	281	-1	284	2
0.43	0.33	0.24	279	284	5	272	-7	276	-3	281	2
0.57	0.17	0.26	278	284	6	273	-5	276	-2	280	2
0.73	0.14	0.13	276	282	6	274	-2	275	-1	279	3

Table 6.2. Experimental WDT data (Metivaud et al., 1999) and different model predictions for C_{18}-C_{19}-C_{20} ternary, at 0.1MPa.

Experimental data			Predictions and deviations (Dev)								
			Exp.	Ideal solid solution		Mutli-pure-solid		Countinhos UNIQUAC		HWWAX	
Mole fraction			WDT	WDT	Dev	WDT	Dev	WDT	Dev	WDT	Dev
C_{18}	C_{19}	C_{20}	/K	/K	/K	/K	/K	/K	/K	/K	/K
0.02	0.02	0.96	309	310	1	309	0	309	0	309	0
0.05	0.05	0.9	309	309	0	309	-1	309	0	309	0
0.05	0.9	0.05	305	305	0	303	-2	304	-1	305	0
0.1	0.1	0.8	308	309	1	307	-1	307	-1	308	0
0.1	0.4	0.5	306	308	2	302	-4	303	-3	306	0
0.1	0.55	0.35	306	307	1	298	-8	300	-6	305	-1
0.14	0.73	0.13	304	306	2	300	-4	301	-3	304	0
0.15	0.15	0.7	307	308	1	306	-1	306	-1	307	0
0.2	0.2	0.6	306	308	2	304	-2	305	-1	306	0
0.2	0.6	0.2	305	306	1	296	-9	296	-10	304	-1
0.26	0.26	0.48	306	307	1	301	-5	302	-4	305	-1
0.33	0.33	0.34	304	306	2	298	-7	299	-5	303	-1
0.4	0.1	0.5	305	307	2	302	-3	303	-2	304	-1
0.43	0.43	0.14	303	304	1	292	-11	297	-6	302	-1
0.48	0.15	0.37	304	306	2	299	-6	300	-4	303	-1
0.6	0.2	0.2	302	304	2	295	-8	295	-7	301	-1
0.79	0.11	0.1	301	303	2	298	-3	299	-2	300	-1
0.9	0.05	0.05	301	302	1	299	-2	300	-1	301	-1

Table 6.3. Experimental WDT data (this laboratory) and different model predictions for C_6-C_{16}-C_{17} ternary, at 0.1MPa.

Experimental data			Predictions and deviations (Dev)								
			Exp.	Ideal solid solution		Mutli-pure-solid		Countinhos UNIQUAC		HWWAX	
Mole fraction			WDT	WDT	Dev	WDT	Dev	WDT	Dev	WDT	Dev
C_6	C_{16}	C_{17}	/K	/K	/K	/K	/K	/K	/K	/K	/K
0.911	0.048	0.041	261	265	4	254	-7	258	-3	261	0
0.905	0.04	0.055	263	266	3	257	-6	260	-3	262	-1
0.794	0.156	0.051	271	273	2	267	-4	268	-3	270	-1

Table 6.4. Compositions of four mixtures containing methane (Daridon et al. 1996).

	Mole%			
Compound	A	B	C	D
C_1	43.70	43.80	43.60	44.00
C_{10}	46.10	45.90	46.15	45.80
C_{18}	0.00	1.65	1.33	6.80
C_{19}	0.00	1.43	1.27	0.00
C_{20}	3.27	1.25	1.16	0.00
C_{21}	2.24	1.15	1.10	0.00
C_{22}	1.53	0.91	1.04	0.00
C_{23}	1.05	0.78	0.98	0.00
C_{24}	0.72	0.67	0.92	0.00
C_{25}	0.49	0.58	0.87	0.00
C_{26}	0.34	0.50	0.81	0.00
C_{27}	0.23	0.43	0.77	0.00
C_{28}	0.16	0.37	0.00	0.00
C_{29}	0.11	0.31	0.00	0.00
C_{30}	0.07	0.27	0.00	3.40

Table 6.5. Experimental (this laboratory) and predicted (using the HWWAX model) WDTs for real reservoir fluids, at 0.1 MPa.

Resevoir fluids	Experimental WDT/K	Predicted WDT/K
LTA97-1	328	321
LTB98-1	309	308
RFS-1 (dead fluid)	323	319

Table 6.6. Compositions for the multi-component mixture representing a highly simplified crude oil system (Pauly et al., 2001).

Component	Mole%	Component	Mole%
C_6	19.50	C_{22}	0.62
C_7	15.92	C_{23}	0.50
C_8	12.68	C_{24}	0.40
C_9	10.19	C_{25}	0.32
C_{10}	8.20	C_{26}	0.26
C_{11}	6.50	C_{27}	0.21
C_{12}	5.24	C_{28}	0.17
C_{13}	4.20	C_{29}	0.13
C_{14}	3.39	C_{30}	0.11
C_{15}	2.77	C_{31}	0.09
C_{16}	2.24	C_{32}	0.07
C_{17}	1.80	C_{33}	0.06
C_{18}	1.45	C_{34}	0.04
C_{19}	1.18	C_{35}	0.03
C_{20}	0.95	C_{36}	0.03
C_{21}	0.76		

6.6. FIGURES

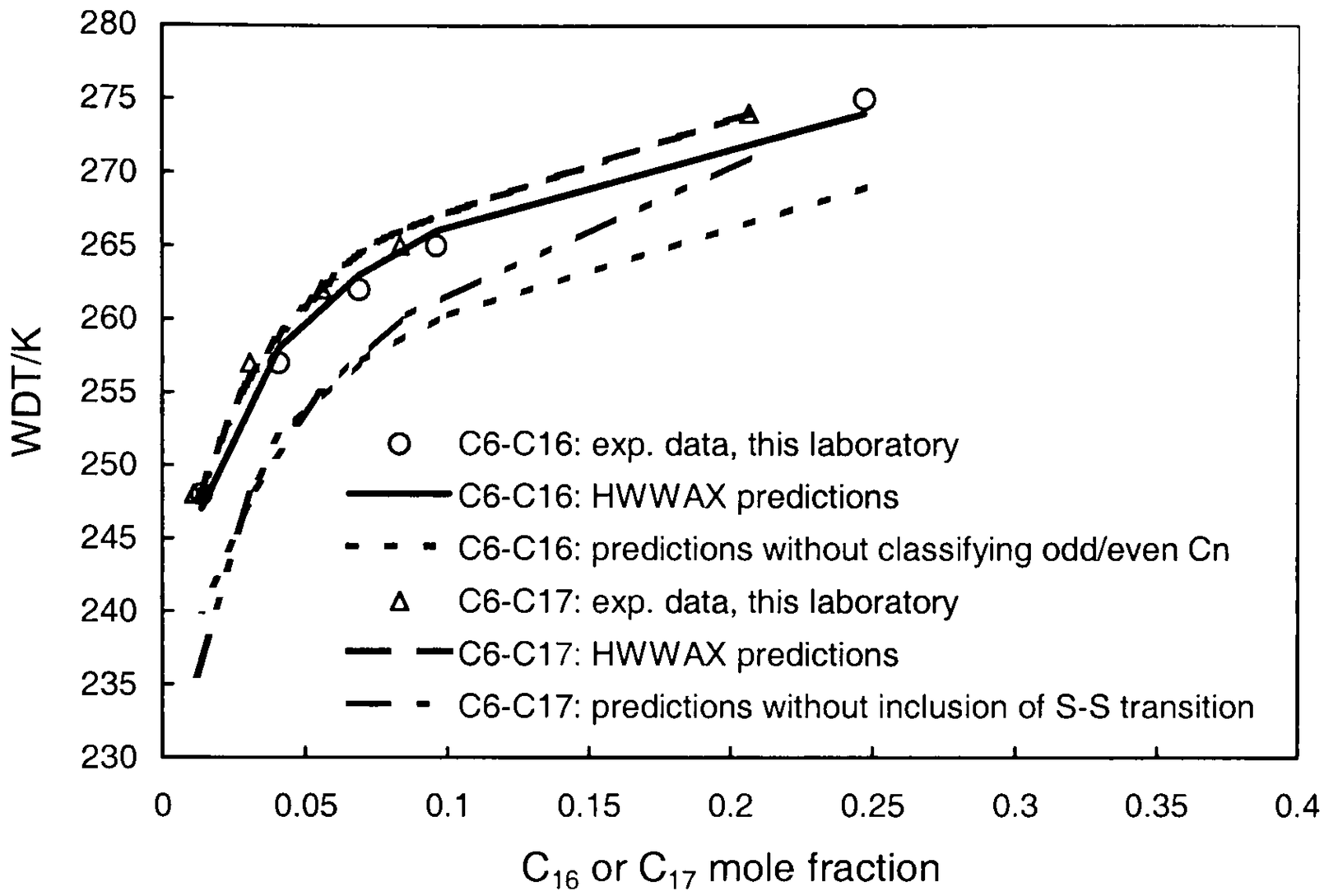

Figure 6.1. Experimental (this work) and predicted WDTs for C_6-C_{16} and C_6-C_{17} binaries.

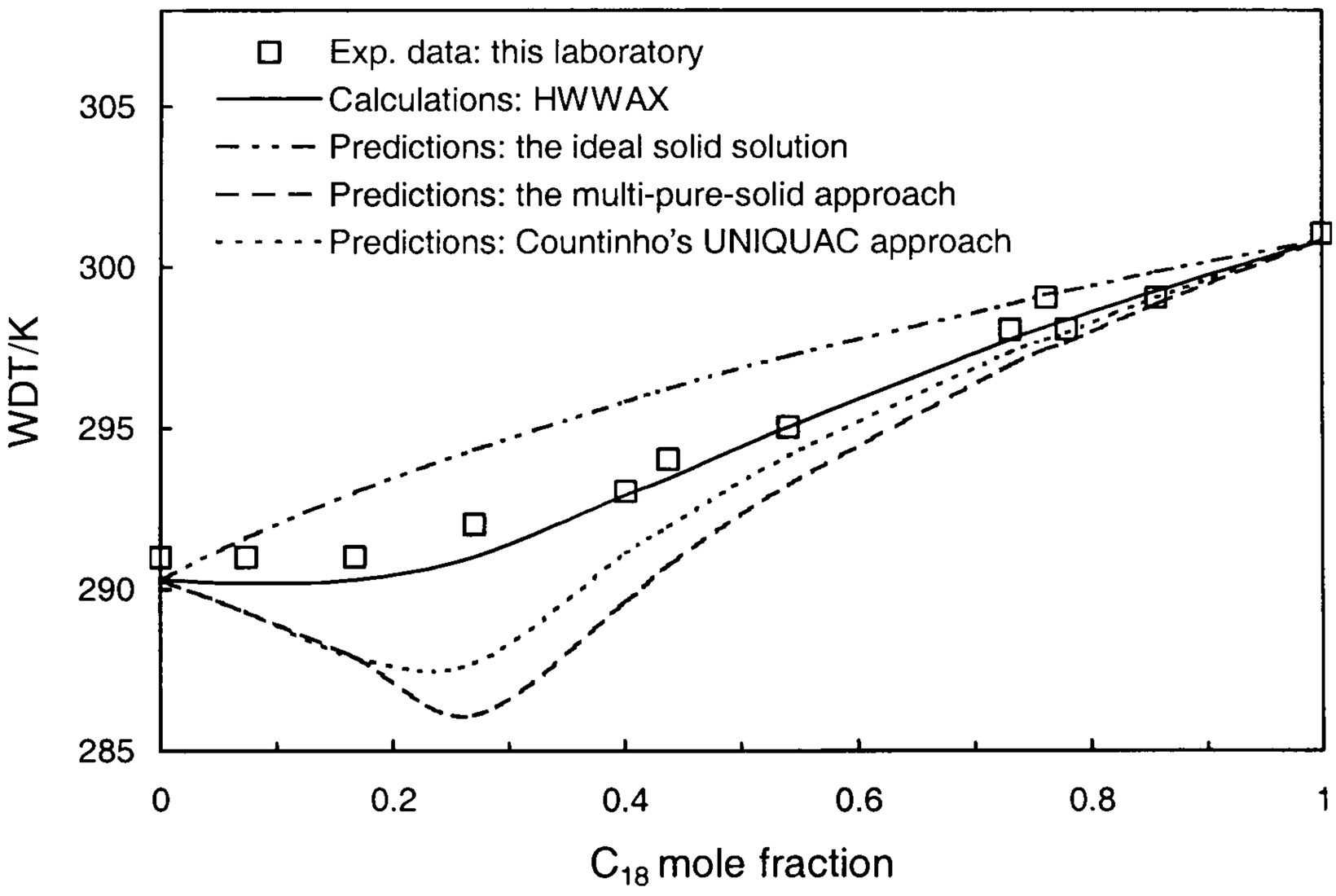

Figure 6.2. Comparison of experimental WDT data (this laboratory) for C_{16} -C_{18} binaries with model predictions using several approaches.

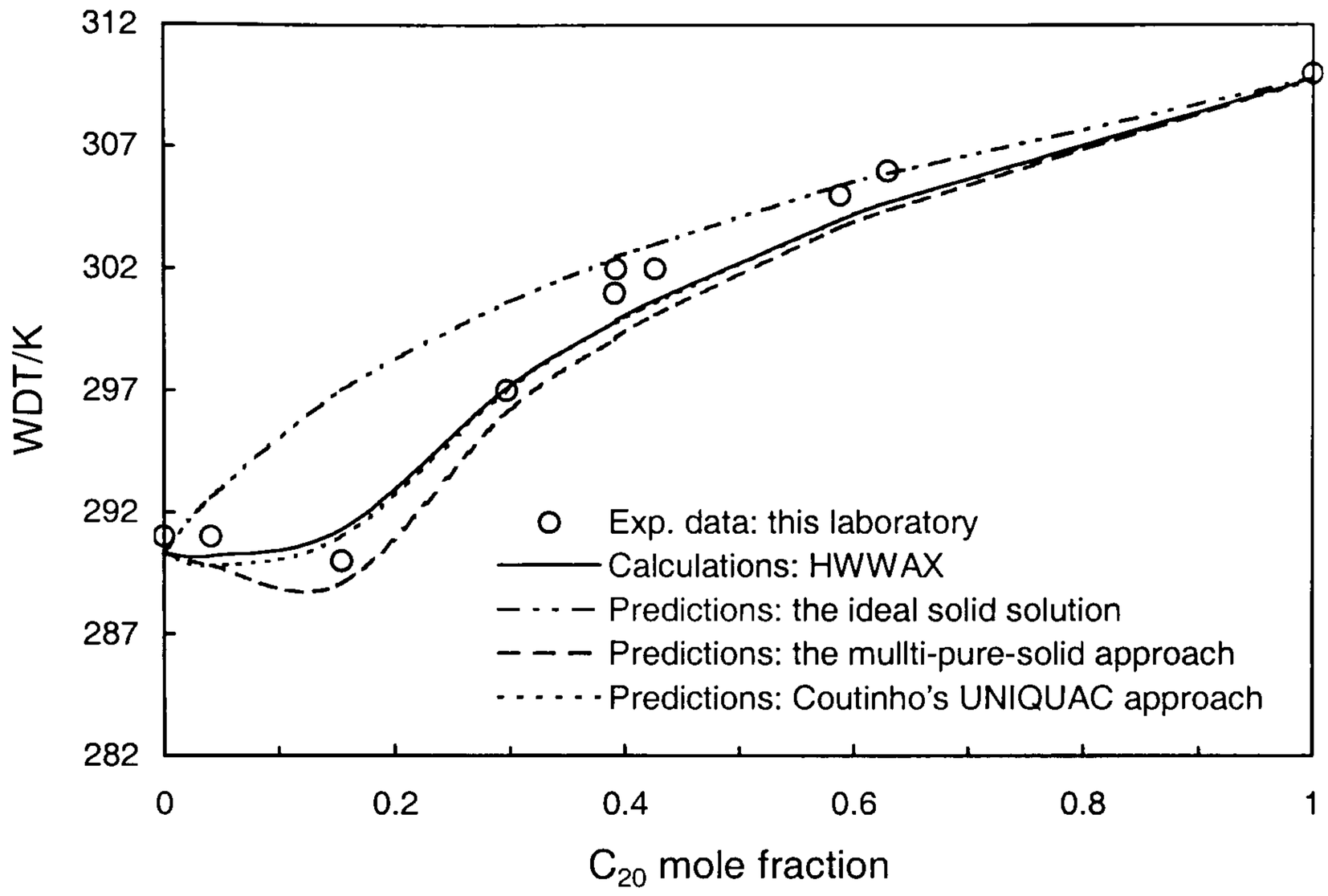

Figure 6.3. Comparison of experimental WDT data (this laboratory) for C_{16}-C_{20} binaries with model predictions using several approaches.

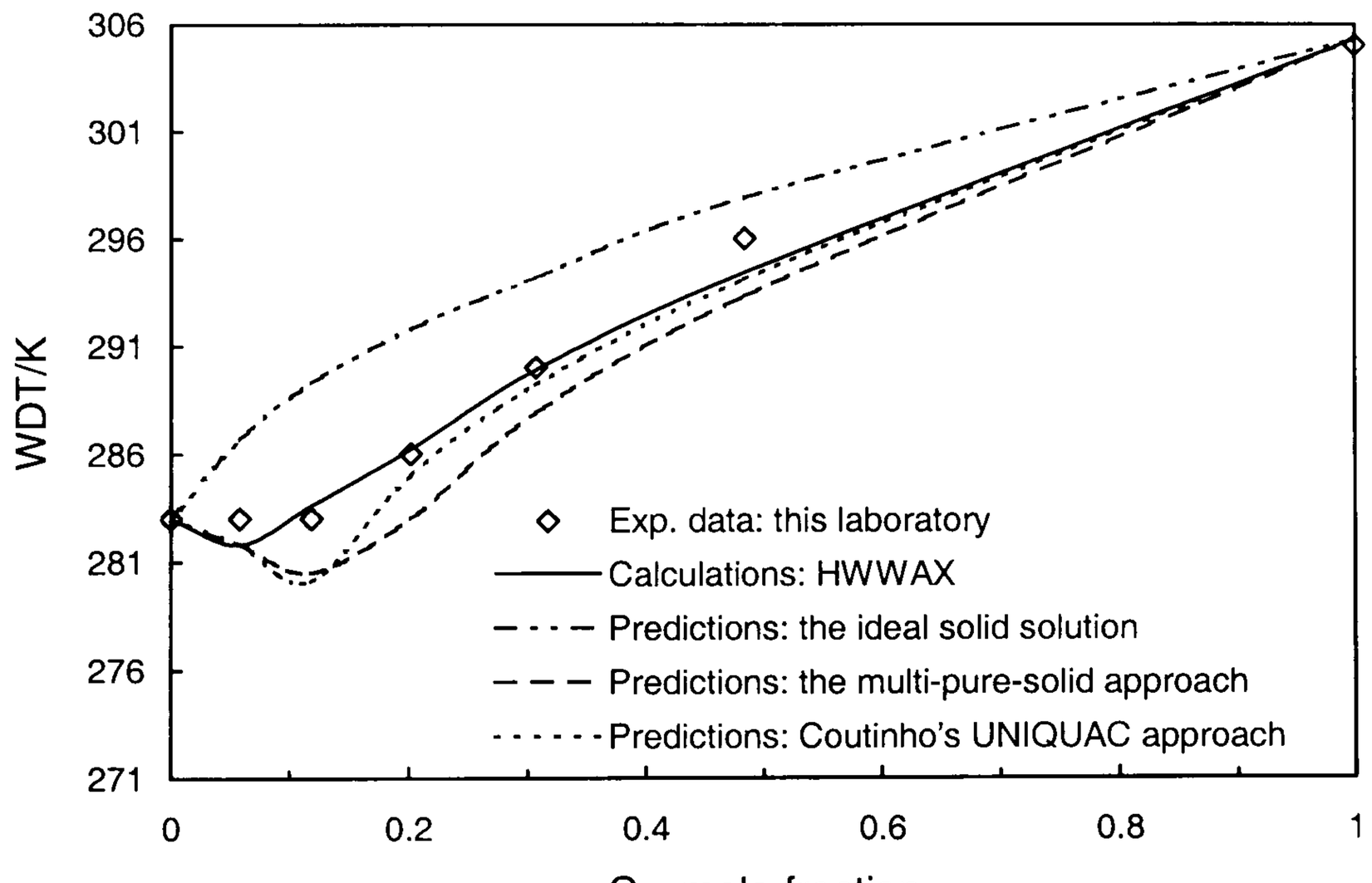

Figure 6.4 Comparison of experimental WDT data (this laboratory) for C_{15}-C_{19} binaries with model predictions using several approaches.

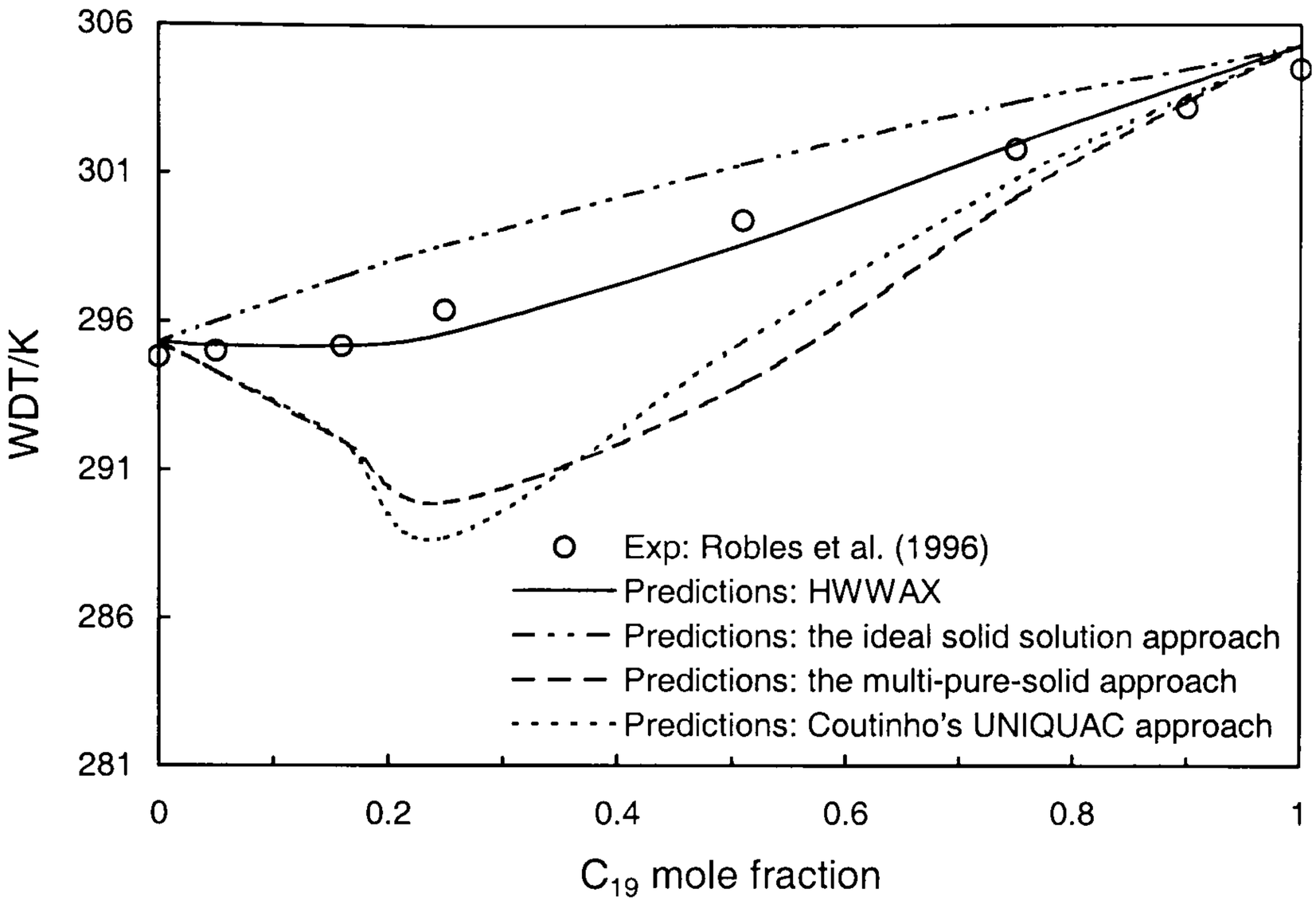

Figure 6.5. Comparison of experimental WDT data (Robles et al., 1996) for C_{17}-C_{19} binaries with model predictions using several approaches.

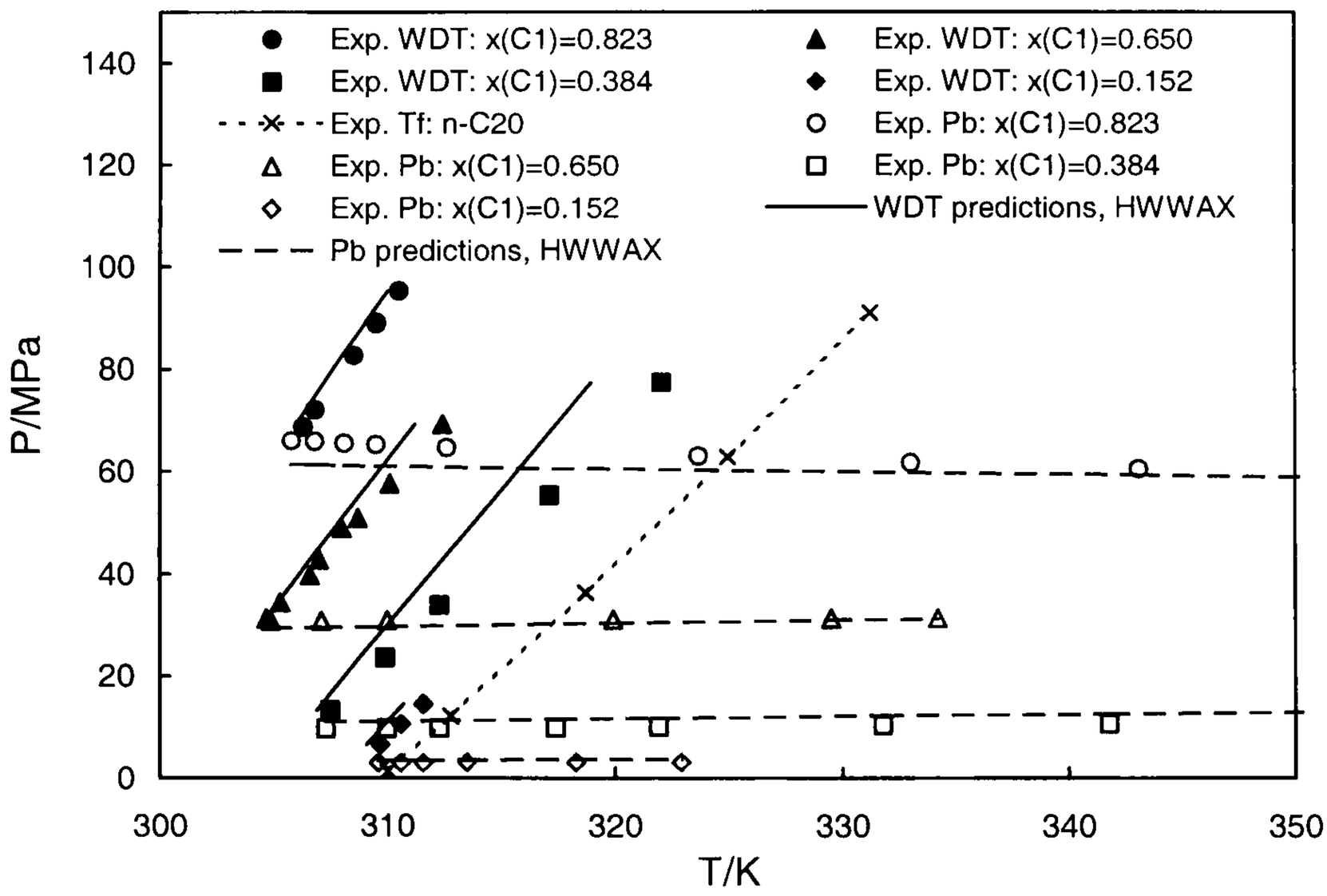

Figure 6.6. Experimental data (Vanderkooi et al., 1995) compared with the HWWAX predictions of P_b and WDT for C_1-C_{20} binaries.

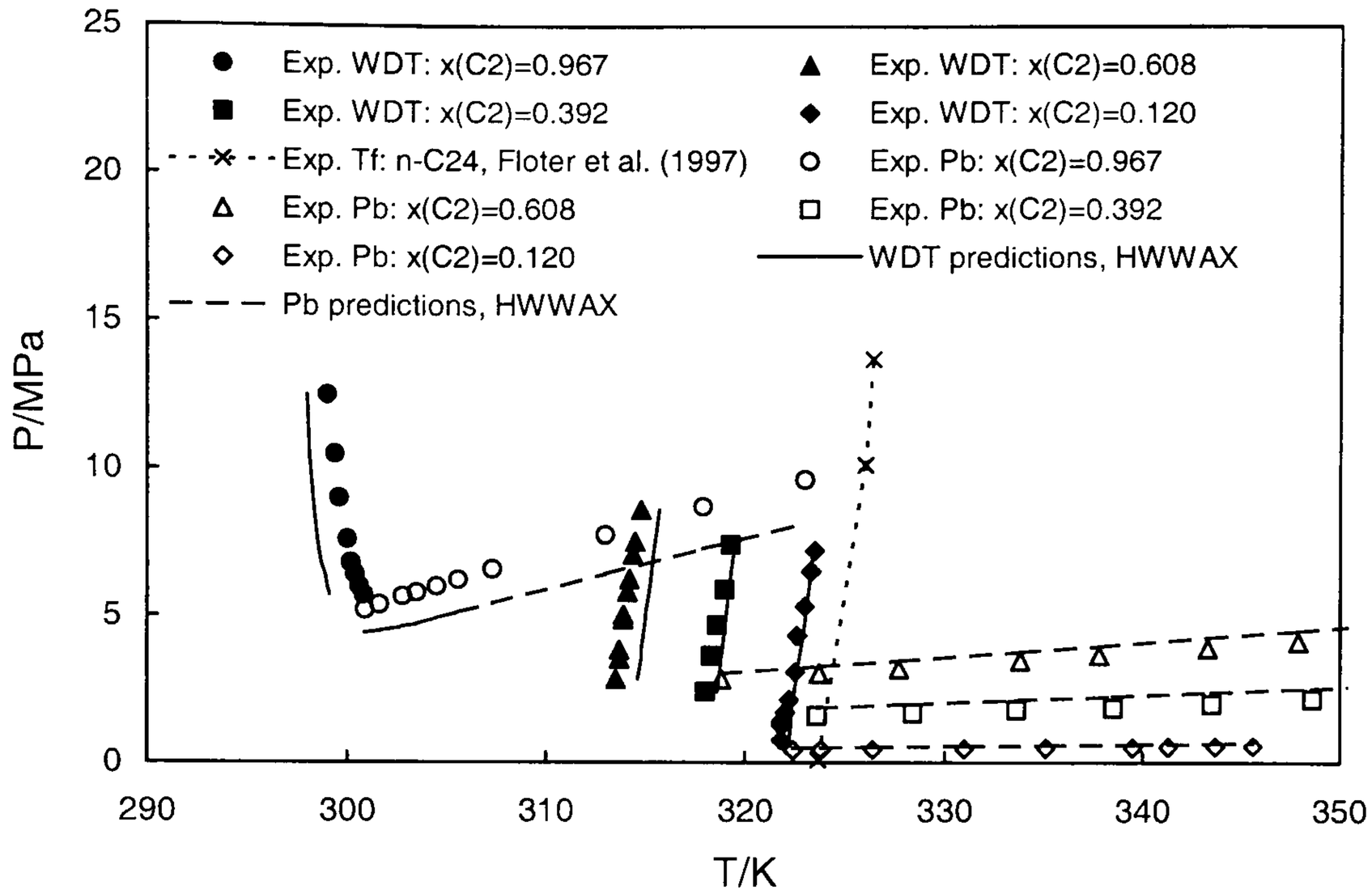

Figure 6.7. Experimental data (Peters et al., 1987) compared with the HWWAX predictions of P_b and WDT for C_2-C_{24} binaries.

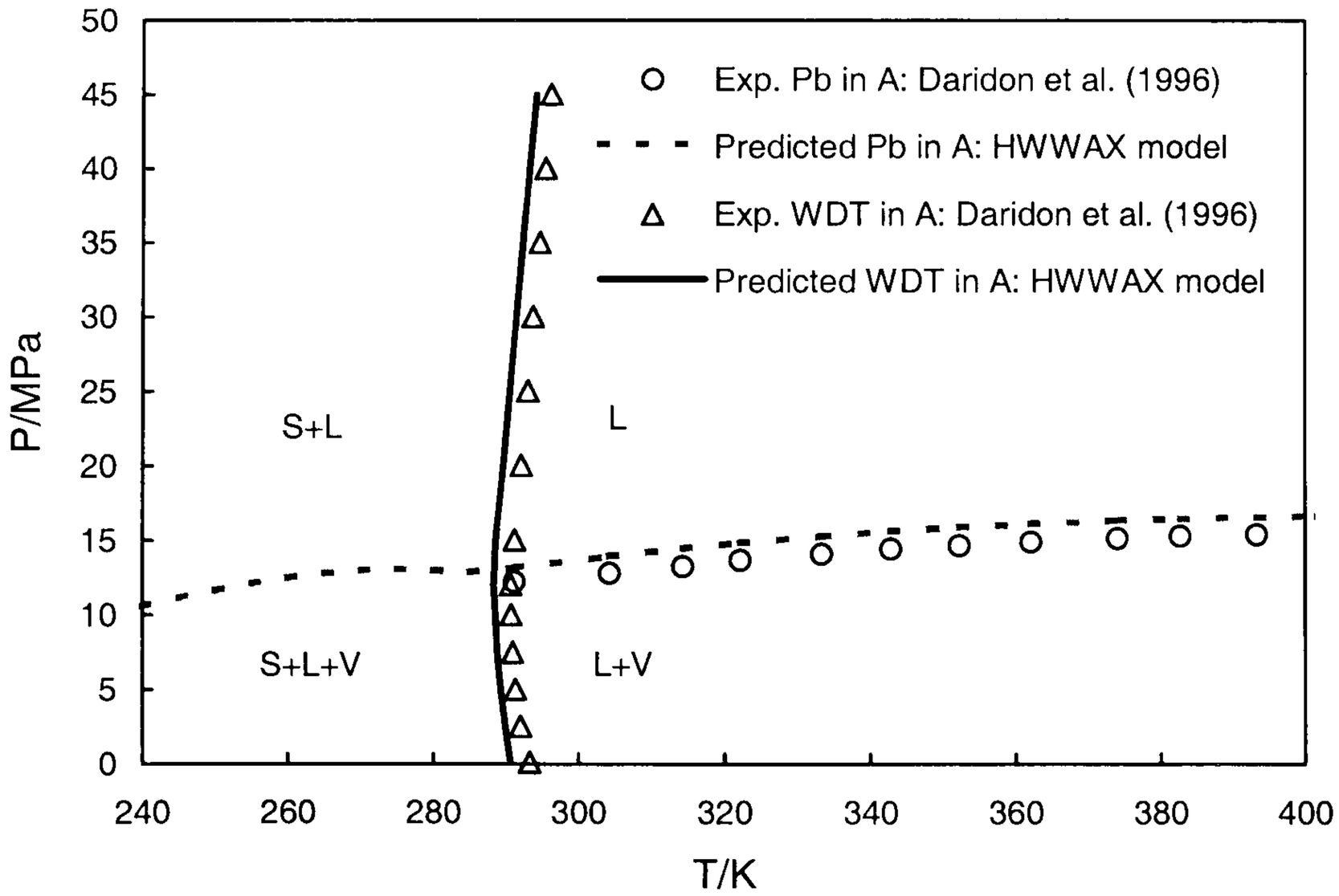

Figure 6.8. Measured (Daridon et al., 1996) and predicted (using the HWWAX model) phase boundaries for Mixture A.

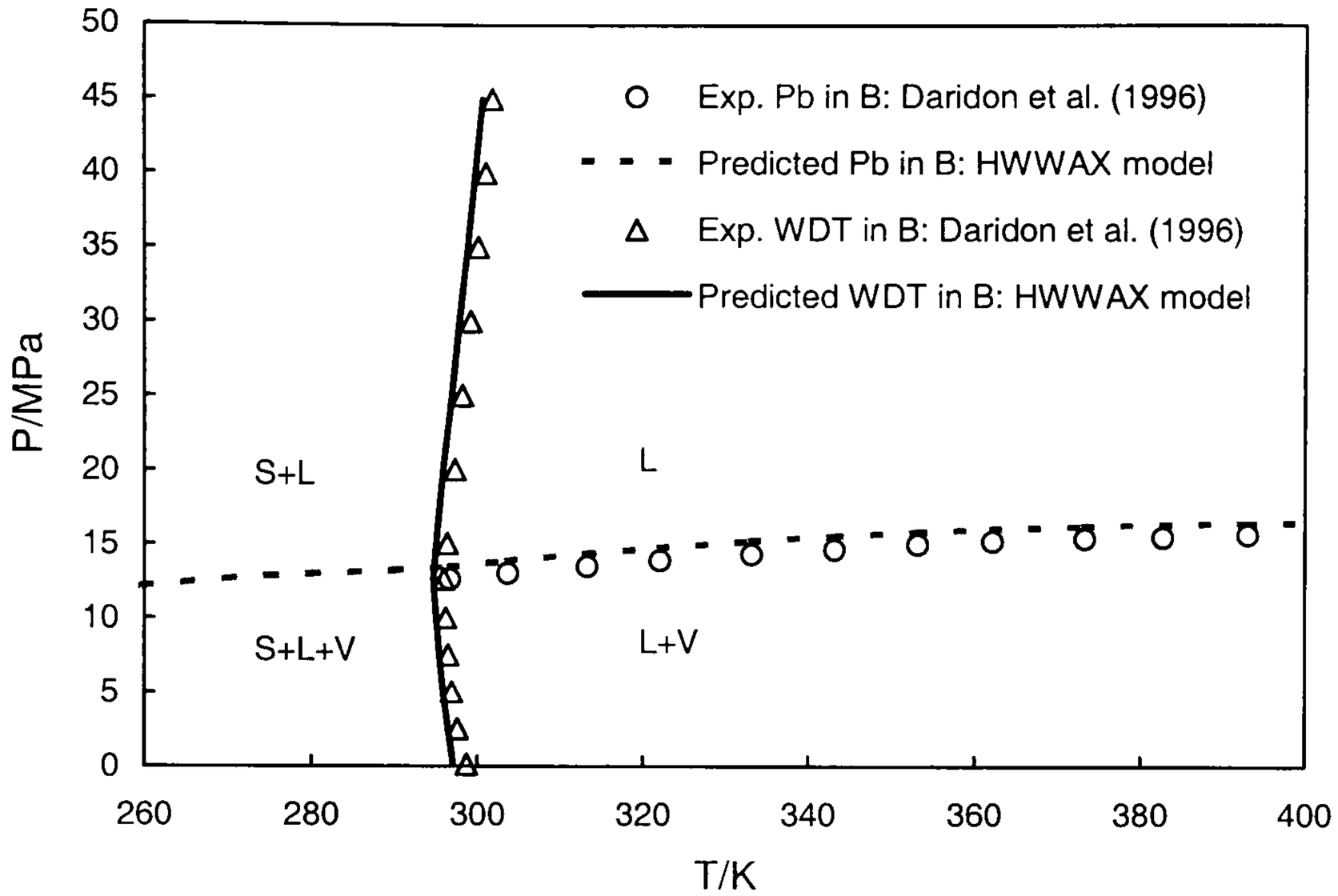

Figure 6.9. Measured (Daridon et al., 1996) and predicted (using the HWWAX model) phase boundaries for Mixture B.

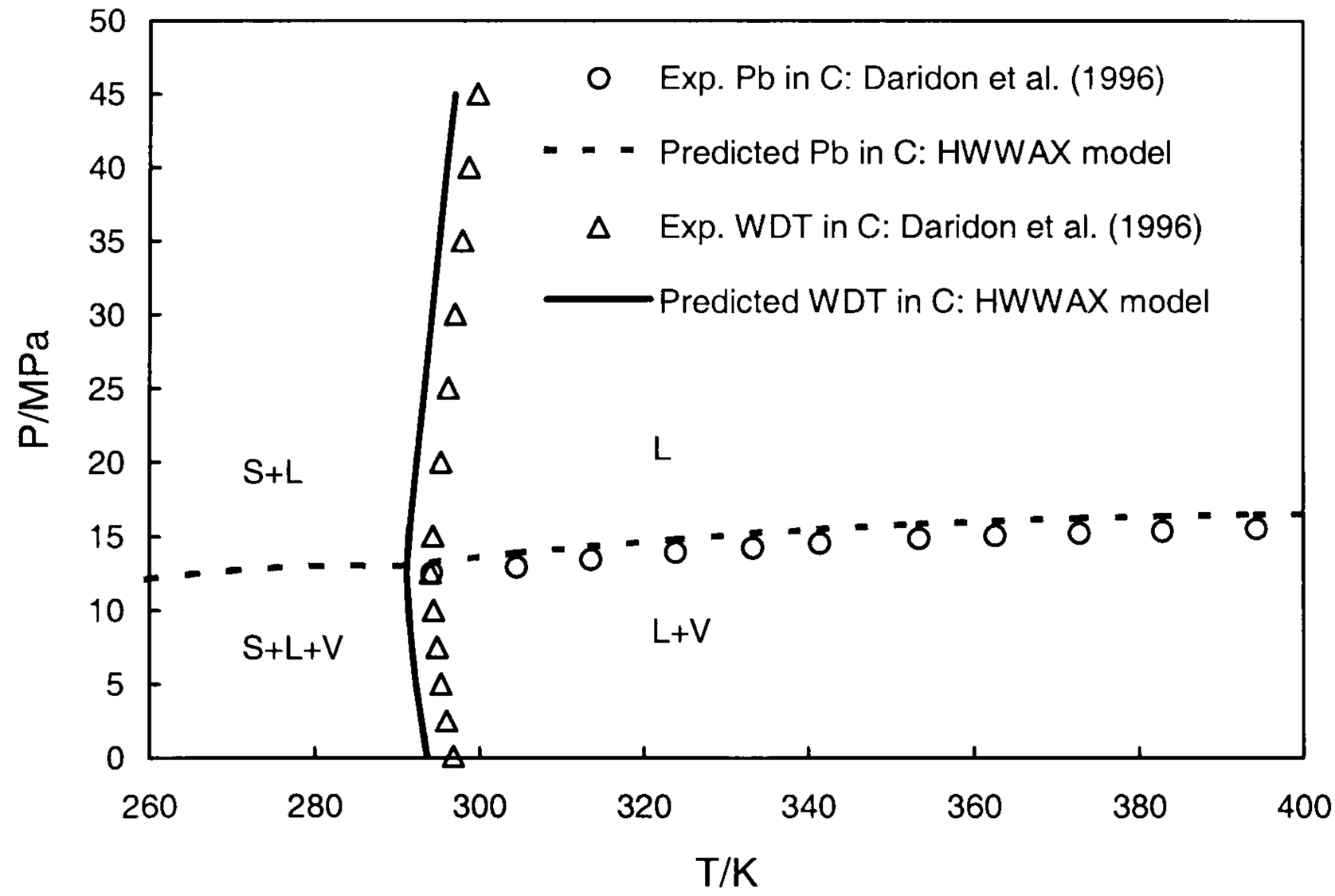

Figure 6.10. Measured (Daridon et al., 1996) and predicted (using the HWWAX model) phase boundaries for Mixture C.

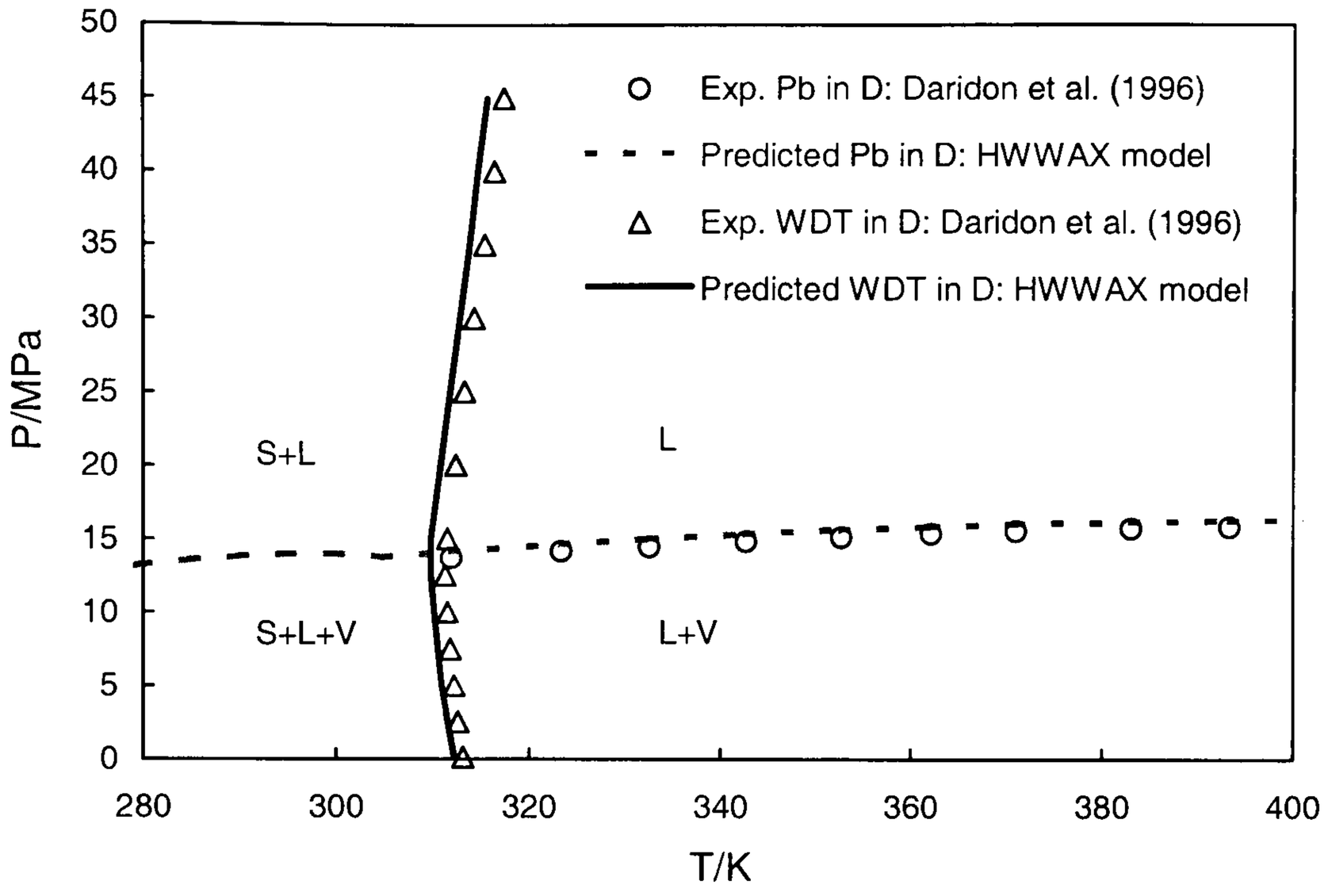

Figure 6.11. Measured (Daridon et al., 1996) and predicted (using the HWWAX model) phase boundaries for Mixture D.

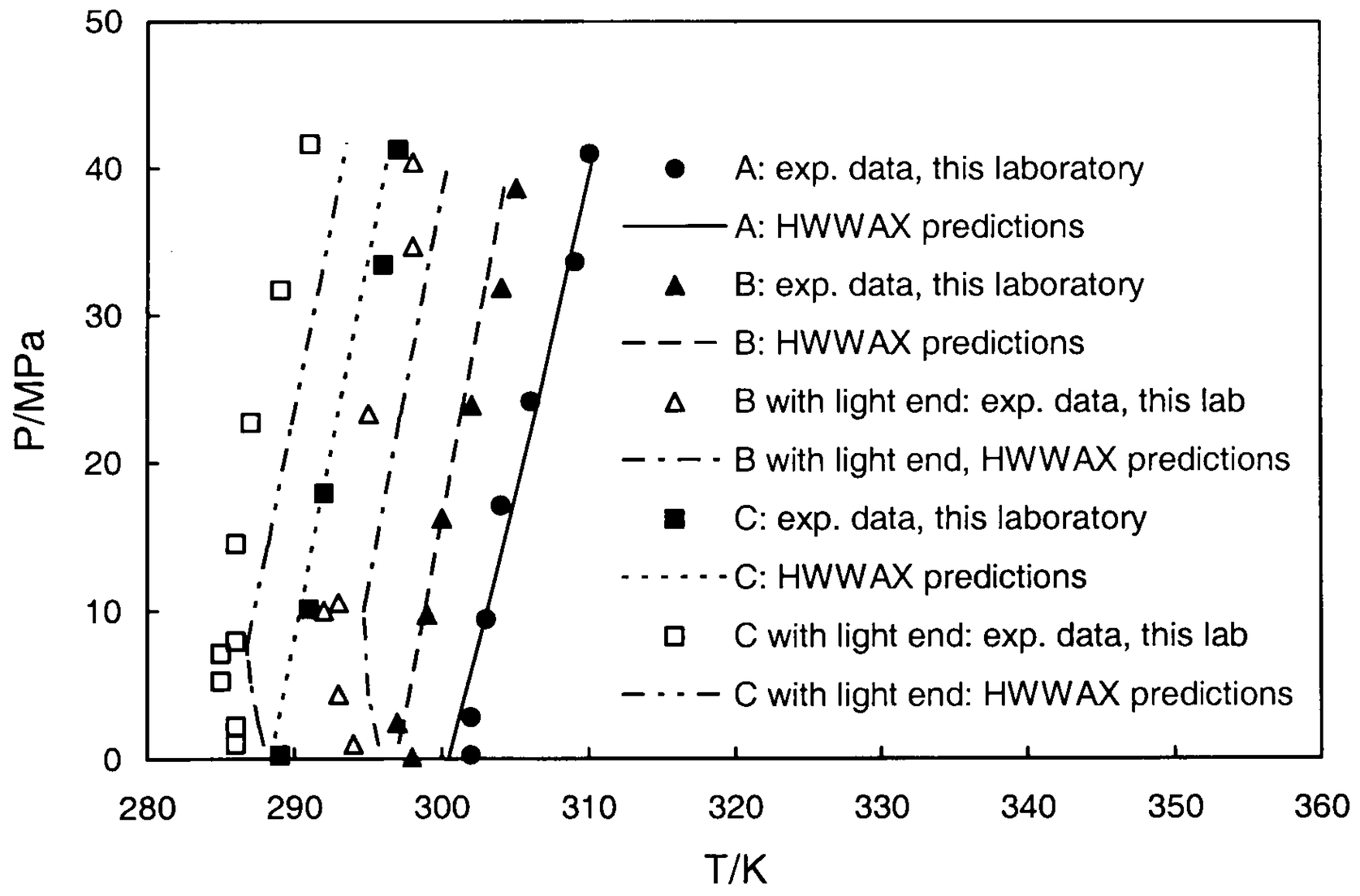

Figure 6.12. Experimental data (this laboratory) and predicted WDTs (using the HWWAX model) for Mixtures A, B and C and their live fluids with C_1-C_4.

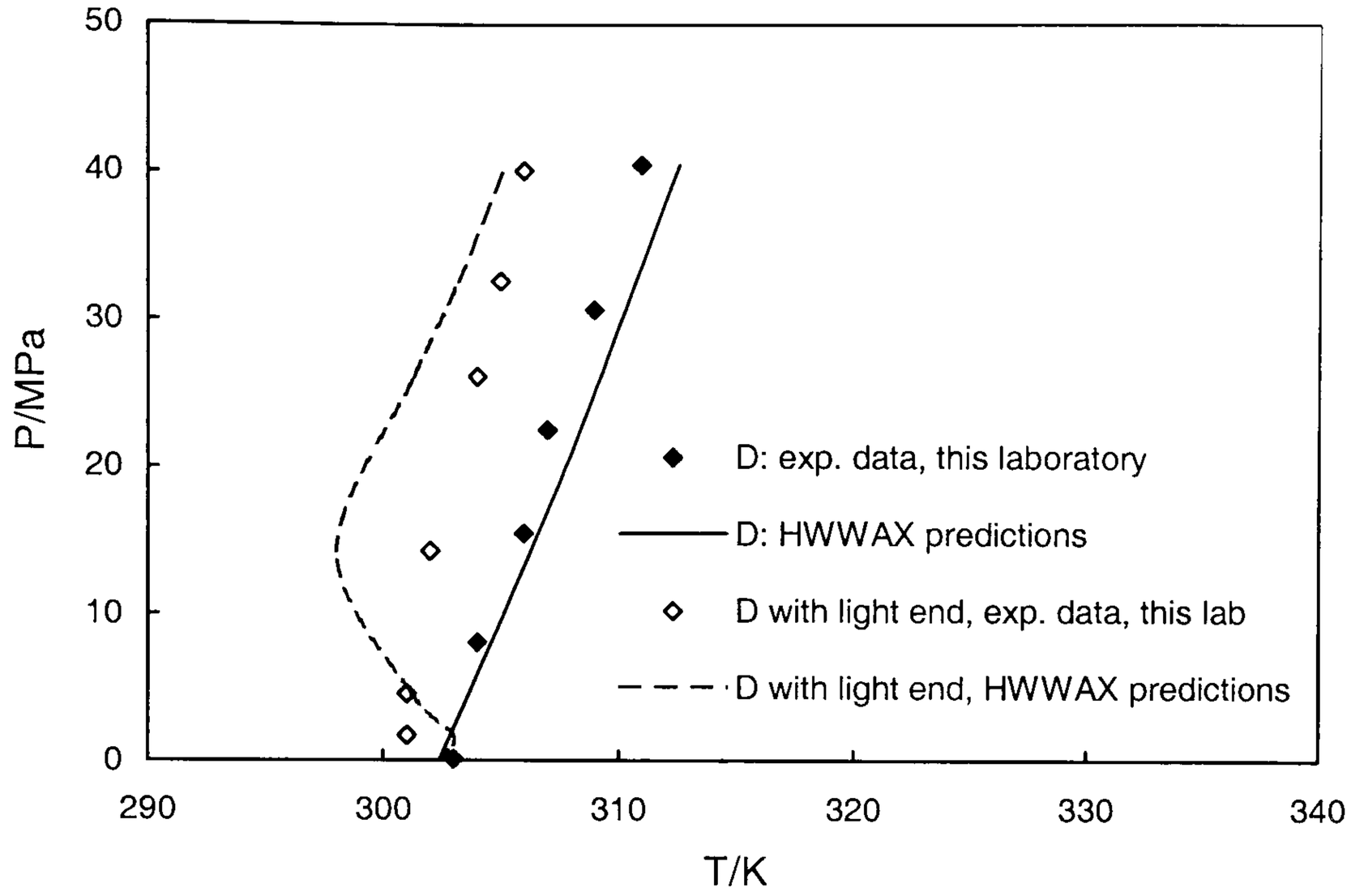

Figure 6.13. Measured (this laboratory) and predicted (using the HWWAX model) WDTs for Mixture D, with and without natural gas.

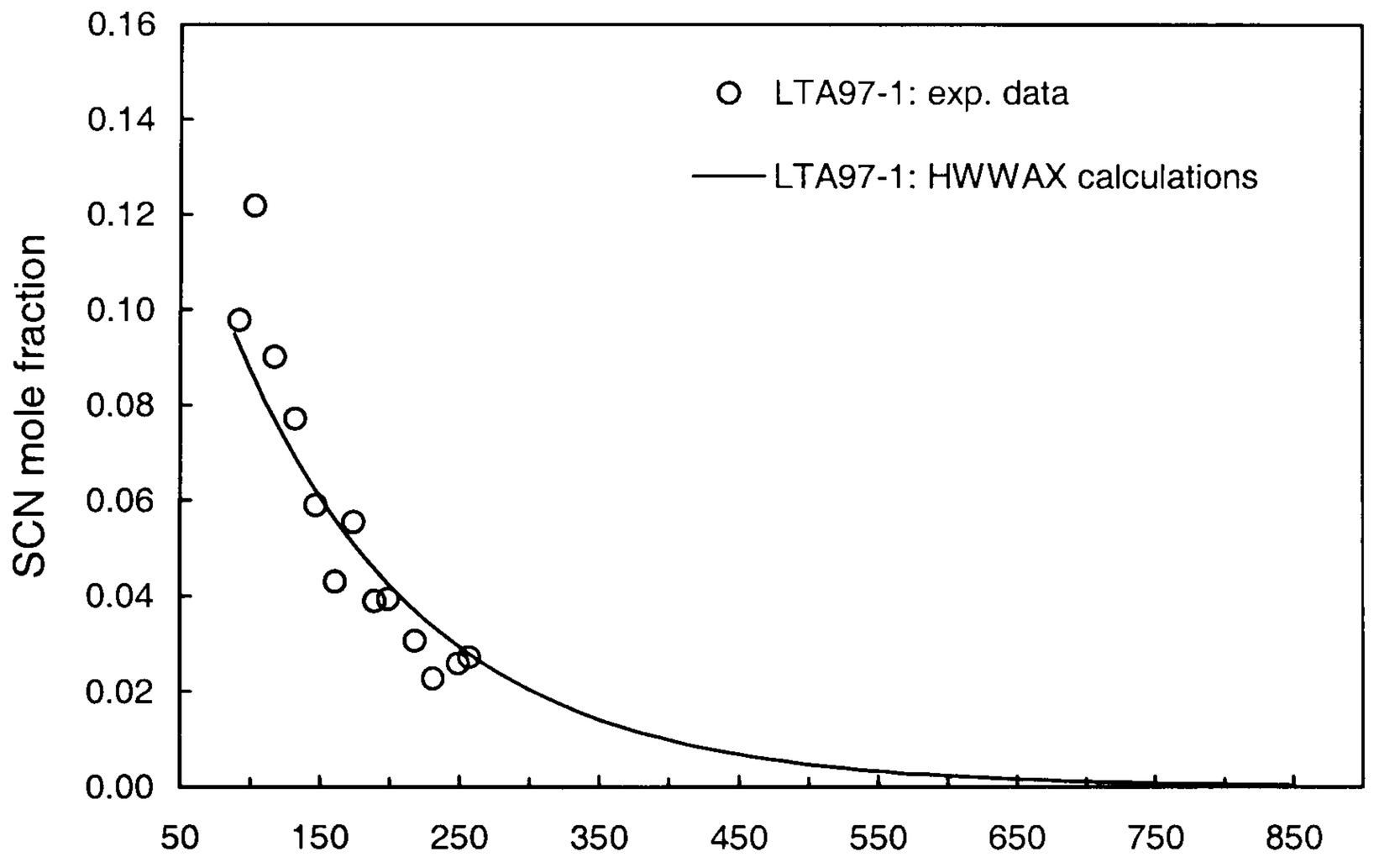

Figure 6.14. Experimental data (Reservoir Fluid Studies Group) and the calculated SCN mole concentrations against molecular weight for the North Sea crude oil LTA97-1.

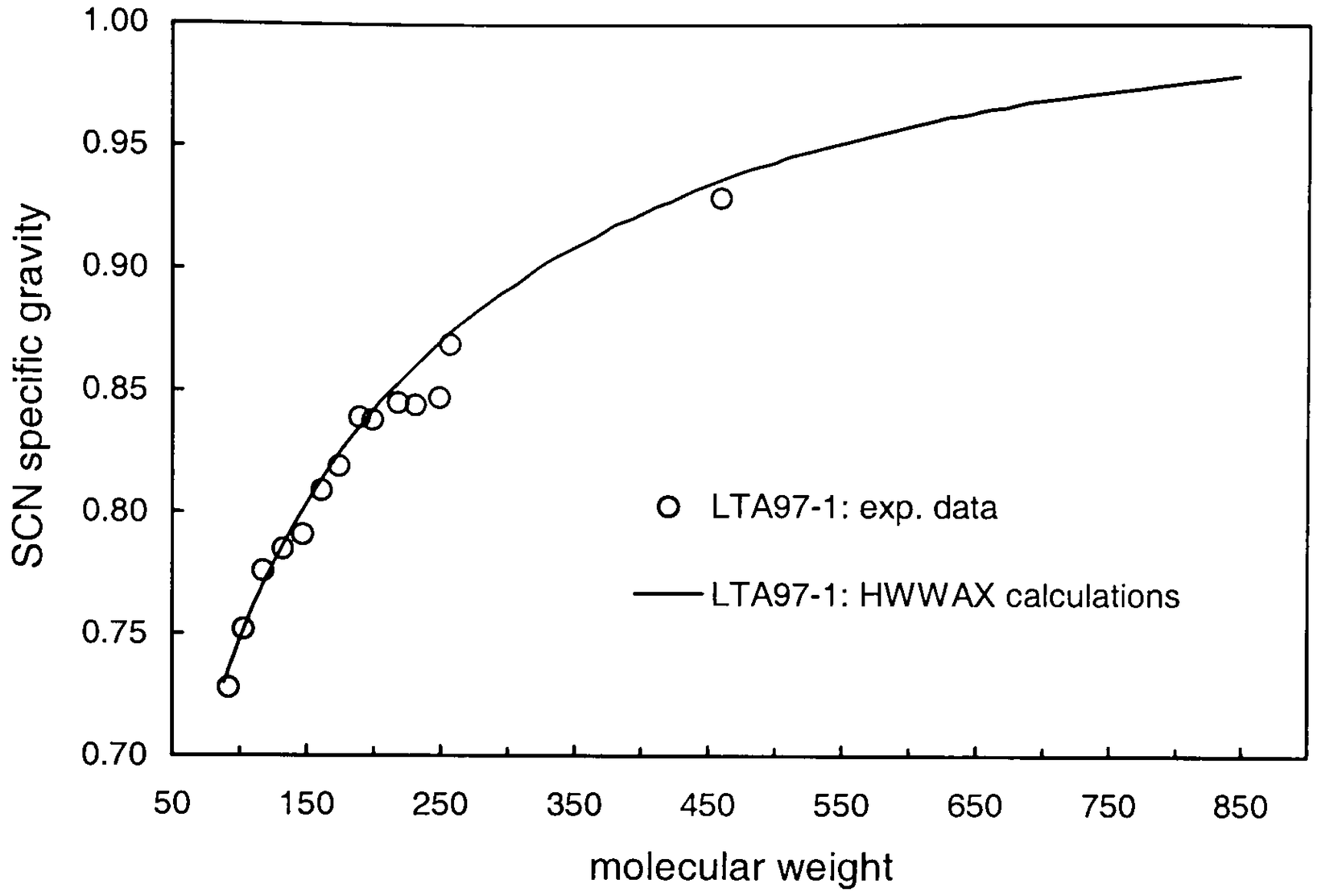

Figure 6.15. Experimental data (Reservoir Fluid Studies Group) and the calculated SCN specific gravities against molecular weight for the North Sea crude oil LTA97-1.

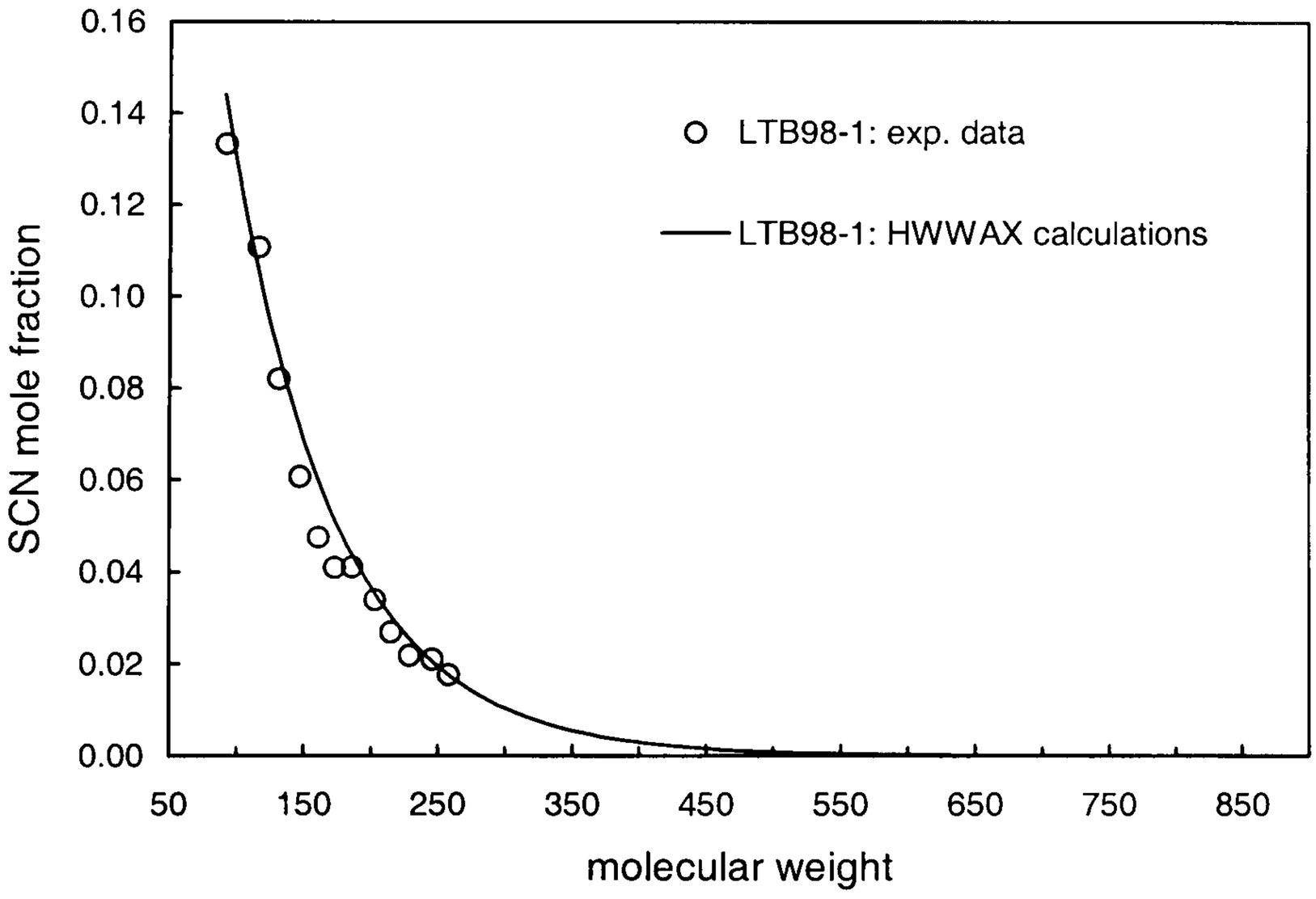

Figure 6.16. Experimental data (Reservoir Fluid Studies Group) and the calculated SCN mole concentrations against molecular weight for Base Condensate LTB98-1.

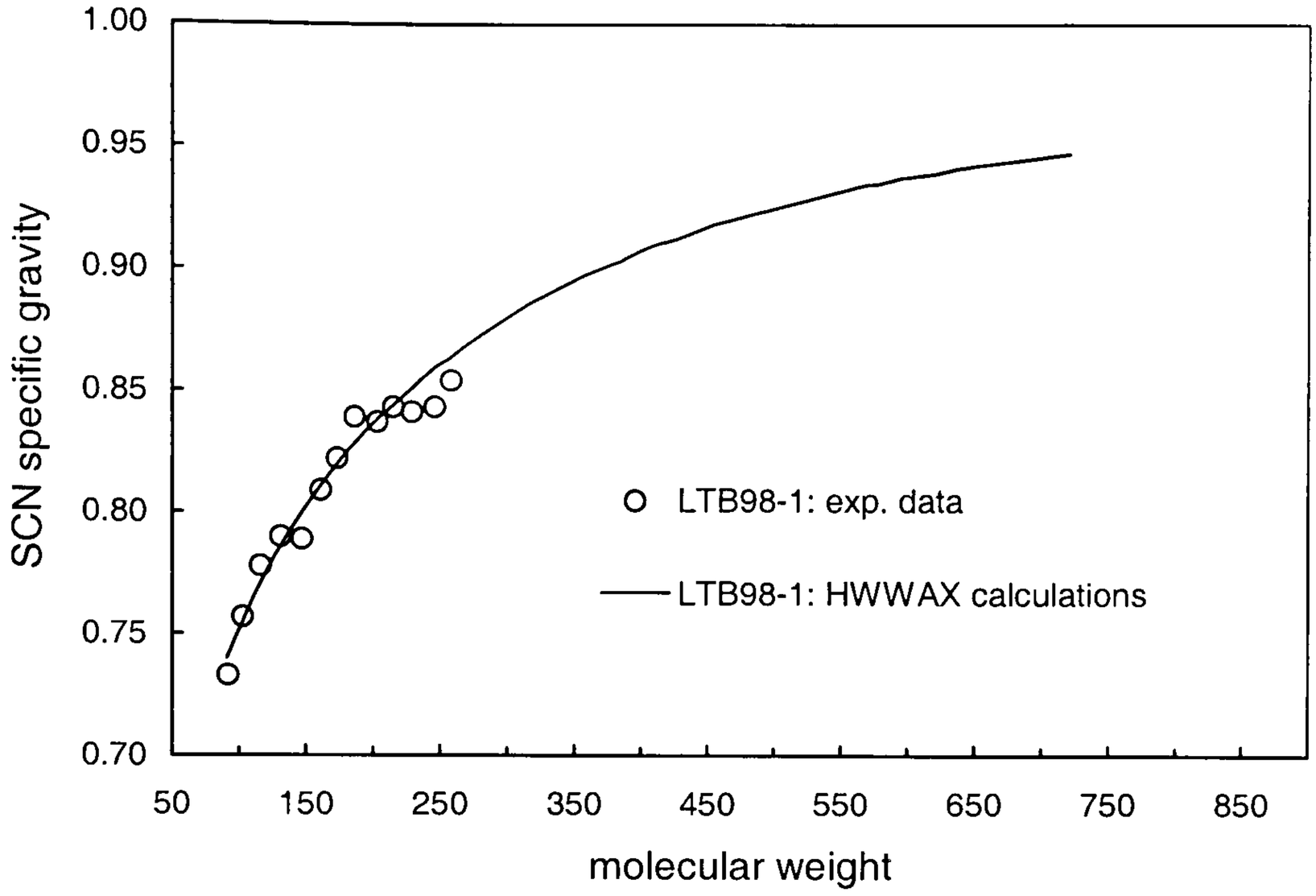

Figure 6.17. Experimental data (Reservoir Fluid Studies Group) and the calculated SCN specific gravities against molecular weight for Base Condensate LTB98-1.

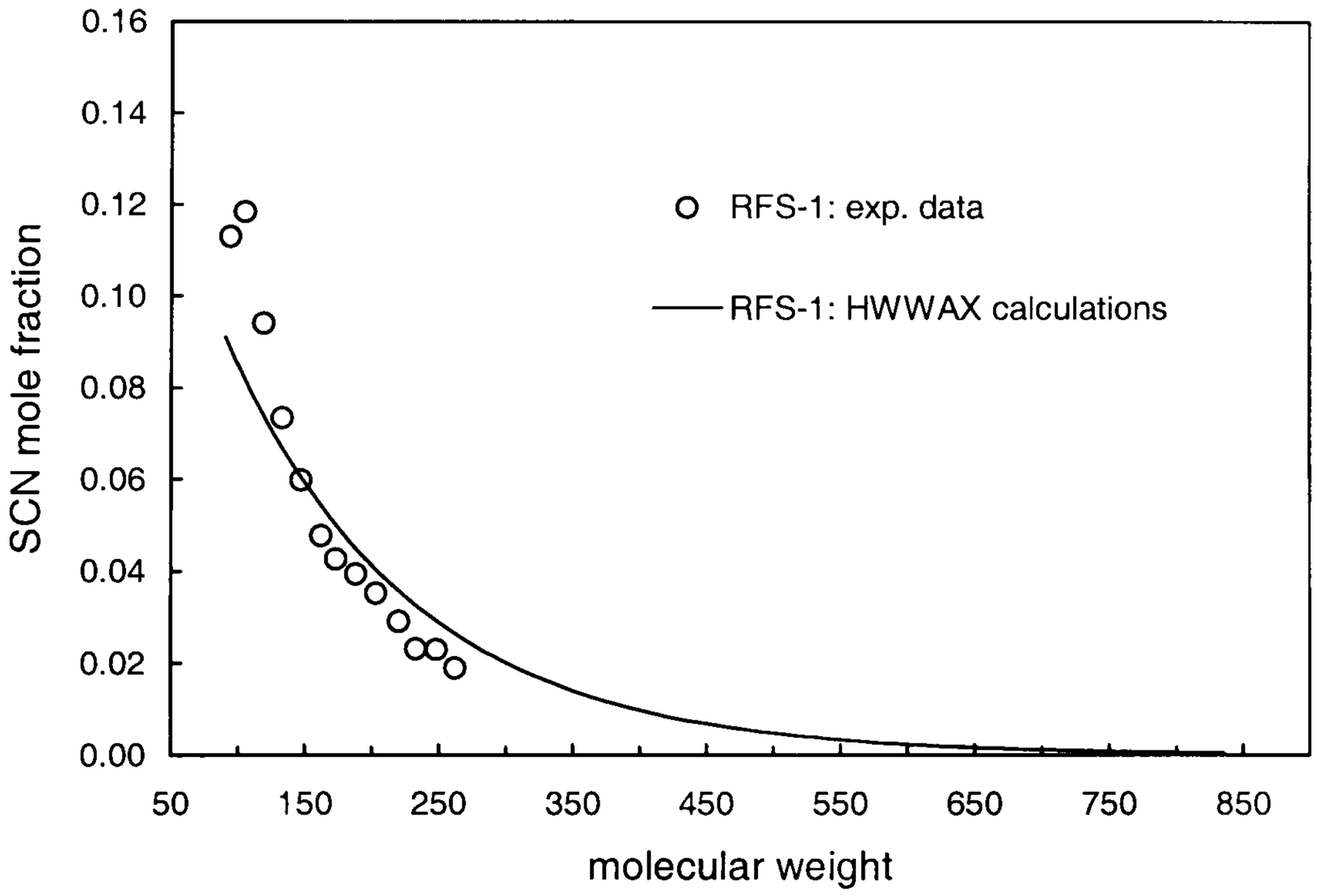

Figure 6.18. Experimental data (Reservoir Fluid Studies Group) and the calculated SCN mole concentrations against molecular weight for Black Oil RFS-1 (dead fluid).

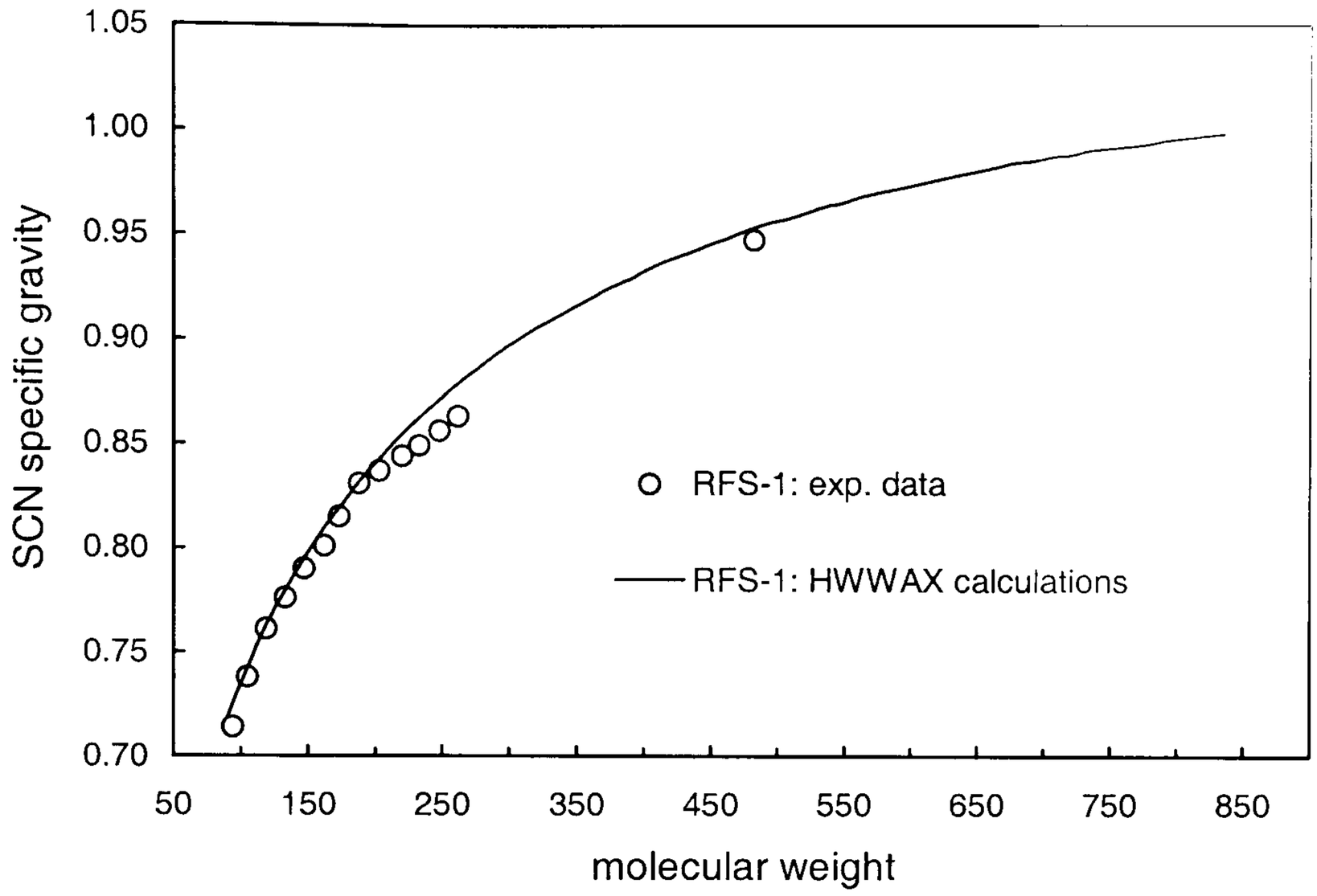

Figure 6.19 Experimental data (Reservoir Fluid Studies Group) and the calculated SCN specific gravities against molecular weight for Black Oil RFS-1 (dead fluid).

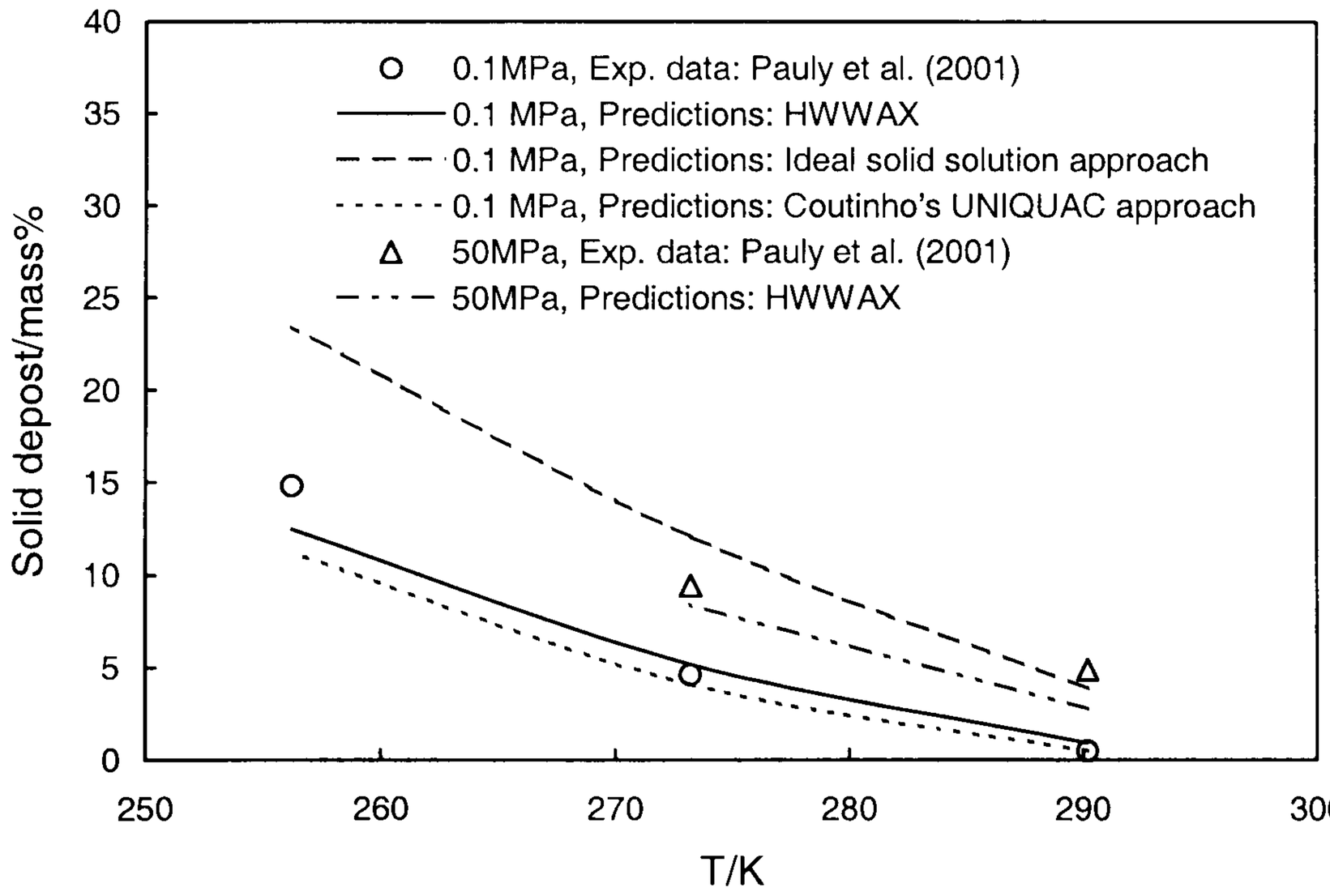

Figure 6.20. Measured wax amounts (mass %) (Pauly et al., 2001) and predicted values using different wax models.

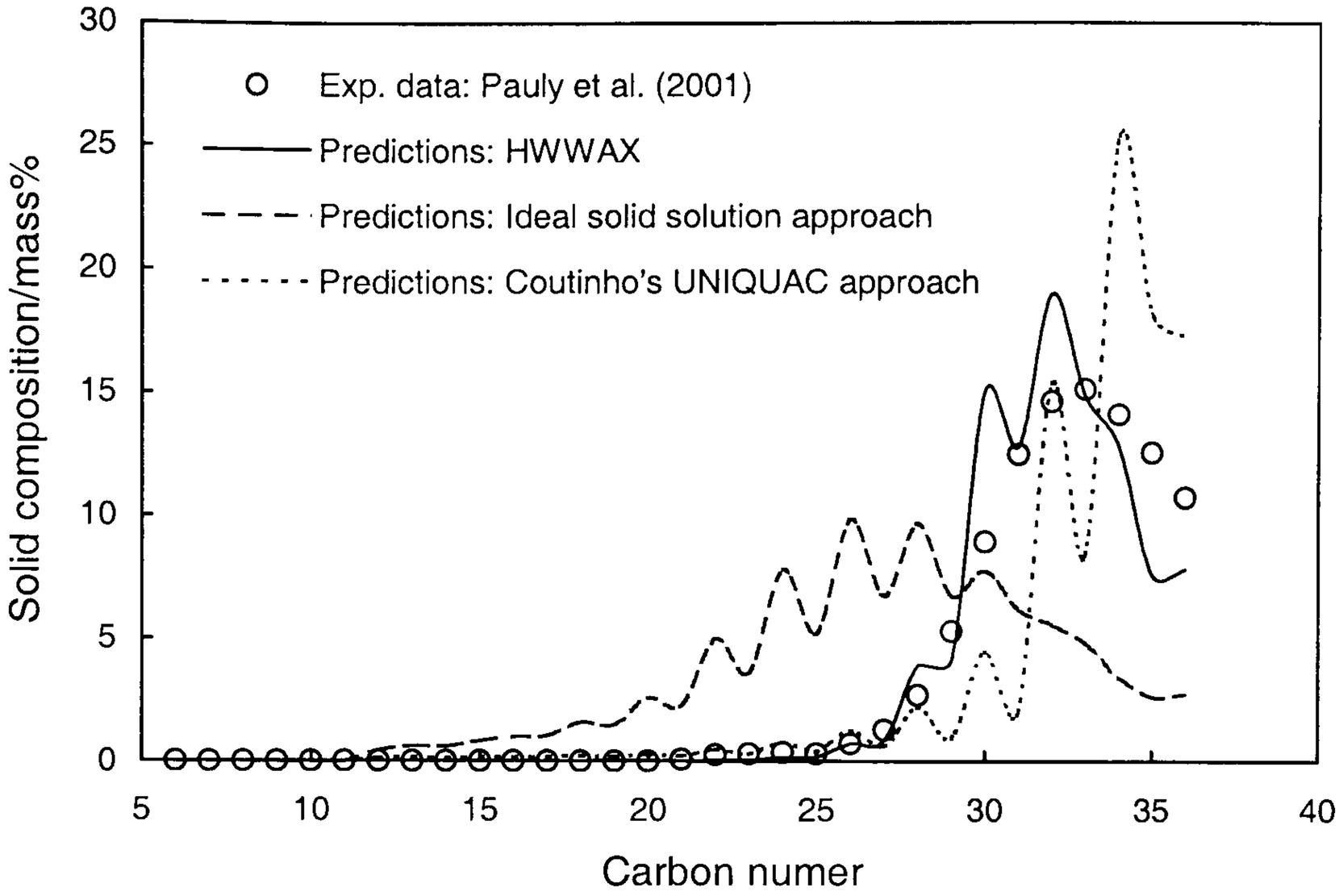

Figure 6.21 Measured (Pauly et al., 2001) and predicted wax compositions using different wax models at 290.2 K and 0.1 MPa.

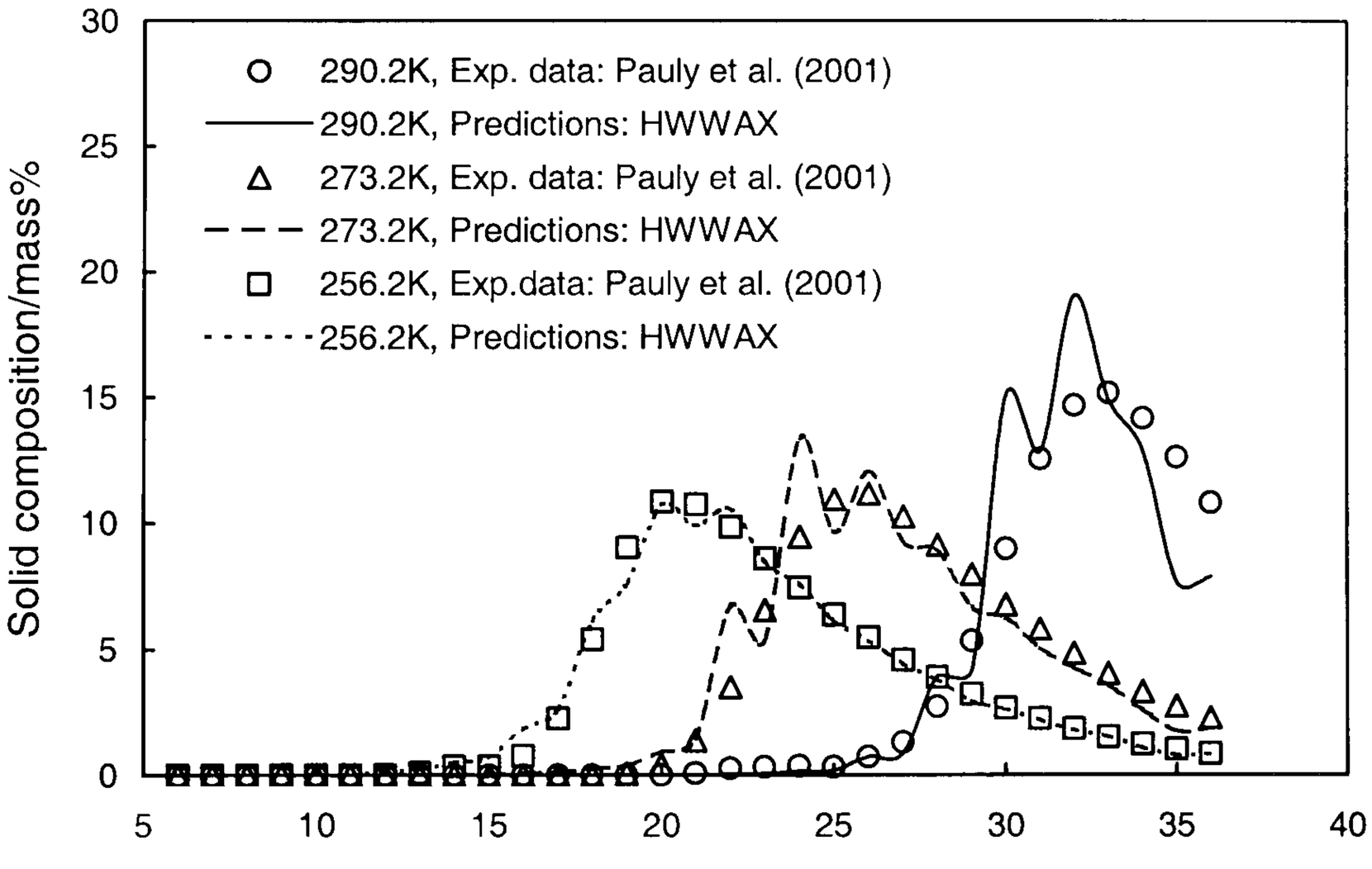

Figure 6.22. Measured (Pauly et al., 2001) and predicted (using HWWAX) wax compositions at different temperature conditions, at 0.1MPa.

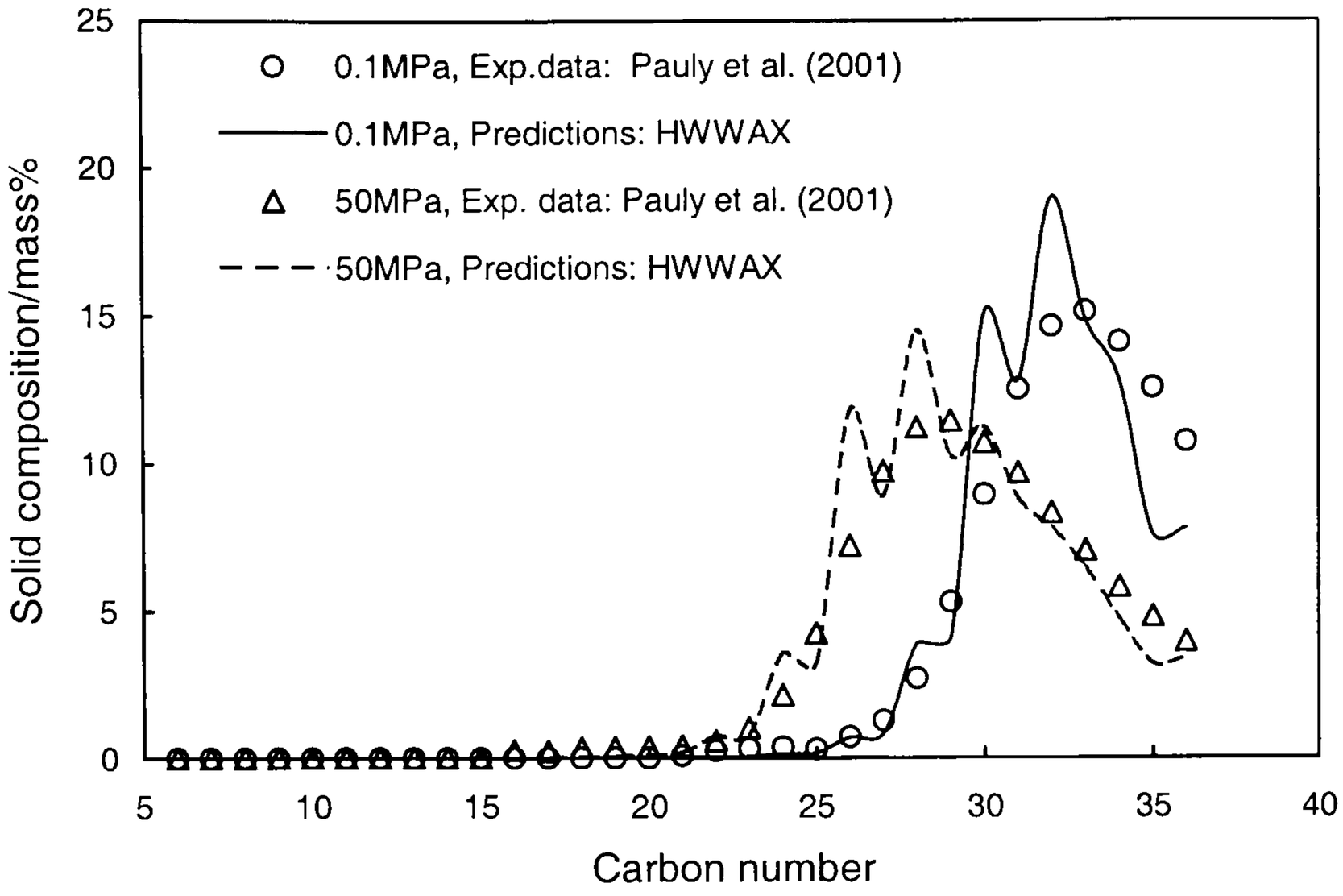

Figure 6.23. Experimental (Pauly et al., 2001) and predicted (using HWWAX) wax compositions at different pressure conditions (290.2K).

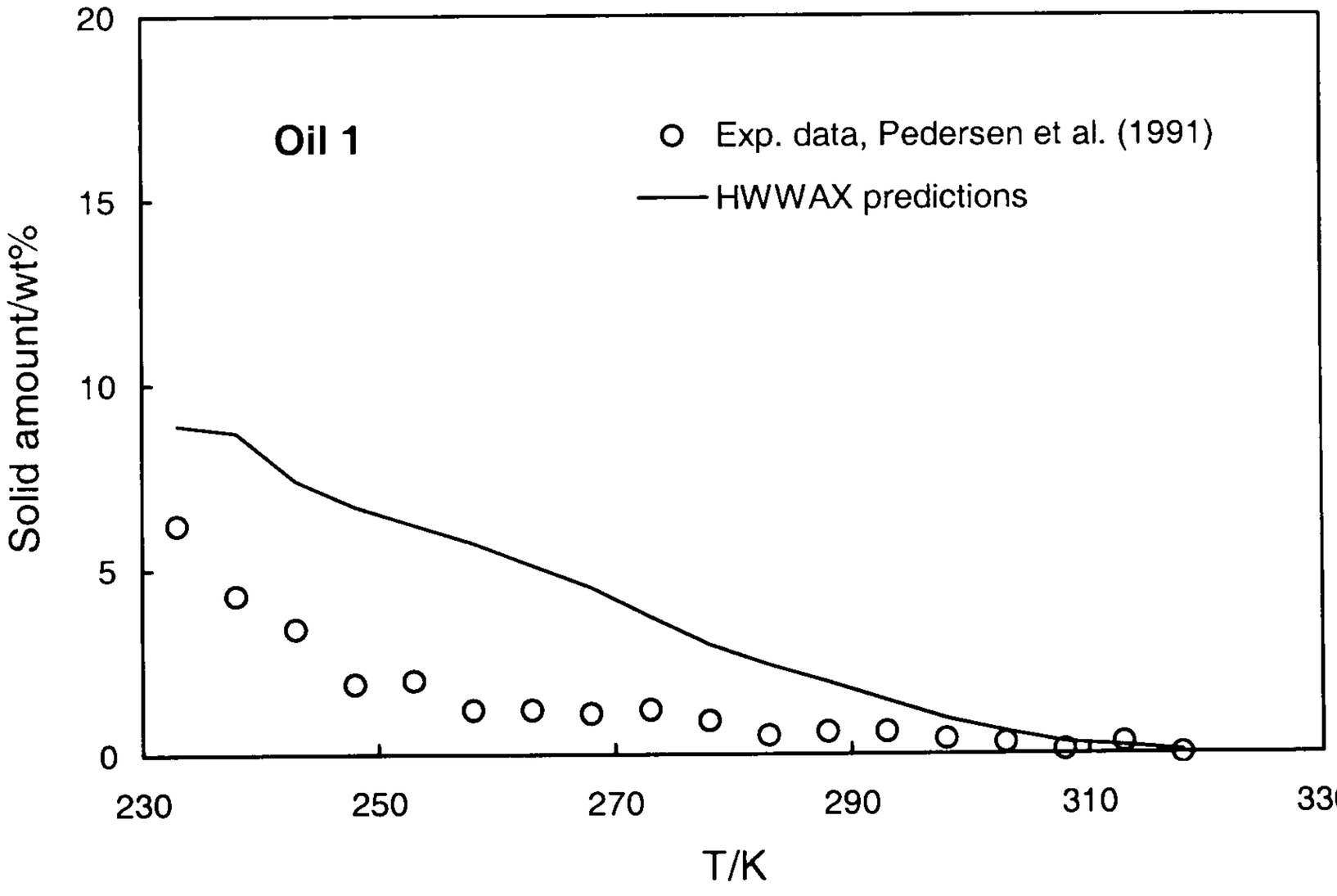

Figure 6.24. Experimental (Pedersen et al., 1991a) and predicted (using HWWAX) wax amounts for crude Oil 1.

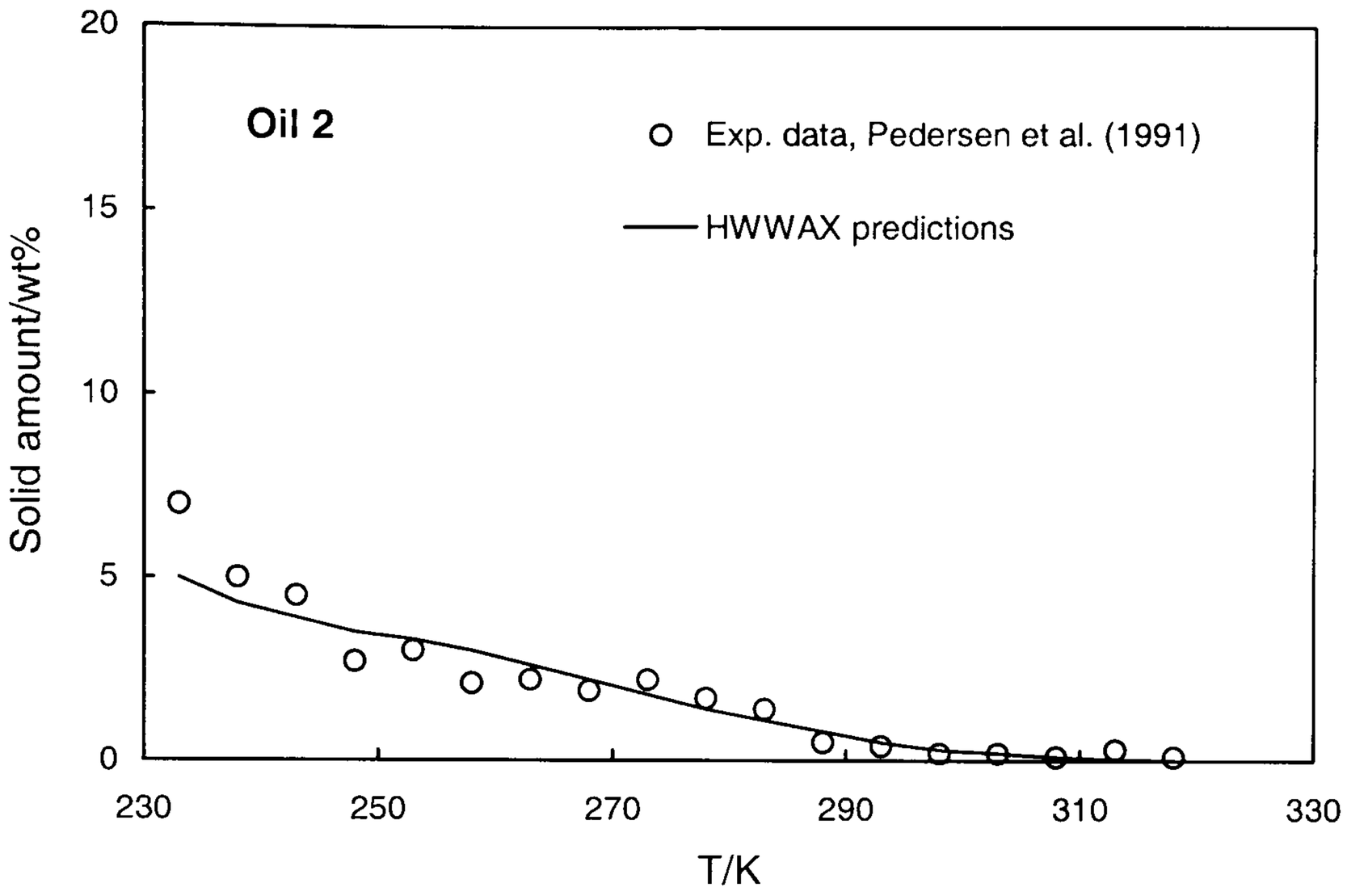

Figure 6.25. Experimental (Pedersen et al., 1991a) and predicted (using HWWAX) wax amounts for crude Oil 2.

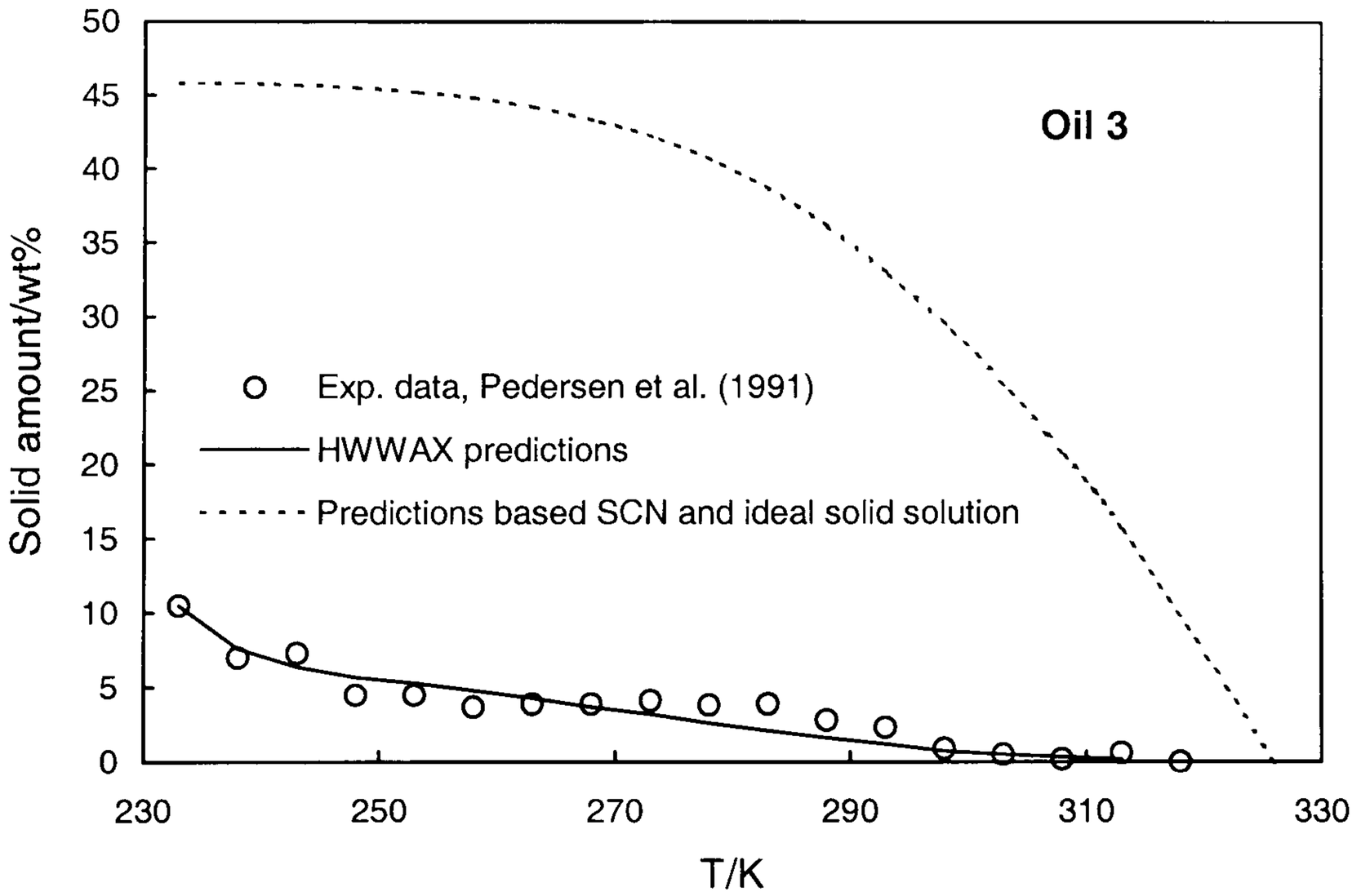

Figure 6.26. Experimental (Pedersen et al., 1991a) and predicted wax amounts (using the HWWAX model and the model based on SCN groups) for crude Oil 3.

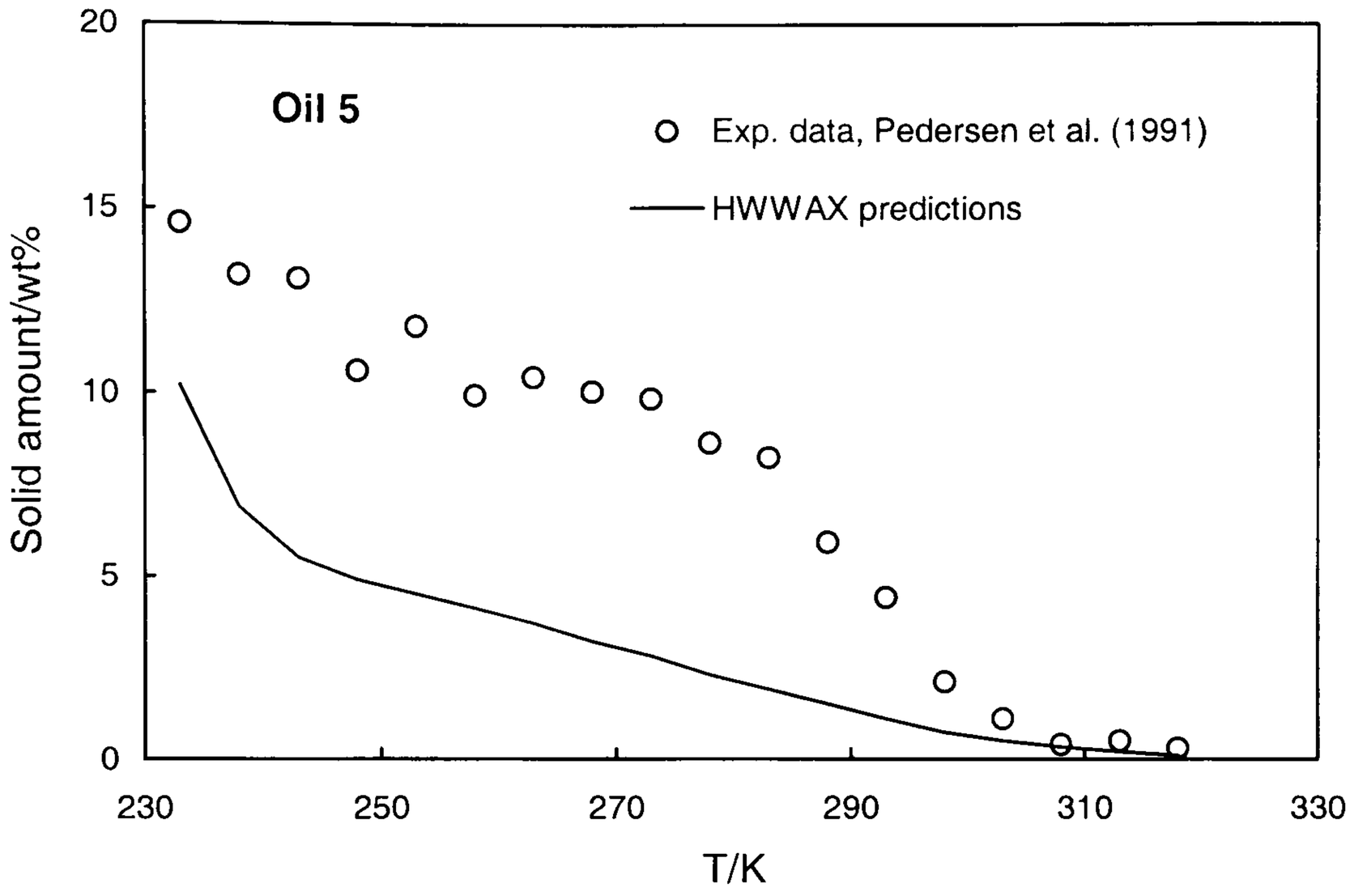

Figure 6.27. Experimental (Pedersen et al., 1991a) and predicted (using HWWAX) wax amounts for crude Oil 5.

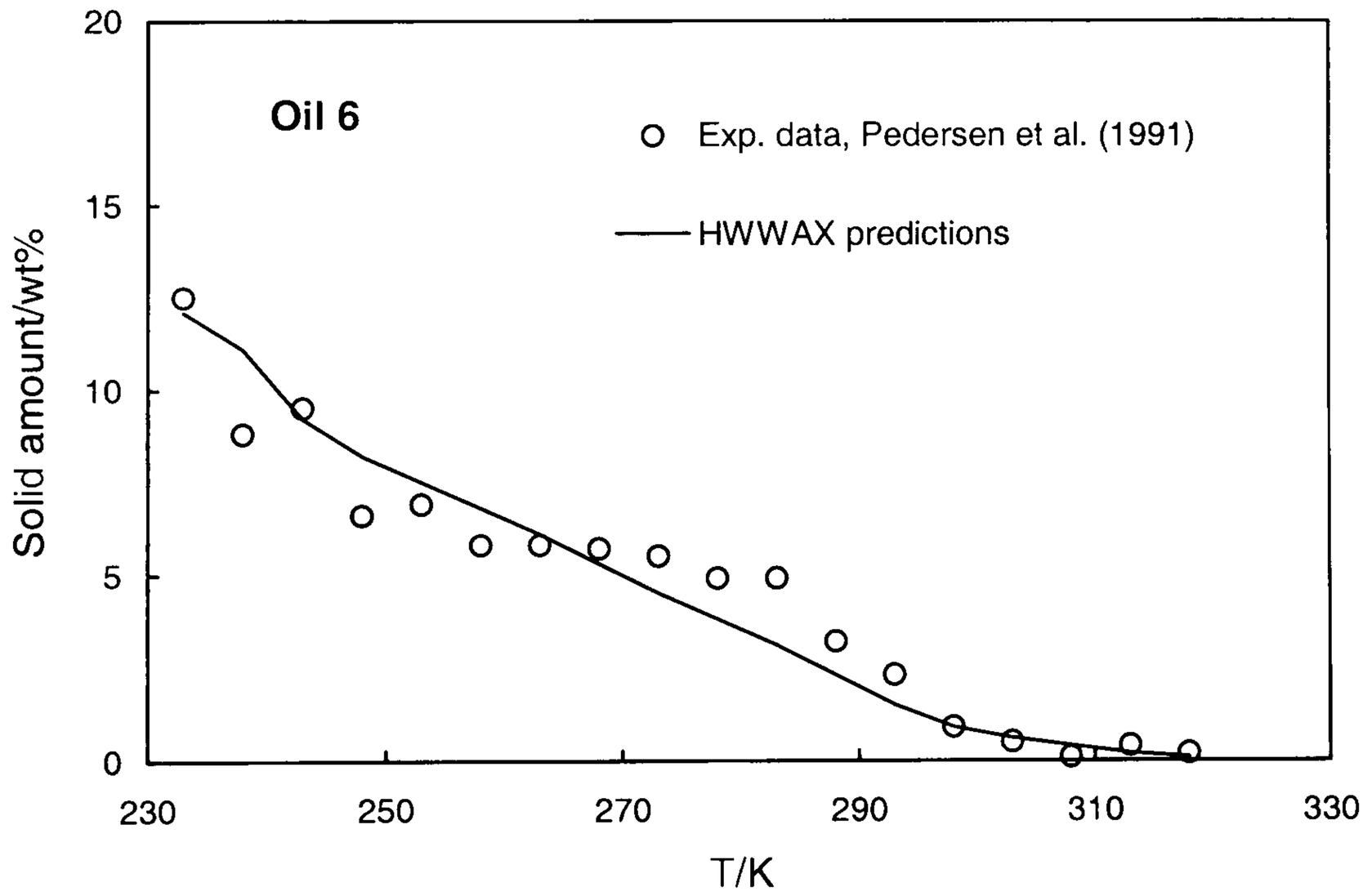

Figure 6.28. Experimental (Pedersen et al., 1991a) and predicted (using HWWAX) wax amounts for crude Oil 6.

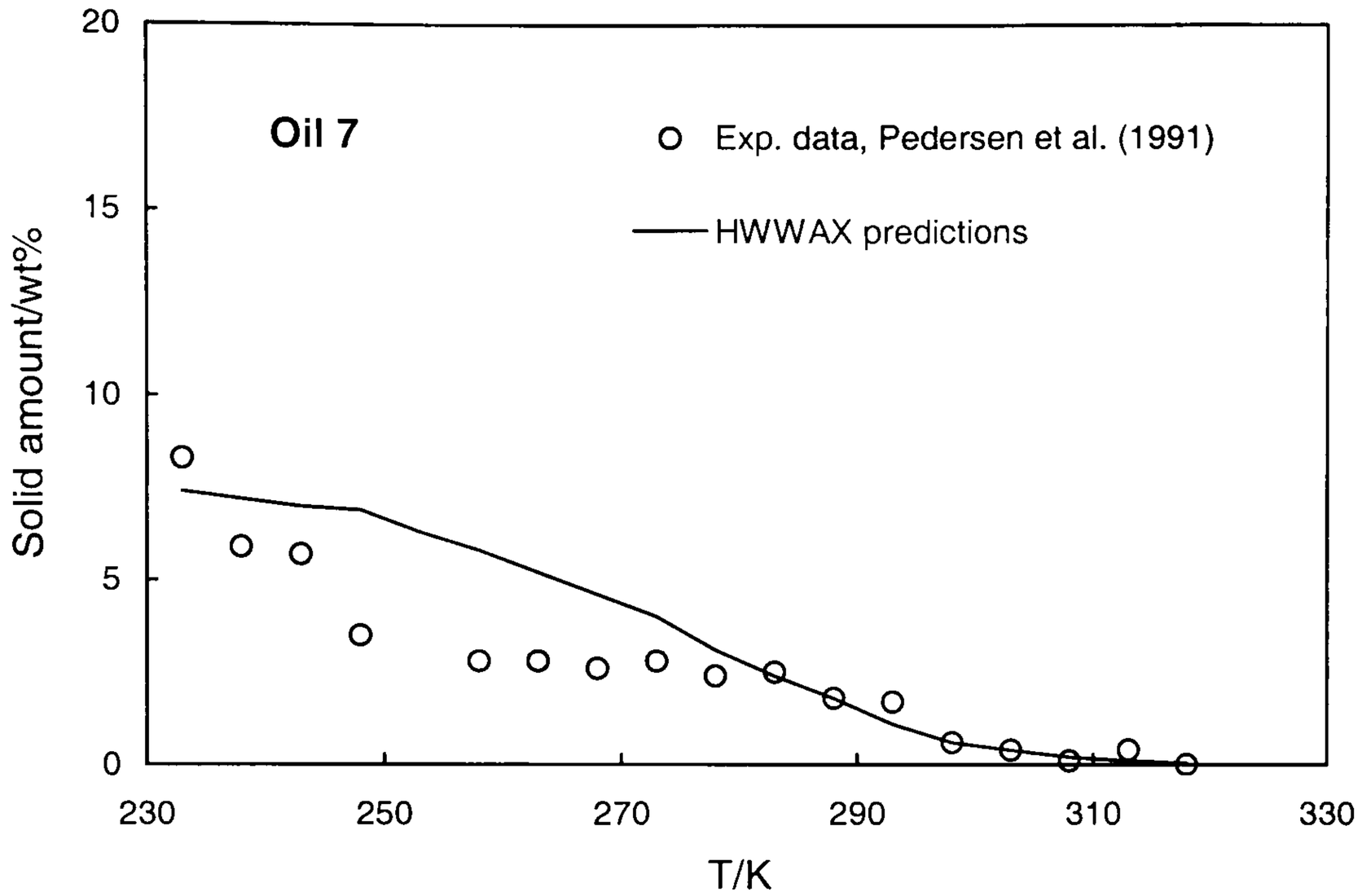

Figure 6.29. Experimental (Pedersen et al., 1991a) and predicted (using HWWAX) solid amounts for crude Oil 7.

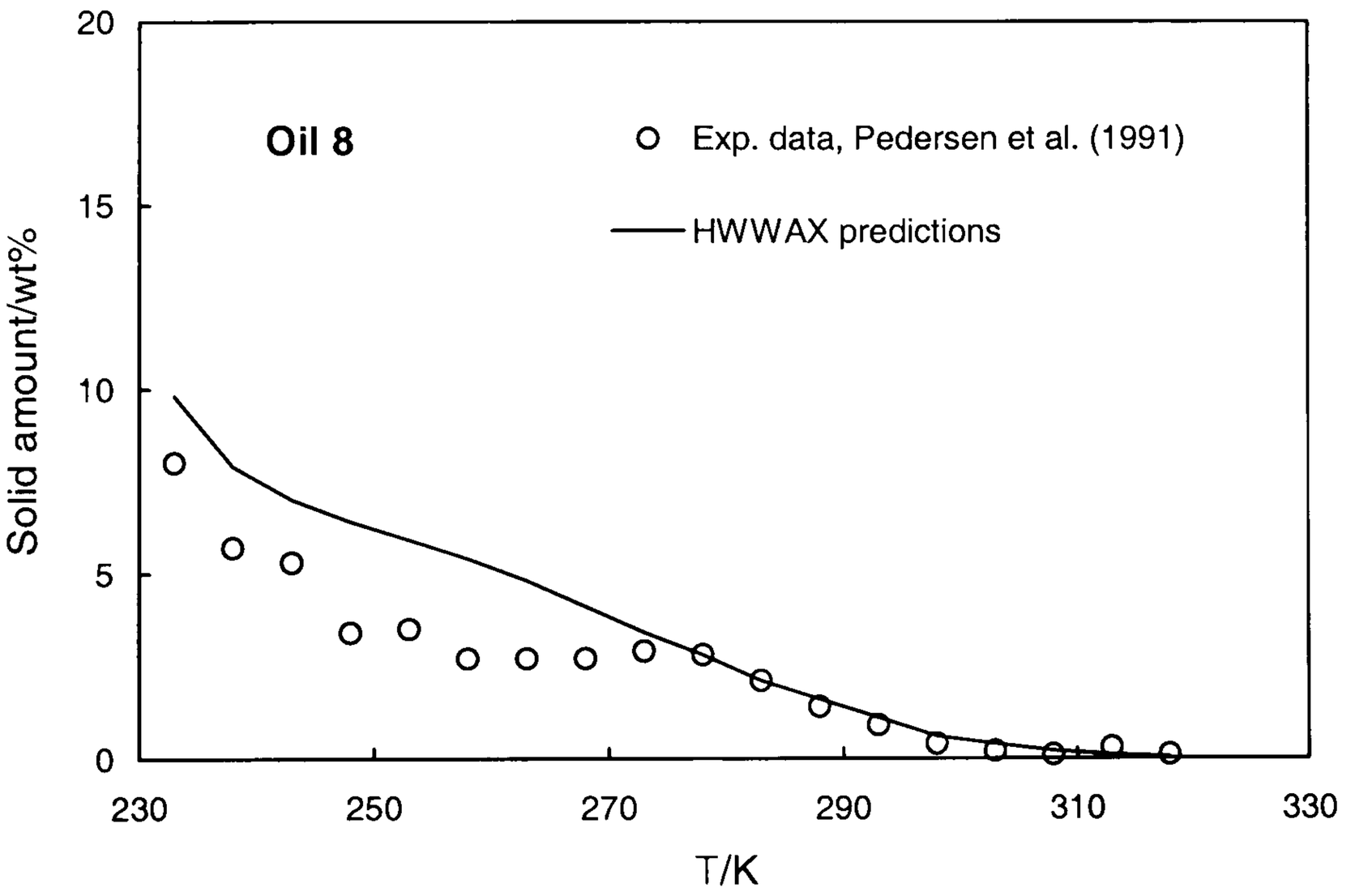

Figure 6.30. Experimental (Pedersen et al., 1991a) and predicted (using HWWAX) wax amounts for crude Oil 8.

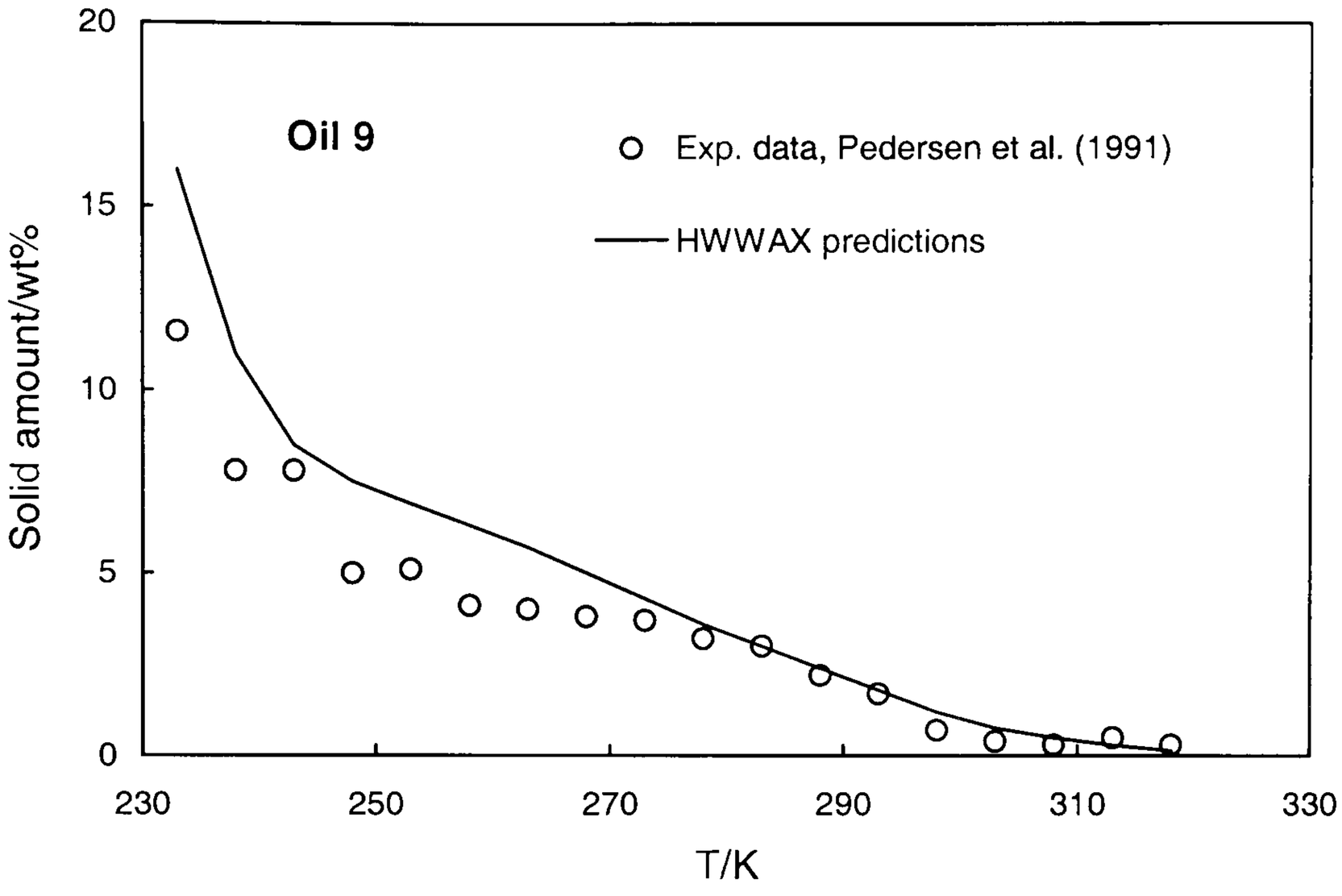

Figure 6.31. Experimental (Pedersen et al., 1991a) and predicted (using HWWAX) wax amounts for crude Oil 9.

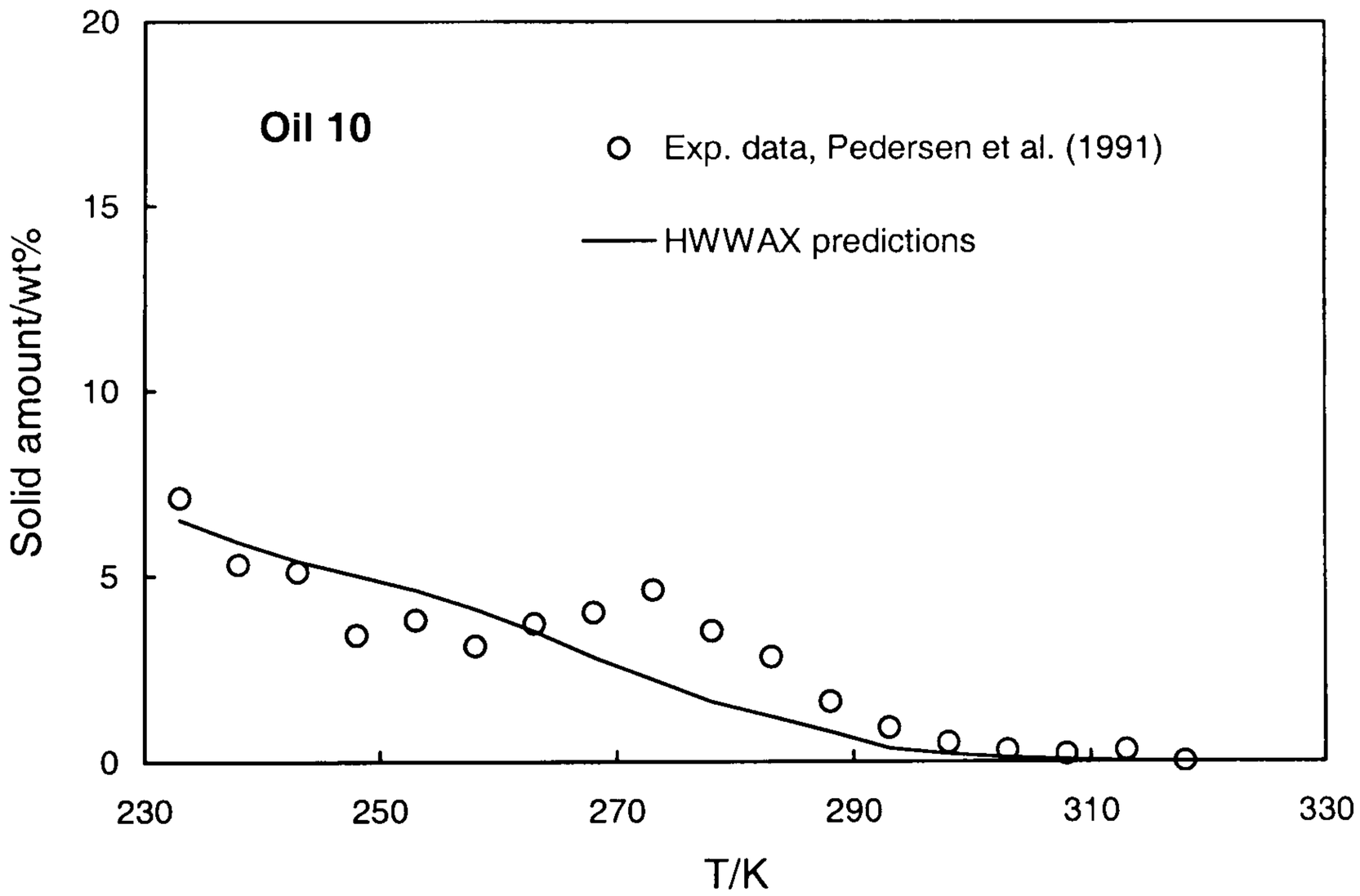

Figure 6.32. Experimental (Pedersen et al., 1991a) and predicted (using HWWAX) wax amounts for crude Oil 10.

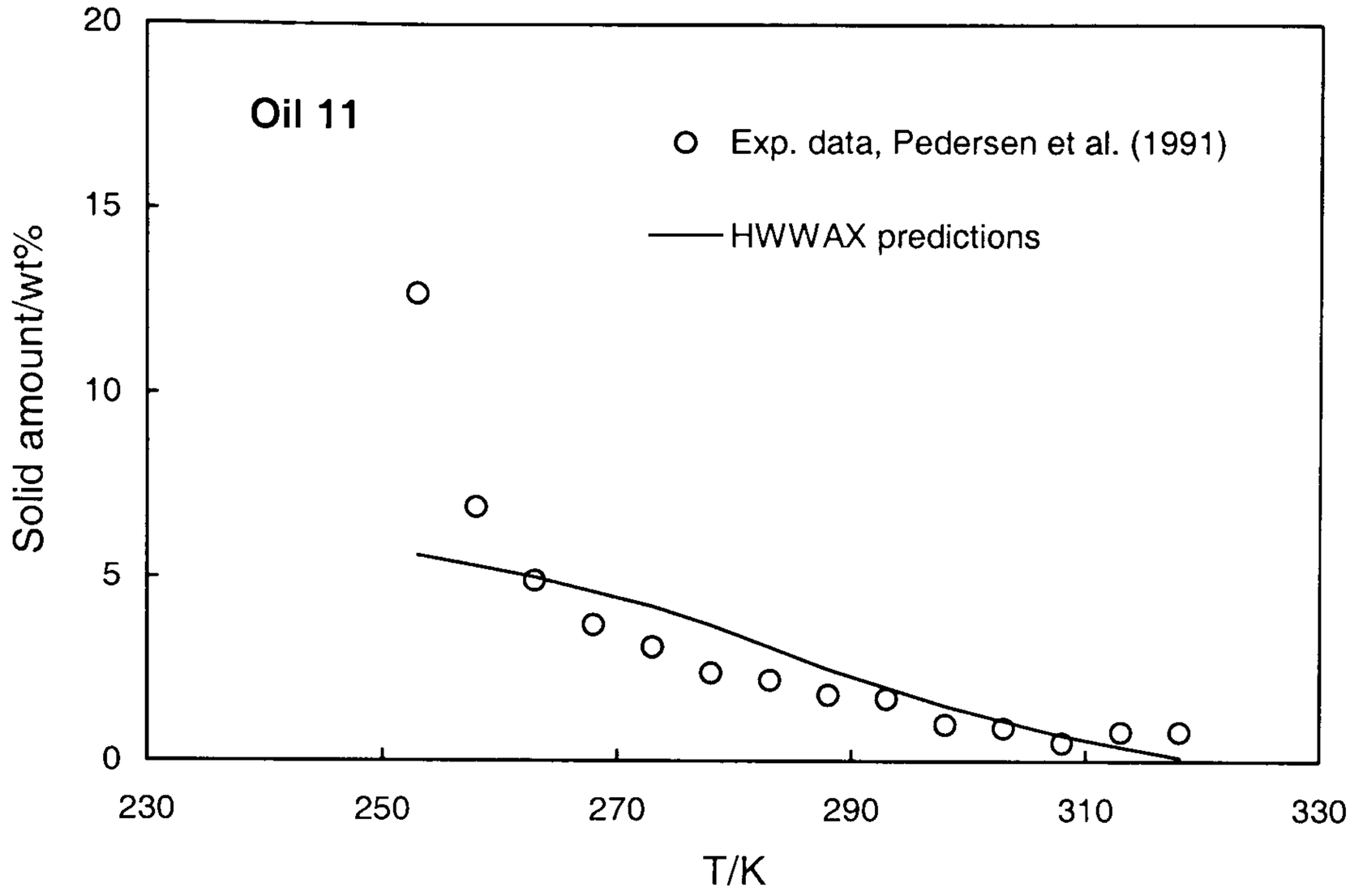

Figure 6.33. Experimental (Pedersen et al., 1991a) and predicted (using HWWAX) wax amounts for crude Oil 11.

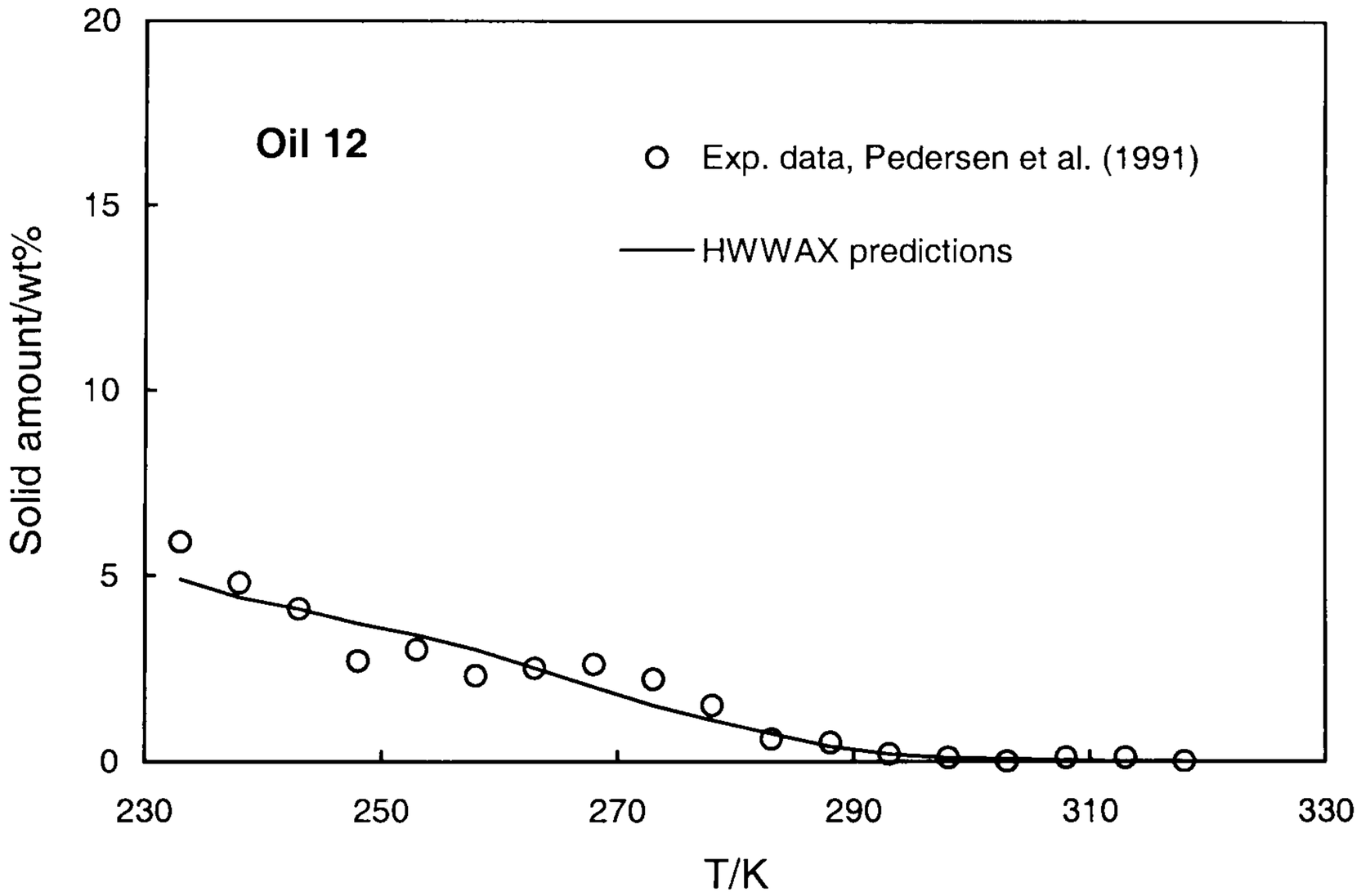

Figure 6.34. Experimental (Pedersen et al., 1991a) and predicted (using HWWAX) wax amounts for crude Oil 12.

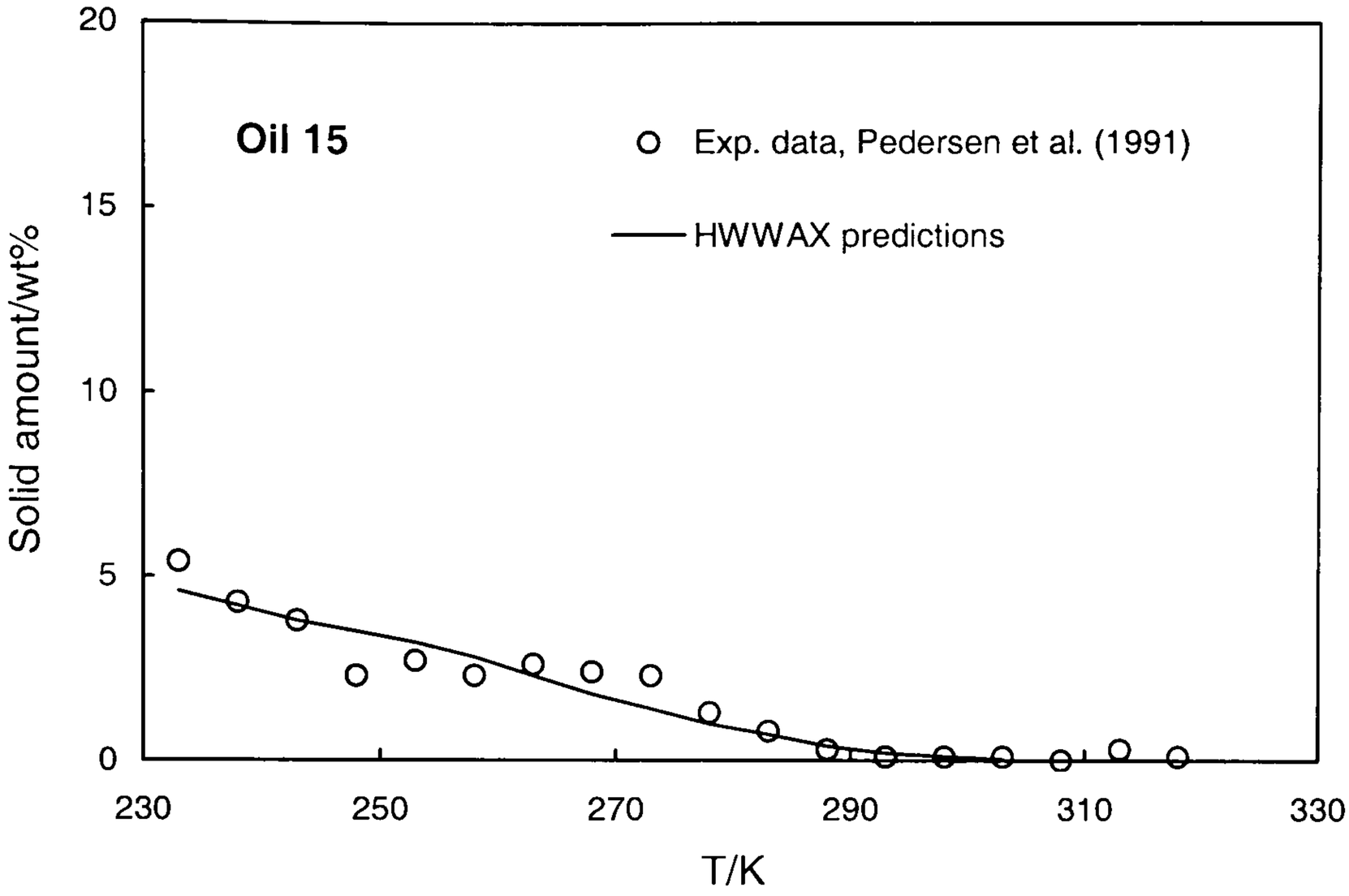

Figure 6.35. Experimental (Pedersen et al., 1991a) and predicted (using HWWAX) wax amounts for crude Oil 15.

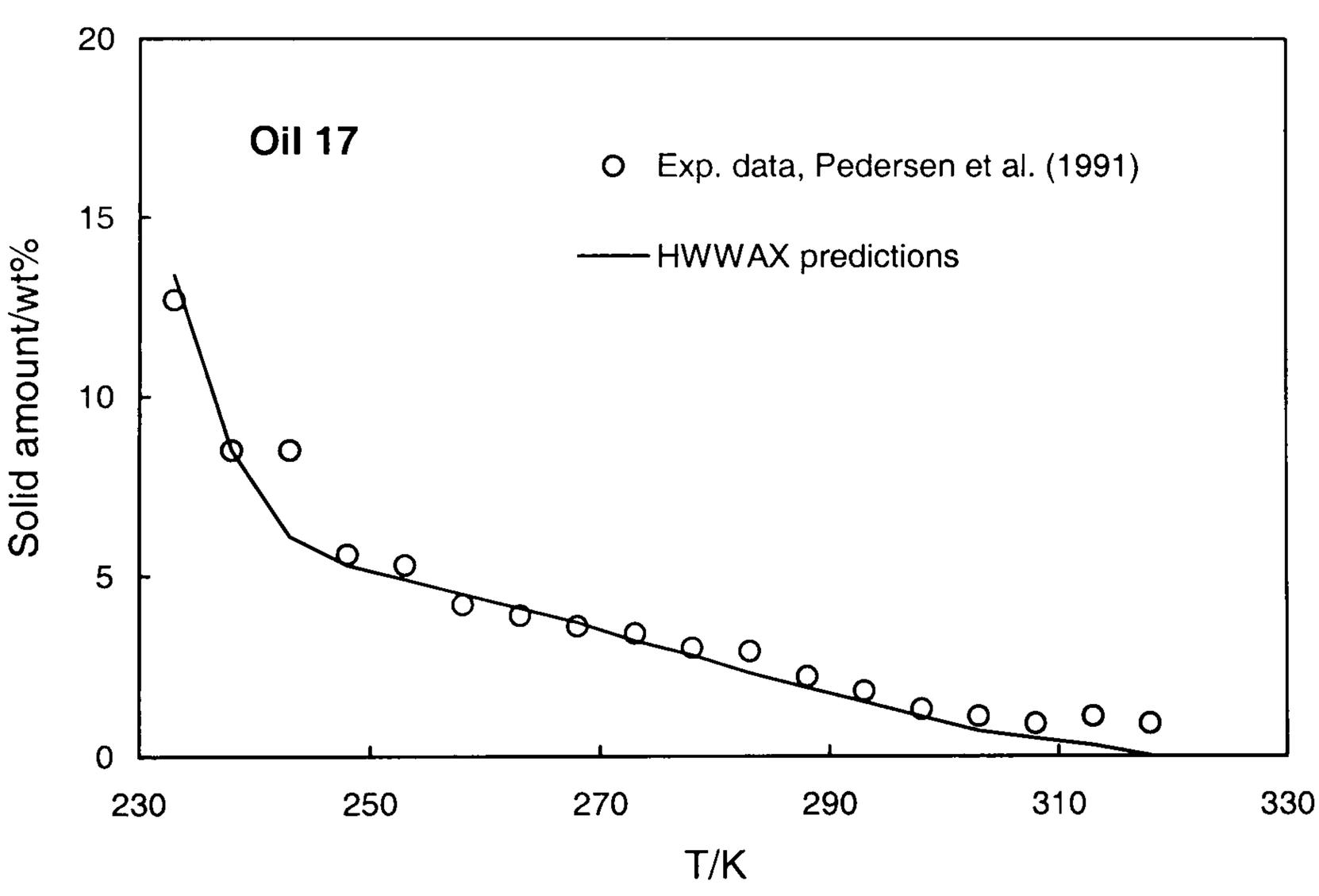

Figure 6.36. Experimental (Pedersen et al., 1991a) and predicted (using HWWAX) wax amounts for crude Oil 17.

CHAPTER-7

INTEGREATED MODELLING OF WAX AND HYDRATE

7.1. INTRODUCTION

In a multiphase system, formation of gas hydrates can remove light components from the fluid phases, subsequently reducing the solubility of waxy compounds that may affect wax phase boundary. On the other hand, wax formation can remove heavy compounds, increasing the relative concentrations of light compounds in the fluid, in which hydrate phase boundary may be affected.

Edmonds et al. (1999) has attempted an integrated modelling of hydrate and wax. In their programme, hydrate phase equilibrium calculation was based on the model of van der Waals and Platteeuw (1959), while the multi-pure-solid model suggested by LiraGaleana et al. (1996) was used for calculating wax phase equilibrium. The LiraGaleana et al.'s wax model was based on WAT, and modelling of wax for real reservoir fluids was based on single carbon number (SCN) groups without differentiating n-paraffins and non-n-paraffins.

For a given fluid, the same compositional data (i.e. the same component number) was used for simultaneous calculations of both hydrate and wax in Edmonds et al.'s model. Since hydrocarbons heavier than C_{20} are responsible for determining wax phase equilibrium, they need to be described as discrete components for the wax modelling. However, these hydrocarbons are not hydrate formers. Their presence as individual components in the hydrate model will not improve the modelling accuracy, but can increase the computation time due to large number of components. In order to reduce the computation time, a 'lumping' procedure was employed by Edmonds et al. to combine SCN components into pseudo-components. This might cause problems in wax modelling, as it was noticed that

wax calculation was sensitive to the 'lumping' procedure; the predicted WATs could differ by over 30 K when using different pseudo-components in the lumping for the given fluid.

In this chapter, I will integrate the new wax model (HWWAX) developed in this work with the hydrate model (HWHYD) developed from the previous studies in the research group. Considering the drawbacks of Edmonds et al.'s model, separated fluid characterisation procedures will be used for wax and hydrate modelling in order to improve the calculation stability and reduce the computation time.

7.2. COMBINING THE WAX AND HYDRATE MODELS

7.2.1. Programme Outline

In terms of thermodynamics, the effects of wax formation on hydrate and vice versa are related to changes in the fluid composition due to solid formation. Light compounds will be removed from the fluid phases by the formation of gas hydrates, while heavy hydrocarbons will be extracted from the liquid phase due to wax deposition.

For a given fluid system, it is important to determine whether wax or hydrate forms first when reducing temperature at a certain pressure. It is assumed that wax will form first if WDT of the fluid at certain pressure is higher than the Hydrate Dissociation Temperature (HDT) at the same pressure, and vice versa. The kinetic effect of wax and hydrate formation is not considered in this work.

If wax forms first, it will change the composition of liquid phase, which will affect the solubility of light ends. This change will then be considered in the calculations of hydrate phase boundary. On the other hand, if hydrate forms first, the effect by removal of hydrate-formers will be accounted for the wax phase boundary prediction. Therefore, the hydrate flash calculation programme will be coupled into the wax models to update the fluid composition after the formation of hydrate, and similarly the hydrate model will be combined with the wax flash calculation.

Figure 7.1 shows the schematic flow-chart (algorithm) for the integrated modelling of wax and hydrate in this work. It should be noted that, when calculating the Wax Disappearance

Temperature (WDT) in the presence of hydrate, the fluid compositions are recalculated using a hydrate flash procedure, in which the light components that formed hydrates were removed from the fluid phases. A similar procedure is used to update the fluid compositions during hydrate calculations in the presence of wax.

In the previous hydrate model, the hydrate dissociation pressure was selected as the unknown variable instead of the dissociation temperature, since, as shown in Chapter 3, several thermodynamic equations describing the hydrate are highly dependent on temperature. In this work, a programme was coded for obtaining the hydrate dissociation temperature, in order to compare with the wax disappearance temperature. Its schematic flowchart is shown in Figure 7.2. When the operating T is inside the wax phase boundary, the wax flash calculation is performed, giving an updated fluid composition for calculating the hydrate dissociation point. Otherwise, the original fluid composition will be used.

7.2.2. Fluid Characterisation

A typical fluid composition report (e.g. Tables A.7-A.9 in Appendix-A) gives discrete components for the non-hydrocarbon gases such as CO_2, and hydrocarbons up to C_6. Compounds such as *methane*, *ethane*, *propane*, *iso-butane*, *n-butane*, *iso-pentane*, CO_2, N_2 and H_2S, are hydrate formers. They are expressed as individual components in both wax and hydrate models.

In the typical fluid composition report, hydrocarbon components heavier than C_6 are commonly given as a series of single carbon number (SCN) cuts, and a plus fraction is used for the remaining heavy end. These compounds do not take part in hydrate formation. So they can be grouped into one pseudo-component for hydrate calculations. The pseudo-component can be determined by matching the bubble point of the fluid (Tohidi, 1995). This grouping procedure will not affect the accuracy of hydrate calculations, but can reduce the number of components and hence the computation time.

For wax calculations, both grouping and splitting procedures are used. As mentioned in Chapters 5 and 6, the plus fraction is first split into SCN groups up to C_{60}, then the non-wax forming SCN groups between C_6 and C_{20} are grouped into one pseudo-component, while each SCN group heavier than C_{20} is further separated into a n-paraffin and a non-n-paraffin component using Equation 5.7.

7.2.3. EoS and BIP

In the hydrate model, the Valderrama modification of the Patel and Teja (VPT) EoS is used for calculating the fugacity in the vapour and liquid phases (Valderrama, 1990). The gas-water binary interaction parameters (BIPs) are determined by matching binary vapour-liquid equilibrium data, and are kept constants.

For an integrated modelling of wax and hydrate, it is better to use the VPT EoS for modelling wax. However, it was found difficult to modify its α function for considering heavy hydrocarbons. The VPT EoS was found incapable of calculating fugacity in vapour phase for the systems containing heavy paraffins. The Binary Interaction Parameters determined for the VPT EoS were strongly dependent on the carbon numbers of compounds. Since the BIP is sensitive in the thermodynamic calculations, the VPT EoS is deemed not suitable for use in calculation of wax formation. Therefore, the SRK and PR EoSs were used in the wax model.

In the SRK and PR EoS, the BIPs for light compounds such as C_1-C_5 are based on the data given in the references (as listed in Appendix-B), while a constant BIP, –0.020 for the SRK EoS and –0.024 for the PR EoS (see Chapter-4), is used for intermediate (the C_6-C_{20} pseudo-component) and heavy components (C_n>C_{20}). Furthermore, the BIP between the major light compound (i.e. the one with the highest mole fraction) and others heavier than C_6 is determined by matching the bubble point pressure of the fluid.

7.3. APPLICATION OF THE INTEGRATED MODEL

Two examples will be given for the application of the integrated wax and hydrate model to numerically study the thermodynamic effect of one solid formation on the other. For each example, I will show the phase boundaries for fluids with different concentrations of light end, indicating the potential shift of phase boundary due to lose or increase of light end fraction. Then, the phase boundaries for hydrate or wax will be predicted with and without considering the existing solid. The effect of existing solid will be analysed using the simulation data of fluid composition change, and backed up with the available experimental observation in laboratory.

7.3.1 Hydrate Phase Boundary: Effect of Wax Formation

Effect of light end on hydrate phase boundary

Black Oil RFS-1 with compositions given in Table A.9 has been studied using the integrated model. As given earlier in Chapter-6, the WDT of the dead fluid was predicted as 319 K, while the experimental WDT was 323K. The live reservoir fluid of RFS-1 (Table A.9) contains 44.7 mole% light ends (i.e. C_1-C_5), 43.8 mole% intermediate hydrocarbons (i.e. C_6-C_{20}) and 11.5 mole% heavy hydrocarbons (i.e. C_{20+}), with the measured saturation pressure of 9.41 MPa at 373.15 K. In order to facilitate the hydrate calculations, all compounds heavier than C_6 are lumped into n-C_{13} by matching the saturation pressure of the live fluid. To assess the effect of the mixing ratio of light ends with the dead fluid on hydrate, several mixtures were assumed by using different mole fractions of light end, as shown in Table 7.1.

The hydrate phase boundaries without consideration of wax formation were predicted for the above mixtures using the combined wax-hydrate model. The results are shown in Figure 7.3. Hydrate phase boundary is shifted toward higher temperatures as the mixing ratio of light ends increases. For instance, at 5 MPa, the hydrate dissociation temperature increases 1 K when the light end fraction increases from 44.7 mole% to 55 mole%. In an extreme case, the hydrate dissociation temperature at 5 MPa can increase by approximately 5 K if the light end content increases from 25 to 95 mole%. It is noted that, if the live reservoir fluid of RFS-1 removes all hydrocarbons above C_{20} due to wax formation, its light end fraction will increase from 44.7 mole% to 50.5 mole%, which would cause the increase of hydrate dissociation temperature less than 1 K.

Effect of wax formation on hydrate phase boundary

As noted in Figure 7.3, for the live fluid RFS-1 with 44.7 mole% light ends, the hydrate dissociation temperature at 5 MPa is approximately 287.3 K. On the other hand, the wax disappearance temperature (WDT) was predicted as 314.5 K at 5 MPa (as shown in Table 7.2). Therefore, wax may form before hydrates.

The integrated wax and hydrate model was used for calculating the hydrate dissociation point at various conditions. Table 7.2 compares the predicted hydrate phase boundaries in the

absence and presence of wax. The data show that the effect of wax formation on the hydrate phase boundary is not notable for the live fluid studied in this case.

Table 7.3 shows the wax flash calculation results at different temperature and pressure conditions. The predicted amounts of wax formed at these conditions are very small (less than 1 mole%), and consequently the change in the light end concentration is small. Therefore there is little effect on the hydrate phase boundary due to wax formation.

7.3.2. Wax Phase Boundary: Effect of Hydrate Formation

The effect of light end composition on wax phase boundary has been discussed in Chapter-6. In this section, it will be further demonstrated using the synthetic mixtures with different fractions of light ends: 0 mole%(no light ends), 45 mole% and 69 mole% light ends. The details of the mixture compositions are shown in Table A.5 (in Appendix A). Figure 7.4 shows experimental WAT and WDT data (listed in Table A.6) as well as the predicted wax phase boundaries for the fluids with different mixing ratios of the light ends.

The wax phase boundaries predicted using the HWWAX model are approximately 1 K higher than the measured WAT data for the fluids with 0 and 45 mole% light end. When considering the subcooling (approximately 1 K as detailed in Chapter 2) for these fluids, it can be concluded that the HWWAX predictions are in excellent agreement with the measured wax phase boundaries. For the fluid with 69 mole% light ends, the model predictions are close to the measured WDT data. As can be observed in the figure, the predicted WDT at 20 MPa increases approximately by 2 K as the light end concentration decreases from 69 mole% to 45 mole%.

The fluid containing 69 mole% light ends was mixed with water by volume ratio of approximately 1:1, and was investigated in the laboratory for hydrate phase boundary measurement. Figure 7.5 shows the experimental and predicted hydrate dissociation points, which are in good agreement. The measured and predicted wax phase boundaries are also shown in the figure. Apparently, hydrates form at higher temperatures than the wax when the system pressure is above 2 MPa.

It was intended to study the effect of hydrate on wax formation by measuring the wax disappearance temperature in the presence of hydrate. However, since both hydrate and wax

formed in this system are white crystals, it was found difficult to correctly detect the last wax crystal disappearing upon heating. It was also found that the detection of wax appearance is possible, as the wax crystal is sparkly and so can be differentiated from the exiting hydrates during cooling. Therefore, in the experiments, the wax appearance temperatures in the presence of hydrate were detected using visual technique. The difference between the measured WATs with and without hydrates was within 1 K. The experimental data indicated that the effect of hydrate formation on the wax phase boundary is not notable for the system studied.

The integrated wax and hydrate model was used to calculate the wax phase boundary with the consideration of hydrate formation. The calculated WDTs with hydrate are compared with those without hydrate in Table 7.4, in which the WDT increases by 0.1 – 0.3 K due to the formation of hydrate.

Table 7.5 lists the distributions of different phases at several equilibrium conditions. It is noticed that significant amounts of hydrate can be formed (about 58 mole% of the system). As shown in the table, the formation of hydrate can remove approximately 6 mole% light compounds (C_1, C_2 and C_3) from the system. Recalling the results shown in Figure 7.4, only 2 K increase of WDT was gained as the light end concentration decreases from 69 mole% to 45 mole%. It may suggest that the increase of WDT due to hydrate formation could be less than 1 K for the system studied. In fact, there is no significant change in the concentration of heavy components such as C_{23} - C_{26} after hydrate formation (as shown in Table 7.5), so it is not surprising that the wax phase boundary is not significantly affected by hydrate formation.

7.4. CONCLUSIONS

In this chapter, the new wax model developed in this work was combined with the hydrate model available from previous studies to form an integrated wax-hydrate model. In the model combination, the hydrate model was coupled with a wax flash calculation, and a hydrate flash calculation was added to the wax model, in order to update the fluid composition after wax or hydrate formation. The new integrated model used different fluid characterisation approaches in wax and hydrate calculations to ensure the reliability of each

model and reduce computing time. The integrated wax and hydrate model can be used to estimate the effect of one solid formation on the other in terms of thermodynamics.

The effect of wax formation on hydrate phase boundary was investigated for a real reservoir fluid with a higher WDT than HDT (hydrate dissociation temperature), in which wax could form before hydrate. The modelling results showed that the hydrate phase boundary was not significantly affected by the wax formation since only small increases of the light compound compositions were introduced after wax formation.

The effect of hydrate formation on wax was studied for a specially designed synthetic fluid, which had a higher HDT than WDT to assure hydrate could form before wax. The simulation results showed that the wax phase boundary was not significantly shifted due to hydrate formation, because only small increases of the heavy compound compositions were induced by the hydrate formation.

It is speculated that the influence of wax formation on hydrate may increase if the wax deposition can cause significant change in fluid composition. On the other hand, the effect of hydrate formation on wax may be notable when a significant amount of light compounds are removed from the fluid due to formation of hydrate. It is suggested to measure and model the wax effect on hydrate using systems containing large amounts of C_{20+} fractions.

7.5. TABLES

Table 7.1. Compositions (mole%) for several mixtures based on different mixing ratios of C_1-C_5 with the dead fluid.

	Light end/ mole%						
Component	15	25	35	44.7	55	75	95
C_1	8.04	13.41	18.77	23.98	29.49	40.22	50.94
C_2	1.34	2.23	3.12	3.98	4.90	6.68	8.46
C_3	1.90	3.16	4.42	5.65	6.95	9.48	12.00
iC_4	0.67	1.12	1.57	2.00	2.46	3.35	4.25
nC_4	1.38	2.30	3.22	4.12	5.07	6.91	8.75
iC_5	0.70	1.17	1.64	2.09	2.57	3.51	4.44
nC_5	0.97	1.62	2.26	2.89	3.55	4.85	6.14
nC_{13}	85.00	75.00	65.01	55.30	45.01	25.01	5.02

Table 7.2. Calculated wax disappearance temperature (WDT) at 5.07 MPa and the hydrate dissociation points without and with taking into account wax formation.

		Calculation of the hydrate dissociation point			
Operating	calculated	without wax		with wax	
P/MPa	WDT/K	T/K	P/MPa	T/K	P/MPa
5.07	314.48	273.50	0.58	273.50	0.57
		278.50	1.30	278.50	1.29
		283.50	2.79	283.50	2.78
		286.00	4.10	286.00	4.09
		287.25	4.99	287.25	4.98
		287.33	**5.06**	287.33	5.05
				287.37	**5.08**

Table 7.3. Distributions (mole %) of equilibrium phases and compositions of the fluid with removal of wax at several temperature and pressure conditions.

	Temperature and pressure at equilibrium						
T/K	273.50	278.50	283.50	286.00	287.25	287.33	287.37
P/MPa	0.69	1.31	2.68	3.92	4.77	4.83	4.86
Phase	Calculated mole% of equilibrium phases						
Vapour	25.99	22.28	15.70	10.17	6.46	6.20	6.07
Liquid hydrocarbon	73.25	77.16	83.91	89.51	93.26	93.52	93.65
Wax	0.76	0.56	0.39	0.31	0.28	0.28	0.28
Input composition	Compositions (mole%) with removal of wax						
C_1 24.03	24.22	24.17	24.13	24.11	24.10	24.10	24.10
C_2 3.99	4.02	4.01	4.00	4.00	4.00	4.00	4.00
C_3 5.66	5.71	5.69	5.68	5.68	5.68	5.68	5.68
iC_4 2.00	2.02	2.02	2.01	2.01	2.01	2.01	2.01
nC_4 4.13	4.16	4.15	4.14	4.14	4.14	4.14	4.14
iC_5 2.09	2.11	2.11	2.10	2.10	2.10	2.10	2.10
nC_5 2.90	2.92	2.91	2.91	2.91	2.90	2.90	2.90
nC_{13} 55.20	54.85	54.94	55.02	55.05	55.07	55.07	55.07

Table 7.4. The calculated hydrate dissociation temperatures (HDT) and the wax disappearance temperatures (WDT) with and without hydrate.

		Calculation of WDT	
Operating P/MPa	Calculated HDT/K	without hydrate WDT/K	with hydrate WDT/K
3.3	281.4	275.2	275.4
6.9	286.6	274.3	274.6
13.4	290.8	273.7	273.8
19.9	293.0	273.8	273.9

Table 7.5. Distributions (mole %) of equilibrium phases and compositions of the fluid with removal of hydrates formed at conditions of a fixed temperature and several pressures.

	Temperature and pressure at equilibrium			
T/K	273.20	273.20	273.20	273.20
P/MPa	3.30	6.90	13.40	19.90
Phase	Calculated mole% of equilibrium phases			
Vapour	22.96	18.50	10.38	1.64
Liquid hydrocarbnon	19.14	23.20	31.12	39.78
Hydrate	57.90	58.30	58.50	58.58
Initial composition	Compositions (mole%) with removal of hydrate			
C_1 60.24	57.61	56.83	56.26	56.06
C_2 3.91	1.54	1.82	2.16	2.35
C_3 1.16	0.21	0.30	0.41	0.46
iC_4 0.16	0.04	0.06	0.08	0.09
nC_4 0.28	0.23	0.27	0.28	0.29
iC_5 0.07	0.08	0.08	0.08	0.08
CO_2 2.24	0.95	0.98	1.01	1.03
N_2 0.94	2.51	2.47	2.36	2.21
C_{10} 30.24	35.92	36.26	36.43	36.50
C_{21} 0.26	0.31	0.31	0.32	0.32
C_{22} 0.18	0.22	0.22	0.22	0.22
C_{23} 0.13	0.15	0.15	0.15	0.15
C_{24} 0.09	0.11	0.11	0.11	0.11
C_{25} 0.06	0.07	0.08	0.08	0.08
C_{26} 0.04	0.05	0.05	0.05	0.05
Light end 68.99	63.17	62.81	62.64	62.57

7.6. FIGURES

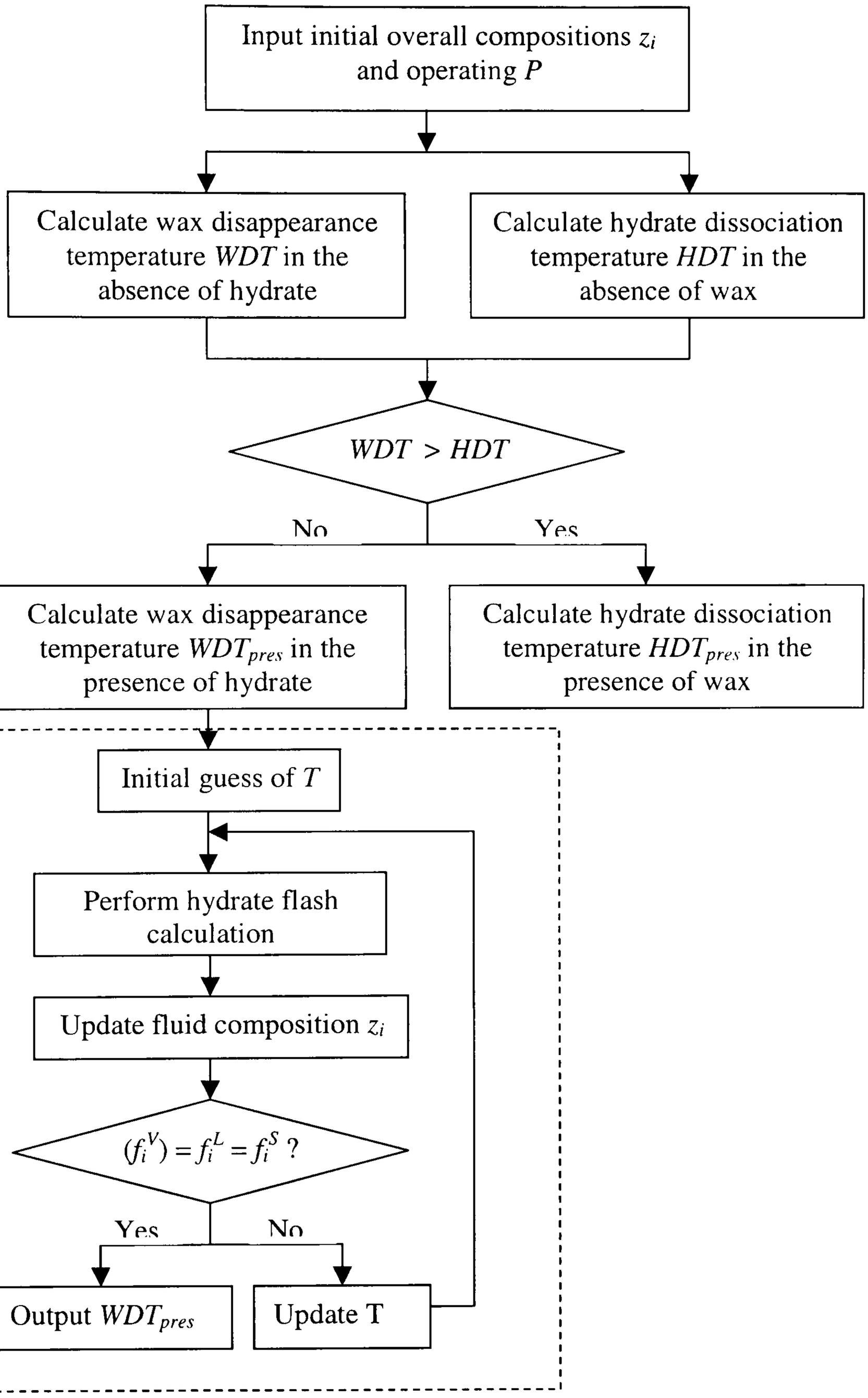

Figure 7.1. Schematic flow-chart for integrated modelling of wax and hydrate (WDT and WDT_{pres} are the wax disappearance temperatures in the absence and presence of hydrate, respectively. HDT and HDT_{pres} are the hydrate dissociation temperatures in the absence and presence of wax, respectively).

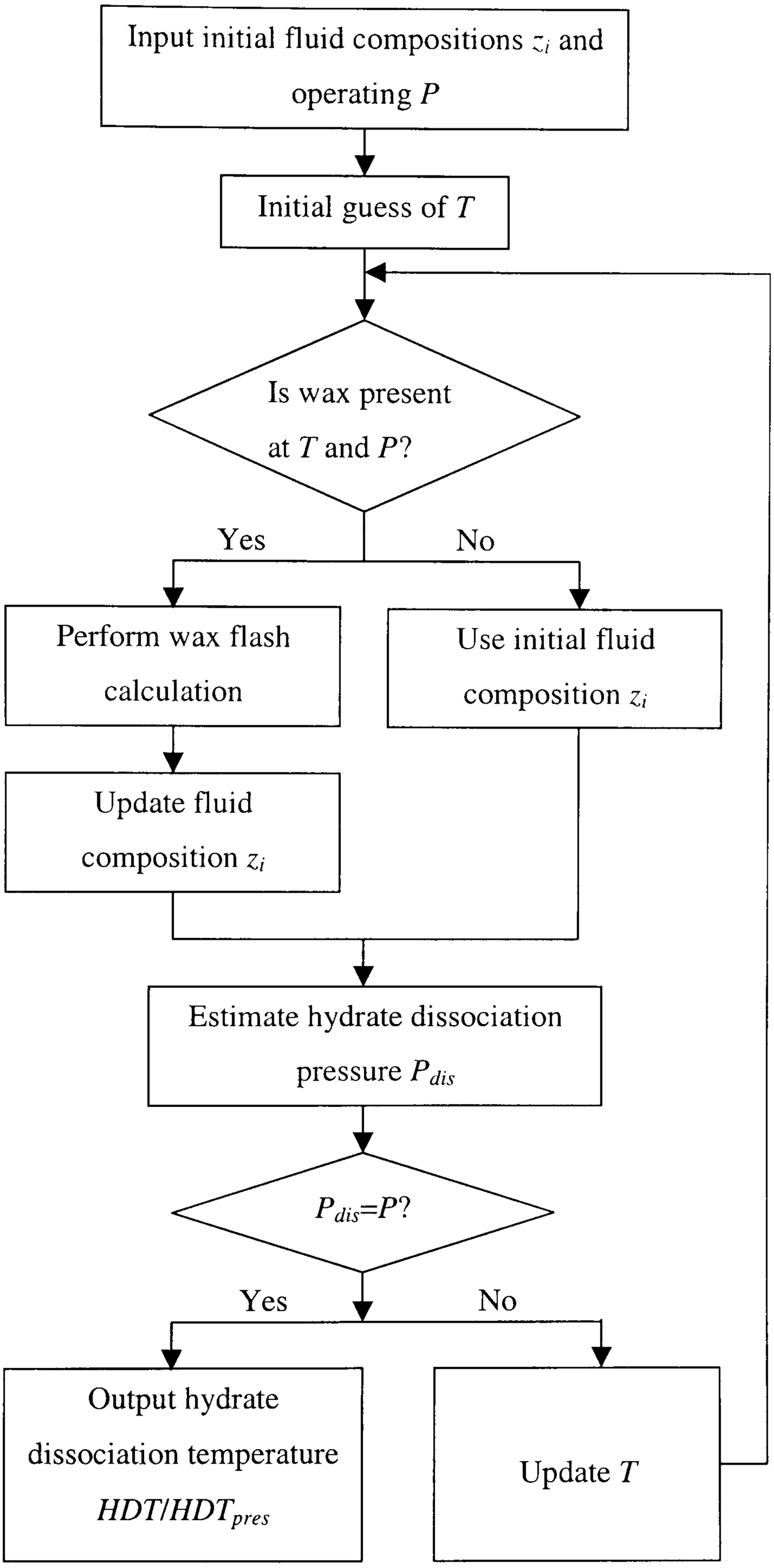

Figure 7.2. Schematic flow-chart for calculating the hydrate dissociation temperature (HDT/HDT_{pres}) in absence/presence of wax.

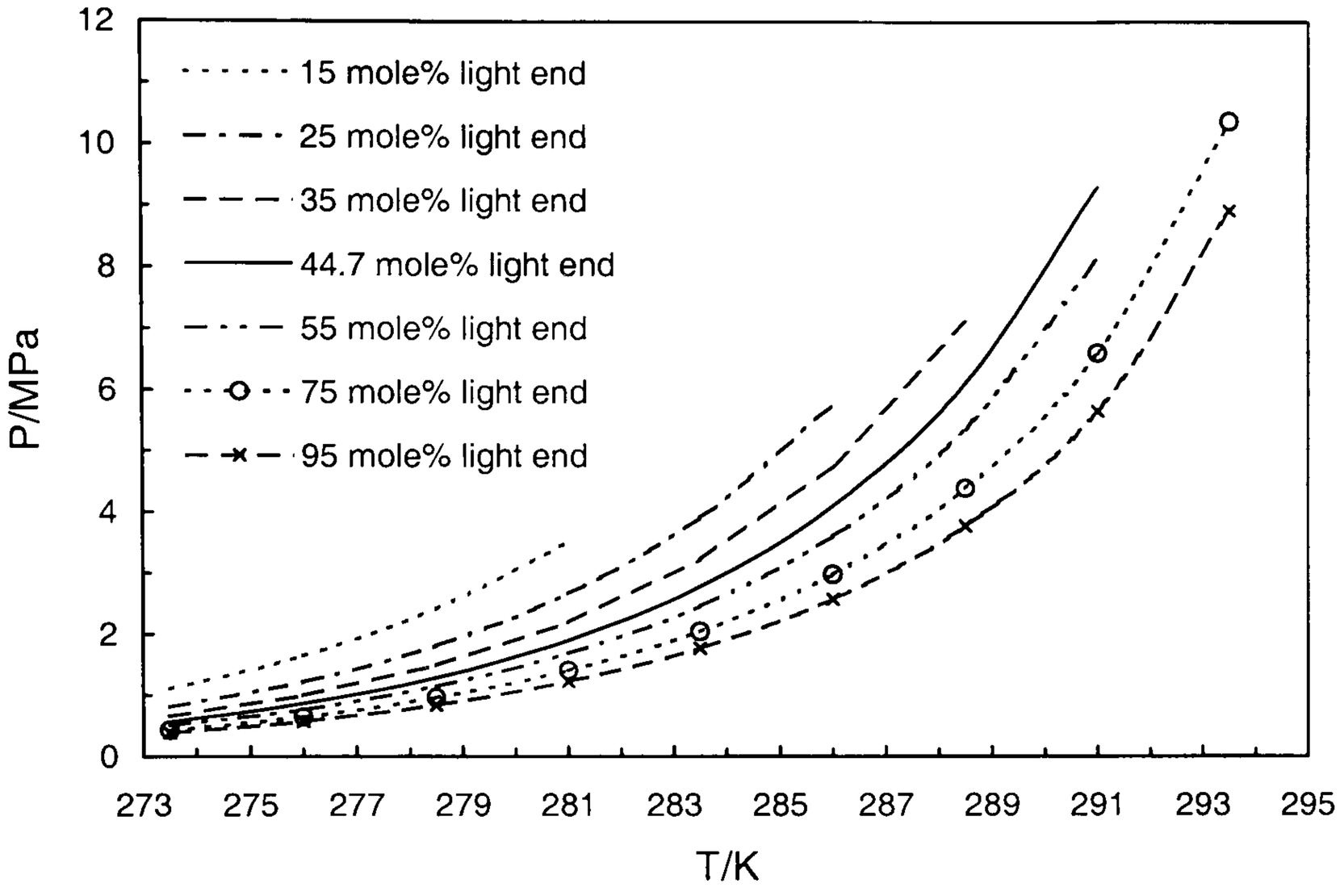

Figure 7.3. Hydrate phase boundaries predicted for several mixtures with different mixing ratios of light ends (C_1-C_5).

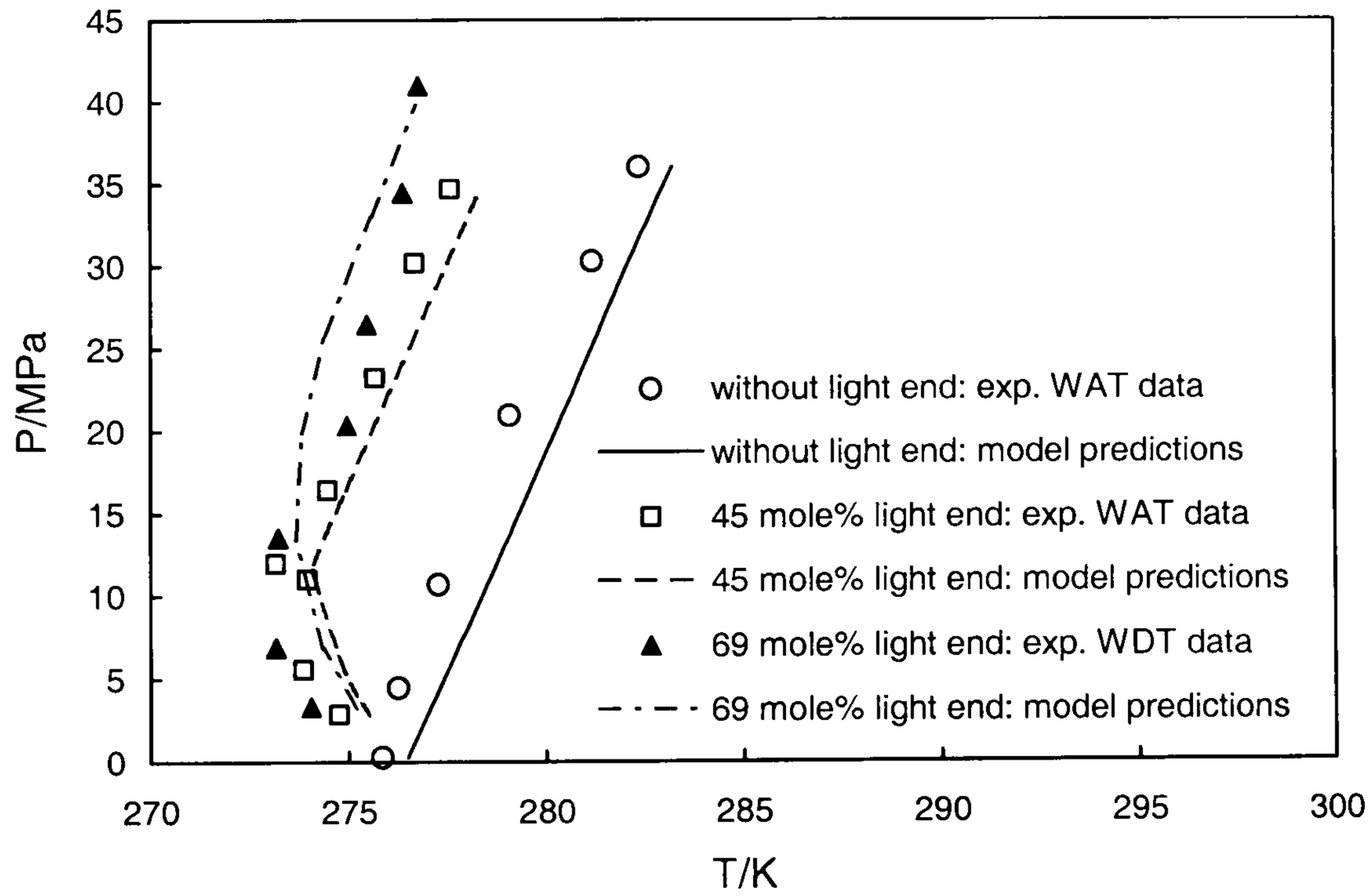

Figure 7.4. Wax phase boundaries for fluids with different concentrations of light end, as compositions listed in Table A.5.

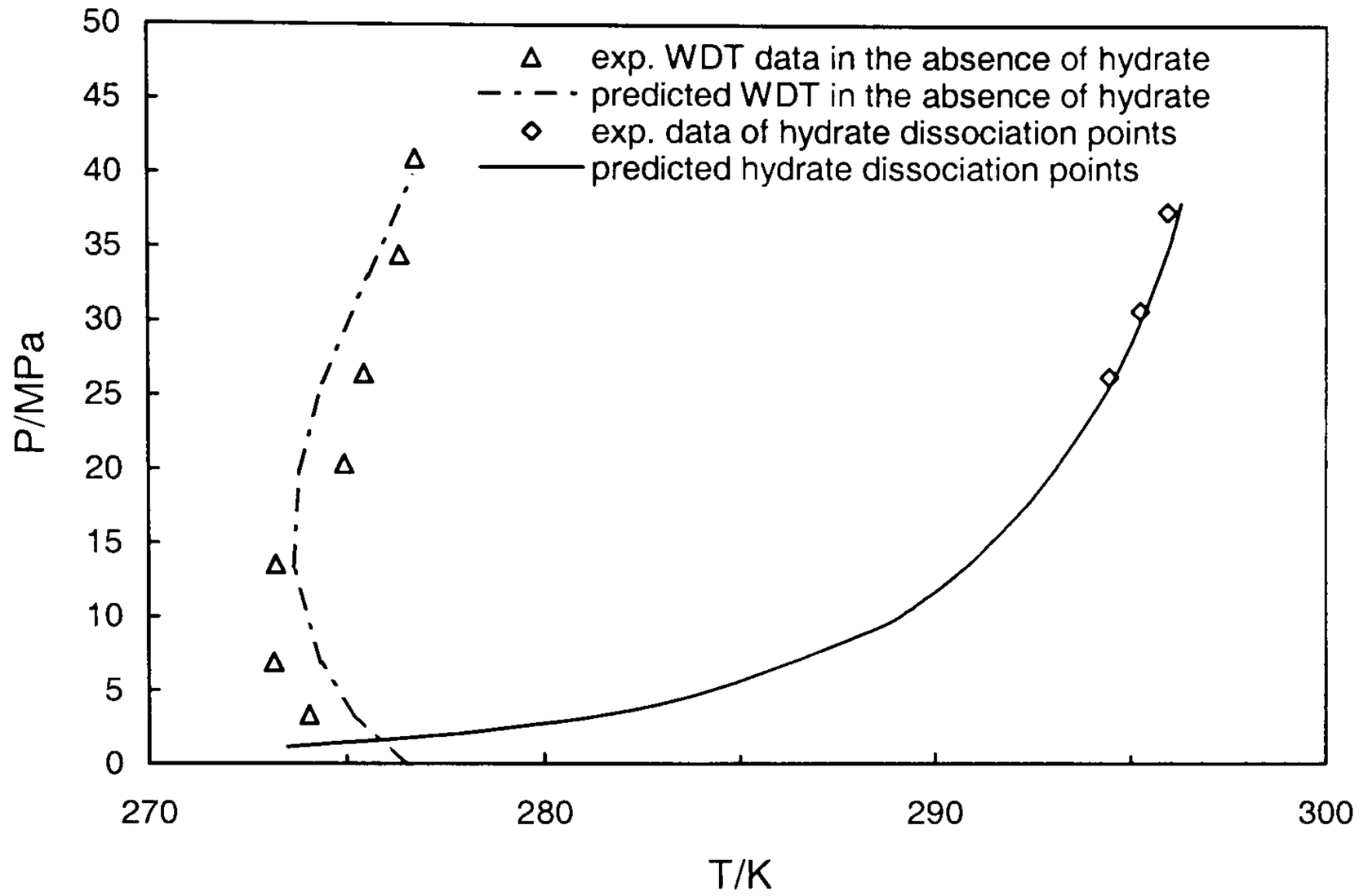

Figure 7.5. The wax and hydrate phase boundaries for the fluid containing 69 mole% light ends (experimental data are generated in this laboratory. Wax and hydrate predictions are based on the HWWAX and HWHYD models).

CHAPTER-8

CONCLUSIONS

The work described in this thesis has sought to develop a comprehensive thermodynamic wax model that can be used to estimate the wax phase equilibrium problem for complex reservoir fluids. The development of the new wax model was based on systematic procedures using reliable experimental data. First, the basic thermodynamic equations for wax formation were modified and tuned using experimental data for synthetic mixtures with known compositions. The model was developed by improving estimated pure compound properties, using a fundamental equation more suitable to describe the melting process, modifying equations of state, and developing a new approach to describe solid mixtures. Then the model was extended to real reservoir fluids using a well-proven fluid characterisation procedure based on conventional oil compositional data. The new model has shown good capability and reliability for predicting the wax phase boundary, amount and composition of wax formed. Finally, the new wax model, named as HWWAX, along with the existing hydrate model (HWHYD) available within the research group, has been integrated to formulate an integrated Wax-Hydrate model. The integrated model is capable of predicting wax and hydrate phase equilibrium and assessing the thermodynamic effect of co-appearance of wax and hydrate.

The conclusions drawn during the course of this study and main features of the new wax model will be described in this Chapter. Some suggestions and recommendations of future work are also presented for further modification and validation of the wax model and for investigation of wax and hydrate co-formation.

8.1 EXPERIMENTAL WORK

The new wax model was based on wax disappearance temperature (WDT), which can be accurately measured at a more realistic equilibrium condition than wax appearance temperature (WAT) that was used in many existing wax models. In Chapter-2, the importance of measuring wax disappearance temperature (WDT) as the basis for developing the new wax model has been clarified. The experimental set-ups and techniques used in this laboratory for wax measurements have been described. Experimental WDT data have been generated for binary systems in this work, and used for tuning the new wax model. WDTs were also measured for multi-component synthetic systems and real reservoir fluids in this laboratory, and used for validation of the new wax model. The experimental work conducted in this study can be summarised below:

- Reliable techniques (visual observation and Quartz Crystal Microbalance) and experimental procedures (step-heating) have been developed and used for measuring wax disappearance temperature (WDT) at solid-liquid equilibrium (SLE) conditions in a practically feasible experimental time scale.

- Experiments have been conducted using several deliberately designed binary systems to produce WDT data for tuning of the new wax model. The WDTs of complex synthetic hydrocarbon systems and real reservoir fluids have been measured and used for validating the new wax model. Experiments have been performed on synthetic hydrocarbon mixtures with and without light hydrocarbon ends (C_1-C_5) at different pressures. The data have been used for validating the model and assessing the effects of light ends and pressure on wax phase boundary.

8.2. DEVELOPMENT AND VALIDATION OF THE NEW WAX MODEL

In general, modelling of wax formation in a complex fluid system is a multi-phase equilibrium problem, in which the fugacities of each component in the vapour, liquid hydrocarbon and solid (wax) phases are equal. In this study, the fugacities of fluid phases were calculated using the SRK EoS or PR EoS. The calculation of fugacity in the solid phase has been related to the nature of the solid mixture, which depends on the difference of

molecular sizes between components. Compounds with significant difference in their carbon numbers can form pure solids, so a multi-pure-solid approach was used for calculating the fugacity in the solid phase. On the other hand, compounds with small difference in carbon numbers can form a solid solution, which was modelled using a non-ideal solid solution theory, while the activity coefficients were calculated using an UNIQUAC equation. The non-ideal solid solution was considered to be more suitable to describe the wax solid phase for real reservoir fluids.

8.2.1. Development of the Wax Model

In Chapter-4, the new wax model was tuned in terms of the fugacities of liquids and solids using a systematic approach. First, new correlations were introduced for calculating the thermo-physical properties of pure compounds based on reliable experimental data. Next, the α functions of SRK EoS and PR EoS were modified for describing heavy hydrocarbons at low temperatures. Then, the adjustable parameter in the UNIQUAC equation was determined for the description of wax solids. Finally, the effect of pressure on the wax phase boundary was included in the model.

The main work conducted and the features of the new model include:

- New correlations have been developed for calculating the thermo-physical properties, such as fusion temperature and heat of fusion, of pure compounds, with improved accuracy due to the consideration of the differences between odd and even carbon numbers.

- The solid-solid transition has been included into the thermodynamic equations for SLE calculations, which was in line with the experimental observations on crystalline structure transformation upon heating.

- The experimental data obtained from binary synthetic mixtures were used for tuning the SRK EoS and PR EoS. The binary mixtures were carefully selected for each system to have components with significantly different carbon numbers, so that the multi-pure-solid model can be used for calculating fugacity in solid phase. The modified equations of state and the use of constant binary interaction parameters have improved the calculation of fugacities for heavy liquid hydrocarbons.

- The adjustable parameter for the UNIQUAC equation was correlated with the difference in carbon numbers for each component pair, which can be used to model the effect of components carbon number distribution in real reservoir fluids.

- Pressure can change the fusion temperature of pure compounds. This effect on wax solid phase has been considered and modelled using reliable pure compound fusion temperatures at different pressures from the literature. Inclusion of the pressure effect has improved the accuracy of the model for predicting wax phase equilibrium at high-pressure conditions.

8.2.2. Modelling of Real Reservoir Fluids

In chapter-5, the wax model was extended to real reservoir fluids. The extension was based on fluid compositional data obtained from the conventional reservoir oil analysis, concerning the general and practical use of the model without needs for extra analytical work. A programme has been developed for splitting the plus fraction (e.g. C_{7+}) into single carbon number (SCN) groups. Then the SCN groups between C_6-C_{20} were lumped into a pseudo-component, while the SCN groups heavier than C_{20} were further separated into n-paraffins and non-n-paraffins using an empirical correlation determined in this work. The major work carried out and the main conclusions drawn in this chapter are as follows:

- Heavy components in real reservoir fluids are the main constitutes in wax formation, therefore the plus fraction obtained from the conventional oil analysis needs to be split into individual components. A Gamma distribution function has been developed to calculate the SCN mole fractions and molecular weights for the splitting of the plus fraction. The parameters such as χ and η of the Gamma function were obtained by matching the measured molecular weight and mole fraction. In this work, the Gamma function parameters were optimised using experimental data of SCN groups up to C_{20}. On the other hand, a logarithmic function has been used to calculate the SCN specific gravity for the splitting of the plus fraction. The parameters of the logarithmic function were obtained using the experimental data of C_7 group and dead oil, and adjusted by the coefficients determined in this work.

- The composition of n-paraffins was considered as the determining factor for the wax phase boundary, while iso-paraffins, and naphthenes were considered only

contributing to the amount of precipitated wax. Though aromatics do not form wax, they were grouped with iso-paraffins, and naphthenes into the non-n-paraffin pseudo-components in this work due to lack of data on individual categories.

- The n-paraffin composition was estimated using an empirical correlation with its parameters determined in this work, requiring only the SCN data. This advocates the model for general application to real reservoir fluids.

8.2.3. Validation of the Wax Model

In Chapter-6, the reliability of the new wax model was validated using various synthetic mixtures and real reservoir fluids with independent experimental data. The model was examined in terms of wax phase boundary (i.e. WDT), and the amount and composition of wax to be deposited at certain pressure and temperature conditions. The new wax model was also compared with several existing wax models, such as the ideal solid solution, multi-pure-solid model and Countiho's UNIQUAC model. In general, for the synthetic mixtures when the details of their compositions are known, excellent agreement between the model predictions and the experimental data has been observed. For the real reservoir fluids with limited compositional data, the model has also showed very good capability for independent predictions. The new wax model has shown superiority to the existing wax models discussed, as a result of modifications made in this work.

In summary, the new model has been improved on the following aspects:

- The model calculation accuracy was improved by the differentiation of odd or even carbon number in the new correlations for calculating the thermo-physical properties (e.g. fusion temperature) of pure compounds, and also by the inclusion of solid-solid transition in the SLE calculation.

- The EoS parameters have been modified, and the modification improved the SLE calculations. Constant BIPs were used for modelling heavy hydrocarbons, which has simplified the model, but proved to be reliable in various complex systems.

- The new UNIQUAC approach improved the description of wax solid phase, and it showed reliability for complex synthetic and real fluids containing multiple components.

- The model successfully reproduced the effect of pressure on wax formation by combined modelling of both changes in gas solubility and fusion temperature. The model predictions of wax phase boundary at different pressures were in excellent agreement with the experimental data for saturated and unsaturated fluids.

- Conventional oil compositional data were used for predicting wax phase boundary for real reservoir fluids. The independent predictions of WDT and wax amount were in general agreement with experimental data for various reservoir fluids such as gas condensate, black oil and paraffinic oil.

8.3. INTEGRATED MODELLING OF WAX AND HYDRATE

In Chapter-7, the new wax model developed in this work was combined with the hydrate model available from previous studies, forming an integrated wax-hydrate model. The integrated model was used in a preliminary study of the thermodynamic effect of wax on hydrate formation and vice versa. The approaches used for combining the models and the main conclusions of integrated modelling of wax and hydrate are described below:

- A start-up programme was introduced to calculate and compare the wax disappearance temperature (WDT) without hydrate and the hydrate dissociation temperature (HDT) without wax, in order to determine whether wax or hydrate forms first, and then to choose the proper combined programme to model the effect of existing solid.

- In the combined programmes, the wax flash calculation was added to the hydrate model and the hydrate flash calculation was coded into the wax model, in order to update the fluid composition after wax or hydrate formation. During the wax and hydrate calculations, different numbers of components were used to properly model heavy compounds forming wax and light components forming hydrate and to ensure the reliability of each calculation.

- The integrated wax-hydrate model was used to predict the effect of wax on hydrate using a real reservoir fluid with the WDT (without hydrate) higher than the HDT (without wax). The calculated fluid composition was analysed, which showed small

changes after wax formation, consequently the hydrate phase boundary was not significantly affected by wax formation in the system studied.

- The integrated wax-hydrate model was also used to estimate the effect of hydrate formation on wax using a specially designed synthetic fluid that has a higher HDT (without wax) than WDT (without hydrate). Due to the small fluid composition changes induced by hydrate formation, the predicted wax phase boundary was not significantly shifted by the presence of hydrate, which was in agreement with the experiment data.

8.4. RECOMMENDATIONS FOR FUTURE WORK

8.4.1 Further Improving the Wax Model Using New Experimental Data

The new wax model formulated in this work was based on a large number of experimental data in terms of wax phase boundary and wax amount. The data were mainly for synthetic fluids saturated and unsaturated with light constituents, and for stabilised reservoir fluids without dissolved gases. There was few experimental data for live reservoir fluids, which will be needed in order to validate and improve the model. The model can be further improved in the following aspects for real reservoir fluids:

Thermodynamic description of the solid phase of wax

In this work, wax solid phase was described using the non-ideal solid solution. which was developed based on the SLE behaviour of n-paraffins. In the modelling of real reservoir fluids, this approach was directly extended to the non-n-paraffin compounds, such as iso-paraffins, naphthenes and aromatics. The solid behaviour of non-n-paraffins may be different from that of n-paraffins. This needs to be verified and considered in the model.

Differentiation of hydrocarbon types

In this work, aromatics were grouped into non-n-paraffin pseudo-components, and assumed to increase wax accumulation. It may actually not be the case. It was noted that the accuracy of predicted wax amount could be improved by taking aromatics out of wax forming components. This needs to be quantified using experimental data.

It was also noted that the empirical correlation (Equation 5.7) used to estimate n-paraffin concentration with only one set of parameters was not accurate enough for all reservoir fluids. It is suggested to improve the correlation parameters by classifying real reservoir fluids according to their n-paraffinic, iso-paraffinic, naphthenic or aromatic natures.

The modelling of real reservoir fluids can also be improved by using novel experimental data for SCN groups. The measured proportions of different hydrocarbons (i.e. n-paraffin, iso-paraffin, naphthene and aromatics) in SCN groups can be directly correlated with the SCN properties such as specific gravity, and to formulate independent correlations.

8.4.2. Effects of Wax and Hydrate Co-Formation

The effect of wax formation on hydrate phase boundary was found to be not significant for the live reservoir fluid studied in this work. However, the influence of wax on hydrate may increase in systems that contain large amounts of wax-forming compounds. It is suggested to further study the effect of wax on hydrate using fluids having different fractions of heavy hydrocarbons. On the other hand, the effect of hydrate formation on wax may be more notable when there is a more significant change in the concentration of light compounds due to hydrate formation. It is hence suggested to measure and model the hydrate effect on wax using different fluids. Furthermore, though the thermodynamic effect of wax formation on hydrate and vice versa could be not significant, the formation of one solid could promote the deposition of the other by reducing the required subcooling due to the existing nucleation sites. It is therefore suggested to study the effects of wax and hydrate co-formation in terms of kinetics.

APPENDIX-A

EXPERIMENTAL DATA

This appendix gives the compositions and experimental WDT data for 10 synthetic mixtures (Tables A.1 – A.6) and one real reservoir fluid (Table A.7). The WDT data were measured using the experimental techniques and procedures described in Chapter-2, and they are used for validation of the new wax model in Chapter-7.

Table A.1. Compositions (mole%) for synthetic Mixtures A, B, C and D without light ends (Centre for Gas Hydrate Research, HWU).

	without light ends			
Component	A	B	C	D
C_7	51.04		47.44	48.99
C_{10}	44.49	80.04	37.76	43.62
C_{13}	1.59			2.56
C_{16}	2.12		6.44	2.05
C_{18}	0.33		2.40	0.33
C_{20}		6.43	3.24	
C_{21}		4.39	1.81	
C_{22}	0.17	2.99	0.22	0.27
C_{23}		2.06	0.30	
C_{24}	0.19	2.34		0.25
C_{28}		1.41	0.21	1.64
C_{30}		0.34	0.18	0.11
C_{36}	0.08			0.18
C_{40}				0.01

Table A.2. Experimental WDT data for synthetic Mixtures A. B. C and D without light ends (Centre for Gas Hydrate Research, HWU).

without light ends							
A		B		C		D	
P/MPa	WDT/K	P/MPa	WDT/K	P/MPa	WDT/K	P/MPa	WDT/K
0.3	302	2.4	297	0.2	289	0.1	303
2.8	302	9.8	299	10.1	291	7.9	304
9.4	303	16.2	300	17.9	292	15.3	306
17.1	304	23.8	302	33.5	296	22.4	307
24.1	306	31.9	304	41.3	297	30.5	309
33.6	309	38.6	305			40.4	311
41.0	310						

Table A.3. Compositions (mole%) for synthetic Mixtures B, C and D with light ends (Centre for Gas Hydrate Research, HWU).

	with light ends		
Component	B	C	D
C_1	28.00	24.41	37.10
C_2	4.04	2.55	2.45
C_3	1.46	5.66	0.70
nC_4	1.12	3.63	0.09
iC_4			0.15
nC_5			0.03
iC_5			0.03
N_2			1.66
CO_2			0.64
C_7		30.24	28.02
C_{10}	52.32	24.07	24.91
C_{13}			1.46
C_{16}		4.11	1.17
C_{18}		1.53	0.19
C_{20}	4.20	2.06	
C_{21}	2.87	1.15	
C_{22}	1.96	0.14	0.15
C_{23}	1.34	0.19	
C_{24}	1.53		0.14
C_{28}	0.92	0.13	0.94
C_{30}	0.23	0.12	0.06
C_{36}			0.10
C_{40}			0.01
Bubble point			
T/K	291	284	299
Pb/MPa	9.3	7.6	12.6

Table A.4. Experimental WDT data for synthetic Mixtures B, C and D with light ends (Centre for Gas Hydrate Research, HWU).

with light ends					
B		C		D	
P/MPa	WDT/K	P/MPa	WDT/K	P/MPa	WDT/K
1.0	294	1.0	286	1.6	301
4.4	293	2.2	286	4.5	301
10.0	292	5.3	285	14.1	302
10.6	293	7.1	285	26.0	304
23.3	295	8.0	286	32.5	305
34.7	298	14.6	286	40.0	306
40.4	298	22.8	287		
		31.7	289		
		41.6	291		

Table A.5. Compositions (mole%) for synthetic Mixture E with different amounts of light-ends (Centre for Gas Hydrate Research, HWU).

	No light end	45 mole% light end	69 mole% light end
C_1		39.42	60.24
C_2		2.56	3.91
C_3		0.76	1.16
nC_4		0.10	0.16
iC_4		0.18	0.28
iC_5		0.05	0.07
N_2		1.46	2.24
CO_2		0.61	0.94
C_{10}	97.52	53.49	30.24
C_{21}	0.84	0.46	0.26
C_{22}	0.59	0.32	0.18
C_{23}	0.41	0.23	0.13
C_{24}	0.29	0.16	0.09
C_{25}	0.20	0.11	0.06
C_{26}	0.14	0.08	0.04
Bubble point			
T/K		273	288
Pb/MPa		12.0	26.3

Table A.6. Experimental WAT and WDT data for synthetic Mixture E with different amounts of light-ends (Centre for Gas Hydrate Research, HWU).

No light end		45 mole% light end		69 mole% light end			
P/MPa	WAT/K	P/MPa	WAT/K	P/MPa	WAT/K	P/MPa	WDT/K
0.3	276	2.9	275	3.3	274	3.3	274
4.5	276	5.6	274	6.9	272	6.9	273
10.7	277	11.0	274	13.4	272	13.5	273
20.9	279	12.0	273	19.9	273	20.3	275
30.3	281	16.4	274	25.8	274	26.4	275
36.0	282	23.2	276	33.0	274	34.4	276
		30.2	277	39.8	275	41.0	277
		34.7	278				

Table A.7. Compositions and physical properties (Reservoir Fluid Studies Group, HWU) of North Sea crude oil LTA97-1 (WDT is measured as 328 K, Centre for Gas Hydrate Research, HWU).

Component	MW	mole%	Specific gravity
nC_4	58	0.11	
iC_5	72	0.56	
nC_5	72	1.24	
C_6s	89	4.03	0.669
C_7s	92	9.77	0.728
C_8s	103	12.18	0.752
C_9s	117	9.00	0.776
$C_{10}s$	132	7.70	0.785
$C_{11}s$	147	5.90	0.791
$C_{12}s$	161	4.30	0.809
$C_{13}s$	174	5.54	0.819
$C_{14}s$	189	3.89	0.839
$C_{15}s$	199	3.93	0.838
$C_{16}s$	218	3.06	0.845
$C_{17}s$	231	2.27	0.844
$C_{18}s$	249	2.58	0.847
$C_{19}s$	257	2.71	0.869
C_{20+}	460	21.23	0.929
the fluid	209		0.851

Note: $C_n s$ is the single carbon number (SCN) group n.

Table A.8. Compositions and physical properties (Reservoir Fluid Studies Group, HWU) of Base condensate LTB98-1 (WDT is measured as 309 K, Centre for Gas Hydrate Research, HWU).

Component	MW	mole%	Specific gravity
C1	16	0.00	
C2	30	0.00	
C3	44	0.12	
iC_4	58	0.18	
nC_4	58	0.84	
iC_5	72	1.28	
nC_5	72	2.29	
C_6s	89	6.13	0.678
C_7s	92	13.32	0.733
C_8s	103	16.50	0.757
C_9s	116	11.06	0.778
$C_{10}s$	131	8.19	0.790
$C_{11}s$	147	6.07	0.789
$C_{12}s$	161	4.75	0.809
$C_{13}s$	173	4.09	0.822
$C_{14}s$	186	4.10	0.839
$C_{15}s$	203	3.39	0.837
$C_{16}s$	215	2.69	0.843
$C_{17}s$	229	2.18	0.841
$C_{18}s$	246	2.10	0.843
$C_{19}s$	258	1.76	0.854
C_{20+}	384	8.98	0.880
the fluid	154		0.803

Table A.9. Single phase compositions and physical properties (Reservoir Fluid Studies Group, HWU) of Black oil RFS-1 (WDT for the dead fluid is measured as 323 K, Centre for Gas Hydrate Research, HWU).

Component	MW	mole%	Specific gravity
C1	16	23.98	
C2	30	3.98	
C3	44	5.65	
iC_4	58	2.00	
nC_4	58	4.12	
iC_5	72	2.09	
nC_5	72	2.89	
C_6s	85	4.10	0.666
C_7s	94	6.25	0.714
C_8s	105	6.55	0.738
C_9s	119	5.20	0.761
$C_{10}s$	133	4.06	0.776
$C_{11}s$	147	3.31	0.790
$C_{12}s$	162	2.64	0.801
$C_{13}s$	173	2.36	0.815
$C_{14}s$	188	2.18	0.831
$C_{15}s$	203	1.95	0.837
$C_{16}s$	220	1.61	0.844
$C_{17}s$	233	1.28	0.849
$C_{18}s$	248	1.27	0.856
$C_{19}s$	262	1.05	0.863
C_{20+}	483	11.50	0.947
the fluid	131.8		
Temperature/K		373	
Saturation pressure/MPa		9.4	
Sat. density/g.cc^{-1}		0.715	

APPENDIX-B

EQUATION OF STATE AND BINARY INTERACTION PARAMETER

Equations of state (EoS) represent the relation between temperature T, pressure P and volume v. Though equations of state are basically developed for pure compounds, they can be applied to multi-component systems by employing appropriate mixing rules. The van der Waals type EoS and the conventional random van der Waals mixing rules are commonly applied to model hydrocarbons fluid phase behaviour, and they will be described in this appendix. Binary interaction parameters are required in the mixing rules, and they will also be given in this appendix for light compounds and intermediate hydrocarbons.

B.1. EQUATION OF STATE

B.1.1 General Form of EoS

The virial equation can be expressed as an infinite series of molar volume:

$$Z = \frac{Pv}{RT} = 1 + \frac{B'}{v} + \frac{C'}{v^2} + \frac{D'}{v^3} + \cdots\cdots \tag{B.1}$$

where Z is the compressibility factor, P and T are pressure and temperature, v is the molar volume. B', C' and D' are the second, third and fourth virial coefficients depending only on temperature for each compound.

Some successful equations of state such as the van der Waals EoS take a cubic form in terms of molar volume (v) or compressibility factor (Z), and so they are often referred as cubic EoS. Intermolecular attractive and repulsive forces are considered in the van der Waals EoS, which is expressed with explicit pressure as:

$$P = \frac{RT}{v-b} - \frac{a}{v^2} \tag{B.2}$$

where $\frac{a}{v^2}$ and b represent the attractive and repulsive terms, respectively.

The van der Waals EoS has been modified in order to improve its representation for complex systems. Almost all popular van der Waals type EoS have improved their capabilities by modifying the attractive term. They can be expressed using the following general form:

$$P = \frac{RT}{v-b} - \frac{a}{v^2 + uv - w^2} \tag{B.3}$$

where a and b represent the attractive and repulsive terms, respectively. u and w are related to the EoS parameters.

The above general equation can be expressed in terms of compressibility factor by:

$$Z^3 - (1 + B - U)Z^2 + (A - BU - U - W^2)Z - (AB - BW^2 - W^2) = 0 \tag{B.4}$$

where A, B, U and W are given by:

$$A \equiv \frac{aP}{(RT)^2} \tag{B.5}$$

$$B \equiv \frac{bP}{RT} \tag{B.6}$$

$$U \equiv \frac{uP}{RT} \tag{B.7}$$

$$W \equiv \frac{wP}{RT} \tag{B.8}$$

The fugacity coefficient is calculated by

$$ln(\varphi) = (Z-1) - ln(Z-B) + \frac{A}{\sqrt{U^2 + 4W^2}} ln\left(\frac{2Z + U - \sqrt{U^2 + 4W^2}}{2Z + U + \sqrt{U^2 + 4W^2}}\right) \tag{B.9}$$

B.1.2 EoS Parameters

The van der Waals type cubic EoS can have two parameters (a and b) or three parameters. A two-parameter EoS predicts the same critical compressibility factor Z_c for all substances. In addition to a and b, a third parameter c is included in a three-parameter EoS for matching both the vapour pressure and volume. The parameter c is generally determined by employing volumetric data.

For two-parameter and three-parameter equations of state, the EoS parameters a, b and c can be calculated using critical temperature (T_c) and critical pressure (P_c):

$$a = \Omega_{a_c} \frac{R^2 T_c^2}{P_c} \alpha \tag{B.10}$$

$$b = \Omega_b \frac{RT_c}{P_c} \tag{B.11}$$

$$c = \Omega_c \frac{RT_c}{P_c} \tag{B.12}$$

where Ω_{ac}, Ω_b and Ω_c are constants. α expresses the temperature dependency of the attraction term; being a function of the reduced temperature and acentric factor.

SRK EoS

Soave-Redlich-Kwong (SRK) equation of state is a two-parameter EoS, which has a constant value of 0.307 for the critical compressibility factor Z_c. When using the general cubic EoS form (Equation B.3) to express the SRK EoS, u and w equal to b and 0, respectively. In the SRK EoS, parameters a and b can be calculated using Equations B.10 and B.11 with Ω_a and Ω_b of approximately 0.42747 and 0.08664.

In order to develop the α function for calculating the parameter a, Soave (1972) used the critical points and vapour pressure data at the reduced temperature of 0.7 for pure compound up to C_{10} (with an acentric factor of 0.492). The α function was selected, and m was correlated with acentric factor ω by equating fugacities of saturated liquid and vapour phases:

$$\alpha = \left[1 + m\left(1 - T_r^{0.5}\right)\right]^2 \tag{B.13}$$

$$m = 0.480 + 1.574\omega - 0.176\omega^2 \tag{B.14}$$

PR EoS

Peng and Robinson (1978) modified the attractive term mainly to improve the prediction of liquid density in comparison with SRK EoS. The PR EoS is also a two-parameter EoS with a constant value of 0.333 for critical compressibility factor Z_c. The PR EoS can be expressed using the general form of cubic EoS with u and w equal to $2b$ and b, respectively. Ω_a and Ω_b of approximately 0.45724 and 0.07780 are used to calculate the EoS parameters a and b.

Peng and Robinson (1976) used vapour pressure data for pure compounds up to C_{10} to determine α when proposing the PR EoS. The temperature range taken into account was the normal boiling point to the critical point. The authors obtained similar α form as the one derived by Soave (1972), as expressed in Equation B.13. m was similarly correlated to the acentric factor (ω) by:

$$m = 0.37464 + 1.54226\omega - 0.26992\omega^2 \tag{B.15}$$

Robinson and Peng (1978) applied Equation 13 and modified the m correlation with a higher degree of acentric factor to improve predictions for heavy components. The m correlation is given by:

$$m = 0.3796 + 1.485\omega - 0.1644\omega^2 + 0.01667\omega^3 \tag{B.16}$$

VPT EoS

Patel and Teja (1982) modified the attractive term by including a more flexible third parameter c. PT EoS can be expressed using the general cubic EoS form (Equation B.3) with $u = b + c$ and $w = \sqrt{bc}$. Ω_a, Ω_b and Ω_c are correlated with adjustable critical compressibility factors, which in turn are correlated with acentric factors.

Valderrama (1990) modified the PT EoS by using critical compressibility factor Z_c instead of the acentric factor ω to calculate Ω_a, Ω_b and Ω_c:

$$\Omega_a = 0.66121 - 0.76105Z_c \tag{B.17}$$

$$\Omega_b = 0.02207 + 0.20868 Z_c \tag{B.17}$$

$$\Omega_c = 0.57765 - 1.87080 Z_c \tag{B.17}$$

In the VPT EoS, the α form as expressed by Equation B.13 is used. It is combined with the *m* correlation give by:

$$m = 0.46283 + 3.58230(\omega \cdot Z_c) + 8.19417(\omega \cdot Z_c)^2 \tag{B.18}$$

B.2. MIXING RULES AND BINARY INTERACTION PARAMETERS

Equations of state are applied to multi-component systems by employing mixing rules to determine the EoS parameters for mixtures. The mixing rules are used to describe the prevailing forces between molecules of different substances forming the mixture. It is common to incorporate binary interaction parameters to express the attractive term between pairs of non-similar molecules.

B.2.1. Mixing Rules

For reservoir hydrocarbon fluids, the van der Waals mixing rules are adequate. The van der Waals mixing rules, often referred as the conventional (or classical) random mixing rules, consider the interaction between pairs of neighbouring molecules and neglect interaction between three or more molecules. The EoS parameters *a*, *b* and *c* for a mixture are expressed using the random mixing rules as:

$$a = \sum_i \sum_j x_i x_j (a_i a_j)^{0.5} (1 - k_{ij}) \tag{B.19}$$

$$b = \sum_i x_i b_i \tag{B.20}$$

$$c = \sum_i x_i c_i \tag{B.21}$$

where x is the composition in mole fraction. Subscript i and j designate components 'i' and 'j'. k_{ij} is the binary interaction parameter between component 'i' and component 'j'.

For mixtures containing highly polar and asymmetric compounds such as water, the random mixing rules are not appropriate, due to non-uniform distribution of molecules. Non-random mixing rules will be used, which calculate the attraction term by:

$$a = a^C + a^A \tag{B.22}$$

where a^C is the conventional random mixing term given by Equation B.19, a^A is the asymmetric term due to polarity. Various expressions have been proposed for the asymmetric term.

The term a^A is independent of pressure, and it is calculated as:

$$a^A = \sum_p x_p^2 \sum_i x_i a_{pi} l_{pi} \tag{B.23}$$

where p indicates the polar compound. l_{pi} is a binary interaction parameter, which is a function of temperature:

$$l_{pi} = l_{pi}^0 - l_{pi}^1 (T - T_0) \tag{B.24}$$

where l_{pi}^0 and l_{pi}^1 are dimensionless constants expected to be positive, and T_0 is the ice point in K.

a_{pi} in Equation B.23 is given as:

$$a_{pi} = (a_p a_i)^{0.5} \tag{B.25}$$

B.2.2. Binary Interaction Parameters

As shown in Equation B.19, binary interaction parameters are required to calculate the attraction term for a mixture. The binary interaction parameter is generally determined by minimising the difference between calculated and experimental data, such as bubble point pressures of binary systems. As only the interaction between two neighbouring molecules is considered in the mixing rules, the binary interaction parameters determined by binary systems are valid for applying to multi-component systems.

The binary interaction parameters between hydrocarbons with little differences in size are generally considered to be zero. However, the binary interaction parameters are not zero for hydrocarbons with significant differences in molecular sizes. As the binary interaction parameter is considered as a fitting parameter and not a rigorous physical term, binary interaction parameters may be different, depending on equations of state.

Tables B.1, B.2 and B.3 list the binary interaction parameters between light compounds (e.g. $C_1 - C_5$, N_2 and CO_2) and intermediate hydrocarbons (C_6-C_{20}) for SRK EoS, PR EoS and VPT EoS, respectively.

Table B.4 lists the interaction parameters between water and several compounds for the non-density dependent mixing rule in VPT EoS.

B.3. TABLES

Table B.1. Binary interaction parameters between light and intermediate compounds in SRK EoS.

	1	2	3	4	5	6	7	8	9	10 - 24
No. Compound	N_2	CO_2	C_1	Ethylene	C_2	Propylene	C_3	iC_4	nC_4	iC_5 - nC_{20}
1 N_2	0.0000									
2 CO_2	0.0000	0.0000								
3 C_1	0.0278	0.1107	0.0000							
4 Ethylene	0.0300	0.1000	0.0189	0.0000						
5 C_2	0.0407	0.1363	-0.0078	0.0026	0.0000					
6 Propylene	0.0800	0.1000	0.0289	0.0000	0.0200	0.0000				
7 C_3	0.0763	0.1000	0.0080	0.0080	-0.0220	0.0033	0.0000			
8 iC_4	0.0944	0.1000	0.0241	0.0900	-0.0010	-0.0144	-0.0100	0.0000		
9 nC_4	0.0700	0.1000	0.0056	0.1000	0.0067	0.0000	0.0000	0.0000	0.0000	
10 iC_5	0.0867	0.1000	-0.0078	0.0120	0.0050	0.0000	0.0078	0.0000	0.0000	0.0000
11 Neopentane	0.0870	0.1000	-0.0078	0.0120	0.0050	0.0000	0.0078	0.0000	0.0000	0.0000
12 nC_5	0.0878	0.1000	0.0079	0.0120	0.0056	0.0050	0.0230	-0.0300	0.0204	0.0000
13 nC_6	0.1400	0.1000	0.0374	0.0140	-0.0156	0.0050	-0.0022	0.0000	-0.0111	0.0000
14 Met.Cyc.Pent.	0.1400	0.1000	0.0400	0.0140	0.0033	0.0050	0.0030	0.0000	0.0000	0.0000
15 Cyc. Hex.	0.1400	0.1000	0.0333	0.0150	0.0230	0.0050	0.0030	0.0005	0.0000	0.0000
16 nC_7	0.1422	0.1000	0.0307	0.0144	0.0411	0.0100	0.0044	0.0005	0.0000	0.0000
17 Met.Cyc.Hex.	0.0145	0.1000	0.0500	0.0150	0.0230	0.0100	0.0050	0.0005	0.0000	0.0000
18 Toluene	0.1500	0.1000	0.0978	0.0300	0.0900	0.0300	0.0300	0.0200	0.0100	0.0000
19 o-Xylene	0.1500	0.1000	0.1000	0.0250	0.0500	0.0300	0.0300	0.0200	0.0100	0.0000
20 nC_8	0.1500	0.1000	0.0448	0.0200	0.0170	0.0100	0.0040	0.0015	0.0000	0.0000
21 nC_9	0.1500	0.1000	0.0448	0.0200	0.0170	0.0100	0.0040	0.0015	0.0000	0.0000
22 nC_{10}-nC_{14}	0.1500	0.1000	0.0550	0.0300	0.0200	0.0150	0.0040	0.0020	0.0010	0.0000
23 nC_{15}-nC_{19}	0.1500	0.1000	0.0600	0.0400	0.0350	0.0250	0.0005	0.0025	0.0010	0.0000
24 nC_{20}	0.1500	0.1000	0.0650	0.0450	0.0400	0.0300	0.0010	0.0050	0.0015	0.0000

From: Knapp, H and Doring, R., 'Vapour-Liquid Equilibria for Mixtures of Low Boiling Substances', Berhens, D, and Eckerman R., Eds (Dechema Chemistry Data Ser.), Part I - Binary System (1986).

Table B.2. Binary interaction parameters between light and intermediate compounds in PR EoS.

		1	2	3	4	5	6	7	8	9	10 - 24
No.	Compound	N_2	CO_2	C_1	Ethylene	C_2	Propylene	C_3	iC_4	nC_4	iC_5 - nC_{20}
1	N_2	0.0000									
2	CO_2	0.0000	0.0000								
3	C_1	0.0311	0.1070	0.0000							
4	Ethylene	0.0500	0.1200	0.0215	0.0000						
5	C_2	0.0515	0.1322	0.0026	0.0089	0.0000					
6	Propylene	0.0600	0.1300	0.0330	0.0000	0.0089	0.0000				
7	C_3	0.0852	0.1241	0.0140	0.0100	0.0011	0.0100	0.0000			
8	iC_4	0.1000	0.1400	0.0256	0.0200	-0.0067	0.0080	-0.0078	0.0000		
9	nC_4	0.0711	0.1333	0.0133	0.0200	0.0096	0.0080	0.0033	0.0000	0.0000	
10	iC_5	0.1000	0.1400	-0.0056	0.0250	0.0080	0.0080	0.0111	-0.0040	0.0170	0.0000
11	Neopentane	0.1000	0.1400	-0.0056	0.0250	0.0080	0.0080	0.0111	-0.0040	0.0170	0.0000
12	nC_5	0.1000	0.1400	0.0236	0.0250	0.0078	0.0100	0.0120	0.0020	0.1700	0.0000
13	nC_6	0.1496	0.1450	0.0422	0.0300	0.0140	0.0110	0.0267	0.0240	0.0174	0.0000
14	Met.Cyc.Pent.	0.1500	0.1450	0.0450	0.0310	0.0141	0.0120	0.0270	0.0242	0.0180	0.0000
15	Cyc. Hex.	0.1500	0.1450	0.0450	0.0310	0.0141	0.0120	0.0270	0.0242	0.0180	0.0000
16	nC_7	0.1441	0.1450	0.0352	0.0300	0.0150	0.0140	0.0560	0.0250	0.0190	0.0000
17	Met.Cyc.Hex.	0.1500	0.1450	0.0450	0.0300	0.0160	0.0150	0.0580	0.0250	0.0200	0.0000
18	Toluene	0.1700	0.1800	0.0600	0.0400	0.0200	0.0210	0.0600	0.0300	0.0110	0.0000
19	o-Xylene	0.1500	0.1400	0.0470	0.0300	0.0160	0.0150	0.0590	0.0260	0.0120	0.0000
20	nC_8	0.1500	0.1400	0.0470	0.0300	0.0160	0.0150	0.0590	0.0260	0.0120	0.0000
21	nC_9	0.1550	0.0145	0.0474	0.0400	0.0190	0.0200	0.0070	0.0060	0.0100	0.0000
22	nC_{10}-nC_{14}	0.1550	0.0145	0.0500	0.0450	0.0300	0.0250	0.0200	0.0100	0.0010	0.0000
23	nC_{15}-nC_{19}	0.1550	0.0145	0.0600	0.0500	0.0400	0.0300	0.0250	0.0150	0.0010	0.0000
24	nC_{20}	0.1550	0.0145	0.0700	0.0600	0.0500	0.0350	0.0300	0.0200	0.0015	0.0000

From: Knapp, H and Doring, R., 'Vapour-Liquid Equilibria for Mixtures of Low Boiling Substances', Berhens, D, and Eckerman R., Eds (Dechema Chemistry Data Ser.), Part I - Binary System (1986).

Table B.3. Binary interaction parameters between light and intermediate compounds in VPT EoS.

		1	2	3	4	5	6	7	8	9	10	11	12
No.	Comp.	C_1	C_2	C_3	iC_4	nC_4	iC_5	CO_2	N_2	nC_5	nC_6	nC_7	nC_8-nC
1	C_1	0.0000											
2	C_2	0.0000	0.0000										
3	C_3	0.0000	0.0000	0.0000									
4	iC_4	0.0000	0.0000	0.0000	0.0000								
5	nC_4	0.0000	0.0000	0.0000	0.0000	0.0000							
6	iC_5	0.0117	0.0000	0.0000	0.0000	0.0000	0.0000						
7	CO_2	0.0920	0.1340	0.1280	0.1260	0.1380	0.0530	0.0000					
8	N_2	0.0350	0.0380	0.0700	0.1340	0.1140	0.0628	-0.0360	0.0000				
9	nC_5	0.0000	0.0000	0.0000	0.0000	0.0000	0.0000	0.1410	0.0880	0.0000			
10	nC_6	0.0000	0.0000	0.0000	0.0000	0.0000	0.0000	0.1180	0.1500	0.0000	0.0000		
11	nC_7	0.0000	0.0000	0.0000	0.0000	0.0000	0.0000	0.1100	0.1420	0.0000	0.0000	0.0000	
12	nC_8-nC_{20}	0.0000	0.0000	0.0000	0.0000	0.0000	0.0000	0.0000	0.0000	0.0000	0.0000	0.0000	0.0000

Table B.4. Binary interaction parameters between water and several compounds in VPT EoS.

		water		
No.	Comp.	k_{21}	l_{21}^0	$l_{21}^1 \times 10^4$
1	C_1	0.5028	1.8180	49.00
2	C_2	0.4974	1.4870	45.40
3	C_3	0.5465	1.6070	39.30
4	iC_4	0.5863	1.7863	37.40
5	nC_4	0.5800	1.6885	33.57
6	nC_5	0.5525	1.6188	23.72
7	nC_6	0.4577	1.5730	31.41
8	nC_7	0.4165	1.5201	35.21
9	nC_8	0.3901	1.5200	35.31
10	xenon	0.2374	0.8870	47.50
11	CO_2	0.1965	0.7232	23.74
12	N_2	0.4792	2.6575	64.46
13	H_2S	0.1382	0.3809	13.24
14	methonal	-0.0789	-0.0149	0.00
15	water	0.0000	0.0000	0.00

From: Avlonitis et al. (1994).

APPENDIX-C

THERMO-PHYSICAL PROPERTIES

Thermo-physical properties, such as fusion temperature, solid-solid transition temperature, latent heat of fusion, latent heat of solid-solid transition, heat capacity of liquid and solid, are required for solid-liquid equilibrium calculations. Correlations to calculate these thermo-physical properties were developed in this work using experimental data for pure n-paraffins. The correlations will be given in this appendix.

C.1. FUSION AND SOLID-SOLID TRANSITION TEMPERATURES

Correlations for calculating fusion and solid-solid transition temperatures have been developed in accordance with the measured values reported in the literature (Schaerer et al., 1955; Broadhurst, 1962). Differentiation between odd or even carbon numbers for n-paraffins is applied to correlations in order to improve accuracy.

C.1.1 Fusion Temperature

n-paraffins with odd carbon numbers

For $C_n \le C_9$

$$T_f / K = 0.3512C_n^3 - 7.6438C_n^2 + 72.898C_n - 73.9$$

For $C_9 < C_n \le C_{43}$

$$T_f / K = 0.0122C_n^2 - 2.0861C_n - 775.598/C_n + 76.2189Ln(C_n) + 156.9$$

For $C_n > C_{43}$

$$T_f / K = 414.3(C_n - 1.5)/(C_n + 5.0)$$

n-paraffins with even carbon numbers

For $C_n \leq C_{10}$

$$T_f / K = -0.0998C_n^3 + 1.0812C_n^2 + 18.602C_n + 49.216$$

For $C_{10} < C_n \leq C_{42}$

$$T_f / K = 0.0031C_n^3 - 0.3458C_n^2 + 14.277C_n + 137.73$$

For $C_n > C_{42}$

$$T_f / K = 414.3(C_n - 1.5)/(C_n + 5.0)$$

Figure C.1 shows the experimental data (Schaerer et al., 1955; Broadhurst, 1962) and regressed fusion temperatures for n-paraffins.

C.1.2 Solid-solid Transition Temperature

n-paraffins with odd carbon numbers

For $C_9 < C_n \leq C_{43}$

$$T_{tr} / K = 0.0039C_n^3 - 0.4239C_n^2 + 17.28C_n - Ln(C_n) + 95.4$$

Others

$$T_{tr} / K = T_f$$

n-paraffins with even carbon numbers

For $C_{22} \leq C_n \leq C_{42}$

$$T_{tr} / K = 0.0032C_n^3 - 0.3249C_n^2 + 12.78C_n + 154.19 + Ln(C_n)$$

Others

$$T_{tr} / K = T_f$$

Figure C.2 shows the experimental data (Schaerer et al., 1955; Broadhurst, 1962) and regressed solid-solid transition temperatures for n-paraffins between C_9 and C_{43}.

C.2. ENTHALPIES OF FUSION AND SOLID-SOLID TRANSITION

The sum of enthalpies of fusion and heats of solid–solid transitions are considered to be dependent on fusion temperature and molecular weight. Correlations have been developed using data reported in the literature (Schaerer et al., 1955; Broadhurst, 1962).

C.2.1 Sum of Enthalpy of Fusion and Enthalpy of Solid-solid Transition

n-paraffins with odd carbon numbers

For $C_n \leq C_9$

$$\Delta h_{sum} / cal \cdot mol^{-1} = 0.119 MW \times T_f + 672.2$$

For $C_9 < C_n \leq C_{33}$

$$\Delta h_{sum} / cal \cdot mol^{-1} = 0.167 MW \times T_f + 432.47$$

For $C_n > C_{33}$

$$\Delta h_{sum} / cal \cdot mol^{-1} = 0.139 MW \times T_f + 3984.8$$

n-paraffins with even carbon numbers

For $C_n \leq C_{34}$

$$\Delta h_{sum} / cal \cdot mol^{-1} = 0.180 MW \times T_f + 522.7$$

For $C_n > C_{34}$

$$\Delta h_{sum} / cal \cdot mol^{-1} = 0.139 MW \times T_f + 3984.8$$

Figure C.3 shows the experimental data (Schaerer et al., 1955; Broadhurst, 1962) and regressed enthalpies for fusion and solid-solid transition.

C.2.2 Enthalpies of Fusion and Solid-solid Transition

n-paraffins with odd carbon numbers

For $C_n \leq C_9$

$$\Delta h_f / cal \cdot mol^{-1} = 1.0 \Delta h_{sum}$$

$$\Delta h_{tr} / cal \cdot mol^{-1} = 0$$

For $C_9 < C_n \leq C_{43}$

$$\Delta h_f / cal \cdot mol^{-1} = 0.74 \Delta h_{sum}$$

$$\Delta h_{tr} / cal \cdot mol^{-1} = 0.26 \Delta h_{sum}$$

For $C_n > C_{43}$

$$\Delta h_f / cal \cdot mol^{-1} = 1.0 \Delta h_{sum}$$

$$\Delta h_{tr} / cal \cdot mol^{-1} = 0$$

n-paraffins with even carbon numbers

For $C_n \leq C_{20}$

$$\Delta h_f / cal \cdot mol^{-1} = 1.0 \Delta h_{sum}$$

$$\Delta h_{tr} / cal \cdot mol^{-1} = 0$$

For $C_{20} < C_n \leq C_{42}$

$$\Delta h_f / cal \cdot mol^{-1} = 0.64 \Delta h_{sum}$$

$$\Delta h_{tr} / cal \cdot mol^{-1} = 0.36 \Delta h_{sum}$$

For $C_n > C_{42}$

$$\Delta h_f / cal \cdot mol^{-1} = 1.0 \Delta h_{sum}$$

$$\Delta h_{tr} / cal \cdot mol^{-1} = 0$$

Figure C.4 shows the experimental data (Schaerer et al., 1955; Broadhurst, 1962) and regressed enthalpies of fusion for n-paraffins.

C.3. HEAT CAPACITY

Correlations have been developed for calculating heat capacity as a function of temperature and carbon number using measured data for n-paraffins (Huffman et al., 1931; Jin et al., 1991; van Miltenburg et al., 1999). Differentiation between odd or even carbon numbers for n-paraffins is applied to correlations when calculating the heat capacity of solids.

C.3.1 Heat Capacity for n-Paraffin Liquids

$$C_p^L / cal \cdot mol^{-1} \cdot K^{-1} = a^L T + b^L$$

With:

$$a^L = 0.01 \times C_n - 0.0138$$
$$b^L = 4.529 \times C_n + 3.8457$$

Figures C.5 and C.6 show the experimental data (Huffman et al., 1931; Jin et al., 1991; van Miltenburg et al., 1999) and regressed heat capacities for liquid n-paraffins with odd carbon numbers and even carbon numbers, respectively.

C.3.2 Heat Capacity for n-Paraffin Solids

$$C_p^S / cal \cdot mol^{-1} \cdot K^{-1} = a^S T^3 + b^S T^2 + c^S T + d^S$$

With:

n-paraffins with odd carbon number (based on data available up to C_{19})

$$a^S = (0.3571 \times C_n + 2.1667) \times 10^{-6}$$
$$b^S = -(0.2014 \times C_n + 0.4300) \times 10^{-3}$$
$$c^S = (0.4579 \times C_n + 0.8105) \times 10^{-1}$$
$$d^S = -(0.0678 \times C_n - 0.0580) \times 10$$

n-paraffins with even carbon number

For $C_n \leq C_{20}$

$$a^S = (0.0929 \times C_n + 4.9286) \times 10^{-6}$$
$$b^S = -(0.0993 \times C_n + 1.5929) \times 10^{-3}$$
$$c^S = (0.3604 \times C_n + 1.9115) \times 10^{-1}$$
$$d^S = -(0.0459 \times C_n + 0.2022) \times 10$$

For $C_n > C_{20}$

$$a^S = (1.6964 \times C_n - 22.5000) \times 10^{-6}$$
$$b^S = -(1.1670 \times C_n - 19.525) \times 10^{-3}$$
$$c^S = (2.4703 \times C_n - 39.848) \times 10^{-1}$$
$$d^S = -(1.5093 \times C_n - 31.209) \times 10$$

Figures C.7 and C.8 show the experimental data (Huffman et al., 1931; Jin et al., 1991; van Miltenburg et al., 1999) and regressed heat capacities for solid n-paraffins with odd carbon numbers and even carbon numbers, respectively.

C.4. FIGURES

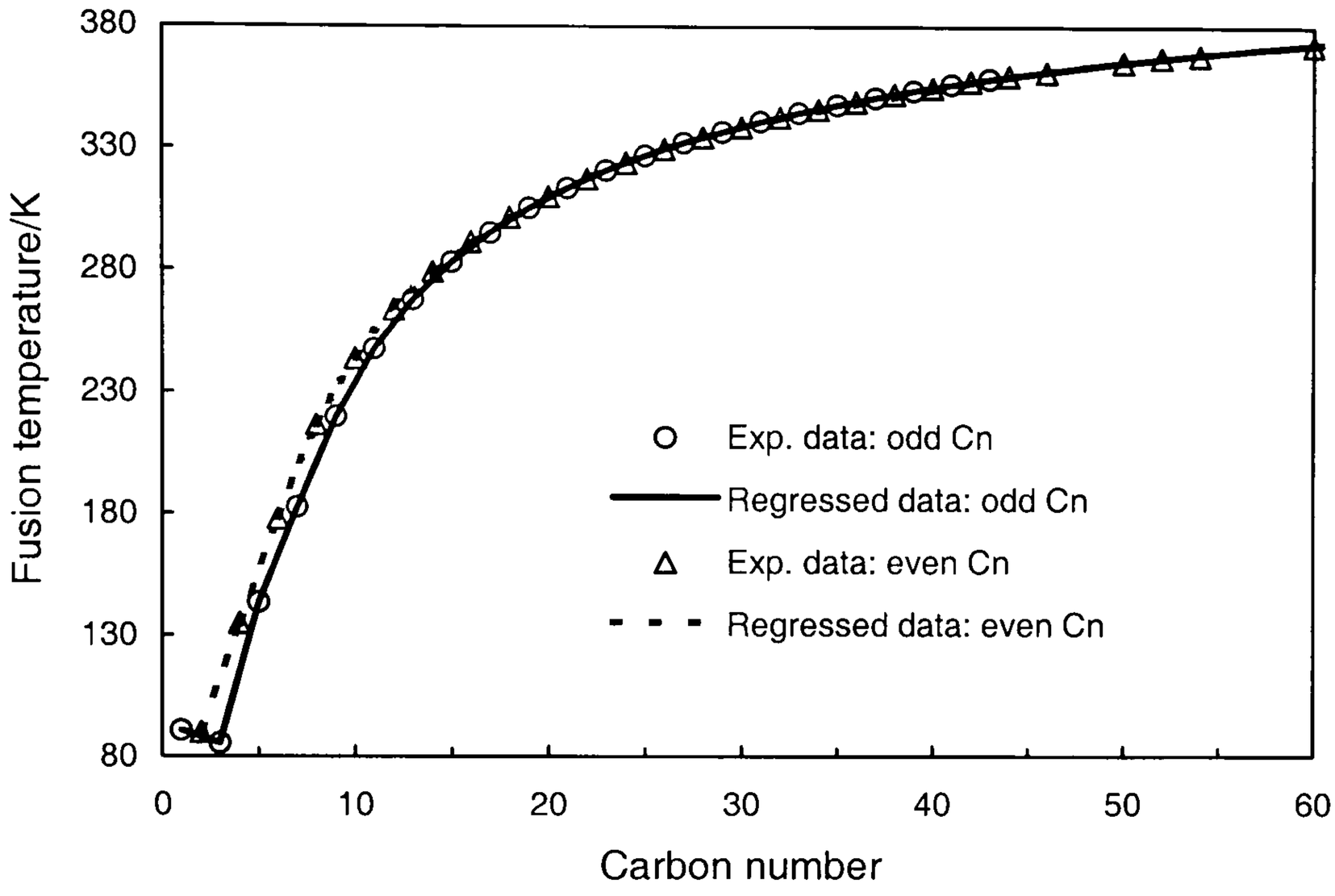

Figure C.1. Experimental data (Schaerer et al., 1955; Broadhurst, 1962) and regressed fusion temperatures for n-paraffins.

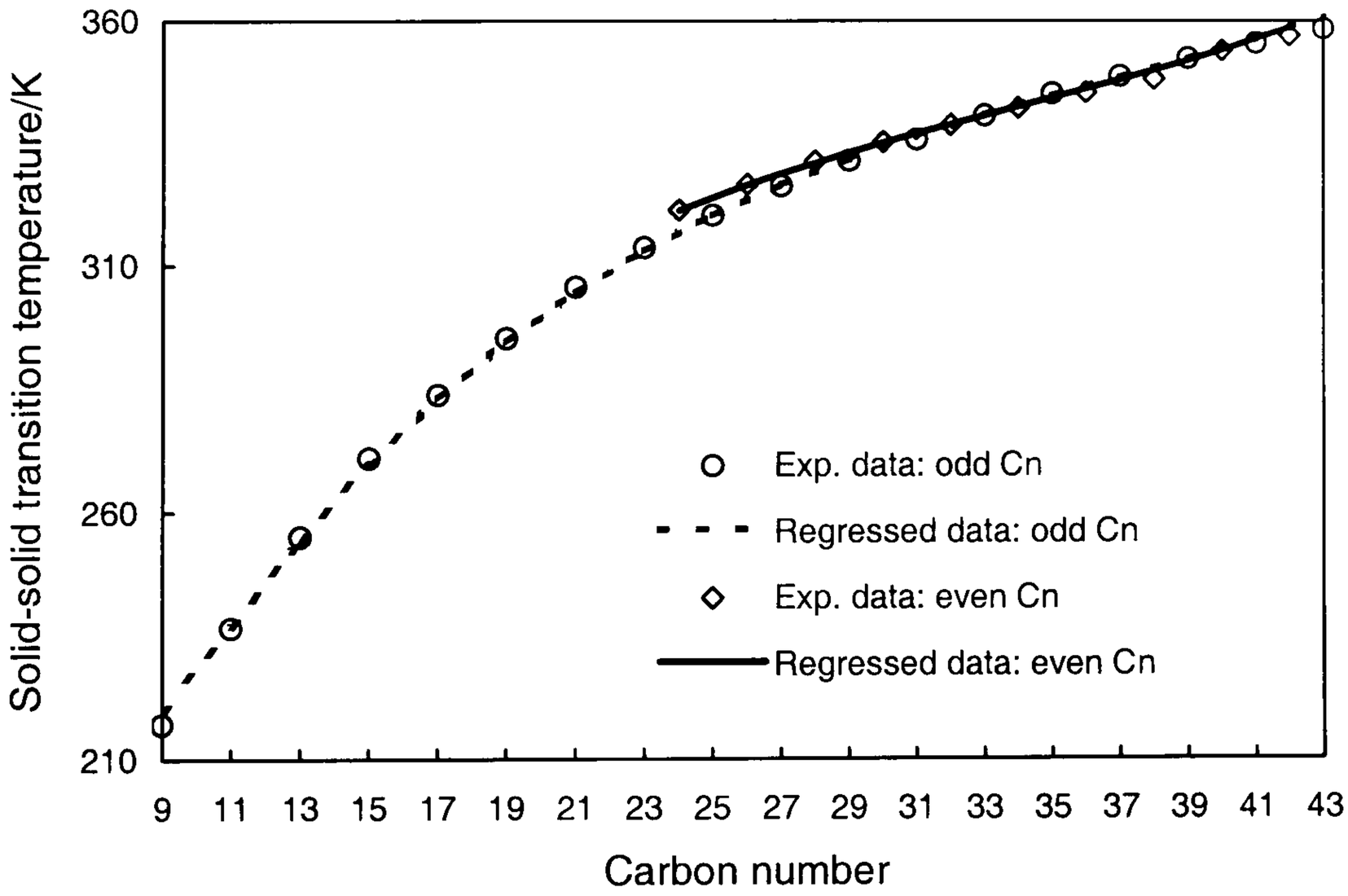

Figure C.2. Experimental data (Schaerer et al., 1955; Broadhurst, 1962) and regressed solid-solid transition temperatures for n-paraffins.

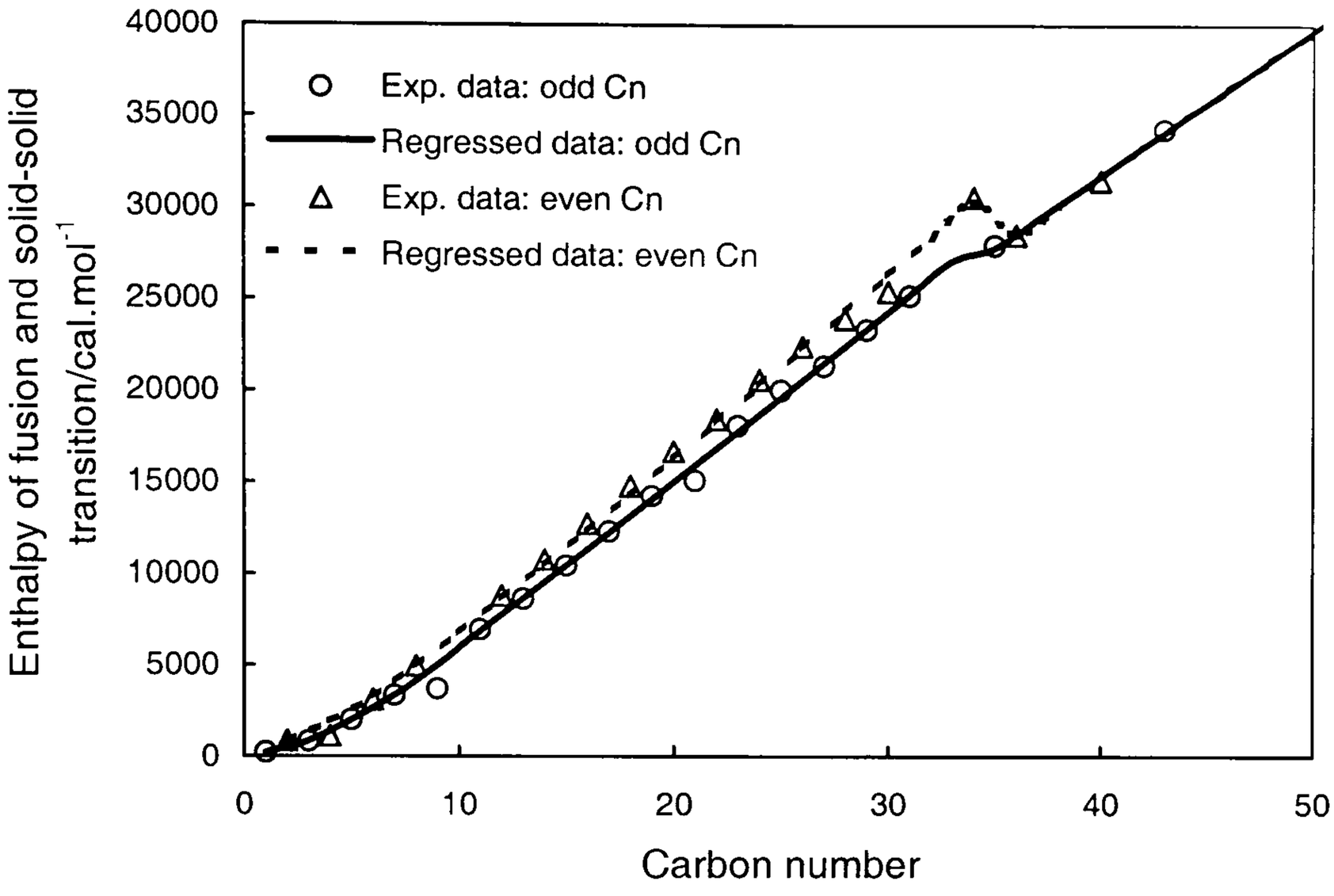

Figure C.3. Experimental data (Schaerer et al., 1955; Broadhurst, 1962) and regressed enthalpies of fusion and solid-solid transition for n-paraffins.

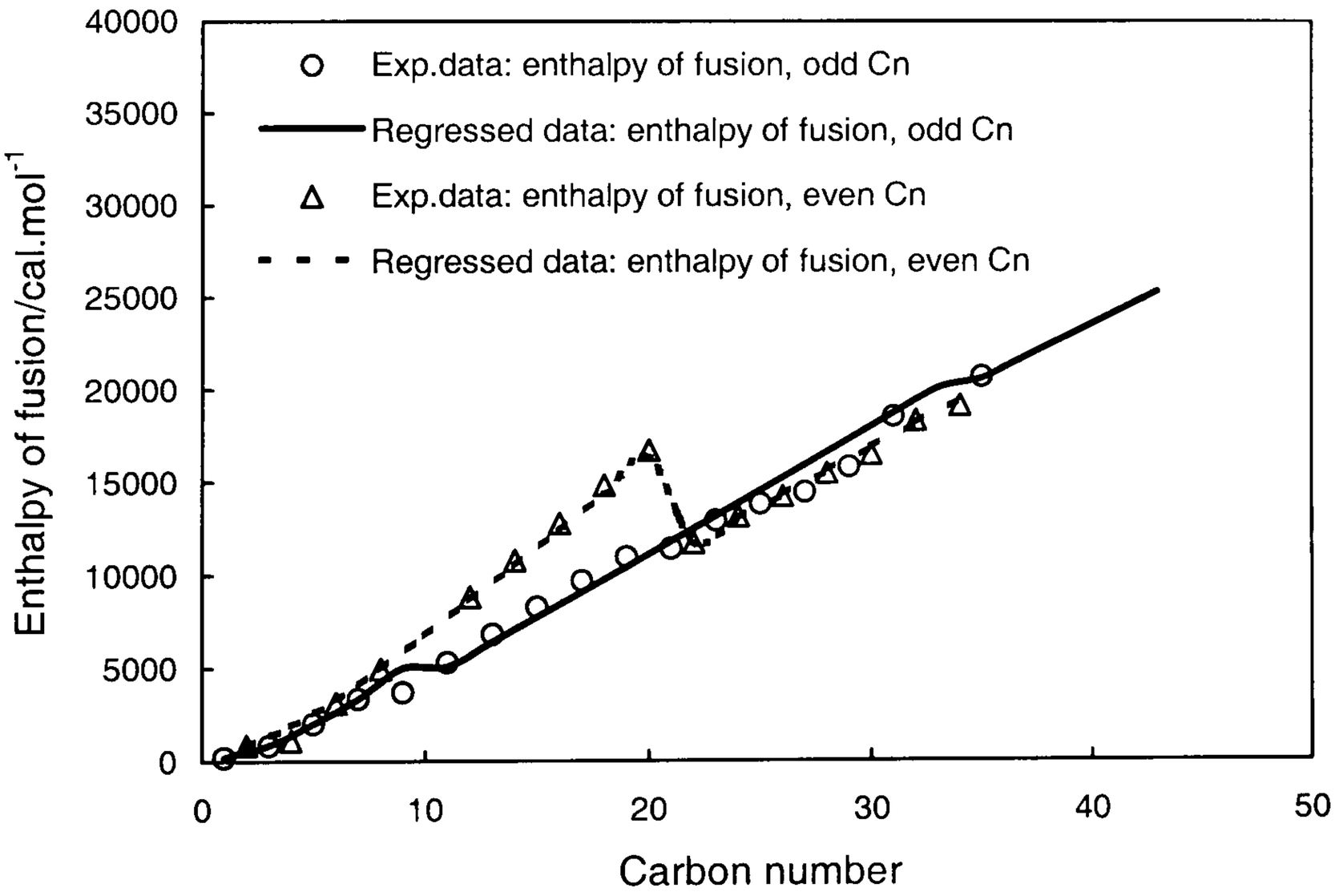

Figure C.4. Experimental data (Schaerer et al., 1955; Broadhurst, 1962) and regressed enthalpies of fusion for n-paraffins.

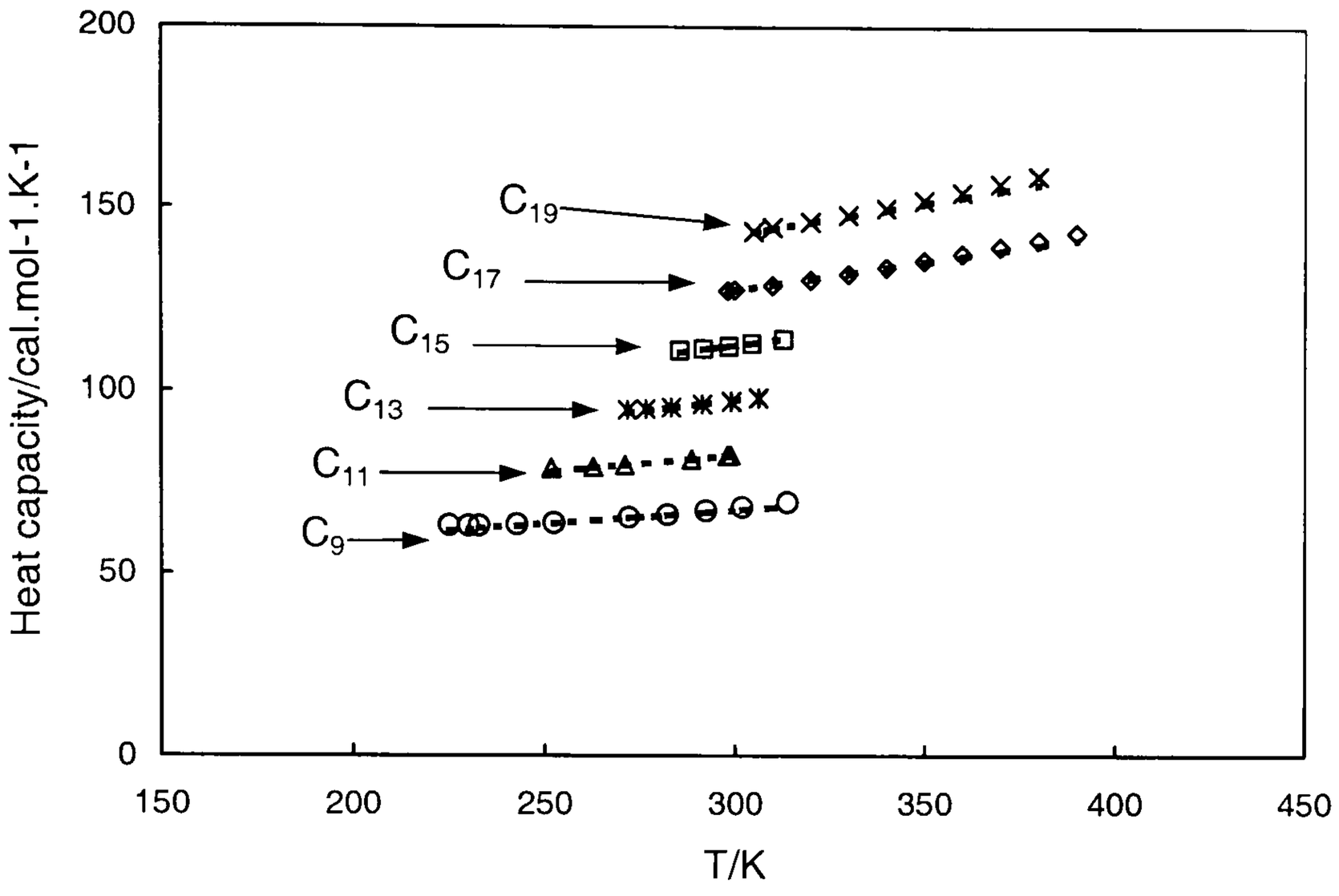

Figure C.5. Experimental data (Huffman et al., 1931; Jin et al., 1991; van Miltenburg et al., 1999) and regressed heat capacities for liquid n-paraffins with odd carbon numbers.

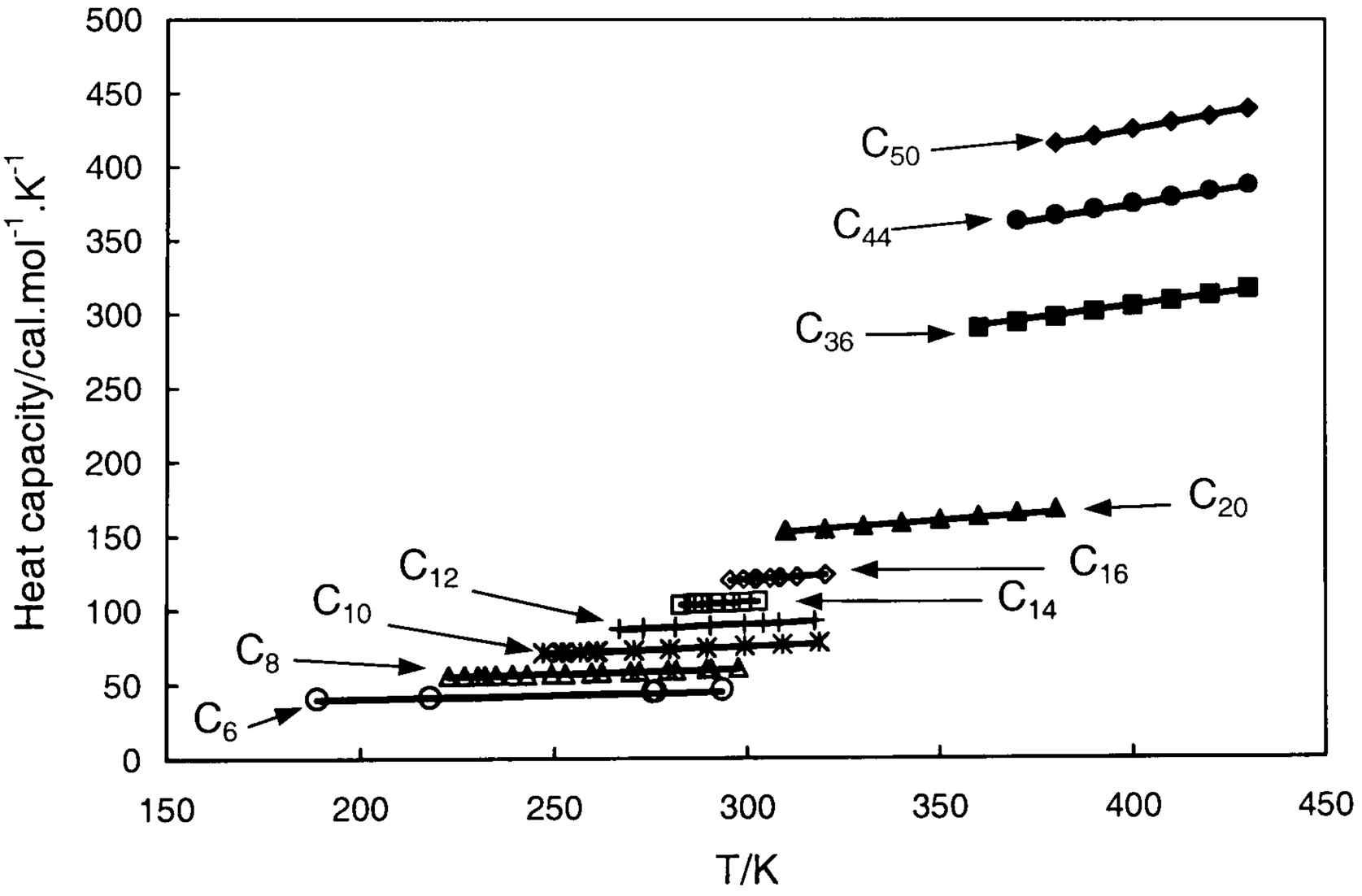

Figure C.6. Experimental data (Huffman et al., 1931; Jin et al., 1991; van Miltenburg et al., 1999) and regressed heat capacities for liquid n-paraffins with even carbon numbers.

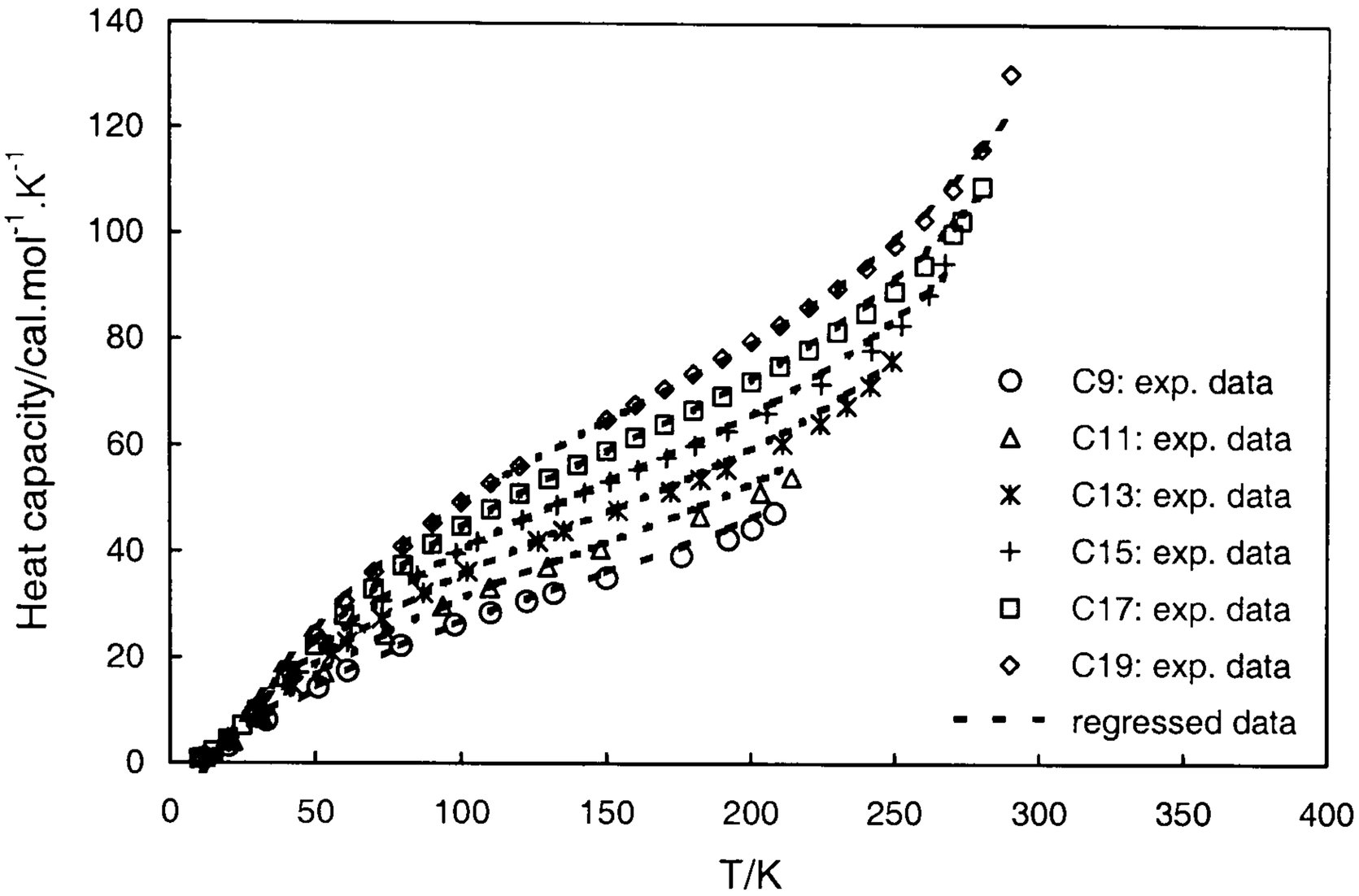

Figures C.7. Experimental data (Huffman et al., 1931; Jin et al., 1991; van Miltenburg et al., 1999) and regressed heat capacities for solid n-paraffins with odd carbon numbers.

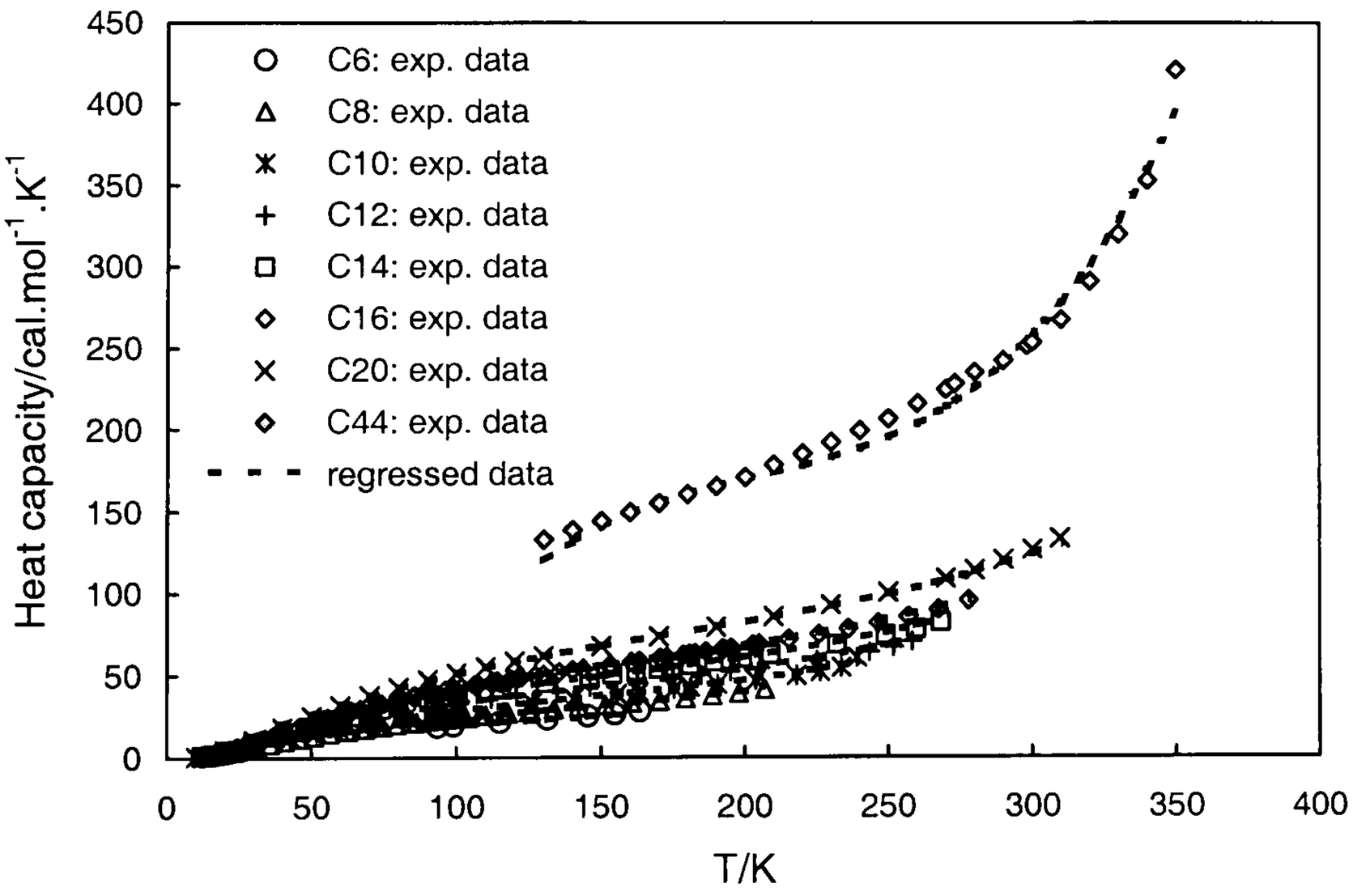

Figures C.8. Experimental data (Huffman et al., 1931; Jin et al., 1991; van Miltenburg et al., 1999) and regressed heat capacities for solid n-paraffins with even carbon numbers.

REFERENCES

Aalto, M., Liukkonen, S., 'Bubble point pressures and densities for the binary systems of propane with triacontane, hexatriacontane, tetracontane, pentacontane, and squalane at 353-373 K and 4.00-7.00 MPa', *Journal of Chemical and Engineering Data*, **41** (1), 79-83, (1996).

Abrams, D. S., Prausnitz, J. M., 'Statistical thermodynamics of Liquid Mixtures: A New Expression for the Excess Gibbs Energy of Partly or Completely Miscible Systems', *AIChE Journal*, **21** (1), 116-128, (1975).

AchourBoudjema Z, Bouroukba M, Dirand M, 'Binary phase diagram of molecular alloys of the consecutive even-numbered n-alkanes n-tetracosane (n-C24H50) and n-hexacosane (n-C26H54)', *Thermochimica Acta*, **276**: 243-256, (1996).

Addison, G. E., '' Paraffin control more cost-effective'', SPE 13391, (1984).

Ambrose, D., National Physical Laboratory Reports Chem. 92, 98 and 107, Teddington, Middlesex, UK, 1978, 1979 and 1980.

Anderson, F. E., Prausnitz, J. M., 'Inhibition of Gas Hydrates by Methanol', *AIChE Journal*, **32** (8), 1321-1333, (1986).

Avlonitis, D.A., ''Thermodynamic of Gas Hydrate Equilibria'', PhD Thesis, Heriot-Watt University, Edinburgh, UK, (1992).

Avlonitis, D.A., Danesh, A., Todd, A.C., ''Prediction of VL and VLL Equilibria of Mixtures Containing Petroleum Reservoir Fluids and Methonal with a Cubic EoS'', *Fluid Phase Equilibria*, **94**, 181-216, (1994).

Becker, J.R., ''Oilfield Paraffin treatments: Hot Oil and Hot Water Compared to Crystal Modifiers'', SPE 63123, (2000).

Bennett, H., ''Chemical waxes'', Chemical Pub. Co., (1944).

Bilderback, CA, McDougall, L.A., ''Complete Paraffin Control in Petroleum Products''. *JPT*, 1151-1156, Sept. (1969).

Bone, J.H.A, ''Petroleum and Petroleum Wells'', J.B. Lippincott & Co., Philadelphia, 26, (1865).

Broadhurst, M.G., 'An Analysis of the Solid Phase Behaviour of the Normal Paraffins'. *Journal of Research of the national Bureau of Standards – A. Physics and Chemistry*, **66A** (3), 241-249, (1962).

Brownawell, P.W., Holliday, W.C., ''Wax Solid Solution in Middle Distillate Fuel Oils and its Effect upon Cloud Point'', *JIP*, **48**, 463, (1962).

Bucaram, S.M., ''An Improved Paraffin Inhibitor'', SPE 1544, (1966).

Buchler, C. C. and Braves, G. D., *Ind. and Eng. Chem.*, 19, 718, (1927).

Burger, E.D., Perkins, T.K., Striegler, J.H., ''Studies of Wax Deposition in the Trans Alaska Pipeline'', SPE 8788, (1981).

Carniani, C., Merlini, M., ''Basic Design of Waxy Oil Transportation Through Improved Lab Testing'', SPE 36836, (1996).

Cavett, R. H., Proc. API Div. of Refining Meeting, San Francisco, 1964.

Chevallier V, Petitjean D, Bouroukba M, Dirand M, 'Mixtures of numerous different n-alkanes: 2. Studies by X-ray diffraction and differential thermal analyses with increasing temperature', *POLYMER* **40** (8): 2129-2137, (1999).

Chevallier V, Bouroukba M, Petitjean D, Dirand M, Pauly J, Daridon JL, Ruffier-Meray V, 'Crystallization of a multiparaffinic wax in normal tetradecane', *Fuel* **79** (14): 1743-1750, (2000).

Clarke, E. W., "Crystal Types of Pure Hydrocarbons in the Paraffin Wax Range", *Industrial & Engineering Chemistry*, **43**(11), 2526-2535, (1951).

Constantinou, L., Gani, R., 'New Group-Contribution Method for Estimating Properties of Pure Compounds', *AIChE J.*, **40** (10), 1697-1710, (1994).

Coutinho, J. A. P., Andersen, S. I., Stenby, E. H., ''Evaluation of Activity-Coefficient Models in Prediction of Alkane Solid-Liquid Equilibria'', *Fluid Phase Equilibria*, **103** (1), 23-39, (1995).

Coutinho, J. A. P., Stenby, E. H., ''Predictive local composition models for solid/liquid equilibrium in n-alkane systems: Wilson equation for multicomponent systems'', *Industrial & Engineering Chemistry Research*, **35** (3), 918-925. (1996).

Coutinho, J. A. P., '' Predictive UNIQUAC: A new model for the description of multiphase solid-liquid equilibria in complex hydrocarbon mixtures'', *Industrial & Engineering Chemistry Research*, **37** (12) 4870-4875, (1998).

Coutinho, J. A. P., Daridon, J. L., '' Low-pressure modeling of wax formation in crude oils'', *Energy & Fuels*, **15** (6): 1454-1460, (2001).

Craig, S. R., Hastie, G. P., Roberts, K. J., Gerson, A. R., Sherwood, J. N., Tack, R. D., ''Investigation into the structures of binary-, tertiary- and quinternary-mixtures of n-alkanes and real diesel waxes using high-resolution synchrotron X-ray powder diffraction'', *Journal of Materials Chemistry*, **8** (4), 859-869, (1998).

Danesh, A., PVT and phase behaviour of petroleum reservoir fluids, Elsevier Science B.V., Amsterdam, The Netherlands, 1998, pp.156.

Daridon, J. L., Xans, P., Montel, F., ''Phase boundary measurement on a methane plus decane plus multiparaffins system'', *Fluid Phase Equilib.*, **117** (1-2), 241-248. (1996).

Daridon, J. L., Pauly, J., Coutinho, J. A. P., Montel, F., '' Solid-liquid-vapor phase boundary of a North Sea waxy crude: Measurement and modeling'', *Energy & Fuels*, **15** (3): 730-735, (2001).

Dernini, S., Desantis, R., 'Solubility of solid hexadecane and tetracosane in hexane', *The Canadian Journal of Chemical Engineering*, **54**, 369-370, (1976).

Dharmawardhana, P. B., Parrish, W. R., Sloan, E. D., " Experimental Thermodynamic Parameters for the Prediction of Natural Gas Hydrate Dissociation Conditions", *Industrial & Engineering Chemistry Fundamentals*, **19**, 410-414, (1980).

Dirand, M., Achour, Z., Jouti, B., Sabour, A., Gachon, J. C., " Binary mixtures of n-alkanes. Phase diagram generalization: Intermediate solid solutions, rotator phases", *MOL CRYST LIQ CRYS A* **275**: 293-304, (1996).

Dirand M, Chevallier V, Provost E, Bouroukba M, Petitjean D, 'Multicomponent paraffin waxes and petroleum solid deposits: structural and thermodynamic state', *Fuel* **77** (12): 1253-1260, (1998).

Dorset, D.L., 'Crystal Structure of an n-Paraffin Binary Eutectic Solid. An Electron Diffraction Determination', *J. Phys. Chem. B*, **101**, 4870-4874, (1997).

Edmonds, B., Moorwood, R. A. S., Szczepanski, R.,''A unified framework for calculating solid deposition from petroleum fluids including waxes, asphaltenes, hydrates and scales'', *Fluid Phase Equilibria*, **160**, 481-489, (1999).

EnDean, H., ''The Paraffin Problem Parts 1-4'', *Champion News*, April-July 1981.

Erickson,D.D., Niesen V.G., Brown, T.S., ''Thermodynamic Measurement and Prediction of Paraffin Prediction in Crude Oils'', SPE 26604, (1993).

Flory, P. J., *J. Chem. Phys.*, **9,** 660, (1941).

Flory, P. J., *J. Chem. Phys.*, **10,** 51, (1942).

Floter, E., deLoos, T. W., Arons, J. D., 'High pressure solid-fluid and vapour-liquid equilibria in the system (methane plus tetracosane)', *Fluid Phase Equilibria*, **127** (1-2), 129-146, (1997).

Fontana, B. J., *J. Phys. Chem.*, 57, 222, (1946).

Gasem, K. A. M., Gao, W., Pan, Z., Robinson, R. L., 'A modified temperature dependence for the Peng-Robinson equation of state', *Fluid Phase Equilibria*, **181** (1-2), 113-125, (2001).

Hammami A., Raines, M. A., ''Paraffin Deposition From Crude Oils: Comparison of Laboratory Results to Field Data'', SPE 38776, (1997).

Hammerschmidt, E. G., ''Formation of Gas Hydrates in Natural Gas Transmission Lines'', *Industrial & Engineering Chemistry*, **26** (8), 851-855, (1934).

Hansen, J. H., Fredenslund, A., Pedersen, K. S., Ronningsen, H. P.. 'A Thermodynamic Model for Predicting Wax Formation in Crude Oils', *AIChE J.*, **34**(12), 1937-1942, (1988).

Hoerr C.W., Harwood, H.J., ''Solubilities of High Molecular Weight Aliphatic Compounds In n-Hexane'', *J. Org. Chem.*, **16**, 779-791, (1951).

Holder, G. D., Corbin, G., Papadopoulos, K. D., 'Thermodynamic and Molecular Properties of Gas Hydrates from Mixtures Containing Methane, Argon, and Krypton', *Industrial & Engineering Chemistry Fundamentals*, **19** (3), 282-286, (1980).

Horne, J. W., Watkins, J. W. and Matjick, A., *Oil & Gas Journal*, **44**, 134, (1946).

Huffman, H. M., Parks, G. S., Barmore, M., ''Thermal data on organic compounds. x. Further studies on the heat capacities, entropies and free energies of hydrocarbons'', *J. Am. Chem. Soc.* **53,** 3876-3888, (1931).

Huggins, M. L., *J. Chem. Phys.*, **9,** 440, (1941).

Huggins, M. L., *Ann. NY Acad. Sci.*, **1,** 431, (1942).

Ji, H-Y., Burgass, R. W., Tohidi, B., Danesh, A., Todd, A. C., ''Developing a reliable technique for measuring wax phase boundary'', submitted.

Ji, H-Y., Burgass, R. W., Tohidi, B., Danesh, A., Todd, A. C., ''Reliable Wax Measurement and a Practical Predictive Model'', in preparation.

Ji, H-Y., Tohidi, B., Danesh, A., 'Experimental measurement and modelling of wax phase equilibrium', 2003 Petroleum Engineering Group (PEG) Technology Forum. Malaysia, Sept. 2003.

Ji, H-Y., Tohidi, B., Danesh, A., Todd, A. C., ''Wax phase equilibria: developing a thermodynamic model using a systematic approach''. *Fluid Phase Equilibria*, **216** (2), 201-217, (2004).

Jin, Y. M., Wunderlich, B., ''Heat-Capacities of Paraffins and Polyethylene''. *Journal of Physical Chemistry*, **95** (22), 9000-9007, (1991).

JIP Reports, 'Gas hydrates in offshore production and drilling', 1999 – 2002; 'Flow assurance: gas hydrates and wax', 2002 – 2004.

Jouti B, Provost E, Petitjean D, Bouroukba M, Dirand M, 'Phase diagram of n-tricosane and n-pentacosane mixtures', *MOL CRYST LIQ CRYS A*, **287**, 275-283, (1996).

Kniaz, K., 'Solubility of Normal-Docosane in Normal-Hexane and Cyclohexane', *Journal of Chemical and Engineering Data*, **36** (4), 471-472, (1991).

Labes-Carrier, C., Ronningsen, H. P., Kolnes, J. and Leporcher, E., "Wax deposition in North Sea gas condensate and oil systems: Comparison between operational experience and model prediction", SPE 77573, (2002).

Lee, B. I., Kesler, M. G., 'A generalized Thermodynamic Correlation Based on Three-Parameter Corresponding States', *AIChE Journal*, **21** (3), 510-527, (1975).

LiraGaleana C, Firoozabadi A, Prausnitz JM, 'Thermodynamics of wax precipitation in petroleum mixtures', *AIChE J* **42** (1): 239-248 JAN 1996.

Lydersen, A.L., Estimation of Critical Properties of Organic Compounds by the Method of Group Contributions, University of Wisconsin, Chemical Engineering Department, *Eng. Exp. Stn. rept. 3*, April 1955.

Madsen, HEL, Roistelle, AR, 'Solubility of long-chain n-paraffins in pentane and heptane', *J. Chem. Soc, Faraday Trans I,*, **72**, 1078-1081, (1976).

Madsen, HEL, 'Solubility of octacosae and hexatriacontane in different n-alkane solvents'. *J. Chem. Soc. Faraday trans I*, **75**, 1254-1258, (1979).

Mansoori, G.A., ''Arterial Blockage in the Petroleum and Natural Gas Industry''. The 1st Conference on Controlling Hydrates, Waxes and Asphaltenes, Aberdeen, UK, 16-17 September, 1996.

McClaflin, G.G., Whitfill, D.L., ''Control of Paraffin Deposition in Production Operations''. SPE 12204, (1984).

Mckoy, V., Sinanoglu, O., 'Theory of Dissociation Pressures of Some Gas Hydrates'. *J. Chem. Physics*, **38** (12), 2946-2956, (1963).

Mehta, A. P., Sloan, E. D., 'A Thermodynamic Model for Structure-H Hydrates'. *AIChE J* **40** (2): 312-320 FEB 1994.

Metivaud, V., Rajabalee, F., Oonk, H. A. J., Mondieig, D., Haget, Y., ''Complete determination of the solid (RI)-liquid equilibria of four consecutive n-alkane ternary systems in the range C14H30- C21H44 using only binary data''. *Can. J. Chem.-Rev. Can. Chim.*, **77** (3), 332-339, (1999).

Monger-McClure, T. G., Tackett, J. E., Merrill, L. S., ''Comparisons of cloud point measurement and paraffin prediction methods''. *SPE Prod. Facil.* **14** (1), 4-15 (1999).

Nelson, W. L. and Stewart, L. D., *Ind. and Eng. Chem.*, 41, 2231, (1949).

Newberry, M.E., ''Crude Oil Production and Flowline Pressure Problems'', SPE 11561, (1983).

Newberry, M.E., Addison, G.E., Barker, K.M., ''Paraffin Control in the Northern Michigan Niagaran Reef Trend'', SPE 12320, (1986).

Nikitin ED, Pavlov PA, Popov AP, 'Vapour-liquid critical temperatures and pressures of normal alkanes with from 19 to 36 carbon atoms, naphthalene and m-terphenyl determined by the pulse-heating technique'. *Fluid Phase Equilibria* **141** (1-2): 155-164 DEC 1997.

Ostergaard, K.K., ''Gas hydrate stability in the petroleum industry and its application in gas-liquid separation''. PhD thesis, Heriot-Watt University, Edinburgh, UK, (2000).

Pan HQ, Firoozabadi A, Fotland P, ''Pressure and composition effect on wax precipitation: Experimental data and model results'', *Spe Production & Facilities*, **12** (4): 250-258, (1997).

Patel, N. C., Teja, A. S., ''New cubic equation of state for fluids and fluid mixtures'', Chemical Engineering Science, 37 (3): 463-473, (1982).

Pauly, J., Daridon, J. L., Coutinho, J. A. P., Lindeloff, N., Andersen, S. I., ''Prediction of solid-fluid phase diagrams of light gases-heavy paraffin systems up to 200 MPa using an equation of state-G(E) model'', *Fluid Phase Equilibria*, **167** (2), 145-159, (2000).

Pauly, J., Daridon, J. L., Coutinho, J. A. P., ''Measurement and prediction of temperature and pressure effect on wax content in a partially frozen paraffinic system'', *Fluid Phase Equilib.*, 187, 71-82, (2001).

Parczewska, B., ''the Static Dilatometric Method with Ultrasonic Liquid Level Detection to Determine Phase Diagrams and (Solid + Liquid) Equilibrium in (Hexadecane + Octadecane)'', *J. Chem. Thermodynamics*, **32**, 777-788, (2000).

Parrish, W. R., Prausnitz, J. M., 'Dissociation Pressures of Gas Hydrates Formed by Gas Mixtures', *Industrial & Engineering Chemistry Process Design and Development*, **11** (1), 26-35, (1972).

Paso, K.G., Fogler, H.S., ''Influence of n-paraffin composition on the aging of wax-oil gel deposits'', *AIChE J.*, **49** (12): 3241-3252 DEC (2003).

Paunovic, I., Mehrotra, A.K., 'Liquid-Solid Phase Transformation of $C_{16}H_{34}$, $C_{28}H_{58}$ and $C_{41}H_{84}$ and their binary and ternary mixtures', *Thermochimica Acta*, **356**, 27-38, (2000).

Pedersen, W. B., Hansen, A. B., Larsen, E., Nielsen, A. B. and Ronningsen, H. P., "Wax Precipitation from North-Sea Crude Oils .2. Solid-Phase Content as Function of Temperature Determined by Pulsed Nmr", *Energy & Fuels*, **5** (6), 908-913, (1991a).

Pedersen, K. S., Skovborg, P., Ronningsen, H. P., 'Wax Precipitation from North-Sea Crude Oils .4. Thermodynamic Modeling', *Energy Fuels*, **5** (6), 924-932, (1991b).

Pedersen, K. S., 'Prediction of Cloud Point Temperatures and Amount of Wax Precipitation'. *SPE Prod. Fac.*, **10** (1), 46-49, (1995).

Peng, D. Y., Robinson, D. B., '' A New Two-Constant Equation of State''. *Industrial & Engineering Chemistry Fundamentals*, **15** (1), 59-64, (1976).

Perry's Chemical Engineers' Handbook, McGraw-Hill Company, Tokyo Japan, (1984).

Peters, C. J., Vanderkooi, H. J., Arons, J. D., 'Measurements and Calculations of Phase-Equilibria for (Ethane + Tetracosane) and (P, Vm-Star, T) of Liquid Tetracosane' *Journal of Chemical Thermodynamics*, **19** (4), 395-405, (1987).

Peters, C. J., Spiegelaar, J., Arons, J. D., 'Phase-Equilibria in Binary-Mixtures of Ethane+ Docosane and Molar Volumes of Liquid Docosane', *Fluid Phase Equilibria*, **41** (3), 245-256, (1988).

Peters, C. J., Vanderkooi, H. J., Deroo, J. L., Arons, J. D., Gallagher, J. S., Sengers, Jmhl, 'The Search for Tricriticality in Binary-Mixtures of near- Critical Propane and Normal Paraffins', *Fluid Phase Equilibria*, **51**, 339-351, (1989).

Prausnitz, J. M., Lichtenthaler, R. N., de Azevedo, E. G., Molecular Thermodynamics of Fluid-phase Equilibria, Prentice-Hall Inc., Englewood Cliffs, N.J., 1986, pp. 240.

Provost E, Balesdent D, Bouroukba M, Petitjean D, Dirand M, Ruffier-Meray V, 'Phase diagram of n-hexacosane and n-octacosane: experimental determination and calculation', *J Chem Thermodyn.*, **31** (9): 1135-1149, (1999).

Rai, R., Sarkar, B., Dalal, V., ''Multiphase Transportation of High Waxy Crudes'', SPE 27061, (1995).

Reyna, E.M., Stewart, S.R., ''Case History of the Remival of a Hydrate Plug Formed During Deep Water Well Testing'', SPE/IADC 67746, SPE/IADC Drilling Conference, Amsterdam, The Netherlands, 27/2-1/3/2001.

Riazi, M. R., Alsahhaf, T. A., 'Physical-Properties of N-Alkanes and N-Alkylhydrocarbons - Application to Petroleum Mixtures', *Ind. Eng. Chem. Res.* **34** (11), 4145-4148, (1995).

Riazi, M. R., AlSahhaf, T. A., '' Physical properties of heavy petroleum fractions and crude oils'', *Fluid Phase Equilibria*, 117 (1-2): 217-224, (1996).

Roberts, K. L., Rousseau, R. W., Teja, A. S., 'Solubility of Long-Chain N-Alkanes in Heptane between 280 and 350-K', *Journal of Chemical and Engineering Data*, **39** (4), 793-795, (1994).

Robinson, D. B., Peng, D. Y., 'The Characterisation of the Heptane and Heavier Fractions for the GPA Peng-Robinson Programme', *GPA Research Report* 28, Tulsa (1978).

Robles, L., Espeau, P., Mondieig, D., Haget, Y., Oonk, H. A. J., ''Polymorphism and molecular alloys in the binary system C17H36- C19H40''. *Thermochim. Acta*, **274**, 61-72, (1996).

Roehner, R. M., Fletcher, J. V. and Hanson, F. V., "Comparative compositional study of crude oil solids from the Trans Alaska Pipeline System using high-temperature gas chromatography", *Energy & Fuels*, **16** (1), 211-217, (2002).

Ronningsen, H. P., Bjorndal, B., Hansen, A. B., Pedersen, W. B., ''Wax Precipitation from North-Sea Crude Oils .1. Crystallization and Dissolution Temperatures, and Newtonian and Non-Newtonian Flow Properties'', *Energy & Fuels*, **5** (6), 895-908, (1991).

Schaerer, A.A., Busso, CJ, Smith, AE, Skinner, LB, ''Properties of pure alkanes in the C17 to C36 range'', *Journal of the American Chemistry Society*, 77, 2017-2018, (1955).

Schanen, A. N., ''Chemical constituents of petroleum'', Reinhold Pub. Corp., (1945).

Seyer, W.F., 'Mutual solubilties of hydrocarbons. II. The freezing point curves of dotriacontane (Dicetyl) in Dodecane, Decane, Octane, Hexane, Cyclohexane and Benzene', *J. Am. Chem. Soc.*, **60**, 827 – 830, (1938).

Shock, D.A., Sudbury, J.D., Crockett, J.J., ''Studies of the Mechanism of Paraffin Deposition and Its Control'', *J. Pet. Tech.*, 23-28, Sept. (1955).

Sifferman, T.R., ''The Flow Properties of Difficult to Handle Waxy Crudes''. SPE 7409. presented at the 1978 SPE annual Technical Conference and Exhibition. Houston. Oct. 1-4.

Singhal, H. K., Sahai, G. C., Pundeer, G. S., Chandra, K., '' Desining and selecting wax crystal modifier for optimum field performance based on crude oil composition'', SPE 22784, (1991).

Sloan, E.D. Jr., ''Clathrate Hydrates of Natural Gases''. Marcel Dekker Inc., New York. 1998, pp. 266.

Soave, G., ''Equilibrium Constants from a Modified Redlich-Kwong Equation of State''. *Chemical Engineering Science*, **27**, 1197-1203, (1972).

Soave, G., 'Improving the Treatment of Heavy Hydrocarbons by the SRK EoS'. *Fluid Phase Equilibr.*, **84**, 339-342, (1993).

Spencer, C. F., Daubert, T. E., *AIChE J.*, **19,** 482, (1973).

Srivastava, S. P., Handoo, J., Agrawal, K. M. and Joshi, G. C., "Phase-Transition Studies in N-Alkanes and Petroleum-Related Waxes - a Review", *Journal of Physics and Chemistry of Solids*, **54** (6), 639-670, (1993).

Srivastava, S. P., Butz, T., Verma, P. S., Purohit, R. C., Rahimian, I., "Study of the temperature and enthalpy of wax crystallization from middle distillate by DSC", *Petroleum science and technology*, **20** (7-8), 831-839, (2002).

Teja, A. S., Lee, R. J., Rosenthal, D., Anselme, M., 'Correlation of the Critical Properties of Alkanes and Alkanols' *Fluid Phase Equilib.*, **56**, 153-169, (1990).

Tipmeester, J. A., Tse, J. S., Ratcliffe, C. I., Powell, B. M., ''A New Clathrate Hydrate Structure''. *Nature* **325** (6100): 135-136 JAN 8 1987.

Tohidi, B. ''Gas Hydrate Equilibria in the Presence of Electrolyte Solutions''. PhD thesis. Heriot-Watt University, Edinburgh, UK. (1995).

Tohidi, B., Danesh, A., Todd, A. C., Burgass, R. W., Ren, S-R., Andersen, R., Yang J-H., Arjmandi, M., Reid, A., Ji., H-Y., Masoudi, R., Biderkab, A. B., Mohammadi, A.H.,

''Gas Hydrates in Offshore Production and Drilling''. *Proceeding of DTI Improved Oil Recovery (IOR) Research Dissemination Seminar*, 25th June 2002. Aberdeen. UK (2002).

Tohidi, B., Danesh, A., Todd, A. C., Andersen, R., Burgass, R. W., Arjmandi. M., Masoudi. R., Ji., H-Y., Mohammadi, A.H., Yang J-H., Ren, S-R., Zain, Z., Mali. G., Jadhawar. P., ''Gas Hydrates and Flow Assurance Studies''. *Proceeding of DTI Maximising Hydrocarbon Recovery from the UKCS Seminar 2004*, 22th-23rd June 2004. Aberdeen. UK (2004).

Twu C.H., 'An Internally Consistent Correlation for Predicting the Critical Properties and Molecular-Weights of Petroleum and Coal-Tar Liquids' *Fluid Phase Equilibria*, **16** (2), 137-150, (1984).

Twu, C. H., Coon, J. E., Cunningham, J. R., 'A New Generalized Alpha-Function for a Cubic Equation of State .2. Redlich-Kwong Equation', *Fluid Phase Equilibria*, **105** (1), 61-69, (1995a).

Twu, C. H., Coon, J. E., Cunningham, J. R., 'A New Generalized Alpha-Function for a Cubic Equation of State .1. Peng-Robinson Equation', *Fluid Phase Equilibria*, **105** (1), 49-59, (1995b).

Valderrama, J. O., ''A Generalized Patel-Teja Equation of State for Polar and Nonpolar Fluids and Their Mixtures'', *J. Chem. Eng. JPN*, **23** (1): 87-91 FEB (1990).

Vanderkooi, H. J., Floter, E., Deloos, T. W., ''High-Pressure Phase-Equilibria of ((1-X)Ch4+Xch(3)(Ch2)(18)Ch3)'', *J. Chem. Thermodyn.*, **27** (8), 847-861, (1995).

Van Miltenburg, J. C., Oonk, H. A. J., Metivaud, V., ''Heat capacities and derived thermodynamic functions of n- nonadecane and n-eicosane between 10 K and 390 K'', *Journal of Chemical and Engineering Data*, **44** (4), 715-720, (1999).

Van der Waals, J. H., Platteeuw, J. C., ''Clathrate Solutions'', *Advances in Chemical Physics*, **2**, 1-57, (1959).

Von Stackelberg, M. and Müller, H. R., "Feste Gashydrate", *Z. für Elektrochemie*, **58**, 25, (1954).

Whitson, C. H., ''Characterizing hydrocarbon plus fractions'', *Society of Petroleum Engineers Journal*, **23** (4): 683-694, (1983).

Won, K. W., 'Thermodynamics for Solid Solution-Liquid-Vapor Equilibria - Wax Phase Formation from Heavy Hydrocarbon Mixtures', *Fluid Phase Equilib.*, **30**, 265-279, (1986).

Won, K. W., ''Thermodynamic Calculation of Cloud Point Temperatures and Wax Phase Compositions of Refined Hydrocarbon Mixtures'', *Fluid Phase Equilib.*, **53**, 377-396, (1989).

Wurflinger, A., Sandmann, M., 'Thermodynamic measurements on n-hexadecane (C16H34) and n- heptadecane (C17H36) at elevated pressures', *Zeitschrift Fur Naturforschung Section a-a Journal of Physical Sciences*, **55** (5), 533-538, (2000).